Durham E-Theses

The climatic significance of tropical forest edges and their representation in global climate models

CAIN, RUSSELL

UNIVERSITY OF DURHAM

THE CLIMATIC SIGNIFICANCE OF TROPICAL FOREST EDGES AND
THEIR REPRESENTATION IN GLOBAL CLIMATE MODELS

RUSSELL JOHN CAIN

B.Sc. (HONS) (DUNELM)

SUBMITTED IN PARTIAL FULFILLMENT FOR THE

DEGREE OF DOCTOR OF PHILOSOPHY

2009

Declaration and Copyright

None of the material presented here has previously been submitted for a degree in this, or any other, university. All of the work described is my own, except where otherwise stated.

Russell John Cain

July 2009

Copyright © 2008 Russell John Cain

The copyright of this thesis rests with the author. No quotation from it should be published in any format without the author's prior written consent.

The author can be contacted at: Russell.Cain@dunelm.co.uk

ABSTRACT

An emerging theme in global climate modelling is whether land covers created in the clearance of tropical humid forests influence water exchange between remnant forest patches and the atmosphere, and, if so, how this affects regional and global water exchange. Fieldwork presented in this thesis ascertains whether the amount of water transferred to the atmosphere from a humid tropical forest situated in Sabah, Northern Borneo, Malaysia, differs between its edge and interior due to the influence of surrounding clearings through horizontal heat transfer. Using satellite imagery to measure the shape and size of tropical forests, field measurements of water transfer were extrapolated to continental and global levels to infer how differences in water exchange with the atmosphere between forest edges and interiors may influence regional and global forest-atmosphere water exchange.

Mean sap flow in trees within 50 meters of a forest-clearing boundary was found to be 73% greater than that in trees further into the forest; an observation supported by the decreased canopy temperature also recorded there. Evaporation from the forest canopy constituted a high fraction of annual rainfall (33%), but showed no edge effect similar to that of sap flow. Edge plots, however, expressed evapotranspiration rates 22% lower than forest interiors (657-890 mm yr^{-1}), owing to the lower number and size of trees there. One edge plot, however, exhibited evapotranspiration 49.5% greater than that of forest interiors. Gradients of air temperature, vapour pressure deficit and wind speed from the adjacent clearing to the forest interior indicated that warm, dry air moving from the clearing to the forest was the most credible cause of increased sap flow of trees near the forest edge. This hypothesis was supported by a strong correlation between the amount of vapour in the air moving from the clearing and tree water use. It was estimated that the influence of differences in water transfer to the atmosphere between the edges and interiors of tropical forest would not alter global water transfer to the atmosphere by more than 0.25-4%, or by 4-7% in the most fragmented tropical continent, Africa.

However, it remains unclear whether the inclusion of tropical forest edge effects within climate models is necessary, as the pioneering nature of this thesis, and of existing studies reviewed within it, means that solid conclusions will be dependent upon future work. This thesis concludes with suggestions for future research that will most effectively consolidate the provisional conclusions and recommendations herein.

ACKNOWLEDGEMENTS

CONTENTS

CONTENTS

Chapter I: The Potential Significance of Tropical Forest Discontinuities and Their Influence on Regional Hydrometeorology

CONTENTS

CONTENTS

CONTENTS

CONTENTS

CONTENTS

CONTENTS

Chapter 5

List of Figures

Forests of the tropical humid biome influence and maintain local, regional and global climate (Cox *et al.*, 2000; Fu & Li, 2004; Hales *et al.*, 2004; Holfman & Jackson, 2000; Kumagai *et al.*, 2004a, 2004b, 2005; Laurance, 1999a; Malhi *et al.*, 1998; Polcher, 1995; Weaver & Avissar, 2001; Werth & Avissar, 2002). This is orchestrated through the bidirectional exchange of energy between the forest and its overlying atmosphere via the transfer of heat, moisture, air momentum and trace gases. Of these quantities, water transport is a key determinant of climate, and the work presented in this thesis thus focuses on the role of water transport in tropical meteorology – i.e. tropical hydrometeorology. Deforestation creates clearings that have little or no vegetation, considerably reducing the amount of water transferred from the land surface to the atmosphere. This means that clearings receiving solar energy instead transfer a large amount of heat to the air immediately above them (i.e. there is a high sensible heat flux from the clearing surface to the overlying air). As a result the air over clearings is hotter and drier than that over the canopies of forest remnants, which are pre-adapted to the stable, moist and relatively cool environment typical of continuous (i.e. homogeneous) forest cover (Harper *et al.*, 2005; Murcia, 1995; Saunders *et al.*, 1991). The aforementioned contrasting energetic responses of tropical forest remnants and clearings (sensible and latent heat flux proportions to the atmosphere above each land cover type for a given amount of incoming solar energy) arise from the physical properties of clearings, which express an altered vegetation fraction, rooting depth, albedo, and thus water status, to that of forest. Thus deforestation forms a fragmented and heterogeneous landscape comprising of many different components (patches) which are heterogeneous in their physical characteristics and energetic responses to incoming solar energy.

Theory suggests that the contrasting energetic responses of heterogeneous landscape components, such as those between clearings and tropical forest remnants, may influence hydrometeorological and associated biogeochemical processes at the edges of different patches through horizontal heat transfer where they meet (Harding *et al.*, 1997; Stohlgren *et al.*, 1998; Veen *et al.*, 1996). In the case of forest clearings within the tropical humid biome, it is suggested that there will be increased transpiration from trees at forest edges where hot dry air passes from clearings into forest edges. Processes that are different at the edges of landscape

components when compared to their interiors, such as altered transpiration at forest edges, are called 'edge effects'. The presence of substantial edge effects within fragmented tropical forest landscapes holds many ramifications for regional and global climate, and its modelling. This is because the transfer rate of quantities important to regional and global climate would not depend on the proportion of tropical forest cover alone, but also on the degree and pattern of fragmentation. Recent studies (Ciencala *et al.*, 2002; Giambelluca *et al.* 2003; Herbst *et al.* 2007b; Klaassen *et al.*, 2002) all conclude that edge effects, and therefore the shape as well as the size of forest patches, should be accounted for in the regionalisation (the generation of regional estimates from point measurements) of key hydrometeorological parameters when considering the meteorology of fragmented forest ecosystems. However, despite unprecedented and unabated conversion and fragmentation of primary tropical forest (Achard *et al.*, 2002a; Whitmore, 1984), almost nothing is known about the actual contribution of edge effects to hydrometeorology.

The six chapters of this thesis distil and compare different hydrometeorological processes at a tropical forest edge and interior, and analyse how these differences aggregate at the regional and global scale, depending on the size and shape of forest remnants found throughout the tropical humid biome.

The first chapter assesses the state of knowledge with regard to the meteorological responses of tropical forests to incoming solar energy, and the importance of these responses to regional and global climate. The respective meteorological responses of forest edges are also considered, and the potential importance of these responses to regional and global climate in fragmented forested ecosystems is discussed. The importance of the moisture status of the land surface is highlighted, and the decision to focus this thesis on the hydrometeorology of tropical forests is justified. The theory upon which the field campaign of Chapter 2 and remote sensing exercise of Chapter 3 are based is introduced. This is supported by analyses of four case studies that examine land surface-climate interactions (LSAIs) at forest edges in terms of their hydrometeorology, and represent the only work of this type conducted to date. Reviewing the methods and limitations of relevant case studies helps define the methodology of Chapters 2 and 3. Values reported by each case study of the altered transpiration responses of trees at forest edges when compared to that of 'interior' trees (i.e. the magnitude of edge influence, MEI) and the extent to which this difference is apparent from the forest edge (i.e. the extent of edge influence, EEI) are

discussed. The need to account for wet canopy evaporation in addition to transpiration when considering the hydrometeorology of forest edges is also highlighted, since all but one of the four case studies presented in Chapter 1 focus on edge effects of transpiration alone.

Chapter 2 details the measurement of transpiration and wet canopy evaporation from a tropical forest patch in Sabah, Northern Borneo, Malaysia. It is shown how the methodologies employed facilitate reliable comparisons of evapotranspiration rates between the edge and interior of this forest patch to ascertain respective values of MEI and EEI. Particular attention is drawn to the use of thermal dissipation probes, which are introduced in Chapter 1, and other techniques that can be employed with equal reliability regardless of distance from the forest edge to estimate evapotranspiration.

Chapter 3 details the methodology used to examine deforestation patterns in Latin America, Africa and Southeast Asia, and how this is aided by classifying Landsat satellite imagery into 'forest' and 'non-forest' based upon the Normalised Difference Vegetation Index (NDVI). Issues relevant to the methodology described in chapter 3 are introduced to clarify why certain methods are chosen, and how the methodology allows an estimation of the proportion of forest cover under the influence of edge effects for each continent, and globally, using an appropriate model (Laurance & Yensen, 1991). Analyses are carried out on 104 satellite images acquired from sample sites, chosen in accordance with the TREES (Tropical Ecosystem Environment Observation by Satellite) project (*cf.* Achard *et al*., 2002a, 2002b). The influence satellite sensors resolution upon measurements is also considered, and existing methodologies aimed at examining scale effects are thus reviewed and selected.

In Chapter 4, 'bottom-up' measurements of sap flow, through-fall, and understory evapotranspiration are made according to the methodology outlined in Chapter 2, and scaled to the level of the forest stand for the field site and three other sites using their respective vegetation data to parameterise scaling. 'Top-down' micrometeorological measurements detailed in Chapter 2 are used to support and validate estimates of transpiration and evaporation made by scaling bottom-up measurements. Chapter 4 shows for the first time that trees at a forest edge in the tropical humid biome experience an edge effect of increased transpiration rates 73% greater than those trees in the forest interior, and that a similar edge effect is not shown for wet canopy evaporation. The influence of hydrological, biological and

micrometeorological components upon net evapotranspiration of the forest is analysed. It is shown that whilst transpiration of the studied forest patch is influenced by hot air advection, both transpiration and the net evapotranspiration of the site are also controlled by physiological, biometric and below-ground factors.

Chapter 5 follows the methodology of Chapter 3 by using the 104 satellite image samples to estimate the proportion of tropical forest, regionally and globally, under the influence of edge effects based on the typical extents to which edge effects are known to penetrate into forest patches. This is achieved by adhering to the TREES sampling scheme, and using the respective TREES weights assigned in the selection of the 104 satellite images, as described in Chapter 3. The magnitude of response (MEI) and extent of penetration (EEI) expressed by different edge effects commonly operating in the tropics are combined with statistics of patch perimeter and area to quantify differences in regional/global estimations of a given parameter incurred by neglecting their respective edge effects (*cf.* Laurance & Yensen, 1991). A scaling exercise is also performed to investigate whether patterns of deforestation show predictable scaling behaviour. This is done with a view to allowing the calibration of coarse resolution satellite imagery available over the entire tropical humid biome with finer resolution imagery. Scaling patterns are examined with respect to patch perimeter-to-area ratios. Perimeter-to-area regressions are stratified by continent and also by the use of texture measures. Patterns of deforestation as represented by trends in forest patch perimeter-to-area ratios are shown not to differ significantly between continents. The attempt to stratify this relationship using texture (pattern) descriptors does not provide sufficient separability in patterns of perimeter-to-area ratio for tropical forest patches. Africa is demonstrated to be the most fragmented continent, in fitting with previous work (Rudel & Roper, 1997). As a result it is estimated that Africa will have the greatest proportion of tropical forest under the influence of edge effects. However, it is shown that even for edge effects of greater magnitude and extent than those reported in chapter 4 (i.e. the largest values in the literature) the maximum difference incurred by not including edge effects in climate models is not expected to be greater than 4%. For the different scenarios of evapotranspiration presented in chapter 4, not accounting for edge effects in climate models is expected to lead to differences of less than 1%, as is also the case for typical meteorological and biological edge effects found in the literature.

The sixth and final chapter provides a summary of the achievements of this thesis and highlights limitations upon which future work can improve. Directions for future research are recommended and methodologies suggested.

There follows an outline of the aims and objectives of this thesis and an overview of key terms and units used. The links between research questions, methodologies, analyses and scale, as derived from Chapter 1, are also presented (Table A) to provide a conceptual map on which this thesis is based and on which future work can be developed.

The relationship between scale, prominent research questions, field measurements and numerical modelling is clarified and shown schematically in Table A; wherein the aims, objectives, and research questions of this thesis are highlighted in red. Thereafter, abbreviations and definitions are presented to clarify terminology used in this necessarily jargon-laden discipline. In Table A and when defining terms, attention is drawn to the multi-faceted nature of this research, and the need to employ methodologies that account for the scale at which measurements are made.

The aim of this thesis is to establish:

Whether edges of tropical forest patches contribute significantly to regional and global hydrometeorology, and need to be included in global climate models.

The objectives required to fulfil the aim of this thesis seek to establish:

1) *Whether tropical forest edges transfer more water to the atmosphere than their respective forest interiors.*

2) *What proportions of tropical forests are under the influence of edge effects, and how this influences the estimation of a given parameter at the regional and global scales.*

3) *Whether a predictable relationship between patch perimeter and area is evident for tropical forest patches, and whether this pattern can be stratified by texture measures, nominal descriptors of fragmentation pattern, or by region.*

Aims & Objectives

- Whether edges of tropical forest patches contribute significantly to regional and global hydrometeorology and need to be included in global climate models.

- Whether tropical forest edges transfer more water to the atmosphere than their respective forest interiors.

- Whether a predictable relationship between patch perimeter and area is present for tropical forest patches, and whether this pattern can be stratified by texture measures, nominal descriptors of fragmentation pattern, or by region.

- What proportions of tropical forests are under the influence of edge effects for different MEI and EEI values associated with common edge effects found in tropical fragmented forest, and how this influences the estimation of hydrometeorological parameters at patch-regional- global scales.

	POINT	PATCH	REGION	GLOBAL
RESEARCH QUESTION	What are the typical magnitudes of water loss at forest edges? Do forest edge species differ in their stomatal resistances?	What are the typical extents of edge effect? Does forest structure influence wet-canopy evaporation?	Do forest patches in tropical regions promote a high perimeter-to-area ratio? Which region has the highest perimeter-to-area ratio? Do patterns of forest fragmentation scale systematically?	Does continuous forest negate the influence of fragmented areas?
METEOROLOGICAL MEASUREMENT	Automated dendrometer bands? Sap flux (Thermal Dissipation Probes) Net radiation, vapour pressure deficit, wind speed Eddy Correlation (EC) over patchy landscapes	Through-fall gauges Canopy water capacity Canopy drying time	(EC Networks)	
ANCILLIARY MEASUREMENT		Vegetation dynamics plots (leaf area, species composition, mortality) Slope, aspect, clearing roughness and moisture, local climate (from nearest automatic weather station)		
MODELS		Second order vegetation dynamics Interception	Core area/length-scale Boundary layer Regional and global climate models	
REMOTE SENSING		Surface temperature, albedo, normalised difference vegetation index, net radiation surface energy balance algorithms (System Pour L'Observation de la Terre satellite) (Landsat satellite) (Advanced Very High Resolution Radiometer) Landscape metrics and texture classifiers (Landsat Satellite) (Advanced Very High Resolution Radiometer)		

Table A: Research questions and their scales, taken from literature review, Chapter1. Attention is drawn to the process of up-scaling by a yellow arrow, which makes clear the contiguity between objectives at each scale. Aims, objectives, and research questions are highlighted in red boxes.

ABBREVIATIONS AND DEFINITIONS

ORGANISATIONS & PROJECTS

CLASSIC - Climate and Land Surface Systems Interaction Centre
SEARRP - South East Asia Rainforest Research Program
AFTE – Aggregating Fluxes in Fragmented Tropical Ecosystems
RS- Royal Society of London
DVMC – Danum Valley Management Committee
EPU - Economic Planning Unit of Malaysia

UMS – Universiti Malaysia, Sabah
MMS - Malaysian Meteorological Service
GAW - Global Atmospheric Watch
TREES – Tropical Ecosystem Environment Observations by Satellite
YSLC – Yayasan Sabah Logging Concession
YSC – Yayasan Sabah Corporation.

TECHNIQUES & EQUIPMENT

SRA – Surface Renewal Analysis
CFC – Closed Flux Chamber
BREB – Bowen Ratio Energy Balance
TDP – Thermal Dissipation Probe
VLDP – Variable Length Thermal Dissipation Probe
EO- Earth Observation
CI - Canopy Illumination Index
PI – Perhumidity Index
EIB- Energy Imbalance
NDVI- Normalised Difference Vegetation Index
AFVI – Aerosol Free Vegetation Index
ARVI – Atmospherically Resistant Vegetation Index.
SPOT – System Pour l' Observation de Terre (20-1000m resolution)

MODIS - Moderate Resolution Imaging Spectroradiometer (250-1000m resolution)
LANDSAT – Land Satellite (30-60m resolution)
AVHRR - Advanced Very High Resolution Radiometer (1000m resolution).
IKONOS – Commercial Satellite, derived from the Greek word eikōn, for image (1-4m resolution)
DWT – Discrete Wavelet Transform
LSAIs- Land Surface-Atmosphere Interactions
AFTE- Author's project- Aggregation in Fragmented Tropical Ecosystems.

MODELS

GCM – Global Circulation Model
RCM - Regional Climate Model
JULES - Joint UK Land Environment Simulator
SAMOSES – Spatially Aware Met. Office Surface Exchange Scheme
MOSES - Meteorological Office Surface Exchange Scheme version 2.2
BLASIUS - Boundary Layer above Stationary In-homogeneous and Uneven Surfaces
NWP - Numerical Weather Prediction

AA (AFFECTED AREA) - The total area of a patch or landscape that is subject to significant EI.

ADIABATIC – A process that does not involve heat transfer, such as the expansion of air, and the transfer of energy by waves or particles (i.e. radiative transfer).

ADVECTION – The horizontal movement of a body of atmosphere (or other fluid) along with the concomitant transport of its embodied temperature, humidity, and other properties; the transport of a scalar by bulk atmosphere or fluid motion.

BOTTOM-UP – The approach of addressing a problem in fashion that starts from a series of lower (more specific) levels and combines information from these lower levels to work towards a higher (more general) level. Bottom-up measurements are thus detailed, and need to be combined to avoid simplistic conclusions.

CA (CORE-AREA) - The total patch or landscape area that consists of interior forest outside the zone of significant EI, i.e. the total forested area- the Affected Area (AA).

CARTESIAN SPACE- The Cartesian coordinate system specifies each point uniquely in a plane by a pair of numerical coordinates, which are the signed distances from the point to two fixed perpendicular directed lines, measured in the same unit of length.

DEI (Depth of Edge Influence) – The point at which the MEI asymptotes to zero.

DIABATIC – A process that involves the transfer of heat, and the opposite of adiabatic. A meteorological example would be the warming of an air parcel due to the absorption of infra red radiation, or the release of latent heat via evaporation/transpiration.

DIEL – Describes events that occur with a 24 hour periodicity.

DIURNAL- Pertaining to the daylight portion of the 24-hour day.

EDGE - The interface between two contrasting patches of the landscape or the point of greatest second-order difference (Canny, 1986).

EEI (EXTENT OF EDGE INFLUENCE) - Exactly the same as DEI, the two are interchangeable (compare Laurance & Yensen (1991) to Harper *et al.* (2005)).

EI (EDGE INFLUENCE) - A named influence of one land cover type on another arising from their horizontal interaction at the point where they meet (i.e. the edge interface).

EXTENT- The distance covered by a phenomenon, or the instantaneous field of view (IFOV) of a given sensor. For example, a Landsat satellite sensor image represents a series of 30m x 30m pixels covering an area of approximately 130km^2. Therefore, the extent of a Landsat image is equal to the IFOV of the sensor, which is 130 km in this case.

FETCH – The distance from a forest edge into its interior (usually, but not limited to, a forest edge orientated into the prevailing wind direction).

FEATURE SPACE- The abstract space where each of a series of pattern samples (features) is represented as a point in n-dimensional space.

FEATURE REDUCTION- The removal of n-dimensions of feature-space to reduce the total number of dimensions of feature space into a more manageable and concise number, whilst aiming to retain as much information as possible.

FLUX - The flow of a given quantity, as a rate per area, which, if measured at a fixed point, would produce altered scalar values (e.g. concentrations or densities) that change with time in proportion to the rate and direction of the flow.

HETEROGENEOUS – The same as inhomogeneous; having many different components of contrasting properties and expressing a high variance.

HETEROGENEOUS INTERACTION - Interaction between two heterogeneous land surface components through the exchange of biota, energy, or heat.

HOMOGENEOUS – The opposite of heterogeneous; being uniform, having components of similar properties, and expressing a low variance.

HYDROMETEOROLOGY- The study of the atmospheric and terrestrial phases of the hydrological cycle with emphasis on the relationship between them.

HYPERDYNAMISM - The increased mortality of tree species within a forest, usually due to anthropogenic disturbance, which leads to altered forest structure, species composition, physiognomy, and function. More broadly, hyperdynamism is the increase in frequency and or amplitude of community, population and landscape dynamics in fragmented ecosystems.

LANDING - The method of transporting from a harvest area to a storage area, also called a landing, or 'stamping ground'.

LAND SURFACE – The canopy of vegetated areas such as forests, or the substrate of non-vegetated areas, such as the soil of forest clearings. The term 'skin' is commonly used to denote the land surface.

LAND SURFACE COMPONENTS – The term for areas of the land surface with different physical properties or characteristics. Land surface components can also be termed 'patches', owing to the overall impression they give when viewing the landscape from above.

LYSIMETER – An instrument that measures the percolation of water through soil contained within it. This allows evapotranspiration to be calculated if precipitation is known.

MATRIX HARSHNESS – The difference in ecosystem type, composition, function, or in microclimate between adjacent land surface components/patches.

Abbreviations and Definitions

MEI (MAGNITUDE OF EDGE INFLUENCE) – The percentage deviation (+/- %) of a quantity at the edge of a (forest) patch from its respective interior value.

ONTOGENETIC- The sequence of developmental stages which an organism passes through during its lifetime, mediated by the extrinsic factors within the immediate environment of the organism that act to suppress or initiate the activity genes specific to it.

OROGRAPHIC - The nature of a region with respect to its elevated terrain. Often refers to influences of mountains or mountain ranges on airflow, but also used to describe effects on other meteorological quantities such as temperature, humidity, and precipitation.

PATH AND ROW A path and row value defines a position and area on the earth's land surface within the instantaneous field of view of a given satellite sensor, such as Landsat.

PCA (PRINCIPAL COMPONENT ANALYSIS) – The mathematical procedure of transforming a number of variables that are all correlated to different degrees into a smaller number of uncorrelated variables called principal components. The first principal component accounts for as much of the variability if the data as possible, with each succeeding component accounting for as much of the variability remaining from previous principal components as possible. PCA is can be thus considered a form of feature reduction.

PHYSIOGNOMY- The outward appearance of something, especially the physical characteristics of a geographical region.

PSCYCHROMETRIC – Pertaining to the physical and thermodynamic properties of the atmosphere and its water vapour.

PSI (PATTON SHAPE INDEX) - A measure of shape that indicates deviation from circularity as a deviation from 1, whereby a circle = 1, and higher values of PSI represent increasingly complex shapes.

RADIATIVE – The transmission of energy in the form of waves or particles.

REGIONALISATION – The most efficient way to find a correct regional value of a given quantity that is based upon, and summarises, many individual point observations made throughout that same region.

RESOLUTION- The minimum measureable SI unit of a given sensor, usually expressed as a distance. For example, the pixels of a Landsat satellite sensor image represent a 30m x 30m area on the ground. Hence the resolution of a Landsat satellite image is 30 m.

RING-POROUS- Having tree rings, comprising xylem vessels more numerous and usually larger in cross section in the springwood, with a resulting more or less distinct line between the springwood and the last season's wood.

Abbreviations and Definitions

DIFFUSE-POROUS- Not having tree rings, and uniformly-spaced xylem elements spaced at a lower density, with poor separation between spring and last season wood.

SEPARABILITY- The capability of being separated.

SWIDDEN - A field in an agricultural production system of shifting cultivation or rotational fallow.

TOP-DOWN – The approach of addressing a problem in a fashion that starts from a higher (more generalised) level and works towards lower (more specific) levels by disassembling the higher level into its constituent pieces. Top-down measurements are thus synoptic, and need to be broken down to reduce the complexity of the problem in hand.

VECTOR - A coherent shape made from many scalar pixels.

Throughout this thesis reference is made to a number of different scales. In some cases these relate to process scales, and in other cases to the scales resolved by regional and global atmospheric models (e.g. GCMs). For clarity, the definitions of seven scales to which frequent reference is made are defined below:

Scale	Description	Typical Length Scale
Point	the scale of a *non-remotely sensed* measurement	2cm-10m
Stand	a series of trees in a roughly *homogeneous* area	50m
Patch	a series of contiguous tree stands	200m
Landscape	a series of forested and non-forested patches	600m-1000m
	- or the local political boundaries of an area (e.g Danum Valley Conservation Area)	
Meso	A functionally delineate system or land cover type	2-100km
	- or the length scales that are typically resolved by RCMs	10km
Regional	the geographical or political bounds of an area	100km+
	-or length scales that can be resolved in GCMs	50 km
Pan-tropical	the entire tropical humid biome	

Roman Alphabet

A	Available energy at the land's surface	$W\ m^{-2}$
AA	Affected area of a forest patch by a given edge influence	ha
AA_{ad}	Adjusted AA using empirical data of Laurance & Yensen (1991)	ha
A_{λ}	Mean amplitude of a given wave	-
A_{ground}	Ground area	m^2
$A_1: A_x$	Ratio of leaf area to active xylem area	-
A	Proportion of a probe in contact with xylem	-
AMPFD	Area- weighted mean patch fractal dimension	-
A_x	Area of water conducting tissue	cm^2
A_i	Area of tissue not conducting water	cm^2
BA	Basal area	m^2
b	Proportion of probe not in contact with xylem	-
CC	Correction coefficient	$W\ m^{-2}$
CA	Core area of a forest patch	ha
Cp	Specific heat capacity of dry air at standard pressure (1.006)	$kJ\ kg^{-1}\ K^{-1}$
C_w	Specific heat capacity of water (4.186)	$kJkg^{-1}\ K^{-1}$
C_s	Specific heat capacity of soil	$kJkg^{-1}\ K^{-1}$
C_d	Specific heat capacity of dry soil	$kJkg^{-1}\ K^{-1}$
d	Depth	mm
d_x	Xylem depth	mm
D	Fractal dimension	-
D_{crown}	Crown depth of an individual tree	m
DLFD	Double log fractal dimension	-
d	Displacement height or distance	m/cm
e	Vapour pressure	Pa
E	Flux density of water vapour in air	mm^3
E_{wet}	Evaporation from a wet surface	mm
$E_{transpiration}$	Evaporation from a transpiring surface	mm
E_{aero}	Evaporation due to aerodynamic surface coupling	mm
E_{rad}	Evaporation due to radiative loading upon a surface	mm
E_{eq}	Equilibrium evaporation of a wet surface	mm
E_{imp}	Evaporation imposed by surrounding and advected air	mm
E_t	Evapotranspiration	$mm\ dy^{-1}$
es	Saturated vapour pressure	Pa
es_{wb}	Saturated vapour pressure at wet bulb temperature	Pa
f	denotes a mathematical function	-
G	Flux density of heat due to conduction	$W\ m^{-2}$
g_c	Canopy conductance	sm^{-1}
$g_c critical$	Critical canopy conductance at which advection is most likely to occur	sm^{-1}
h	Relative humidity	$Pa\ Pa^{-1}$
H	Flux density of heat due to convection in air	$W\ m^{-2}$
H_{ad}	Flux density of heat due to advection in air	$W\ m^{-2}$
I	Energy imbalance at the land surface	Wm^{-2}
j	denotes scale	-
K	Von Kármán's Constant (0.41)	-
k	A constant in the Granier equation (equation 2.23, Chapter 2)	-
L	Latent heat of vaporisation of water (2.5×10^6)	$J\ kg^{-1}$
LAI	Leaf Area Index	m^2m^{-2}

Roman Alphabet

$L_{incident}$	Incoming longwave radiation flux density	$W\ m^{-2}$
$L_{emitted}$	Emitted longwave radiation flux density	$W\ m^{-2}$
L_{net}	Net longwave radiation flux density	$W\ m^{-2}$
L_f	Micro-front period	hz
MPFD	Mean patch fractal dimension	-
Mr	Mixing ratio	-
Mrs	Saturation mixing ratio	-
P	Atmospheric pressure at sea level (1013250l)	Pa
P	Precipitation	mm
P	Perimeter of a forest patch	m
PE	Potential evapotranspiration	mm
PSI	Patton shape index	-
Pr	Rainfall flux density	$kg\ m^{-2}\ s^{-1}$
q	Specific humidity	$kg\ kg^{-1}$
q_{sat}	Saturated specific humidity	$kg\ kg^{-1}$
Q_s	Sap flux density	$kg\ m^{-2}\ s^{-1}$
R	Gas constant (8.31)	$J\ mol^{-1}\ K^{-1}$
Rw	Gas constant for water	$J\ mol^{-1}\ K^{-1}$
Rn	Net radiation flux density	$W\ m^{-2}$
r_a	Aerodynamic resistance	$s\ m^{-1}$
r_c	Canopy resistance	$s\ m^{-1}$
r_h	Resistance to heat transports	m^{-1}
r_{st}	Stomatal resistance	$s\ m^{-1}$
R	A line space (Hilbert Space)	-
R	Sap flow ratio	-
S	Storage term	-
$S_{incident}$	Incoming short wave radiation flux density	$W\ m^{-2}$
$S_{reflected}$	Reflected short wave radiation flux density	$W\ m^{-2}$
S_{net}	Net short wave radiation flux density	$W\ m^{-2}$
SF	Wet canopy stemflow	mm
SR	Stem radius	cm
$S^n_{(r)}$	Ramp parameters for surface renewal analysis (Equation 2.12)	-
T	Temperature	°C,K
TA	Total area of a forest patch	ha
TF	Wet canopy throughfall	mm
T*	Surface/skin temperature	°C,K
θT_{max}	Maximum temperature difference between a heated/unheated sensor	°C,K
θT	Temperature difference between a heated/unheated sensor	°C,K
u	Horizontal wind speed	$m\ s^{-1}$
v	Velocity of sap flow	$cm\ dy^{-1}$
V	Volume	m^3
VPD	Vapour Pressure Deficit	kPa
w	Vertical wind speed	$m\ s^{-1}$
w_i	Weighting factor	-
D_x	Xylem depth	cm
z	Measurement height	m
z0	Momentum roughness length	m

Roman Alphabet

z_{soil} Depth of surface soil layer ....m
Z   A series of integers ....-

Greek Alphabet

α   Surface albedo .... -
α   Priestley-Taylor coefficient (1.26) ....-
αu   Constant to account for the uneven amount of a scalar ....-
γ   Psychrometric constant..Pa K^{-1}
Δ   Change in saturation vapour pressure with temperature ....Pa K^{-1}
ε   Ratio of water vapour and air (0.622) .... -
ε   Surface emissivity (0.98)..-
Θv   Volumetric soil moisture ....m^3 m^{-3}
Θm   Mass of (gravimetric)soil moisture......................................kg m^{-3}
θsoil   Soil moisture as fraction of saturation .... -
λ   Volumetric latent heat of vaporization (225.8)......................... KJ m^{-3}
λE   Latent heat flux.. W m^{-2}
π   Pi constant (3.141) ....-
ρair   Density of air at standard pressure ....kg m^{-3}
ρb   Bulk density of soil..kg m^{-3}
ρbw   Density of water ....kg m^{-3}
σ   Stefan-Boltzmann constant(5.67E-8) ....W m^{-1} K^{-4}
σ   Density .... kg kg^{-1}
τ   Momentum flux density .... kg m^{-2}s^{-1}
Τ   Mean frequency of a given wave ....Hz
Ψ   Wavelet family..-
Ω   Decoupling coefficient (McNaughton & Jarvis (1983)) ....-

Lesser-known Subscipts

n cm   Denotes a depth of n centimetres where in is a numerical value ....-
air   Denotes reference to air ....-
water   Denotes reference to water ....-
h   Denotes reference to heat ....-
m   Denotes reference to momentum ....-
q   Denotes reference to water vapour..-
ad   Denotes reference to the process of advection...-
x   Denotes reference to xylem ....-
i   Denotes an area of inactive xylem ....-
stand   Denotes reference to a stand of trees ....-
ground   Denotes ground area..-
gauges   Denotes gauges collecting water ....-
chamber   Denotes reference to a closed flux chamber ....-
stem   Denotes reference to the stem, trunk, or excised limb of a tree...................-
tr   Denotes reference to an individual tree ....-
basal   Denotes basal area of an individual or group of trees ....-
plot   Denotes a plot ....-
trans   Denotes transpiration... -

Lesser-known Subscipts

T	Denotes temperature	-
t	Denotes total (e.g. E_{standt} = Total stand evaporation)	-
u	Denotes reference to forest understorey vegetation	-
wet	Denotes a wet canopy	-
eq	Denotes equilibrium	-
m	Denotes moving sap flow sensor	-
s	Denotes stationary sap flow sensor	-
imp	Denotes evaporation imposed by surface conditions	-

CHAPTER I: THE POTENTIAL SIGNIFICANCE OF TROPICAL FOREST DISCONTINUITIES AND THEIR INFLUENCE ON REGIONAL HYDROMETEOROLOGY

Chapter I: The Potential Significance of Tropical Forest Discontinuities and Their Influence on Regional Hydrometeorology

43

The atmosphere and land surface are fundamentally coupled at almost all spatial scales. This interaction is dominated by a bidirectional and rapid turbulent exchange of trace gases, water and heat between the atmosphere and the land surface (Malhi *et al*., 1998). As the atmosphere passes over the land it can carry moisture, heat and other climatically important quantities from one land cover type and transfer them to different land cover types nearby. This effectively allows different land surface components to interact and to influence one another through the horizontal transfer of energy. Horizontal energy transfer (advection) acts in concert with vertical energy transfer between land surface components and the atmosphere above. Like vertical energy transfer, advection is bidirectional. Advection from one land surface component to another is solely diabatic (i.e. there is a transfer of heat), whereas vertical energetic inputs to the land surface (i.e. radiation) are mainly adiabatic (i.e. there is no heat transfer, only radiative energy transfer). Where land surfaces are heterogeneous in terms of physical properties, such as bare ground/forest and marsh/forest transitions, great horizontal energy transfer between these disparate surfaces can occur (Giambelluca *et al*., 2003; Klaassen *et al*., 2002). At small spatial scales, advective interaction between different land cover types can induce changes in fluxes of moisture, heat, and other meteorological quantities from the land surface at the edges of land cover transitions. This can lead to the edges of land cover patches having fluxes of these quantities that are divergent from those found many metres into the patch –i.e. the patch 'interior'. Such interactions are termed heterogeneous interactions, and the consequent effect termed an edge effect. At larger scales, heterogeneous interactions between different patches of much larger sizes are of sufficient magnitude to form mesoscale flows, whereby a circulation is formed between patches that can significantly alter the convective boundary layer (Fisch *et al*., 2004; Roy *et al*., 2003). Lateral energy transfer (advection) across large and small scales occurs in the tropical humid biome where dry bare ground is left after the clearance of tropical forest. The dry ground rapidly warms, and the warm dry air from the bare ground can pass over the nearby forest. For small clearings this leads to increased water use (i.e. increased latent heat flux) at the edges of the forest (e.g. Giambelluca *et al*., 2003), whereas larger clearings form mesoscale flows known as 'forest breezes', which are similar to offshore winds in their nature (Fisch *et al*., 2004). Like vertical and horizontal energy transfer, the interaction between larger

Chapter I: The Potential Significance of Tropical Forest Discontinuities and Their Influence on Regional Hydrometeorology

scale heterogeneous interactions (and those smaller-scale heterogeneous interactions nested within them) is bidirectional.

There has been noticeable advancement in our knowledge of large-scale heterogeneous feedbacks within heterogeneous forested landscapes (Shuttleworth, 1988; Weaver & Avissar, 2001; Weaver *et al.*, 2002; Werth & Avissar, 2002). However, there remains great uncertainty as to whether smaller-scale heterogeneous components can be represented by simple area-averages when attempting to scale their point-scale measurements of energy fluxes up to the region level (Giambelluca *et al.*, 2003). Recent studies (e.g. Herbst *et al.*, 2007b) suggest that this is not the case owing to edge effects at transition boundaries such as forest edges. As edge effects induce flux properties at forest edges divergent from those of their respective interiors, it is likely that in the highly fragmented tropical regions (such as those where a high amount of deforestation is present) the shape, and not just the size, of forest patches could also significantly contribute to regional.

After briefly describing some earlier pioneering work, I focus this review on recent advances in understanding the interaction of heterogeneous land components in forested ecosystems through the discussion of notable case studies, and how they relate to tropical forests. Given the critical role of the moisture status of the land's surface in land surface-atmosphere interactions (LSAIs), I focus the review upon hydrometeorology. I examine how efforts to elucidate those dominant processes of heterogeneous interaction are limited by the scale, extent and direction of observations. A series of suggestions are presented for future research stating those processes, questions, scales and measurements which need addressing further.

Land surface-atmosphere interactions (LSAIs) of different regions form the cornerstone of plant biogeography (Bailey, 1976; Holdridge, 1947; Koppen, 1936; Walter *et al.,* 1975), and the bidirectional relationship between climate and plant function is a central theme in plant ecophysiology (Lambers *et al.,* 1998; Mooney *et al.,* 1987; Woodward, 1987; Woodward & McKee, 1991) and climate change science (Cutrim *et al.*, 1995; Pielke,2001; Pielke *et al.*, 1998; Pitman *et al.*, 2003, 2004; Rabin *et al.*, 1990; Souza *et al.*, 2000; Xue & Shuklda, 1996a, 1996b; Zeng & Neelin,2000). Traditionally, both disciplines have viewed vegetation as being in equilibrium with its overlying atmosphere. In reality, this is rarely the case (Irvine *et al.*, 1997; Kabat *et al.*, 2003; Klaassen, 1992; Klassen & Claussen, 1995; Klassen & Sogachev, 2006; Klaassen *et al.*, 2002; Woodward & Lomas, 2001) as land cover is undergoing intensive anthropogenic modification (e.g. deforestation, agriculture, silviculture, irrigation), and the overlying atmosphere is changing constantly as it is influenced by each surface over which it passes (Klaassen *et al.*, 2002). The gaseous nature of the atmosphere means that it is not only influenced by those surfaces over which it travels, but also that it can carry and transfer moisture, heat, trace gases, and other climatically important quantities from one area of land to another. In short, quantities such as heat and moisture that are created by one land type can be carried horizontally by the atmosphere over other land cover types and influence them. This horizontal transfer is termed advection. Advection is particularly pronounced where anthropogenic disturbance (e.g. deforestation in the tropics) creates an area that has a stark physical contrast to its surroundings (e.g. a relatively dry and hot clearing, and a moist and relatively cool forest). Two such contrasting areas are said to be heterogeneous land surface components/cover types, and the interaction between the two a heterogeneous interaction, mediated by advection. The atmosphere passing over a clearing in the tropics would be much hotter and drier than that typically found over forest, and therefore if this air passed over a forest edge the trees there would be surrounded by much hotter and drier air. The higher vapour pressure deficit of the air from the clearing passing over the trees at the forest edge would lead to increased water use by those trees, should they have easy access to water. As the dry and hot air receives more water from the trees below, it would gradually converge to the same state of the atmosphere over the forest with distance (i.e. fetch) from the clearing/forest transition (also known as an 'edge'). The smoother surface of the clearing would also allow wind speeds to increase over it,

meaning that turbulence would be created when this wind passes over the aerodynamically rough trees of a forest edge, increasing the efficiency of advective energy transfer. Measurements of moisture and temperature scalars in the atmosphere made further and further into the forest downwind of this transition would reflect air from the clearing inducing a change at the forest edge by a departure from values typical of the clearing. Within increasing distance into the forest patch (fetch), temperature and moisture scalars would gradually return to values typical of the forest, reflecting the adjustment of air from the clearing to its new underlying (forest) surface. It stands to reason that larger clearings would lead to greater energy transfers of a given quantity.

When discussing the lateral energy transfer between non-forest (Amazonian pasture) and forest (tropical humid Amazonian forest), Shuttleworth (1988) categorizes heterogeneity into 'organised' (type 'A', >10km) and 'disorganised' heterogeneity (type 'B'<10km), depending on the spatial scale over which land components are deemed to coherently interact with one another by means of their heterogeneity, the separation between the two being about 2-10km (Laurance, 2004; Roy & Avissar, 2000; Roy *et al.*, 2003; Woodward & Lomas, 2001). The important defining notion behind organised heterogeneity is that this is the scale at which heterogeneous land surface components begin to interact significantly with one another through the atmosphere. This defined by Shuttleworth (1988) as when the convective boundary layer is altered by circulations forming between the atmospheres over heterogeneous land cover types. This means that the land surface components in question are no longer considered two disparate, 'disorganised' units, but instead must be considered as a heterogeneous 'organised' unit defined by their coherent atmospheric interaction. This is best demonstrated by the coherent mesoscale flows that are created between large areas of adjoining forest and pasture in the tropics ('forest breezes'). Whereas large-scale examples are made more obvious by the magnitude and coherence of their interaction, the situation for small-scale heterogeneity is somewhat unclear due to what Shuttleworth (1988) terms its 'disorganised' nature. It was postulated by Shuttleworth (1988) that calculations of regional energetic fluxes could take the form of simple area-weighted averages for 'type B' (small-scale) heterogeneous landscape components, as they had no significant interaction with one another.

However, with apparent contradiction, the literature is replete with the ecological impacts of small-scale heterogeneous interactions leading to forest edges having

different properties to their interiors. These heterogeneous interactions are typified by cleared areas created where continuous (*homogeneous*) forest once was, forming a heterogeneous area of discontinuous forest perforated or surrounded by such clearings. Clearings can be actively maintained (by burning, cropping, grazing etc.) crops/pasture or left dormant (termed 'swidden'). Swidden tends to recover to a forest state with time, whereas maintained crops/pasture does not alter. Swidden and actively maintained crops/pasture can be very similar in their physical properties to each other and forest, depending on how much forest is cleared initially, the species that grow in the clearing, and the extent to which it is allowed to recover back to the forest state. Where physical differences between pasture/crops/swidden and forest are great, a difference between properties of forest edges and their respective interiors is reported. This is due to lateral transfer of biota (e.g. seed dispersal) and energy between the forest and clearing. As biota and energy pass between the forest and clearing, their influence perforates different distances across the edge, and usually converges to a level typical of the respective cover type's interior. A plethora of studies reporting this 'edge effect' have lead to numerous ecological reviews describing differences at forest edges when compared to their respective interiors, arising from this 'edge effect' (Harper *et al.* 2005; Murcia, 1995; Saunders *et al.*, 1991). It is now also apparent that there are significant within- and below-canopy microclimatic gradients at forest edges. In particular, gradients of soil moisture, wind speed, solar radiation, and humidity suggest trends in hydrometeorology. These aforementioned studies cannot, and often do not, aim to clarify whether, or quantify by how much, forest canopies at forest edges possess energy flux properties divergent from those of forest interiors. Results tend to be contradictory and unclear because although previous, ground-based/below-ground techniques are much easier to employ, they are made under the canopy and thus are decoupled from land surface-atmosphere interactions (LSAIs). These techniques moreover lack temporal resolution and do not capture the diurnal variation LSAIs.

There have been a few notable cases where the remote sensing of energy flux proxies, such as forest canopy temperature, which is a proxy for tree water use (i.e. latent heat flux), directly address the coupled (canopy) component of the forested land surface. However, remotely sensed images, and the measurements based upon them, are subject to potentially significant calibration errors. Satellite imagery also inherently involves a trade-off between the resolution of an image and its instantaneous field of view (i.e. the smallest resolvable unit and the area covered by

a satellite image, respectively). As an example, urban heat island effects penetrating into forest edges are captured well by Landsat satellite imagery, as the edge effect extends 1km or so into the forest remnants, and can be easily resolved by the 60m Landsat pixels. However, smaller-scale interactions typical of disorganised heterogeneity, such as increased tree water use at the edges of forests adjacent to smaller clearings, are expected to be one order of magnitude less in extent. Thus the 60m resolution of the Landsat thermal band pixels is too coarse to resolve altered tree water use and similar small-scale interactions. Importantly, remote sensing images and the measurements based upon them are typically limited to a certain 'snapshot' during the day at a certain time of year owing to the nature of the platform, and thus still cannot comprehensively describe seasonal and diurnal patterns in the land's energetic status.

There is much observational and modelling evidence to support the concept of heterogenic meteorological interaction at the meso- (2-100km) and macro- ($>10^6$km) scales (Moorcroft, 2003; Pitman *et al.*, 2003). More recently, Laurance (2004) provided a review of climatic feedbacks in the fragmented tropics at a variety of spatial scales, but this was limited to ecological, biodynamic and disturbance perspectives. Veen *et al.* (1996) review the state of knowledge at forest edges with regard to increased momentum flux of air entering forest edges. However, for small-scale heterogenic interactions, reviews still neglect the hydrometeorology that governs the climate system (Harding *et al.*, 1997; Klaassen, 1992; Pitman *et al.*, 2003). This leaves open the question of whether small-scale ('disorganised') heterogeneity also represents a significant contributor to local climate, though theoretical and observational evidence suggests that this may well be the case (Baldocchi & Rao, 1995). The downward momentum flux of air (i.e. increased turbulence) has been shown to cause significant damage to large trees (Laurance *et al.*, 2000) and also to increase deposition at forest edges (Draaijeers *et al.*, 1994). Whilst it has been shown that increased turbulence at forest edges influences regional carbon balances and deposition in fragmented landscapes (de Jong & Klaassen, 1997; de Ridder *et al.*, 2004; Draaijeers *et al.*, 1994; Laurance *et al.*, 1998b; Weathers *et al.*, 2001), there have recently (post-2000) been notable advances in our understanding of how altered hydrometeorology arising from the downward momentum flux of air at forest edges may also influence regional hydrology (Ciencala *et al.*, 2002; Giambelluca *et al.*, 2003; Herbst *et al.*, 2007b; Taylor *et al.*, 2001).

The size of large scale heterogenic interactions makes them inherently important to regional hydrometeorology, but the abundance of smaller clearings and thus small-scale interactions means they may be just as significant. This holds important implications for the regionalisation of hydrometeorological parameters, i.e. how to find in a simple way a correct regional value on the basis of point observations, which is itself a specific issue within the larger problem of 'scale' (Veen *et al*., 1991). This is particularly crucial in the fragmented tropics whereby not only the absolute amount of deforestation is an important determinant of climate but possibly also the pattern of deforestation, should many non-forest/forest transitions/edges occur (i.e. there be a high degree of fragmentation).

This new direction in land–atmosphere studies is likely to be of particular relevance to ecologists and climatologists alike, owing to the increasing and unabated deforestation throughout the world (Achard *et al.*, 2002a; Kabat *et al.*, 2003). This seems particularly relevant for heavily modified areas; for example, Laurance (2004) states that the average size of land fragments in the anthropogenically modified tropics (in this case Brazil) is below 1 km^2, with others (Gascon *et al*., 2000; Imbernon & Branthomme, 2001; Santos *et al.*, 2008) asserting that these patches are constantly decreasing in size. More recently, is has been shown that forest water use is still highly variable and cannot be explained by leaf type, leaf area index, canopy height and roughness, soil water access and species composition alone (Herbst *et al.,* 2007b). Herbst *et al*. (2007b) suggest that regional water use could indeed be influenced by edge effects, and thus by the shape and size of forest patches in a landscape. Following the logic of Herbst *et al.,* (2007b), it can be seen edge effects may influence the regionalisation of hydrometeorological parameters (Dolman & Blyth, 1997; Giambelluca *et al.*, 2003; Herbst *et al*., 2007a; Klassen, 1992; Klassen & Claussen, 1995; Kruijt *et al.*, 1991; Noilhan *et al.*, 1997; Woodward & Lomas, 2001) and flux measurement corrections in fragmented landscapes (Klaassen & Sogachev, 2006; Lloyd, 1995). LSAIs at forest edges furthermore act to influence long-term vegetation dynamics. It is now widely accepted that edges are not static phenomena but go through a physical recession phase (termed 'expansion', Figure 1.1) that is dependent on local climatic conditions and the maintenance of clearings by burning, grazing, cropping *etc.* (D'Angelo *et al*., 2004; Gascon *et al*., 2000; Harper *et al.*, 2005). This in turn would be expected to reduce the size of fragments and alter further the climatic state of the edge environment (Gascon *et al*., 2000). For example, forest edges are more prone to penetration by wind (Savill, 1983; Somerville, 1980), fire

(Cochrane & Laurance, 2002) and microclimatic influences (Chen *et al*., 1995; Matlack, 1993; Saunders *et al*., 1991). Forest edges consequently exhibit a decline in biomass through the death of large trees (D'Angelo *et al*., 2004; Laurance *et al*., 2000; Mesquita *et al*., 1999; Nascimento & Laurance, 2002, 2004; Nascimento *et al*., 2006). It should be noted, however, that forest edges are also capable of 'sealing' due to increased light interception at edges and consequential secondary growth, such as lianas (Figure 1.1). Sealed edges can act to shelter the forest edge, causing a 'softening' of the forest edge response to the adjacent swidden, expressed as a reduction in the difference between forest edge and interior responses (i.e. the magnitude of edge influence, MEI, Figure 1.1). As time goes on and a forest edge adjusts to its surroundings, the MEI can decrease, but the extent to which an edge influence penetrates into the forest can increase (i.e. and increased extent of edge influence, EEI, Figure 1.1) if the forest has already thinned in acclimatising to its surroundings. Forest edges can also express an increase of biomass, then, not only because of their sealing by lianas, but also because of increased tree growth at the very edge of the forest due to lowered competition for light and moisture there. Indeed, the various ways in which the vegetation of tropical forest edges responds to adjacent clearings in terms of its physical, composition, and structural responses (shown in Figure 1.1) form the basis of tropical forest edges being termed 'hyper-dynamic' (Laurance*, 1997, 2002).
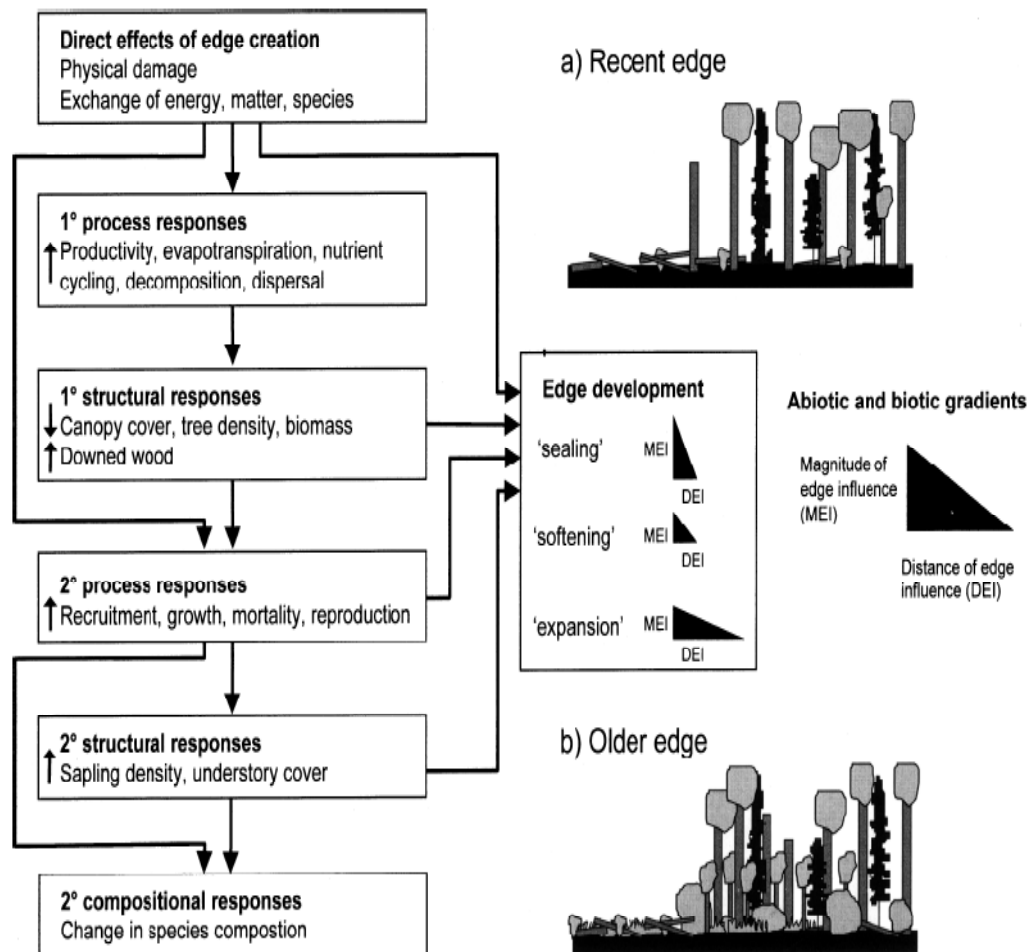
Figure 1.1 *The physical depiction of a forest edge at different ages (reproduced from Harper et al. (2005)). In the tropics, a great physical contrast between a cleared area and the remaining forest can lead to the death of large trees, and an overall decline in biomass that increases the depth of edge influence (DEI). Adaption of this nature, however, reduces the deviation of a given quantity from values found in the edge interior, i.e. the Magnitude of Edge Influence (MEI). Thus, forest edges can increase and decrease in biomass depending on the compositional and structural responses that result from a particular combination of direct effects of edge creation. The effect of edge creation upon compositional and structural responses is dependent on the nature and extent of forest clearing, the composition and structure of the forest at the time of edge creation, and local climate.*

However, despite recent advances, there remain many unanswered questions with regard to forest edges, and our understanding of their influence on climate is rudimentary in comparison to other concepts. This is due to the difficulty of measuring fluxes at forest edges, and it is therefore important that a review of field experiments is presented to overview the state of affairs and draw attention to gaps in our knowledge.

1.2 The Potential Climatic significance of Tropical Forest Fragmentation

Pioneering work such as that of the Anglo-Brazilian Amazonian Climate Observation (ABRACOS, *cf.* Gash & Nobre, 1997; Gash *et al.*, 1997) and the Large-Scale Biosphere Atmosphere in Amazonia (LBA, *cf.* Avissar & Nobre, 2002) studies revealed the stark energetic contrasts between deforested and forested land covers, and have formed the basis of subsequent studies which have looked at their interaction. Deforestation imposes different conditions upon forest remnants pre-adapted to stable conditions typical of *homogeneous* cover (da Silva & Avissar, 2006; Harper *et al.*, 2005; Murcia, 1995; Saunders *et al.*, 1991). Typical parameters for forest and non-forest cover are presented in Table 1.1. Table 1.1 demonstrates that, as a consequence of their different physical properties, deforested areas exhibit a differing interaction with the atmosphere in the form of greatly altered heat fluxes, particularly in the tropics where there is a high radiation load on the land surface.

 As explained earlier, heterogeneous land components (e.g. pasture/forest) can readily interact with one another via the transport of energetic quantities (namely heat and moisture) by the overlying atmosphere, which is ideally suited to the efficient transfer of large amounts of energy over large scales relatively quickly. What proportions of heat and moisture are transferred between non-forest and forest in the tropics depends on the moisture status of the land surface.

The moisture status of the land surface alters its energetic responses, and thus the proportions of moisture and heat transported from it to the atmosphere. This in turn determines the magnitude and direction of lateral transfer between forest and non-forest patches. If the surface is moisture-replete, the higher roughness and lower stomatal conductance of the forest compared with that of cleared areas leads to a higher sensible heat flux in the former than the latter. This occurs since the rough forest captures incoming radiation more effectively, provides a higher resistance to water transport, and because turbulence arising from the rough surface transfers sensible heat to the atmosphere with greater efficiency. Fisch (1986), and later Lynn *et al.* (1995), Dias & Reginer (1997), Sa *et al.* (1997), and Fisch *et al.* (2004), concluded that the contrast in land surface-atmosphere interactions between forest and non-forest is of such magnitude that mesoscale circulations, termed 'forest breezes', can be formed of sufficient strength to influence the planetary boundary layer.

Under drier conditions, however, the deep rooted nature of the forest (Kleidon & Heimann, 2000; Oliviera *et al*., 2005) means that forest trees are less water-stressed (Hodnett *et al*., 1995, 1997a, 1997b) than pasture/swidden species (typically grasses). These have much shallower roots, and cannot access water once water in the top soil layer is exhausted, which is a common problem due to compaction of soil that occurs in clearing forest and subsequent high rainfall run-off. The higher stomatal resistance of forest trees is significantly less than in the hydraulic pathway of the drought-stressed swidden species. Thus, under dry conditions, the situation of moisture-replete landscapes is reversed, and clearings have much higher surface temperatures, and greater sensible heat fluxes than forests (Giambelluca *et al.*, 2000; Giambelluca *et al.*, 1999, Jipp *et al.*, 1998; Lyra *et al*., 2003; Wright *et al.*, 1992). There is, however, much variation in the numerous physical properties (Table 1.1, Figure 1.1) and energetic responses (Table 1.1) of non-forest and forest land cover types. Table 1.1 indicates how a great variation in the quantity, type, and direction of lateral energy transfer between non-forest and forest land cover types will be expressed throughout the tropics. Table 1.1 also demonstrates the need for a direct, site-specific calibration and comparison between the physical properties and energetic/hydrometeorological responses of a forest, non-forest, and edge (assuming a Distance of Edge Influence (DEI, Figure 1.1)) patch. The rarity of these directly comparative measurements is apparent; with only Giambelluca *et al*. (2003) making measurements of physical properties and energetic responses in a swidden, forest, and edge patch (Table 1.1).

Parameter	Non-Forest Value	Forest Value
Physical Properties		
Vegetation height (m) [cefgj]	0.53	33
Canopy cover (%) [m]	0.85	100
Rooting depth (m) [klm]	1.5-2.0	4.0-18
Leaf area index [ce]	1.0-2.7	5.2
Albedo [bd]	0.18, 0.165[i]	0.13 , 0.13[viii]
Zero plane displacement (m)[hjm]	0.66h	0.86h
Roughness length (m) [m]	0.10	2.35
% Intercepted Rainfall		73-77[xxi], 79 [xxiii], 83[xxii], 0.05, 0.5[iii] 18[xxv] 39[xxvii] 21[xxiii] 9[xxv] 17 [xxi] 7, 14 [xxii]
Bulk Density (kg^{1}kg^{-1})	1.49 [xix]	1.03 [xix]
Soil Moisture		
Energetic Responses:		
Sensible heat flux (wet) (Wm^{-2})	[29[xiv], 46[j], 46*] 46[xvi]	[42[vii], 0[xxi],-] 16.4[xi] 35[xvi]
Latent heat flux (wet) (Wm^{-2})	[88[xiv], 108[j], 132*] 83[xvi]	[94[vii], 96[xxi], 118] 78[xi] 104 [xvi]
Sensible heat flux (dry) (Wm^{-2})	[89*, 60*, 55[j], 64*, 67[xiv], 31*] 38[xvi]	[20[vii],-, 23[v], -, -] 21[xi], 46[xvi]
Latent heat flux (dry) (Wm^{-2})	[11*, 45*, 60[j], 85*, 91[xiv], 143*] 64[xvi]	[18[vii],64[vi], 94[v], 105[vi], 129[vi]] 109[xi] 123[xvi]
Surface temperature (dry) (˚C)	35[ii] 37(32-42) [xix]	32[ii]
Surface temperature (wet) (˚C)	17[xv]	16.1[xv]
Relative humidity (wet) (%)	84[ii]98.2[xv]	95[ii]98.6[xv]
Relative humidity (dry) (%)	80[ii]	93[ii]
Air temperature (wet) (˚C)	30[ii]	29.5[ii]28.9[xi]
Air temperature (dry) (˚C)	23[xx]	28.5[xx] 27.4[xi]
Sap flux density (av, wet) (cm^{1}dy^{-1})	-	2.0-15.1[ii]
Sap flux density (av, dry) (cm^{1}dy^{-1})	-	84-288 (0-1320) [xxv],
	-	3.4-25.2[ii]
Sap flux density (maximum) (cm^{1}dy^{-1})	-	60-300[xxiv]
Wind speed (dry) (ms^{-1})	-	2.9[64(xi)]
Wind speed (wet) (ms^{-1})	4.22[xii]	2.5[64(xi)] 2.4[xii]
Boundary layer height (dry) (m)	1650[xix], 2200[xviii]	1100[xix], 1200[xviii]
Boundary layer height (wet) (m)	1000[xix]	1000[xix]
Bowen Ratio (wet)	0.70[j], 0.74*, 0.75[xiv], 0.56[xvi]	1.0[h], 0.69[vii], 0.74[xvi]
Bowen Ratio (dry)	0.11*, 0.35*, 0.52[j], 0.57*, 0.75*, 0.82*, 0.64[xvi]	0.13[h], 0.8[vii], 0.77[xvi]

Table 1.1: Typical biophysical parameters of forest and non-forest covers (continued on following page).

As collated by Wright et al. (1996b), in Gash & Nobre_, 1997 :_ Culf et al. (1996)[a]_, Lloyd et al.(1988)_ [b]_, McWilliam et al.(1993)_ [c]_, McWilliam et al. (1996)_ [d]_, Roberts et al.(1996)_ [e]_, Sa et al. (1996)_ [f]_, Shuttleworth et al., (1984)_ [g]_, Shuttleworth (1989)_ [h]_, Ubarana (1996)_ [i]_, Wright et al. (1992)_ [j]_, Wright et al. (1995)_ [k]_, Wright et al. (1996a)_ [l]_, Wright et al. (1996b)_ [m] _[All TRF in Amazonia, see further (_Gash & Nobre_, 1997)]_

As collated by author (Modified and extended from Giambelluca et al., 2000)*:

i) Giambelluca et al.(2000),(ii) Giambelluca et al. (2003), (iii) Schellekens et al.(1999), (iv)Bruijnzeel (1990): TLF, (v) Shuttleworth (1988): Central Amazonian TRF, (vi) Roberts et al. (1993): Central Amazonian TRF, (vii) Pinker et al. (1980): Central Thailand TRF, (viii) Kumagai et al. (2004b): MDRF, Sarawak, Borneo, (ix) Kume et al. (2006): MDRF, Sarawak, Borneo, (x) Kumagai et al. (2005): MDRF, Sarawak, Borneo, (xi) da Rocha et al. (2004): Eastern Amazonian TRF. (xii) Nieuwenhuis (2005): Montverde TCF; (xiii) Wright et al. (1992): Amazonian PA, (xiv) Holsher et al. (1997): 2 y.o. SW, (xv) Nieuwenhuis (2005): Montverde SW, (xvi) von Randow et al. (2004): TRF, SW Amazonia, (xvii) Richards & Flint (1994): Various sites across South East Asia, (xviii) Lyra et al. (2003): TRF, SW Amazonia, (xix) Pinard & Putz (1996): MDRF, Sabah, Borneo, (xx) Brooks & Spencer (1997): TLF, Sabah, Borneo, (xxi) Sinun et al. (1992)TLF, Sabah, Borneo, (xxii)Bidin & Chappel (2003): TLF, Sabah, Borneo, (xxiii) Calder et al. (1986): TLF, West Java, (xxiv) Lloyd et al. (1988): TRF, Amazonia, (xxv) Lloyd et al. (1988): TRF, Central Amazonia.

Key:

* = Direct measurement, Giambelluca et al., 2000.

[] = Grouped values of different studies for ease of comparison (coloured, from Giambelluca et al., 2000, including direct measurements from Giambelluca et al., 2000).

[nn]_= Comparative measurements of individual studies grouped for ease of comparison._

[nn] _= Individual measurements of different individual studies._

- = no recorded value for sensible heat as Bowen ratio = 1 (i.e. 100% of available energy used for water transport, expressed in the corresponding latent heat flux)

y.o. = year old.

TRF = Tropical Rainforest.

TCF = Tropical Cloud Forest

TLF = Tropical Lowland Forest

MDRF= Mixed Dipterocarp Rainforest (Tropical Lowland Forest)

Av. = mean over a given period.

Table 1.1 (continued): Typical biophysical parameters of forest and non-forest covers.

Theoretical investigations on the influence of advection on the adjustment of water fluxes between adjacent surfaces are numerous (Claussen, 1987, 1991a, 1991b; Klaassen, 1992; Kroon, 1989; Kroon & Bink, 1996; Kroon & de Bruin, 1993, 1995; McNaughton, 1976a; 1976b; Naot & Mahrer, 1991; Philip, 1959, 1987; Rao *et al.*, 1974). A notable investigation into small-scale heterogeneity was that of Harding *et al.* (1997), using the UK Meteorological Office Boundary Layer Above Stationary Inhomogeneous and Uneven Surfaces (BLASIUS) model (Mason, 1988). The model was initially used to investigate hill-flows (changes in air turbulence/flow with orography), and was modified to incorporate a simple available energy term and surface resistance in its lower boundary. Harding *et al*. (1997) based modelling work on measurements made by the HAPEX-MOBIHLY experiment (Lloyd, 1995) and focused on the striped vegetation of the African Sahel, called 'Tiger Bush'. Tiger Bush comprises of different trees and shrubs that grow together in vegetation strips tens of metres wide and many metres in length. Rainfall in the region is limited and therefore prevents vegetation from covering the entire landscape. Instead, the trees and shrubs that form Tiger Bush establish by tapping into ground water at great depths, accessing it in a way very similar to that of tropical rainforest trees in dry seasons. The creation of root macropores (large diameter pores > 50nm) allows better access to water, and consequent leaf litter falling from the Tiger Bush prevents water from evaporating so easily. Thus the Tiger Bush is limited in its size by rainfall, but in strips it can thrive. The areas between Tiger Bush strips are bare ground, and the lack of plant life inhibits water transport from the land surface to the atmosphere. Tiger Bush thus presented a combination of cool, wet, readily-transpiring vegetation that was adjacent to dry and thus hot bare ground. As the region (Nigeria) receives a very high solar load and very little rainfall, a great amount of energy was available to generate strong sensible heat fluxes over the bare ground and strong latent heat fluxes over the transpiring Tiger Bush. The contrast in the strong opposing fluxes of sensible and latent heat lead to exceptionally efficient lateral transfer (advection) between the two land covers and made this a highly idealised system in which to study land heterogeneity-climate interactions. Harding *et al.* (1997) demonstrate that a 'leading edge' effect is expressed upon the transition from a hotter dry patch to a cooler moist patch. The hotter, drier air from the upwind patch combines with the turbulence generated by the vegetation edge to increase the transport efficiency of water vapour and induce a greater latent heat flux at the edge of the wetter cooler patch (see also Oke, 1983).

Blyth (1995) found that a dual-source model which allowed for the horizontal movement of energy best represented experimental measurements of fluxes made over this region (*cf*. Blyth *et al.*, 1993, 1995, 1999). Harding *et al.* (1997) importantly show that there is an increased latent heat flux at the upwind edge of the patch, but not an opposite response at the reverse transition. Consequently, the response of the land surface is non-linear *at this scale*, and is strongly dependent on the length scale of heterogeneity. That is, for a given amount of deforestation, those land surfaces with more wet-dry transitions will be cooler and wetter than those with fewer (Harding *et al.*, 1997; Li & Yu, 2007; Li *et al.*, 2007; Veen *et al.*, 1991). Giambelluca *et al.* (2003) propounded that all other things being equal a response of this nature could be expected to off-set the drying of the earth's atmosphere resulting from deforestation in tropical areas. However, *natural* forest edges are far from 'equal' to forest interiors, and can express differences in species composition, tree size, wood density, leaf area index and aerodynamic roughness; they are also more similar to secondary forest in physiognomy (Santos *et al.*, 2008). These aforementioned differences can all influence the hydrometeorology of tropical forest edges. Furthermore, forest clearings will not necessarily be bare ground, and thus may not offer such a stark contrast in their physical properties and energetic responses to adjacent forest interiors as reported for Sahelian Tiger Bush. The aforementioned differences between the physical properties of natural tropical forest edges and forest interiors, and the likelihood that forest clearings in the tropics will not contrast as greatly to remnant forest as bare ground does readily-transpiring vegetation (e.g. Tiger Bush), necessitate field-based investigations of the exact physical properties and energetic/hydrometeorological responses of tropical forests, their edges, and adjacent forest clearings, and how they contrast between these cover types. Field based investigations comparing and calibrating physical properties (namely albedo and vegetation cover fraction) and energetic responses (namely moisture and heat fluxes) between forest clearings, forest edges and their respective interiors will provide parameters of natural tropical forest edges and forest clearings that are likely to differ greatly from idealised systems such as Tiger Bush.

Field observations into atmospheric fluxes at forest edges are mainly restricted to fluxes of air momentum – i.e. turbulence (Gardiner *et al.*, 1995; Gash, 1986a, 1986b; Irvine *et al.*, 1997; Kruijt *et al.*, 1991; van Breugel *et al.*, 1999a, 1999b; Wilson & Flesch, 1999). Such investigations focus on the increased turbulence produced where wind that has gathered speed moving over an aerodynamically smooth clearing

rapidly slows as it travels over a forest edge containing aerodynamically much rougher trees present there. This leads to a downward momentum flux and increased turbulence, increasing the transport of quantities such as heat and moisture up into the atmosphere. This has lead to the assumption that they are special 'high flux' environments owing to the increased mixing of air over forest edges (Veen *et al.*, 1996). This implies that atmospheric effects upon fluxes of water and heat at forest edges are expected to extend over much greater extents over the canopy (100-200m) than those typically measured below the forest canopy (10-50m) (Klassen & Sogachev, 2006). Rider *et al.* (1963), Dyer (1963), and Dyer & Crawford (1965) were among the first to measure advection directly, but they only examined the horizontal adjustment of temperature and humidity scalar profiles.

Lang *et al.* (1974), Brakke *et al.* (1978) and Naot & Mahrer (1991) quantified the adjustment of latent heat transfer (LE) with distance from the leading (downwind) edge of short crops adjacent to bare ground, but their studies suffered from reliance on the inferential flux-gradient method. The flux-gradient method is limited in that it assumes that scalars of moisture are transported along the concentration gradient of scalars as measured at different heights over the forest edge. Only by measuring the vector (i.e. concurrent measurements of wind direction in all planes and changes in moisture concentrations) can a true flux be calculated. Support for increased latent heat flux at vegetation edges occurring through advection is seen particularly in agricultural meteorology and, as mentioned previously, other systems that offer great contrast in physical properties and energetic responses such as Tiger Bush (Baldocchi & Rao, 1995; Blyth & Harding, 1995; Boegh *et al.*, 1999; Brunet *et al.*, 1994; DeBruin *et al.*, 2005; Gay & Berhoffer, 1991; Li & Yu, 2007; Mcaneney *et al.*, 1994; Prueger *et al.*, 1997; Rosenberg, 1969; Smith *et al.*, 1997, Todd *et al.*, 2000). As with the Tiger Bush, advection in these studies is very likely a result of transitions of bare ground and water-replete (usually irrigated) vegetation in arid environments.

When a surface is in equilibrium with its overlying atmosphere, the energy balance of the surface is described as 'closed'. Thus, in terms of latent heat (λE, Oke, 1983):

$$\lambda E = (Rn - G) - H \qquad\qquad [W\ m^{-2}] \qquad\qquad (Equation\ 1.1).$$

Where (λ) is the volumetric latent heat of vaporization, (Rn) net radiation, (G) ground heat flux, and (H) the sensible heat flux (Following Oke, 1983 - *cf*. Li & Yu, 2007). In an 'open' or advective state, the system expresses an imbalance. This is because extra energy transferred laterally from one patch to another is present in addition to

energy received vertically by the land surface. Comparisons between fetch (down-wind distance from the forest edge) -independent (radiative, adiabatic, vertical) and fetch-dependent (psychrometric, diabatic, lateral/vertical) energetic quantities are typically used to estimate an energy 'imbalance' (I) to calculate fluxes of latent heat that cannot be solely accounted for by the available energy at the land surface directly below (Kochendorfer *et al.*, 2007):

$$I = (Rn - G) - (H + \lambda E) \qquad [W\ m^{-2}] \qquad (Equation\ 1.2),$$

or:

$$\lambda E = (Rn - G) - (H + H_{Ad}) \qquad [W\ m^{-2}] \qquad (Equation\ 1.3).$$

Early work compared lysimeter (i.e. fetch-dependent) and net radiation measurements (fetch-independent) to estimate (I) (e.g. Rosenberg, 1969). However, forests differ significantly from the idealised systems found in agricultural meteorology (e.g. Kochendorfer *et al.*, 2007), and indeed those like the Tiger Bush of Nigeria, where the contrast between the moisture status of irrigated crops/readily transpiring vegetation and bare ground is highly conducive to advection. Moreover, the application of techniques commonly used in agricultural meteorology, such as lysimeters (containers holding an entire vegetation 'unit' such as a plant or tree to measure its water use), is not practicable for single trees, let alone forest stands. It is for this reason that flux measurements at forest edges have been sparse until recently. More recent work exploits the use of eddy correlation systems to make direct atmospheric measurements in place of lysimeters. At a mixed temperate forest in the Netherlands, Hujtes *et al.* (1996) and later Klaassen *et al.* (2002) used eddy correlation to show an increased net heat flux at a 'wet' (marsh land) to 'dry' (forest) transition of about 16% greater than the net radiation at the land surface directly below. This corresponds to I = 40- 56 Wm^{-2}. As heat flux from the surface exceeds net radiation received by the surface in the vertical (i.e. the fetch-independent part of the energy balance, see Equation 1.5), it was taken that the extra 40-56 Wm^{-2} was due to advection (i.e. the lateral transfer of energy, *cf*. Li & Lu, 2007).

The above studies illustrate the potential for significant feedbacks between LSAIs at forest edges, and infer their climatic significance when aggregated at the regional scale. However, their findings have remained controversial owing to the comparatively 'idealised' situations in which measurements are made. These exclude a number of potentially important feedback mechanisms that may act to either maintain or, alternatively, to counteract the meteorological state of naturally forested regions. The known connections between the composition, structure and physiology of vegetation and the climate of different regions (Bailey, 1976; Holdridge, 1947; Koppen, 1936; Lambers *et al.,* 1998; Mooney *et al.,* 1987; Walter *et al.,* 1975; Woodward, 1987; Woodward & McKee, 1991) suggest that ecosystems will respond to novel structural regimes through a variety of biological, physiological, compositional and physical mechanisms *specific to that land cover type,* acting on different time-scales, with consequences for their climatic feedback (e.g. Cox *et al.,* 2000). Tropical forest edges could possibly represent the most complex combination of such mechanisms, exhibiting a much greater aerodynamic roughness than forested area alone (de Jong *et al*., 1999), greater porosity (Kapos *et al*., 1993), species-diversity (Whitmore, 1984) and greater structural diversity (Murcia, 1995; Harper *et al*., 2005). An overview of how forest edge effects can be expected to integrate within the bi-directional feedback between the land surface and regional climate is presented in Figure 1.2, which incorporates those processes (such as large tree mortality) that can be dramatically altered at forest edges and lead to complex edge effects (Camargo & Kapos, 1995; Kapos, 1989) and 'hyper-dynamism' (Harper *et al*., 2005; Laurance, 1997; Laurance, 2002; Laurance *et al*., 1998a; Figure 1.1) at forest edges.

LANDSCAPE PATTERN & INFLUENCE ON FOREST PATCH PROPORTIONS

PROPERTIES OF A CREATED CLEARING

LATENT HEAT

SENSIBLE HEAT

EDGE EFFECTS AT A FOREST EDGE

LATENT HEAT

SENSIBLE HEAT

EDGE EFFECTS

ENERGY FLUXES

ANTHROPOGENIC

LANDSCAPE PATTERN

NATURAL

FEEDBACK UPON ITSELF

POSITIVE EFFECT

NEGATIVE EFFECT

A POSITIVE OR NEGATIVE EFFECT FROM ONE BOX TO ANOTHER ASSUMES A POSITIVE VALUE IN THE PRECEDING BOX.

Figure 1.2   *The potential role of forest edges in regional hydrometeorology (modified from Laurance, 2004, following Laurance & Williamson (2001) and Laurance et al. (2001)). A positive or negative effect imposed by one box upon another (denoted by arrows and +/- signs) assumes a positive value in the first, imposing, box.*

There are only a few case studies where forest plantations (Ciencala *et al.*, 2002; Taylor *et al.*, 2001), or temperate (Herbst *et al.*, 2007b) or tropical forests (Giambelluca *et al.* 2003) have been monitored for edge effects relating to hydrometeorology. Each study makes its own assumptions, explicitly and implicitly, which must be assessed to determine what questions still remain with regard to energy fluxes at forest edges. Investigating altered water fluxes at forest edges is a complex task because the process of advection is exceptionally hard to measure across these boundaries (Klaassen *et al.*, 1996). The main reason for this is that many micrometeorological techniques are fetch-dependent (i.e. biased by the distance they are positioned downwind of a forest edge), and it is precisely this fetch-dependence (i.e. change in a given quantity, such as water flux, with distance downwind of a forest edge) that is the subject of hydrometeorological inquiries at forest edges (Giambelluca *et al.*, 2003; Herbst *et al.*, 2007b).

Fetch-independent techniques traditionally used in agricultural meteorology, such as lysimeters, eddy correlation – or even leaf-based measurements, such as infrared gas analysers (IRGAs) - are exceptionally hard to employ in forest edges. As a result, Thermal Dissipation Probes (TDPs (Granier, 1985, 1987; James *et al.*, 2002)) are the most practical and popular method to measure energy fluxes in such scenarios (Kumagai *et al.*, 2005; Wullschleger *et al.*, 2001). Sap velocity is determined from a differential temperature measurement between an upper, heated, probe situated above an unheated lower probe, both of which are installed in tree xylem. The temperature differential is then calibrated to the volume of water moving over the probe pair on a sapwood area basis. Probes are installed in a series of trees within predefined 'edge' and 'interior' zones. Information from TDPs is used to determine the amount of water transported from forest edge and interior trees to the atmosphere, and then used to make estimations of latent heat fluxes from interior and edge zones by multiplying the measurement by the total sapwood area (xylem) in each stand. Whereas TDPs are not truly 'fetch-independent' (*cf.* Giambelluca *et al.*, 2003), their installation within individual trees delineates naturally the position of the water source. This implicitly accounts for the mixing of fluxes once they leave tree canopies, and avoids errors associated with the footprints of bulk measurements or soil moisture measurements. TDPs furthermore have the exclusive property of being able to be used at the ground level whilst measuring water-use and associated processes occurring at the forest canopy, where 90% of available energy is absorbed (Cox *et al*., 1998). TDP systems are monitored via automated data loggers and thus

also provide high temporal and *relatively* high spatial resolution (Giambelluca *et al.*, 2003). Measurements of water use of individual trees can be used in conjunction with meteorological measurement to ascertain which meteorological variables influence, or are influenced by, tree water use the most (D'Alessandro *et al.*, 2006; Granier *et al.*, 1992, 1996a, 1996b, 2000; Hubbard *et al.*, 2004; O'Brien *et al.*, 2004; Oren & Pataki, 2001; Oren *et al.*, 1999a, 1999b, 2001; Pataki *et al.*, 1998; Phillips & Oren, 1998, Phillips *et al.*, 2001).

There are, however, numerous significant scaling errors associated with the bottom-up approach of TDPs. At the individual level, these are namely radial (James *et al.*, 2002, 2003; Zang *et al.*, 1996) and azimuthal (Clearwater *et al.*, 1999; Ford *et al.*, 2004a, 2004b; James *et al.*, 2003; Jiminez *et al.*, 2000; Meinzer *et al.*, 2001a; Nadezhidina *et al.*, 2002; Philips *et al.*, 1996; Poyatos *et al.*, 2007; Wullschleger & King, 2000) variations in sap flow. At the same time, appropriate sampling of representative species must be taken to make accurate stand-scale estimates. This means that TDP systems require a large number of logger channels, great power (0.2W per probe, typically) and intensive maintenance (*cf.* Giambelluca *et al.*, 2003) to accurately represent a low number of trees. Hence great care has to be taken when making sap flow measurements at forest edges to ensure that remaining questions regarding forest edge water use are addressed appropriately to prevent the use of TDPs becoming impractical. This is particularly important in the tropics where power and other logistical constrictions can be severely limiting, and analyses are likely to be confounded by the inherent genetic and ontogenetic (i.e. the genetic potential of individual trees and their particular expression of that potential as influenced by different environmental conditions) and structural complexity of forest edges (*cf.* Wullschleger *et al.*, 2001).

Despite the limitations of TDPs, this technique has considerably improved our knowledge of energy exchange at forest edges. Following these successes (i.e. the subsequently-reviewed case studies) at capturing forest-edge-atmosphere feedbacks, researchers have begun to make tentative conclusions about the importance of forest edges in the climate. The following four case studies highlight some of the recent progress in understanding climatic feedbacks at forest edges, and how the appropriate use of sap-flow probes has been brought to bear on research questions important to forest edges.

Taylor *et al.* (2001) were the first to address differences between tree water use at forest edges and interiors, following a logical progression from agricultural meteorology (their sampling of a monospecific silviculture of Blue Gum (*Eucalyptus globulus*) in Southern Australia). Their study assessed how tree water use was dependent upon the influence of advection and different soil moisture conditions between the forest edge and interior zones by combining meteorological measurements with TDPs installed at the plantation edges and interior. The Penman-Monteith equation (Monteith, 1965) is an extended theoretical description of the actual evaporation (*Et*) from a vegetated surface for a given net radiation (i.e. Rn, which is equal to the available energy at the land surface, A):

$$\lambda Et \ = \frac{\varDelta A + \sigma C_p \left(\frac{VPD}{r_a}\right)}{\gamma + \varDelta \frac{r_a}{r_s}} \qquad\qquad [W\ m^{-2}] \qquad\qquad (Equation\ 1.4),$$

where (VPD) denotes vapour pressure deficit, (C_p) the specific heat capacity of air, (σ) the air density, (λ) the latent heat of vaporisation of water, (γ) the psychrometric constant (=σ C_p/λ), and ($\varDelta$) the slope of the saturated vapour density curve with temperature. (r_a) and (r_s) are aerodynamic and stomatal resistances to water transport, respectively. The Penman-Monteith (1965) equation incorporates all the weather variables with direct effect upon the evapotranspiration process. Taylor *et al.* (2001) used a diagnostic analysis of the Penman-Monteith (1965) equation similar to that of McNaughton & Jarvis (1983), who broke the equation down into its constituents:

$$\lambda Et = E_{rad} + E_{aero} = \Omega E_{eq} + (1 - \Omega)E_{im}\,, \qquad\qquad [W\ m^{-2}] \qquad\qquad (Equation\ 1.5),$$

where (E_{eq}*),* or potential evapotranspiration (PE), is due to radiation alone (i.e. E_{rad}) and is estimated solely from available energy (A) and psychrometric constants. McNaughton & Jarvis (1983) define E_{aero} as that evaporation *imposed* by the properties of the surrounding air, i.e. E_{im}:

$$E_{im} = \rho c_P VPD r_a \lambda \gamma r_c \qquad\qquad [W\ m^{-2}] \qquad\qquad (Equation\ 1.6).$$

A decoupling factor (Ω) incorporates aerodynamic and canopy resistances (r_a and r_c, respectively (Jarvis, 1976; Jarvis & McNaughton, 1986; Pereira, 2004)):

$$\Omega = \left(\frac{1+\gamma}{\varDelta + \gamma} \frac{rc}{ra}\right)^{-1} \qquad\qquad [-] \qquad\qquad (Equation\ 1.7).$$

Terms r_c and r_a can be calculated:

$$r_c = \left(\frac{VPD\sigma C_p}{\gamma \lambda E}\right) + r_a \left(\frac{\Delta A}{\gamma \frac{\lambda E - \Delta}{\gamma - 1}}\right) \qquad [sm^{-1}] \qquad \text{(Equation 1.8)},$$

$$r_a = \ln\left(\frac{\left(\frac{z-d}{z0}\right)^2}{k^2 u z}\right) \qquad [sm^{-1}] \qquad \text{(Equation 1.9)}.$$

Aerodynamic resistance requires additional measurements of wind speed (u) at height (z) and relies upon the van Karman constant (K). Sap flow (Q_s) was normalised with potential evapotranspiration (PE) as derived from the Priestley-Taylor equation (where α is commonly assumed to = 1.26 to account for advection, Priestley & Taylor, 1972):

$$PE = \alpha \; \frac{\gamma}{\Delta + \gamma} A \qquad [mm\ dy\text{-}1] \qquad \text{(Equation 1.10)}.$$

Pereira (2004) showed α to be inversely proportional to Ω (compare Equations 1.10 and 1.7).The Priestley-Taylor equation estimates the maximum evapotranspiration from a wet surface as a function of available energy (A) only, i.e. the net radiation received at the land surface (E_{rad}, Equation 1.5). Importantly, the Priestley-Taylor (Priestley & Taylor, 1972, Equation 1.10, this chapter), Penmann-Monteith (Monteith, 1965, Equation 1.4, this chapter), and Jarvis-McNaughton decoupling coefficient (Jarvis & McNaughton, 1986, Equation 1.7, this chapter) equations do not account for below-ground limitations such as soil moisture.

Following the Priestley-Taylor (1972) equation, it can be seen that this equation is dependent solely on radiation available at the land surface (A) if α is fixed at 1.26. Thus, by normalising sap flux with potential evapotranspiration, Taylor *et al.* (2001) established whether tree water use at the forest edge was predominantly due to vertical, fetch-independent, adiabatic energy transfer, or to lateral, fetch-dependent, diabatic energy transfer (i.e. advection, E_{aero}, Equation 1.5) imposed by the overlying atmosphere as it passed over the forest edge (Figure 1.3). It was shown that tree water use of both the edge and inner trees increased with PE initially and then became independent as PE increased further (Figure 1.3). The plots indicate that minor but significant differences in Qs (normalised sap flow (cm^3 cm^{-2} sapwood area day^{-1})) between inner and edge trees existed at low PE and that these differences increased with increasing PE until Qs became independent of PE (Figure 1.3). Thus, vertical energy transfer only accounted for some of the variation in tree water use, both for trees at the edge of the plantation and those further in to the plantation. However, under advective conditions, it would be expected that edge trees express a different relationship between PE and Qs to trees in the plantation 'interior'.
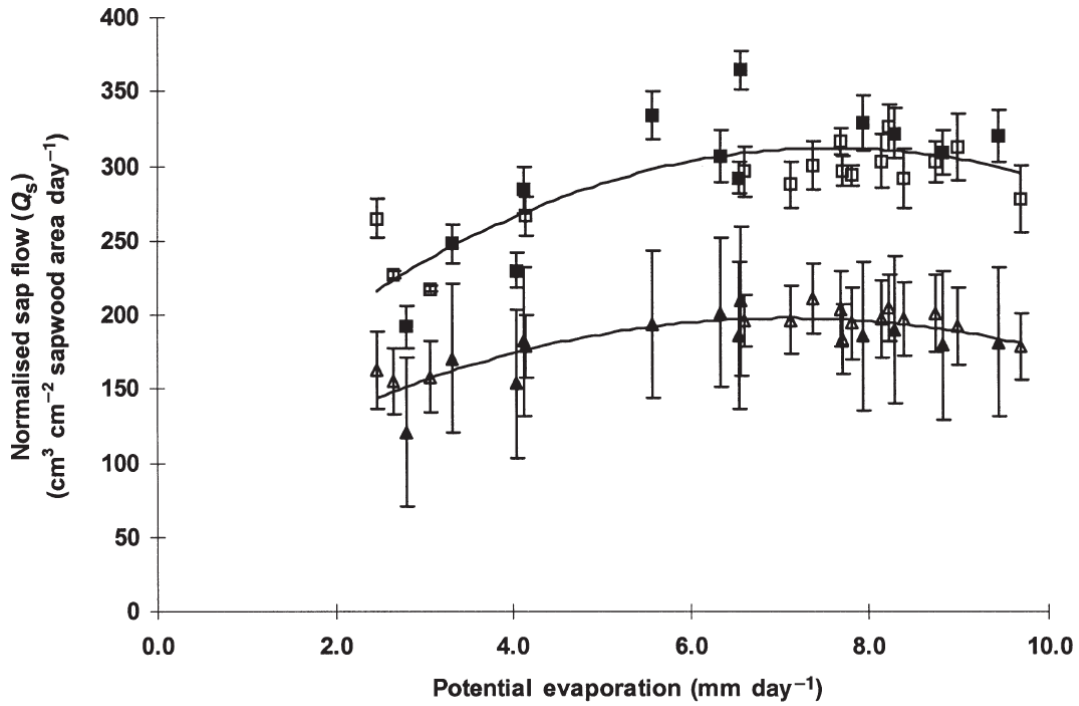
Figure 1.3 *Relationships between normalised (per unit sapwood area) daily sap flow (Q*$_s$*)*
and potential evaporation for edge trees (squares) and inner trees (triangles).

Taylor *et al.* (2001) then inverted the Penman-Monteith (1965) equation to establish
a critical canopy conductance value that diagnosed when hot air advection was most
likely to occur. When surface (canopy) temperature (T*) < air temperature (T$_a$)
canopy conductance (g$_c$) is above the critical value, and transpiration increases with
wind speed because *T** increases toward *T*$_a$. The opposite happens when *g*$_c$ is below
this value. If canopy conductance is equal to the critical value, then transpiration is
independent of wind speed. The critical value was obtained by rearranging the
Penman-Monteith (1965) equation and setting evaporation to be independent of
aerodynamic conductance (Thornley & Johnson 1990, Equation 14.6e in Taylor *et al.*,
2001). This is the equivalent of removing the E$_{aero}$ term in Equation 1.5, and takes the
form:

$$g_c critical = \frac{\Delta A}{\lambda VPD(\Delta + \gamma)} \qquad [sm^{-1}] \qquad (Equation\ 1.11).$$

Days when tree canopy conductance (g$_c$) exceeded g$_c$critical were thus more likely to
represent when the plantation was under advective influences. The calculation of g$_c$
critical required additional measurements of above-canopy vapour pressure deficit
(VPD) in addition to the energy balance (i.e. net radiation, Rn) measurements needed
for the calculation of the Priestley-Taylor coefficient. Such a requirement highlights

the added logistical demands for canopy-level ancillary measurements, which in this case allowed the inversion of the Penman-Monteith equation:

$$g_c = \frac{E}{(\frac{\Delta Rn}{\gamma \lambda g_a} + VPD) - (\frac{\Delta + \gamma}{\gamma g_a})E} \qquad [mms^{-1}], \qquad \textit{(Equation 1.12)}.$$

Subsequent regressions showed that, for the four days when canopy conductance was least likely to exceed the critical value, a strong linear relationship existed between Qs values of the four edge trees and of the four inner trees, whose conductance never exceeded the critical value. For the days when canopy conductance of edge trees was more likely to be greater than the critical value, the relationship was weakened, the slope of the line was steeper and approached the significance level ($P = 0.08$), indicating greater transpiration of the edge trees with respect to the inner trees. This was taken to be evidence for enhancement of transpiration of the edge trees due to advection.

There was a reasonably close correlation between the transpiration rates of interior and edge trees, indicating that soil moisture differences between interior and edge zones were also partially responsible for the different transpiration rates between interior and edge trees. This demonstrates the influence not only of the above ground conditions upon transpiration, but also that of the moisture status of the ground, thus limiting the diagnostic application of the Priestley-Taylor equation, which does not include below-ground influences in its estimation of PE. Interestingly, edge trees demonstrated a different relationship between sap velocity and sapwood area from that of the linear relationship expressed by interior trees, further supporting the presence of a more 'general' edge effect.

Taylor *et al.* (2001) conclude that the optimal design for interception belts (the planting of trees to alleviate rising ground water associated with dry land salinity, as was the case for the plantation in this study) incorporates wide tree spacing to maintain high canopy conductance, increased wind energy to the entire canopy and thus the maximized transpiration of groundwater. This supports the conclusions of Harding *et al.* (1997), who also link the number of 'edges' (in this case widely-spaced rows) to an increased latent heat flux within a fragmented region, or, in this case, forest stand. Given the increased gap frequency (Kapos *et al.*, 1993) and mortality of large trees (Laurance *et al.*, 2000) at natural forest edges, a supporting argument could be presented wherein, at the individual scale, forest edge trees would be well-positioned for increased light interception, turbulence exposure, and water accessibility, thus increasing their transpiration rates. This further highlights the

relevance of biodynamical phenomena, operating additionally to micrometeorological influences upon the transpiration of natural forest edges, which are normally more uniform at the equivalent edges of agricultural and silvicultural regimes or semi-natural forest. It should also be noted that the planting of readily transpiring shelter bests within the arid location of this study is highly conducive to advection and far from a 'natural' scenario for forested systems. This situation is idealised in the same way as the Tiger Bush and agricultural landscapes of arid environments as mentioned previously. 50% of TDPs failed in the study of Taylor *et al.* (2002), limiting substantially the number of trees (19 trees) measured for transpiration, and also the time period over which measurements of transpiration were made (30 days).

1.6 CASE STUDY 2 : THE INFLUENCE OF SOIL MOISTURE ACCESSIBILITY

Ciencala *et al.* (2002) measured water use in a 70 year-old mono-specific pine (*Pinus sylvestris L.*) stand growing on poor sandy soils, in the northern boreal zone of Sweden, Heden, 60km NW of Umea. Ancillary measurements were made below the canopy (ground frost and snow depth, soil moisture and soil temperature) in conjunction with standard micrometeorological diagnostics (relative humidity, air temperature, precipitation, and shortwave radiation), to elucidate how below-ground factors influenced water use at the edge zone as well as above-ground meteorology. This represented a step forward from the analysis of Taylor *et al.* (2001), which only measured the influence of above-ground meteorology on tree water use. Thus, whilst Taylor *et al.* (2001) had to infer the influence of below-ground conditions (i.e. soil moisture) upon tree water use, Ciencala *et al.* (2002) were able to describe empirical relationships explicitly.

It was found that the main mechanism operating on tree water use at the forest edge was the soil temperature and freezing of water within the rhizozone, which restricted water access of individual trees. Above-ground meteorology was not found to influence tree water use, demonstrating the limitations of the Priestley-Taylor equation and approaches such as that of Taylor *et al.* (2001), who based experiments on the same assumptions (i.e. tree water use is only affected by above-ground micrometeorology). Thus, the below-ground measurements made by Ciencala *et al.* (2002) lend pivotal and independent support to conclusions that, in this instance, could only have been inferred from above-ground micrometeorological data alone. The influence of soil moisture and temperature upon transpiration explained a

relatively weak correlation between the calculated PE and tree water use, which r^2 ranged between 0.22 and 0.75 (mean r^2= 0.52). It could be argued, however, that measurements of diabatic variables (humidity and temperature) were made too low in the canopy to rule out the influence of canopy-level micrometeorology upon tree water use. This is the case as meteorological measurements were made at 9m, but the majority of trees measured were 10-15m high. Indeed, although tree water use at the forest edge was attributed to soil conditions, Ciencala *et al.* (2002) concede that only a more comprehensive measurement protocol could conclusively demonstrate the influence of soil conditions on tree water use.

The site used in this study was purposefully chosen as a north-facing edge. As the orientation of the edge was opposite to the prevailing wind direction, the influence of wind and other subsequent microclimatic effects upon transpiration that were not the subject of the study were assumed to be eliminated. However, the assumption of eliminating microclimatic affects relied heavily on literature describing the influence of below-canopy microclimate on tree water use of south-facing edges. Given the aforementioned issue of how appropriate the measurement height of 'canopy level' meteorology was in this study, it remains questionable whether above-ground micrometeorological influences on tree water use were also eliminated.

Ciencala *et al.* (2002) also measured tree and stand biometry (crown exposure, tree height, diameter breast height, and sapwood area). However, due to the high tree-level variability in this study, it was concluded that these variables would not significantly alter stand-scaled sap flux estimates. It should be noted, however, that trees at the forest edge had more sapwood, which Ciencala *et al.* (2002) attributed to light competition. This pattern is similar to the increased sapwood area for a given sap flux density expressed by trees at the edge of the plantation as studied by Taylor *et al.* (2001). The altered water use of trees at the forest edge was linked to the lower competition rates there. Thus, both Taylor *et al.* (2001) and Ciencala *et al.* (2002) link tree water use to density and growth rate of trees at forest edges, highlighting the potential for altered bio-dynamics and hyperdynamism associated with forest edges to influence tree water use there.

The work of Giambelluca *et al.* (2003) in Ban Tat hamlet, Hoa Binh, Vietnam, represents the first attempt at measuring transpiration of trees within a mixed-species stand, and a significant step forwards in addressing edge effects in a 'natural' forest. Giambelluca *et al.* (2003) first conducted a species inventory, and then measured four tree species that were dominant at the forest edge and interior. This ensured that estimations of water fluxes from the land surface were as representative of the forest surface as practically possible – a factor not needing consideration in monospecific stands. Transpiration measurements of individual trees were normalised by their respective species mean to obtain an estimate of their increased transpiration as a departure from 'normal'. However, due to TDP failure and the natural variability of water use between species, the conclusions from sap flow probe data were not conclusive, but rather suggestive, as the effective study period when all equipment was functioning was only one month. Poorly-exposed trees did not exhibit an edge effect upon transpiration, but an increased transpiration rate of about 50% at the forest edge was found for well-exposed trees. It should be noted that this trend was strongly dependent on one individual tree at the very edge of the forest, which alone kept the trend within the bounds of significance (Figure 1.4, highlighted by a red box).

Supplementary measurements of relative humidity, wind speed, air temperature, net radiation, wind direction and surface (canopy) temperature were made above the canopy at the forest edge, interior, and adjacent unused clearing (i.e. swidden) sites using micrometeorological equipment placed on masts, adding support to tentative conclusions drawn from sap flow data. Wind speed decreased sharply across the forest patch boundary, along with midday air temperature, which also declined towards the patch interior; surface temperature was lowest at the forest edge. Relative humidity at the same reference height increased into the patch. It was also found that the air temperature over the forest edge was, on average, higher than that of the surface temperature, suggesting a downward flux of sensible heat into the forest canopy from the clearing and a concomitant increased water (latent heat) flux from the canopy to the atmosphere above. The edge effect was dependent on the moisture status of the land surface, with a greatly increased edge effect upon transpiration being observed in drier periods.

Chapter I: The Potential Significance of Tropical Forest Discontinuities and Their Influence on Regional Hydrometeorology
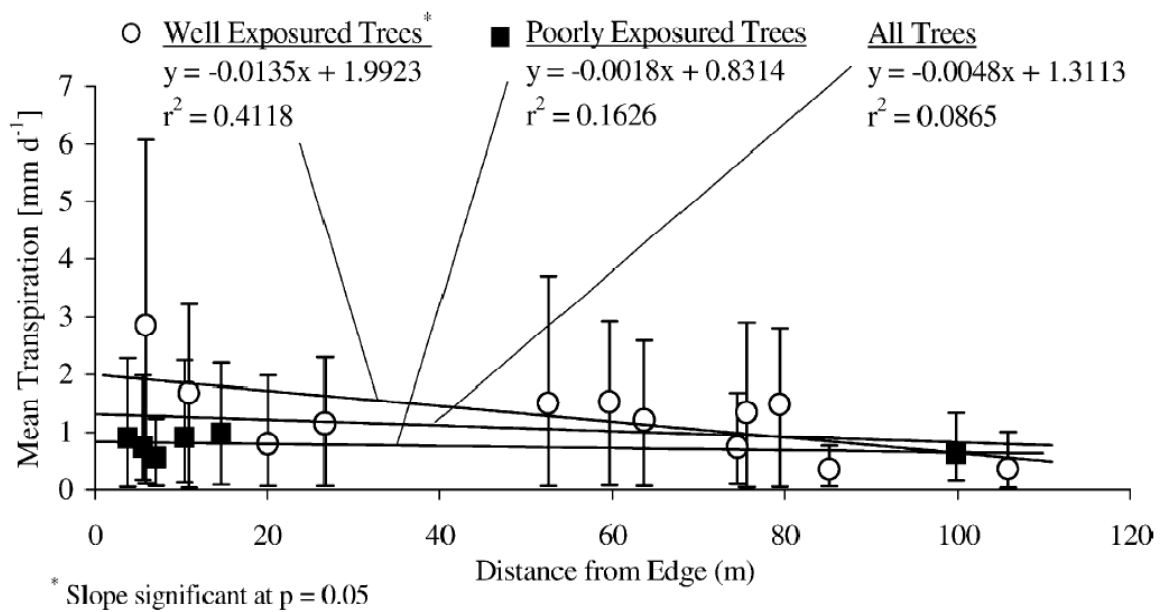
Figure 1.4 *Mean whole-period transpiration (24th March- 20th June, i.e. 'dry' and 'wet' periods) of individual trees as a function of distance from the forest edge. Rates of well-exposed trees (those rated as having good or fair exposure to sunlight and wind) and poorly-exposed trees are shown as open circles and closed squares, respectively. Lines shown for well-exposed, poorly-exposed, and all trees, are based on regressions of mean transpiration versus distance from the forest edge (Reproduced from Giambelluca et al., 2003). Red box shows the one tree in the 'Well-Exposed' category that renders the linear fit between mean transpiration and distance from edge significant.*

Transpiration in both edge and interior stands was more highly correlated with net radiation, air temperature, and relative humidity measured in the clearing than with corresponding measurements within the stands. These results suggest that transpiration in the forest patch is enhanced during relatively clear, sunny periods when the clearing is dry and hot, i.e. periods when conditions are conducive to high positive heat advection. Giambelluca *et al.* (2003) also note that the high correlation between the water use of some individual interior trees and the energetic conditions of the swidden could suggest advective effects extend well beyond the pre-defined 'edge' zone of this study, something that is supported by the spatial interpolation of results (Figure 1.5). Caution must be applied, however, when using remotely-positioned equipment. It was not noted in this study what instantaneous field of view was offered by the infrared thermometers, and furthermore, albedo of the forest was presumed to be equal between the forest edge and its interior. This could lead to unrepresentative sampling of surface values of temperature and albedo, and subsequent calculations of net radiation over the study area. The interpolation from

sap flow probes to large spatial extents is also questionable, although this approach appears to provide sensible results.
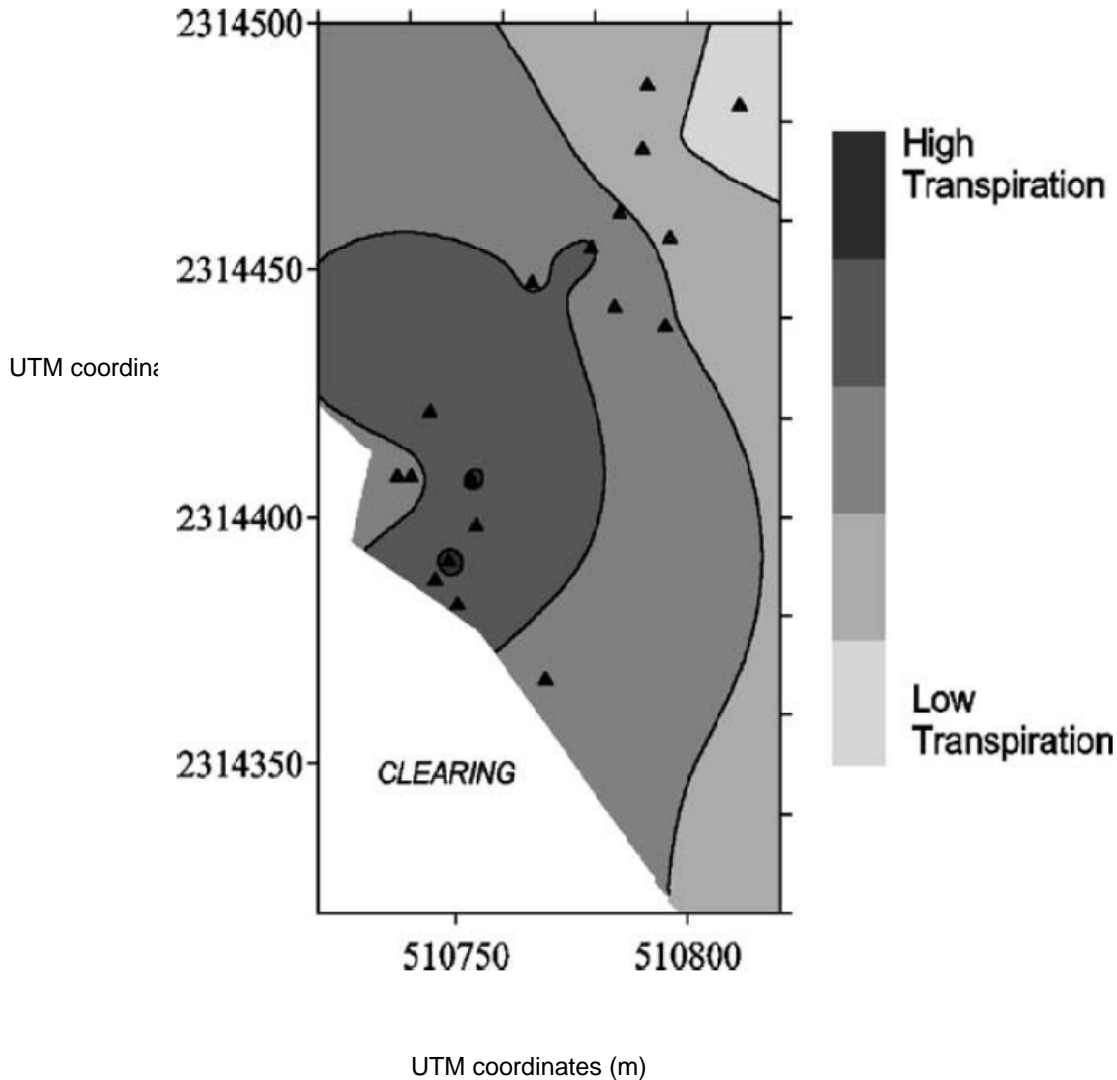
UTM coordinates (m)

Figure 1.5 *Normalized transpiration within the study area of Giambelluca et al. (2003) based on spatially interpolated means of 'wet' and 'dry' periods spanning 24th March- 20th June 1998. Axes values give UTM coordinates (m), and individual trees monitored for transpiration are marked with a triangle (reproduced from Giambelluca et al., 2003).*

Total evaporation, calculated using energy balance methods (Equation 1.1), was also higher at the edge site than at the swidden or forest interior. This was estimated using top-down measurements of net radiation, sensible heat flux and ground heat flux, whereby E is estimated by forcing closure of the energy balance. Giambelluca *et al.* (2003) note that, because this method is itself fetch-dependent (see Equations 1.2 and 1.3), results based upon forcing closure of the energy balance in this case must be treated with caution. Whilst calculating evaporation from energy balance closure acts as a practical diagnostic (as opposed to eddy correlation measurements, which

are not particularly practical for measuring evaporation at forest edges) for water use of the land surface as a whole, the errors associated with this method are unknown so the results must be treated with caution. However, for mixed stands expressing a high level of structural diversity, there is no other option than this to obtain a synoptic view of the land surface as a whole, as there are bound to be errors in scaling exceptionally species-diverse stands from the bottom–up point measurements. Only a full eddy correlation analysis could offer a better diagnostic measurement of the land surface as a whole in the context of individual sap flux measurements, but the use of an eddy correlation system in tropical forest has significant practical constraints. Soil moisture also increased into the patch by the end of the dry season, adding power to the suggestion of greater cumulative evapotranspiration at the forest edge, in agreement with similar studies previously conducted at tropical forest edges (Camargo & Kapos, 1995; Kapos, 1989).

Although it was found that the spatial pattern of transpiration was dependent on wind direction, Giambelluca *et al.* (2003) note that this not only influences the edge effect but also increases the natural variation in the system, as one individual tree in the forest 'interior' transpired at a high rate similar to those trees in the forest 'edge' zone. This sensitivity to wind speed most likely occurs because wind speeds in the tropics are typically low, making the forest canopy predominantly limited by the boundary layer and its turbulence rather than stomatal control (i.e. it is decoupled from the atmosphere, having a high Ω value, following Equation 1.7). This probably leads to increased transpiration by emergent individuals and thus greater variability in the system.

1.8 CASE STUDY 4: SPECIES COMPOSITION WITHIN A SEMI-NATURAL TEMPERATE FOREST

Herbst *et al.* (2007b) noted that in all previous studies addressing transpiration at forest edges sampling densities of tree transpiration rates were low, and were consequently confined to few tree species. By using a 'roving' sap flow probe system to measure sap flux (Fd) they were able to greatly improve their sampling size and diversity in semi-natural woodland in Wytham Woods, Oxford, UK. The roving system worked in the same fashion as standard TDP measurements, but involved moving the probes to different trees after a relatively short time period. This approach rendered a much more powerful data set, doubling both the spatial resolution and temporal extent of the data set. However, unlike Giambelluca *et al.* (2003), measurements were made under semi-natural conditions, demonstrating how measuring the

transpiration of natural tropical forests using TDPs is much more difficult than when measuring semi-natural temperate forests, as the latter tend to be more accessible. Whereas all other studies lasted about a month, the work of Herbst *et al.* (2007b) lasted five months. However, moving TDPs on a regular basis required that Fd measurements were standardised by PE. Calculations of PE were made by Herbst *et al.* (2007b) by inter-calibration between a radiation balance mounted over the forest itself and existing weather station in a nearby field, approximately 100-150m away from their measured trees. This allowed the use of the Priestley–Taylor coefficient to extrapolate shorter measurement periods of Fd to annual estimations using values of net radiation as measured over the field, as the forest radiation balance system was removed after two weeks. The calculation of PE followed Equation 1.10, and thus assumed no variation in advection and no limitation of soil moisture or resistance in the rhizosphere-xylem pathway. Hence, the short time period of measurement allocated to a single tree raises the question of whether this approach greatly improves the characterisation of forest edge fluxes over a series of hydrological conditions, whereby sap flux may not necessarily be controlled predominantly by radiation and thus standardisation of Fd by PE may not be appropriate.

A trend similar to that of Taylor *et al.* (2001) was found, with Fd becoming independent of potential evapotranspiration (PE) at $PE > 0.4 \, \text{mm h}^{-1}$, and the influence of radiation being reduced even further in trees located at the edge when compared with trees in the forest interior. Shuttleworth & Calder (1979) recommend extreme caution when using PE in connection with forests because, if vegetation and the atmosphere are closely coupled, surface factors (E_{aero}, Equation 1.5) rather than the energy input (E_{rad}, Equation 1.5) determine the water loss. Herbst *et al.* (2007b), however, note that neither the uncertainties in the calculation of *Fd* data and their relation with PE nor the variability in Fd caused by conditions other than proximity to the forest edge, weaken any of the statements made about the magnitude (and spatial extension) of the edge effect, since all trees, inner and edge, are affected in the same way. The annual stand transpiration rates seem plausible as transpiration from the forest interior was close to the average rates of forest transpiration for the region (Roberts, 1983) and transpiration from the forest edge compared well with hedgerow transpiration (Herbst *et al.*, 2007a) with respect to its similarity to PE.

Herbst *et al.* (2007b) also was the first study to attempt to account explicitly for understorey evaporation, which would be expected to contribute significantly to total land surface evaporation within the secondary-forest nature of the vegetation

typical of forest edges. In agreement with Giambelluca *et al.* (2003), it was shown that understorey species showed little enhancement of transpiration at the forest edge.

1.9   SCALING EDGE EFFECTS

Once point measurements of LSAIs made at the patch scale have established that there is indeed fetch dependence (i.e. influence on a given property with distance from the forest edge) at forest edges, it becomes important to extrapolate those point measurements appropriately to landscape and regional spatial extents. At the patch scale, scaling is based on the magnitude and extent of edge effect (e.g. Laurance *et al.*, 2000; Laurance *et al.*, 1998b). At the landscape/regional level such scaling must also incorporate measures of landscape edge frequency, using a length-scale model (e.g. de Ridder, 2003; de Ridder & Mensink, 2003; de Ridder *et al.*, 2004), or patch perimeter-to-area ratios using a core area model (e.g. Laurance*, 1991; Laurance & Yensen, 1991). This is difficult since, at the regional, level forest patches are very hard to quantify and monitor (*cf.* de Ridder *et al.*, 2004). Thus scaling analyses to date have been limited to modelling patch size and shape distributions or their measurement over limited (landscape) spatial scales. For example, Herbst *et al.* (2007b) assumed that all forest patches where square in shape using a quadratic function when predicting the transpiration of forest patches in the UK (Figure 1.6).
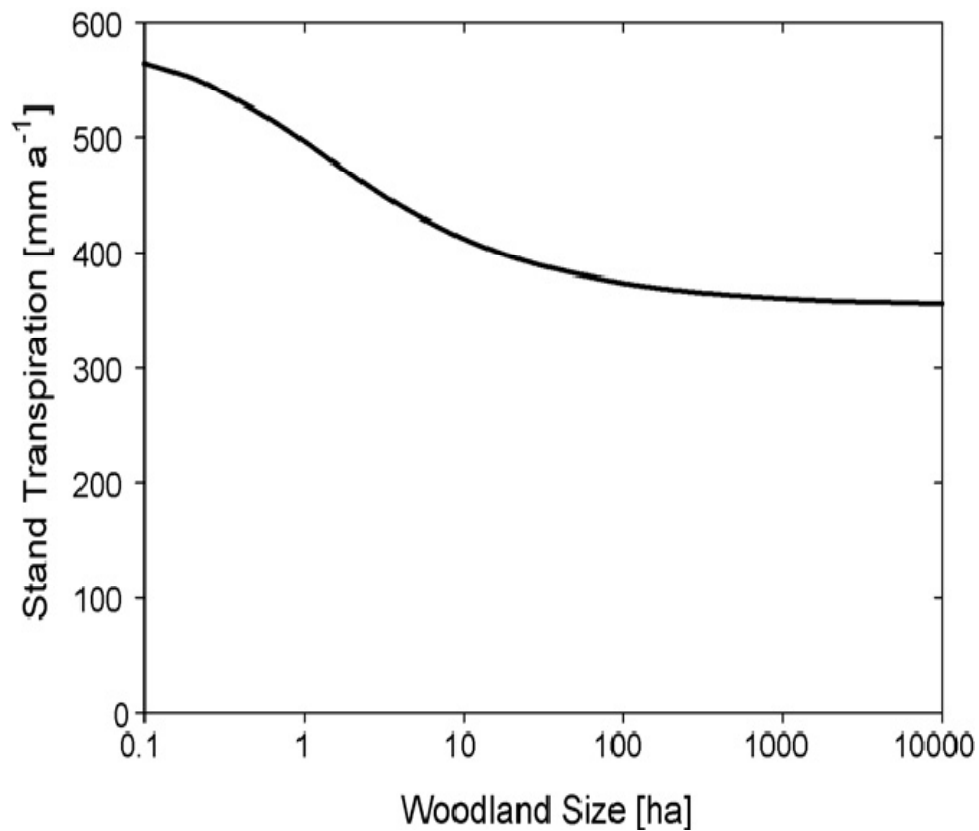
Figure 1.6 *Hypothetical annual transpiration from deciduous forests depending on the area covered by forest, assuming quadratic ground area - i.e. square forest patches (Herbst et al., 2007b).*

Making the assumption that all forest patches within the landscape are square in shape permits an efficient initial indicator of edge influence on regional water use. However it is unlikely that such an assumption will capture effectively the more diverse patterns of deforestation typical of areas such as the tropics, where the landscape is not confined to square remnants but instead displays a variety of shapes and sizes (Imbernon & Branthomme, 2001, and Figure 1.7, this chapter). Thus in highly-fragmented landscapes where edge influences will potentially dominate within patches of remnant forest, and thus the landscape as a whole, the pattern of deforestation (and thus the shape of forest patches) can be an important determinant of landscape function if complexed patterns of deforestation are expressed. Taking Figure 1.7 as an example, it can be see that, although each landscape has a similar proportion of forest, assuming that forest patches are all square would not represent the differences in deforestation patterns between each site. Given the highly fragmented nature of each site in Figure 1.7, and the consequent potential dominance of edge influences in each landscape, assumptions

of square forest patches would lead to poor representation of overall landscape function (such as estimates of total evapotranspiration), should edge influences be present in those landscapes. It should be furthermore noted that edge effects can be additive when forest edges meet at their patch corners (Malcolm, 1994).
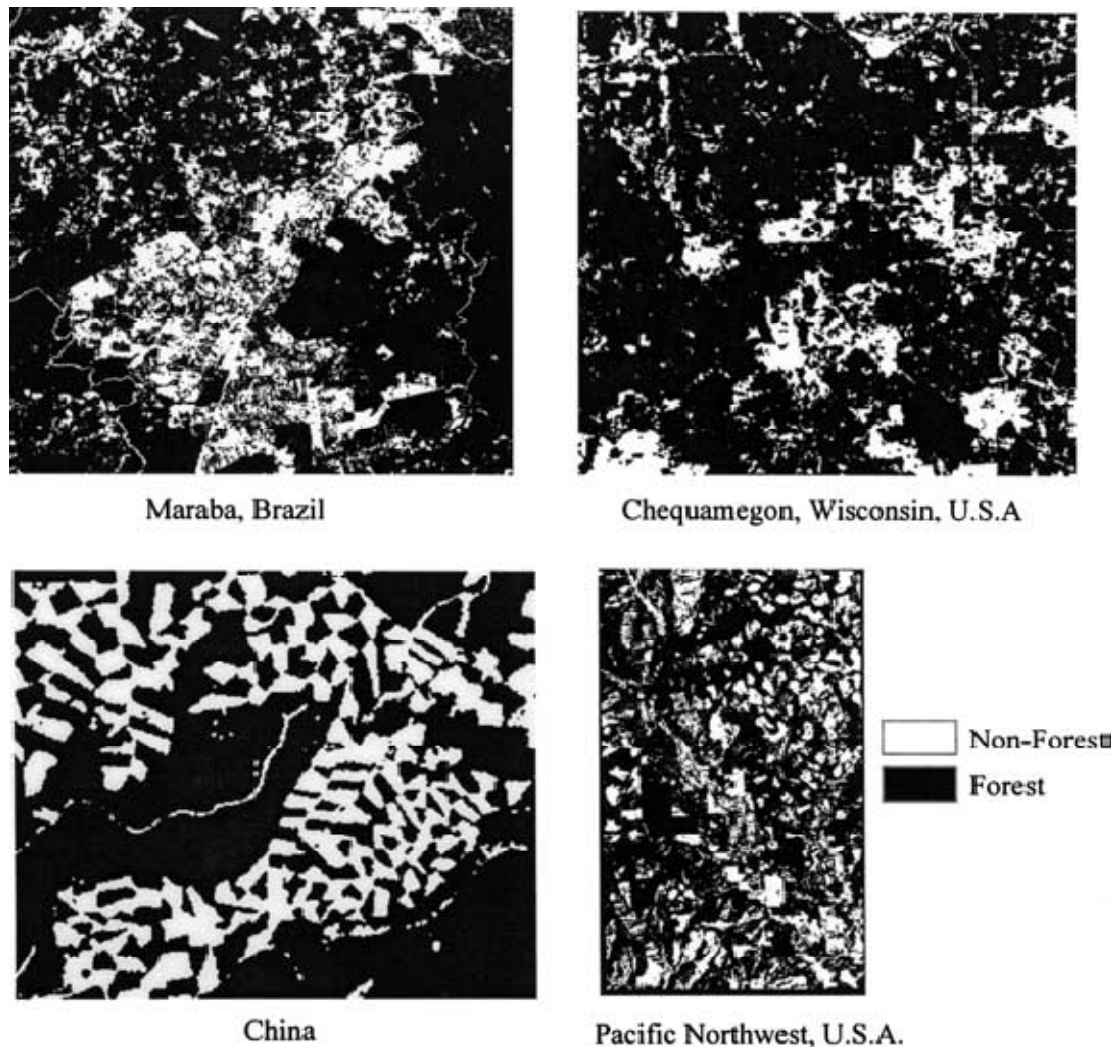
Figure 1.7 *Fragmentation patterns within 20km x 20km landscapes (11.7 x 34km for Pacific Northwest). The configuration of edges is largely determined by human-induced disturbances including timber harvesting, agricultural expansion, and urbanisation. Different fragmentation patterns can result in varying amounts of edge in the landscape. About 70-81% of these landscapes are still described as forest, but the amount of forested area falling within 60m of edges is 34, 24, 33 and 56%, respectively. In all these landscapes, the area of edge influence has the potential to be a dominant component of the landscape matrix (Harper et al., 2005).*

The issue of when a fragmented forested landscape becomes dominated by edge effects also becomes pertinent when viewing Figure 1.7. The deforestation patterns all show a relatively high degree of fragmentation, with 34-56% of forested area

falling within 60 m of forest edges. However, it can be seen that the point at which the processes operating in these landscapes are dominated by edge effects depends not only on the degree of fragmentation, but also the process, the DEI/EEI and the MEI. Thus spatial analyses of landscape pattern alone cannot uncover the precise degree of fragmentation at which landscapes become predominately influenced by edge effects, or indeed the point at which the landscape as a whole can be considered to function as 'forest' or 'non-forest'. Put simply, analyses of edge effect processes and landscape patterns are mutually dependent on one another when making accurate regional-scale estimations of LSAIs in the process of regionalisation.

The Tropical Ecosystem Environment observation by Satellite (TREES, Achard *et al.*, 2002b) initiative defines three deforestation patterns based on their random-stratified sampling of the tropical humid biome, these being Linear, Massive and Diffuse. This approach is somewhat more rigorous, as landscape structure is defined by sampling representative of deforestation 'hotspots'. Laurance *et al.* (1998b) extended this theme to model three different land pattern classes, and established a percentage of forest influenced by edge effect based on each pattern using a shape–index value to prescribe a numerical descriptor of shape to each land pattern class in the Amazon, as described by Laurance (1991). However, these classes were prescribed shape-index values by visual assessment only; a much better option would be to calculate landscape metrics, which describe the landscape pattern in a more objective fashion. Such landscape metrics are, however, inherently ambiguous, since there is no known sole numerical descriptor of shape (Myint & Lam, 2002).

As a result of this ambiguity, a large number of patch metrics exist, and great care is needed when selecting appropriate parameters in order to reduce the volume of data and avoid confusion. Various authors (Cain *et al.*, 1997; Imbernon & Branthomme, 2001) have used statistical analysis to eliminate redundancy in landscape metrics to ascertain those that are truly independent measures of landscape pattern.

A remaining issue in the calculation of landscape metrics in the tropical humid biome, however, is that studies to date have been unable to base calculations of landscape metrics upon areas representative of the entire biome, or to cover the absolute (pan tropical) extent of deforestation. For example, Laurance *et al.* (1998b) extrapolate their modelled area-influences to the humid tropical biome, but are forced to limit their analysis to the broad categorisation of four regions (Brazilian Amazon, South

America, Central Africa, and Southeast Asia) into linear, massive and diffuse deforestation patterns, which were chosen subjectively, having no comprehensive, objective sampling scheme behind their selection. These limitations are the result of the trade-off in the spatial extent and resolution offered by satellite sensors, which is the crux of the problem in any broad-scale remote sensing study (*cf*. Gabriel *et al*., 1988). For example, Laurance (2004) states that the majority of forest patches in an area of the Amazon are below 0.1 ha (e.g. a 10x10m pixel), and later state that high-resolution imagery (Landsat) is needed to capture these inherently small-scale phenomena. This renders medium-resolution satellite imagery such as MODIS (250m) ineffective. Conversely, the expansive and dynamic nature of land cover conversion means that higher-resolution satellite imagery such as Landsat (30m resolution) is of insufficient spatial extent and temporal frequency owing to its lower instantaneous field of view (IFOV).

One solution to this problem would be to use a predefined sampling scheme, such as Imbernon & Branthomme (2001), who adopt the TREES sampling system. Such sampling systems, while highly effective, require intensive labour. Another solution would be to use a proxy for deforestation at medium resolutions to either (a) define strata for intensive sampling or (b) correlate directly to a useful landscape metric, such as the perimeter-to-area ratio, for inverse calibration purposes (Brown, 1982; Mayaux & Lambin, 1995, 1997). However, the efficacy of proxies would be dependent on there being a systematic and stable (i.e. predictable) scaling pattern between medium and high resolution sensors. Specific textural analysis such as wavelets and fractals (essentially scale-independent edge detectors which account for the number of pixels included in the calculation process), which are inherently scale-invariant, offer an exciting way of classifying satellite imagery to elucidate regions expressing textural patterns that change predictably over a series of scales (*cf*. Kushwaha *et al*., 1994). Indeed, textural analysis has been shown to greatly improve the classification of complex landscape patterns, yet, to date, the extraction of spatially explicit data from texture measures has not been attempted for fragmented tropical forest despite numerous cases of scale-stable texture classifiers being demonstrated for forested regions (e.g. Mayaux & Lambin, 1995, 1997).

Accurate calibration is also dependent upon the relationship between scales being consistent not only spatially but also temporally. Therefore, it could be argued that inverse calibration procedures would need recalibrating at an appropriate frequency using high-resolution imagery that has been sampled in a statistical fashion to ensure

calibrations remain appropriate as deforestation continues and fragmentation patterns change. As the initial creation of a sampling scheme takes many years (including the identification of deforestation 'hot spots' (e.g. Achard *et al*., 1998), associated broad-scale maps (e.g. Mayaux *et al*., 1998), and creation of sampling units (e.g. Richards *et al*. (2000) created tessellating hexagons as a icosahedrons within a sphere to over the globe) etc. etc. (Achard *et al*., 2002b)), it remains to be seen whether this approach is practically possible. However, given recent progress in remote sensing, such investigations show definite promise and allow the opportunity to examine patterns with greater temporal frequency. Indeed, recent work by Ewers & Laurance (2006) concludes that the consistent fractal dimensions (a measure of self-similarity over scale) expressed by patterns of deforestation demonstrate that deforestation patterns are relatively consistent over time, considering that satellite images do not offer a 'snapshot' of landscape pattern but rather a cumulative picture of the process. Should this be the case, it would then be made possible to examine time series of fragmentation patterns at relatively high frequency through inverse-calibration/statistical sampling that is not offered by high-resolution platforms. This could be made possible by taking advantage of systematic scaling behaviour of deforestation patterns. An empirical relationship between coarse- and fine-resolution satellite imagery could be used to calibrate coarse-resolution imagery, eliminating the need for fine-resolution imagery. As course- resolution satellite imagery has a greater instantaneous field of view (IFOV), the revisit intervals for a given area are shorter than those for higher- resolution imagery. Thus, high-frequency, low-resolution satellite imagery could be made practicable, without loss of spatial information, via calibration.

1.10 <u>DISCUSSION - THE CURRENT STATE OF AFFAIRS</u>

The case studies in this review are invaluable because they confirm that forest edges differ in their hydrometeorology from forest interiors for a wide variety of forest types. All four case studies report that the transpiration rate of 'edge' trees exceeds that of 'interior' trees by about 50%. Although this agreement seems to indicate consensus, it should be noted that the reported value of Giambelluca *et al.* (2003) was for 'well-exposed' trees only, and that the removal of one individual tree at the very edge of the forest reduced the trend of edge effect to insignificance. Furthermore, only the study of Herbst *et al.* (2007b) measures an appropriate number of trees. The four case studies all report similar increases in transpiration extending similar distances into forest edges, but they represent very different forest

types, ranging from plantations to natural forests, and are conducted in very different biomes (tropical dry, Mediterranean, boreal, temperate). Agreement between the four case studies of this chapter may just be similar by coincidence, or it may be that a similar control is altering transpiration at the forest edges of all four studies. The only possible phenomena operating across the forest edges in all four case studies are dependent on forest density, such as altered light interception or water accessibility. However, the four studies presented here supplement sap flux measurements with either biotic or meteorological measurements, but never the two combined, owing to the cumbersome nature of maintaining all these measurements together. Thus it is uncertain which controls predominantly influence transpiration of forest edges.

Recent suggestions for standardising measurements characterising the biological nature of forest edges (Harper *et al.*, 2005) highlight the lack of a standardised methodology for characterising LSAIs at forest edges. Without the comprehensive and standardised characterisation of forest edge meteorology (above and below canopy air psychrometrics, wind speed, radiation etc., and below ground measurements of soil moisture, rooting depth, soil temperature etc.) and structure (basal area, canopy fraction, xylem area, tree exposure etc.), it is impossible to determine the exact context of sap flux measurements. This is important as the land surface expresses a bidirectional feedback (i.e. vegetation influences meteorology, and meteorology influences vegetation) with the atmosphere (Moorcroft, 2003), so forest edge structure (and, implicitly, edge biodynamics), and below-ground influences (such as soil moisture) will act in concert with meteorological factors. One example would be the measurement of soil moisture, which is a particularly important determinant in tree water use and can invalidate analyses involving the Priestley-Taylor coefficient (including the four case studies presented here). A comprehensive and standardised series of meteorological and vegetation structure measurements would furthermore allow cross-study comparisons, and clarify common variables acting to control transpiration across the four case studies here.

Established study sites would most likely be already well-charachterised in terms of their meteorology and vegetation structure, but they tend not to focus around forest edges. Moreover it could be argued that those established sites where forest edges are present may not be particularly representative of this inherently dynamic phenomenon (e.g. vegetation dynamics of forest edges within well-conserved study

sites may be more stable that those surrounded by actively maintained clearings outside conservation areas).

Harper *et al.* (2005) note that there is a temporal maturing of forest edges associated with a significant change in their structure (Figure 1.1). This involves the death of larger trees through wind-throw (snapping/uprooting of trees from high winds) and microclimatic stresses (e.g. water stress), and also a sealing of the forest edge by under-storey and pioneer species. Differences in light interception, total leaf area index, gap fraction, species composition, water accessibility and soil moisture are expected to influence the water use edge trees (Harper *et al.*, 2005), as well as the nature of 'matrix harshness' (i.e. the contrast in the physical properties of adjoining forest/non-forest covers (*c.f.* Gascon *et al.*, 1999, 2000; Nascimento *et al.*, 2006)) and alterations in sapwood area and tree height (Ciencala *et al.*, 2002). To date, no study has compared the water use of older vs. younger edges, or the potential confounding density effects. Whilst direct comparisons would be desirable, these would necessitate a cumbersome number of measurements. Instead, the standardised characterisation of forest edges, as mentioned in the previous paragraph, would allow comparison across studies, and thus a practical alternative to direct comparisons when comparing LSAIs between forest edges of different ages, or, indeed, biomes.

To date, studies reveal little information about the extent of altered transpiration at forest edges, which, so far, has been assumed to be no further than 50m into the forest from its boundary. Many studies assume that below-canopy wind inflow into forests, which decreases rapidly as it enters at the forest edge (Fritschen, 1985; Raynor, 1971), is a dominant factor in their micrometeorology. However, it remains unclear whether above-canopy wind-flow influences the evaporative fluxes of trees at forest edges. This would certainly appear to be the case given the more distinct edge-influence upon well-exposed trees; quantitative description of a 'well-exposed' tree would help clarify this matter. Momentum and scalar quantities take a considerably longer time to adjust to the underlying conditions of forest edges when the air carrying them passes *over* forest edges than they do when that same air flows *into* forest edges. Whereas inflow effects take 10-20 meters to adjust to the conditions *under* a forest canopy, momentum and scalar quantities passing *over* forest edges take 16-35 and 20 tree heights, respectively, to adjust to the new *underlying* canopy surface (Gash, 1986a; Irvine *et al.*, 1997; Kruijt *et al.*, 1991; Sogachev *et al.*, 2005), in fitting with the extent of wind damage at forest edges as

observed by Laurance (1997), Savil (1983) and Somerville (1980). Supporting this, de Ridder *et al.* (2004) note that the atmospheric deposition model used in their study adequately captures altered fluxes without including inflow effects. Giambelluca *et al.* (2003) furthermore conclude that the edge effect experienced at their tropical site in Vietnam could extend well beyond 100m, which would include all the trees in all 'interior' plots as defined by work to date.

This chapter has so far considered transpiration. No equivalent edge effect has been reported for wet-canopy evaporation, which can constitute an important component of tropical forest hydrometeorology. Should such an effect exist, increased transpiration effects would be confounded by altered wet-canopy evaporation and this would in turn influence total water use estimates. Wet canopy evaporation (assumed to be equal to precipitation interception by the forest canopy) is calculated as the residual of precipitation minus the water that falls from/through the canopy to the ground below the canopy (i.e. throughfall). Neal *et al.* (1993) found that the interception loss of a deciduous temperate forest in the UK did not change between the interior and 20 m from its edge. Klaassen *et al.* (1996) attributed similar findings in a temperate forest in the Netherlands to enhanced evaporation of water from wet forest edge canopies, due to increased turbulence being counterbalanced by a lower water storage capacity of forest edge canopies. This may well be the case for tropical forests, given the greatly reduced canopy cover reported at their edges (Kapos *et al.*, 1993), and the increased throughfall associated with canopy gaps, but it remains to be seen whether there is a consequent decrease in wet-canopy evaporation at forest edges due to structural alterations that may not necessarily have been present in the studies of Klaassen *et al.* (1996) or Neal *et al.* (1993). An effect of this nature would be expected to reduce the influence of increased transpiration at forest edges. Herbst *et al.* (2007b) addressed rain shadows behind the lee edge of a temperate forest fragment, as such an effect had been observed previously for single trees and hedgerows (David *et al.*, 2006; Herbst *et al.*, 2006, 2007a). It was found that there was little effect at the lee edge, and this in part confirms the assumptions of non-linearity at the landscape scale as described by Harding & Blyth (1996). However, altered wet-canopy evaporation at the windward and leeward sides of tropical forest edges has yet to be measured.

The study of Giambelluca *et al.* (2003) addresses various important aspects to measuring natural forest edges, in particular the need to incorporate a wide variety of species. However, practical limitations of TDPs prohibit this somewhat, despite the

important influence of the variety of tree species within forests, and also that of altered species compositions at their edges, upon forest water use. Wullschleger *et al.* (*2001*) described the empirical relationship between the stomatal conductance of dominant tree species, and coupled their stomatal behaviour to micrometeorological and biophysical variables using a prognostic model based on the comprehensive measurement of a single species. The authors consider this a feasible approach of representing tree water use in mixed-species forests, given that, in this instance, 85% of variance in tree water use of a single species can be explained by net radiation and vapour pressure deficit. Such an approach would be a practical alternative in circumstances where a roving arrangement, such as employed by Herbst *et al.* (2007b), cannot be undertaken.

Given the highly variable nature of wind flow over forest edges, and the significant influence of topographic and local structure on wind direction measurements, it is important that comprehensive measurements of local microclimate are made in a remotely-sensed fashion over the forest canopy. However, making such measurements above the canopy is exceptionally hard, as few forest towers exist at forest edges. Giambelluca *et al.* (2003) overcame this problem by using mobile towers to measure wind direction and speed along a transect into their forest patch. This approach, however, is somewhat limited to smaller trees, which in this case were only about 10m high.

This review also highlights the essential inclusion of representative remotely-sensed spatial parameters from satellite imagery when making regional estimates of water use in fragmented tropical forests. This is especially important given that regional estimates made to date have relied upon simplistic estimations of the proportion of forest edges in the landscape. Remote sensing can also play an important role in measuring the energetic status of the land surface using appropriate surface energy balance algorithms (Batiaassenn, 2000; Batiaassenn & Chandrapala, 2003; Batiaassenn *et al.*, 1998a, 1998b; de Ridder *et al.*, 2004) to determine not only the number of edges but also the 'matrix harshness' (Gascon *et al.*, 2000) in terms of energetic quantities (i.e. the likelihood of hot air advection between patches of varying energetic disparity). For example, in the only study of its kind, Klaassen *et al.* (2002) show an increased heat flux downwind from a transition opposite to that documented in the case studies presented in this chapter. Defining edges in energetic terms would influence classification and thus scaling, as can be seen by

examining the equivalent regional analysis of de Ridder *et al.* (2004) when scaling chemical deposition in a fragmented region of the Netherlands.

1.11 CONCLUSIONS

This chapter documents, but does not necessarily confirm, the possible existence of significant advective and micrometeorological influences upon LSAIs that violate the assumptions of homogeneity by micrometeorologists and climate modellers alike in small-scale estimates of water transfer. This is due to a limited number of studies addressing the hydrometeorology of forest edges (since work of this nature is still in its infancy), the bidirectional nature of LSAIs, hyperdynamism of forest edges and, to a large extent, limitations in our ability to accurately measure for forest edges at a number of scales. However, the potential for forest edge water use to influence climate highlights a need for scientists to overcome these limitations to improve modelling approaches. It is intended that this review will draw attention to the multi-faceted nature of forest edges, and those scales at which outstanding research questions need to be addressed to determine if forest edges contribute significantly to the regional hydrometeorology of the tropical humid biome.

It is recommended that standardised analyses of forest edge meteorology and vegetation are conducted to place sap flow measurements in an appropriate context, so comparisons can be made between studies conducted on forest edges of different ages and biomes. Paradigms should be drawn from existing reviews which call for a standard methodology in ecological settings. As the climate system is profoundly influenced by the biota it supports, adapting those same protocols comes at little cost and offers great benefit. In reality, it is impossible to measure all the variables that influence hydrometeorological parameters at forest edges. It is therefore essential to provide a comprehensive site description to link the existing study together with previous works. Only under this construct can a necessarily assumption-laden study design be trusted and deemed stringent enough to make this research discipline viable. Such a format could include good stand-scale practice such as that outlined by Sheil (1995), with additional measurements such as soil moisture, wind speed, LAI or gap fraction. This is of particular importance as established study sites rarely offer natural forest edges. This chapter highlights the crucial role of Thermal Dissipation Probes in studying water movement in forest edges, but other methods – such as automated dendrometer bands - also offer much promise when calibrated appropriately.

Chapter 2: The Hydrometeorology of a Humid Tropical Forest Patch – Methods

This chapter describes the field methodology employed in this thesis to establish "w*hether tropical forest edges transfer more water to the atmosphere than their respective forest interiors"* (Aims and Objectives, Preface).

Fieldwork took place in Sabah, Borneo Island, Malaysia, within the Yayasan Sabah Corporation logging concession near the Danum Valley Field Centre, both of which are introduced in this chapter. The study area was chosen due to the relatively accessible nature of recently-created clearings adjacent to secondary forest edges. The climate as measured at the Danum Valley Field Centre is reviewed to place the measurements of land surface atmosphere-interactions described in this chapter in context of the hydrometeorological regimes at other Neotropical sites. Methodologies are detailed with regard to the selection and positioning of instrumentation and how relevant calculations are used to characterise and compare hydrometeorological parameters of a single forest edge, and compare them with those of its respective forest interior. Particular attention is paid to describing how estimations of forest water use (i.e. evapotranspiration) are influenced by limitations of measurement scale and directionality, and how these effects are addressed by using a combination of 'bottom up' and 'top down' methods. Consideration is paid to how 'fetch' (distance from the forest edge) invalidates the assumptions of methods commonly used to estimate forest evapotranspiration, and the consequential need to employ instruments, such as Thermal Dissipation Probes (TDPs), that can be applied with equal reliability anywhere in a forest patch, regardless of fetch. The methodology described here relied on a considerable amount of equipment built by the candidate, and thus attention is also paid to how such instruments were appropriately calibrated. Results from application of the methodology detailed here are presented in Chapter 4.

Chapter 2: The Hydrometeorology of a Humid Tropical Forest Patch –Methods

2.1. INTRODUCTION: DANUM VALLEY FIELD CENTRE AND CONSERVATION AREA

The Danum Valley Field Centre (DVFC) is located at 117 ^{o}48.75' E and 5° 01.01' N on the east coast of the Malaysian state of Sabah, Northern Borneo (Figure 2.1). The station lies on the edge of the 43.8 km ^{2} Danum Valley Conservation Area ,an area of Class I protected rainforest (Figure 2.1, red), in the Ulu Segama Forest Reserve, part of the 972.8 km^{2} Yayasan Sabah forestry logging concession (Figure 2.1, green, and Figure 2.2, upper box).

The Yayasan Sabah Logging Concession (YSLC, Figure 2.1, in green) has been selectively logged by the Yayasan Sabah Corporation (YSC) from the early 1970's onwards, and logging continues to date. The YSC logging operation comprises a combination of tractor logging in areas of moderate terrain, and cable or 'high-lead' yarding on steeper slopes, which leaves a mosaic of different disturbance patterns. High-lead yarding involves dragging towards a central collection point around the high-lead machine itself, resulting in highly degraded areas around the collection point (typically ±20 ha), with further severe damage extending out along winching 'corridors'. High-lead yarding was banned by the Sabah Forestry Department in 1996. Tractor yarding results in a more varied mosaic of damage including highly degraded areas with little vegetation such as skid tracks, and clear-felled areas of bare ground called 'stamping' areas where timber is stored. Stamping areas can be considered swidden (i.e. forest clearings with rotational use and maintenance) similar to that described by Giambelluca *et al.* (2003). However, lightly disturbed to completely untouched forest remains in areas where tractor yarding has been used to harvest timber.

The YSC logging operation removes about 8 trees ha^{-1}, less than the average extraction rate of 12-15 trees ha^{-1} typical in the rest of Malaysia (Marsh, 1995). Compared with other selectively logged forests in Sabah and Malaysia, some parts of the logged forests in the YSLC can be considered as 'good quality' forest, due to relatively low extraction rates, less human disturbance (such as illegal logging), and modified logging practices such as tractor yarding. This can mean that relatively undisturbed forest remains. Typically, though, selectively logged forested areas within the YSLC are dominated by pioneer trees, such as those of the genera *Macaranga, Octomeles, Neolamarkia* and *Duabanga* (Willot *et al.*, 2000). Selectively logged forests in YSLC also usually have abundant vine cover, climbers, and herbs such as *Melastoma malabathricum*, *Piper* spp., and ginger (Zingiberaceae spp.),

(Ahmad, 2001). Forest remaining after the YSC logging operation is typically interspersed with open clearings which have little or no vegetation (Willott *et al.*, 2000). Vegetation recolonisation is limited in these open clearings, since the organic topsoil is usually removed to reveal highly compacted mineral soil during the various YSCL clearing operations. Should organic soil be left behind in the clearing process, it can become covered with grasses, ferns, vines, and climbing bamboo (e.g. *Dinochloa* spp.), although recolonisation usually takes a long time owing to the compaction of any remaining organic soil by logging machinery. Soils in the YSLC include ultisols, inceptisols and alfisols (Marsh & Greer, 1992; Newbery *et al.,* 1992).

Legend

Yayasan Sabah Logging
Concession (YSCL)
Danum Valley
Conservation Area (DVCA)
* Study Site

Annual Precipitation

>3500mm
3000mm - 3500mm
2500mm - 300mm
2000mm - 2500mm
1500mm - 300mm
<1500mm

Isohyet map courtesy of
Sabah Forestry Department
w w w . s a b a h . g o v . m y
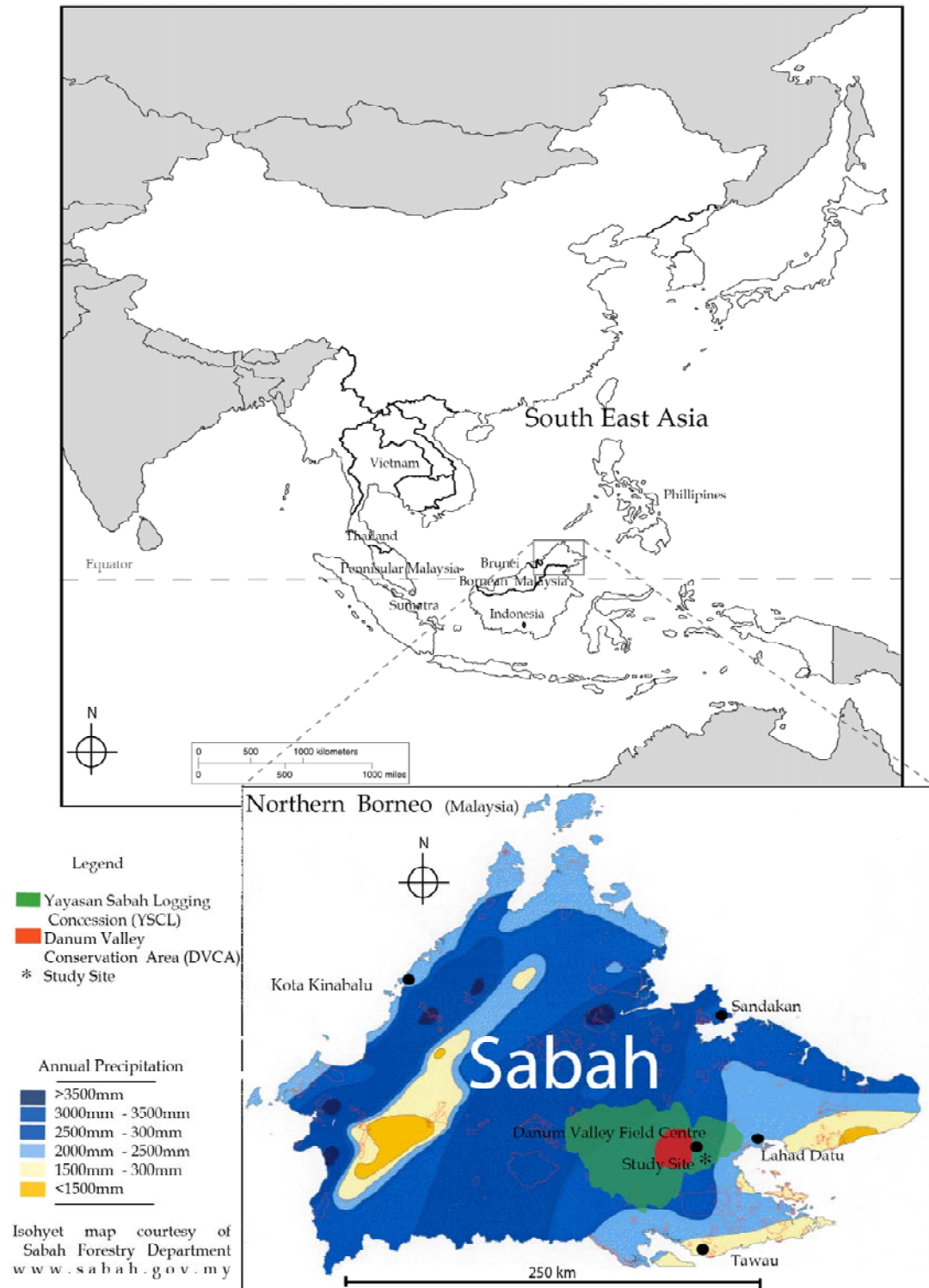
Figure 2.1   Location of Study Area (*), in relation to the Danum Valley Conservation Area (red), both of which are situated in the Yayasan Sabah Logging Concession (green), in Sabah, Northern Borneo, near the town of Lahad Datu. It can be seen that the study site receives an annual rainfall in between the higher amounts found further inland and those lower levels experienced in coastal area.
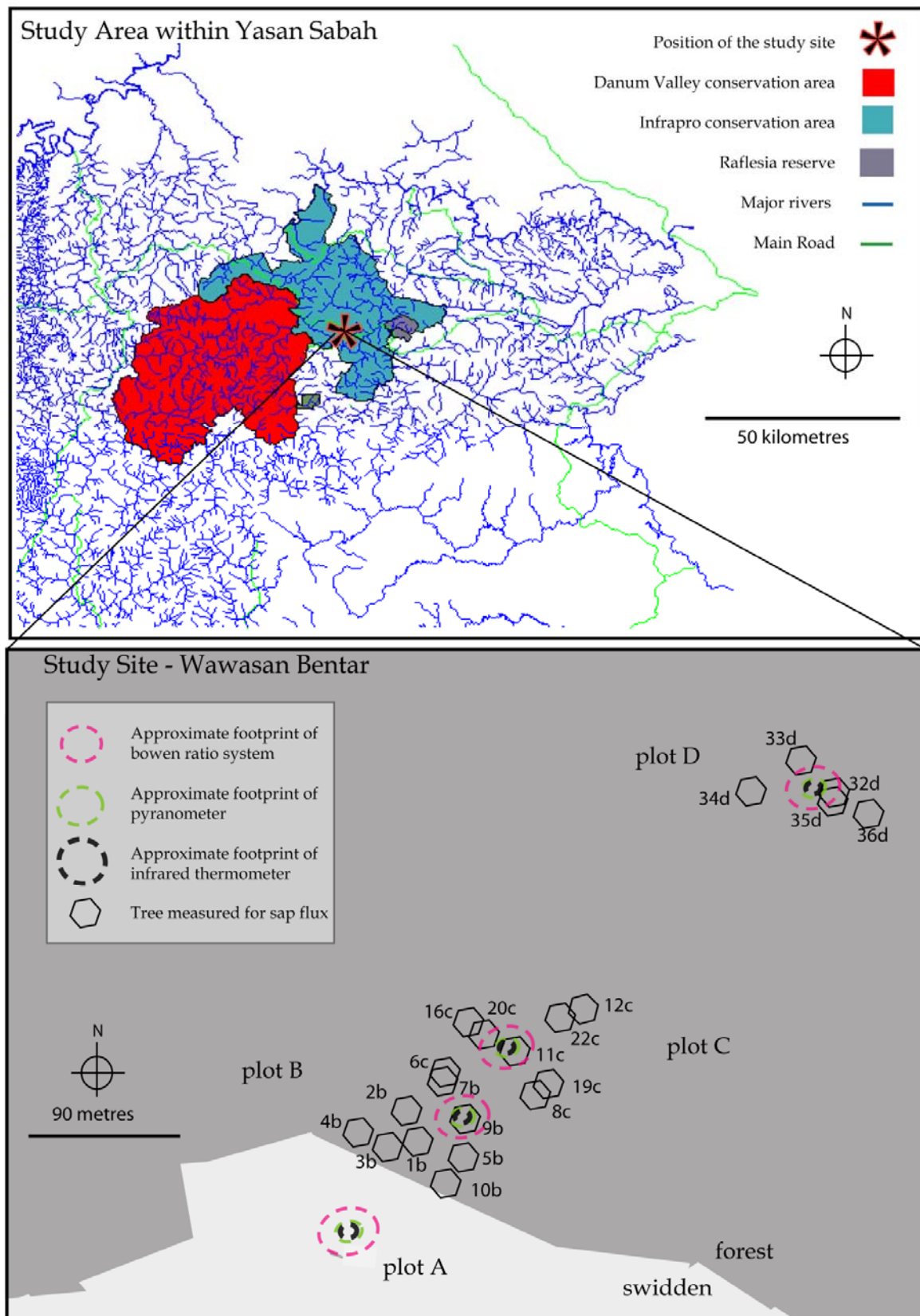
Figure 2.2   The study site location. The positions of meteorological tower/masts are shown (meteorological measurements are detailed in section 2.4) alongside the position of each study plot (A-D). Trees monitored for sap flux measurements are represented by hexagons (sap flux measurements are detailed in section 2.8).

Measurements described in this chapter focussed on the clearing, and forest adjacent to, Wawasan Bentar Sdn. Bhd., a small (1.6 Ha), clear-felled area made for the purpose of storing timber harvested in the process of tractor yarding, often called a stamping ground. The position of Wawasan Bentar is shown in Figure 2.2. Wawasan Bentar was created in June 2006 but, as of October 14th 2007, was yet to be used. Thus, Wawasan Bentar can be classed as a swidden clearing similar to those examples in Chapter 1 (e.g. Giambelluca *et al.*, 2003). At the time of the field campaign ground cover in the Wawasan Bentar swidden was limited, and the clearing was mainly bare soil (approximately 70%), this being sparsely covered by creepers. Organic soil had been removed in the clearing process to expose the mineral under-layer. Regeneration in the swidden took the form of substantial but patchy grass cover about 20 meters before the adjacent forest edge due to the presence of some remaining organic soil. The adjacent forest patch (itself 36 Ha) is dominated by *Macaranga* and *Mallotus* genera individuals. Average canopy height of the adjacent forest is approximately 22m. There remained one *Koompasia* spp. individual (55m approx.) in the swidden itself, close to the edge of the forest. A list of dominant species in the forest is presented in Table 2.1. Both the clearing and the forest lie on a slight slope (8°). For this kind of study, a flat site is preferred, but it was impossible to find such a site and thus a study on flat terrain could be almost certainly considered irrelevant (*cf.* Giambelluca *et al.* 2003). Soils in the forest adjacent to Wawasan Bentar are predominantly ultisols, having high clay and organic matter content, being relatively acidic, and yellow-red in colour.

Family	Species	Total No. of Individuals
Euphorbiaceae	*Macaranga hypoleuca*	13
Euphorbiaceae	*Macaranga pearsonii*	10
Euphorbiaceae	*Macaranga gigantea*	9
Rubiacae	*Neolamarkia cadamba*	9
Euphorbiaceae	*Mallotus peltatus*	6
Lythracea	*Duabanga* sp.	6
Euphorbiaceae	*Mallotus lackey*	5

Table 2.1: Dominant species present in the forest adjacent to the Wawasan Bentar swidden. Total numbers of individuals as counted within 20 randomly selected 5x5m plots (cf. Giambelluca et al. (2003).

Chapter 2: The Hydrometeorology of a Humid Tropical Forest Patch –Methods

Introduction

Temperatures and relative humidity at Danum are typical of the tropical humid biome. Monthly mean temperatures range only 1.9°C around the annual mean of 26.7°C, and the mean daily range, which also varies little throughout the year, is 8.4°C. Temperatures exceed 34°C only rarely, usually during prolonged dry spells. As at most rainforest locations, relative humidities are close to saturation at 0800h. Relative humidity reaches a minimum in the early afternoon, averaging 72% at 14.00h, and up to 81% at wetter sites (Walsh & Newberry, 1999). Climatic data for Danum are presented in Figures 2.3-2.6. These data were kindly provided by Professor Rory Walsh, University of Swansea.
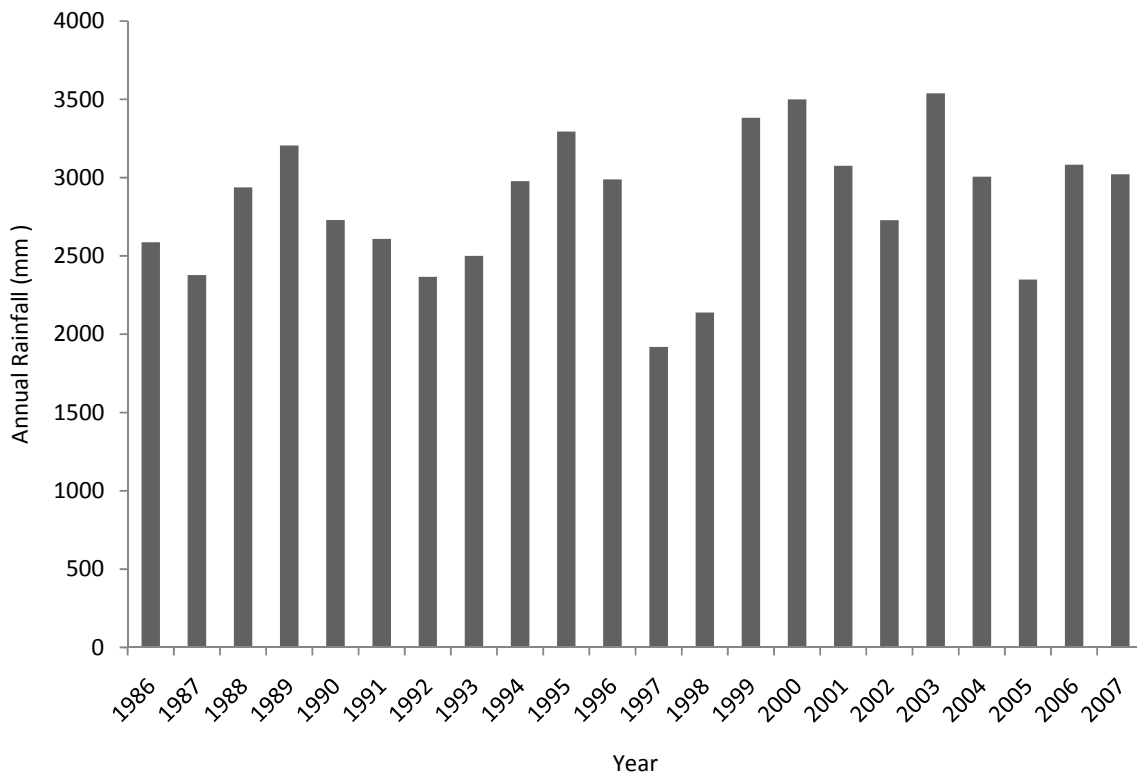
Figure 2.3   Total annual rainfall (mm) at Danum Valley (1985-2007).

Chapter 2: The Hydrometeorology of a Humid Tropical Forest Patch –Methods
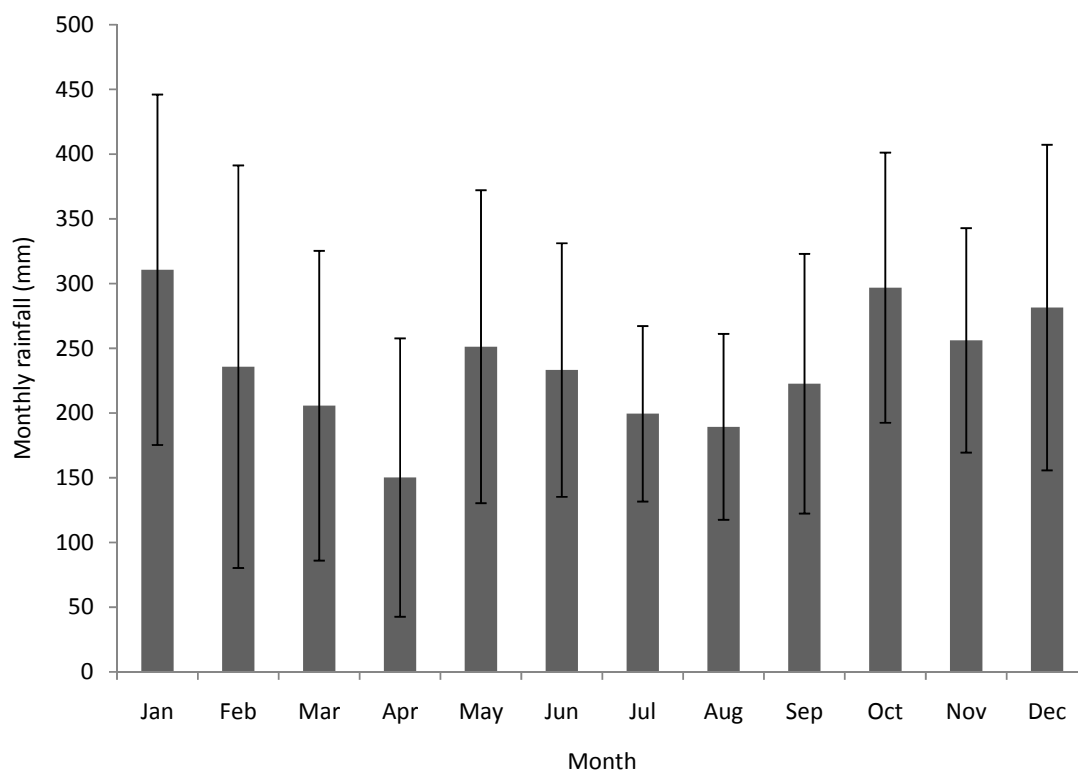
Figure 2.4   Average total rainfall (mm) received each month at Danum Valley (1985-2007). Error bars show standard deviation of yearly values for each month.
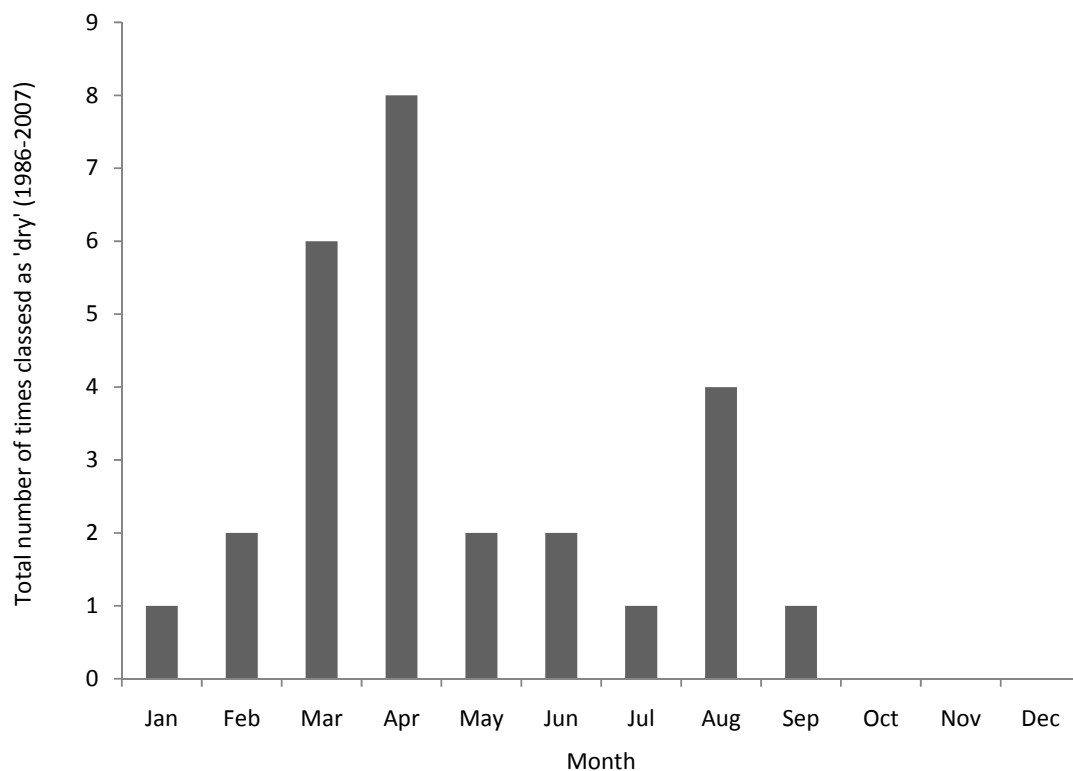
Figure 2.5   Total number of 'dry' month occurrences (defined as <100mm rainfall in a given month) for each month of the year at Danum valley (1986-2007).

Figure 2.4 gives details of monthly rainfall recorded at DVFC. Danum is intermediate in wetness between the drier east coast of Borneo and wetter regions of south western Sabah, Sarawak, and Western and Central Kalimantan. Rain falls for, on average, 218 days per year. Among other sites in North Borneo, Tawau (Southern North Borneo, Figure 2.7) receives, on average, rain 186 days per year, Kuching (Western North Borneo, Figure 2.7) 214 days per year, and Mulu (Central North Borneo, 200km SEE of Miri, Figure 2.7) 275 days per year (Walsh, 1982).
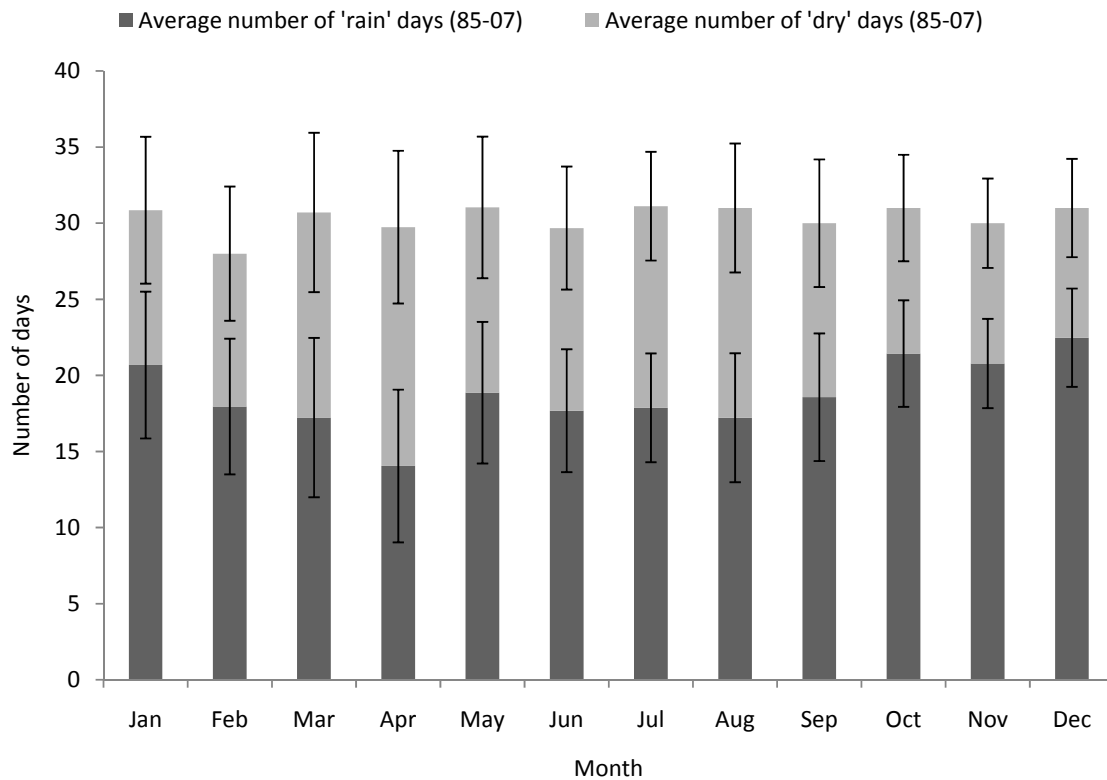
Figure 2.6   Average number of 'wet' and 'dry' days (< 1mm and >1mm of rainfall in a given day, respectively) at Danum Valley for each month (1985-2006). Error bars show standard deviation of yearly values for each month.

Ecoclimatology of Danum within the context of the humid tropics

The degree of continuity of wetness of a rainfall regime can be assessed using the perhumidity index (Walsh, 1992, in Walsh & Newberry, 1999) in which months averaging 100mm or greater are ascribed positive scores, and dry months with less than 100mm negative scores. Rainforest locations have scores ranging from +4.5 to +24. By global standards, Danum, with a perhumidity index of 20, is classified between the 'wet' (perhumidity index of 10-19.5) and 'super-wet' (20-24) classes of system based on this index (Walsh, 1996). Perhumidity index values over most of Borneo are 20-24, but some east-coast stations have values less than 15. The drought

duration magnitude-frequency of Danum Valley (Danum, Figure 2.7) is compared with that of other Neotropical sites in Figure 2.7.
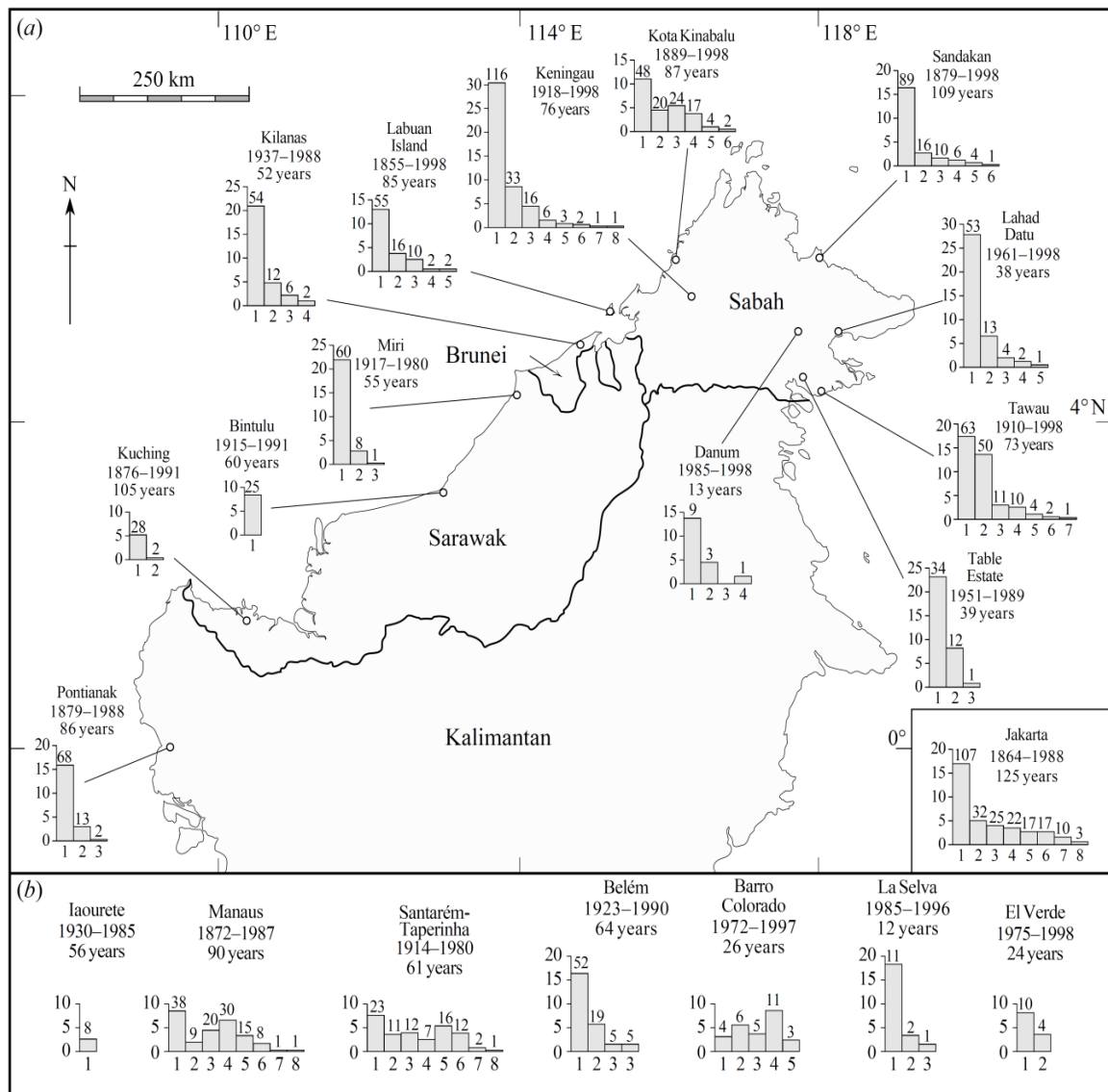
Figure 2.7   The drought duration magnitude-frequency (a) in Northern Borneo and (b) at Neotropical locations in Amazonia (Laourete, Manaus, Santarem-Taperinha, and Belem), Panama (Barro Colorado Island), Costa Rica (La Selva) and Puerto Rico (El Verde). Vertical axis: frequency per 20 years; horizontal axis: drought duration (successive months with < 100mm) in months. The numbers above each bar are the total number of droughts of that duration recorded in the entire record. Record dates and durations are also presented under site names (reproduced from Walsh & Newberry (1999)).

Introduction

Measurements of micrometeorological (humidity, air temperature, wind direction, wind speed, surface temperature, incoming longwave and shortwave radiation and surface albedo), hydrological (sap velocity, rainfall, through fall, stemflow understorey evapotranspiration), and biodynamic (tree basal area, density, crown exposure, crown area, canopy gap fraction and ground cover proportion) variables were made within the Wawasan Bentar swidden and its adjacent forest (Figures 2.1 and 2.2) between 1st April and 1st October 2007.

Issues of direction, scale, and distance

Meteorological methods for estimating forest water flux to the atmosphere generally require a fetch (distance into the forest from its border with the swidden) of 10 tree heights or more (i.e. about 220m in this study). In the case of edge effect studies, the influence of distance from the forest edge (fetch) upon meteorological variables such as water flux (i.e. forest evapotranspiration) is precisely the subject of the research. For this reason it was ensured that the set of methods employed in this study could be applied with equal reliability anywhere in a forest patch, regardless of the distance from the forest edge. These methods involve delineating the area over which a water flux is measured: TDPs, throughfall gauges and closed flux chambers all work within enclosed spaces (tree xylem elements, collecting vessels, and a plastic chamber, respectively), delineating the area over which a water flux is measured, and so are not biased by the distance they are positioned in from a forest edge.

'Top-down' and 'bottom-up' measurements were made. Top-down measurements address the land surface as a whole (e.g. an area of forest) from a remote position, such as a tower, which sits over, and 'looks down' onto, the land surface below. Bottom-up measurements are made upon individual land surface components (such as individual trees and plants) at a series of points within a given area, and grouped in order to represent the land surface as a whole. Top-down measurements can be somewhat redundant, and bottom-up measurements can be somewhat incomplete. As a result, a combination of top-down and bottom-up measurements were employed in this study to compensate for each other's aforementioned limitations.

Chapter 2: The Hydrometeorology of a Humid Tropical Forest Patch –Methods

Top-down measurements

The effective land surface of tropical forest is its canopy, which is typically situated between about 20-50m above the ground. The forest canopy receives 90% of the net radiation that provides energy to forest water transport. Thus, top down micrometeorological measurements of forest atmosphere hydrometeorological interactions must be made at a height above that of the functional surface (i.e. the forest canopy) in a remotely-sensed fashion. Top-down 'bulk' measurements of land surface kinetics (air composition and movement: relative humidity, air temperature, wind speed, wind direction) and the available energy at the land surface (net radiation, comprising an energy balance of incoming and outgoing longwave and shortwave radiation) were made using meteorological masts designed and built by the author. Meteorological masts were mounted in emergent trees at a height of 26 metres so that the top of the mast penetrated the 22 metre-high canopy (i.e. the effective land surface) by approximately 4 metres (+/- 50cm). Emergent trees were selected to ensure masts could be installed at an appropriate distance into the forest edge in a secure manner. Meteorological instruments were mounted on a horizontal 'T' section running perpendicular to the upright aluminium pipe of each meteorological mast. Surface temperature measurements were made with an infra red thermometer (IRT) mounted on the mast so that it pointed down on the canopy below. This was used to calculate outgoing longwave radiation, and also acted as a proxy for latent heat flux from the forest canopy below. In the swidden, micrometeorological measurements were made on a small tower at a height of 3 metres.

Bottom-up measurements

Whereas the hydrometeorological interaction between the swidden and its overlying atmosphere could be characterised well using a meteorological tower, the same could not be said of the forest, owing to its more complexed vegetation structure. Thus, in the forest, bottom-up 'point' measurements of individual tree water use, throughfall, stem flow, and understorey evapotranspiration were made at the ground level.

Point measurements of water movement caused by transpiration through 'canopy' trees (defined as having a crown exposure > 4, Figure 2.15, section 2.10) were made by sap flow probes inserted into the xylem of selected individual trees (Figure 2.2) at

breast height. Under-storey contributions to evapotranspiration (and thus latent heat flux) were measured at ground level through a roving chamber arrangement whereby chambers were positioned over understorey vegetation at different points. Precipitation, throughfall and stemflow measurements were also made at ground level to allow an estimation of wet-canopy evaporation, with precipitation being measured in the swidden. The combination of wet-canopy evaporation measurements with those transpiration measurements made by sap flow probes allows the estimation of latent heat flux from the forest canopy. To allow the accurate estimation of forest transpiration at the stand scale (i.e. on a ground-area basis) from TDP point measurements of tree water use, a set of forest structure measurements (tree basal area, crown exposure, tree density, canopy gap fraction and ground cover proportion) were conducted in the forest adjacent to the Wawasan Bentar swidden. The same forest structure measurements were also made at three other sites, in order to represent four distinct forest edge physiognomy types (old degraded, new degraded, old preserved, new preserved) as recorded in the literature (Harper *et al.*, 2005; Herbst *et al.*, 2007b, Laurance *et al.*, 2000).

Instrument positioning and site selection

 A measurement transect was positioned to run from the Wawasan Bentar clearing into the adjacent secondary forest. The instrumentation transect extended over 200 meters into the forest, starting about 40 metres into the swidden, running through, and perpendicular to, the forest edge. Observations focussed on the south-west facing forest edge because of its distinct physiognomic boundary (a relatively high number of large trees), the high physical contrast provided by its neighbouring patch (i.e. the bare soil of the swidden adjacent to the relatively dense vegetation of the forest) and the expectation of wind blowing into the patch (as suggested by wind direction measurements made at the site before it was chosen). Measurements were taken at four study plots along the transect (A-D, Figures 2.2 & 2.8), comprising three forest sites (B-D) and one swidden site (A). The approximate distances of plots A-D are -40, < 50, 50-100 and >270 metres in from the forest edge (Figures 2.2 & 2.8). Micrometeorological measurements (longwave radiation, shortwave radiation, humidity, air temperature, wind speed and wind direction), as well as the height of each meteorological mast upon which meteorological instrumentation was mounted at each sites' measurement station (A-D), are shown in Figure 2.8. The positions of soil heat flux and soil moisture measurements are also shown in Figure 2.8, and are addressed further in section 2.5. A full list of measurements made in the field

campaign is also presented in Table 2.2, along with respective instrumentation, instrument mechanisms, manufacturers, models, and accuracies.

Other possible study sites considered were rejected due to excessively steep slope, inaccessibility (a previously chosen site had its road washed away one month after selection), and elephant activity. Automatically logged information was relayed to three solid-state data loggers (CR 1000, Campbell Scientific, UK) via three AM25T (Campbell Scientific, UK) solid state multiplexers using screened and shielded waterproof cable (2508680806, Radiospares, UK). All automated equipment was sampled every 10 seconds and averages recorded every 10 minutes, with the exception of fine wire thermocouples, which were sampled and recorded at 10Hz. Data were resampled to a common 30-minute time vector to allow comparisons on a half-hourly basis. Data was uploaded to a portable laptop on a weekly basis via a PCIA card and adapter (CFM100, Campbell Scientific). Power was supplied by a 450 Ah (3 x 150 Ah) battery bank present at each station.

schematic diagram of meteorological mast/tower

| tower(3m) | mast(26m) | mast(26m) | | mast(26m) | tower/mast and measrurement height (z) |

| A | B | C | | D | plot |

| Swidden (-40m) | \| Forest Edge (50m) | Extent of Edge Influence \| (100m) | | Forest Interior (>270m) | category distance of tower/mast into forest |

displacement height (d)

Measurement	Term
Infrared surface temperature	(T^*)
Incoming shortwave radiation	$(S_{incident})$
Incoming longwave radiation	$(L_{incident})$
Reflected shortwave radiation	$(S_{reflected})$
Horizontal wind direction	(V)
Horizontal wind speed	(U)
Wet bulb temperature	(T_w)
Dry bulb temp	(T_d)
Soil moisture	$(\emptyset)$
Soil heat flux	(G)
Soil temperature gradient	(T_{soil})
Rainfall	(P)

direct measurement   presumed homogenous over domain   estimated

Figure 2.8 The position and height of meteorological measurements made along the measurement transect, and the distance from the forest edge that defines each plot (A-D). Where direct measurements were not possible, variables were either presumed homogeneous across the domain (i.e. the measured value is assumed to be the same for each station), or are estimated from the literature (green boxes). Also shown is a schematic of displacement height (d= 0.67 * vegetation height) along the transect path from swidden to forest, and the assumed extent of edge influence in this study. Within the displacement height box, a theoretical gradient of magnitude of edge effect (MEI) is shown from the swidden into the forest interior from the forest edge. The point where the gradient returns to that colour of the forest interior (i.e. light grey) denotes the theoretical extent of edge influence (EEI) and a MEI value of zero.

Variable/Term	Instrument	Model	Mechanism	Accuracy
$L_{incident}$	Pyrogeometer	CG3[a]	Thermopile	10%
T*	Infrared Thermometer	irT/c.5[b]	Thermopile	0.1 C/
	(Instantaneous Field of View = $5m^2$)			
$S_{incident}$	Pyranometer	SKS1110[h]	Thermopile	2%
$S_{reflected}$	Pyranometer	SKS1110[h]	Thermopile	2%
T_{air}	Fine-wire Thermocouple	SXCSS[c]	Seebeck effect	0.1
Q_{air}	Fine-wire Thermocouple	SXCSS[c]	Seebeck effect	0.1
RH	Hobo Pro Datalogger	H08-032-08[g]	Thermistor	3%
T_{air}	Hobo Pro Datalogger	H08-032-08[g]	Hygrometer	0.4 F
U	Anemometer	A100R[d]	Switch-closure	$0.1ms^{-1}$
V	Wind Vane	WP200[d]	Potentiometer	1%
$\emptyset_v$	Soil Moisture Probe	MLX2[e]	Dielectric Potential	$0.05m^3m^{-3}$
$\emptyset_m$	Mass balance	-	Pressure transducer	0.01g
ρ_b	Mass Balance	-	Pressure transducer	0.01g
G_{8cm}	Soil Heat Flux Plate	HFP01[j]	Thermopile	20%
SF	Thermal Dissipation Probe	Granier(1985)[c,i]	Differential Seebeck effect	0.2
Tsoil	Averaging Thermocouple	-[c]	Parallel Seebeck effect	0.3
P	Rain gauge	AGR100[f]	Tipping Bucket Switch- closure	4-8%
TF	Throughfall gauge	-	Volumetric storage	0.01mm
SF	Stemflow gauge	Plastic pipe	Volumetric storage	0.01mm
LAI	Hemispherical photo	HEMIPHOTO	Photo/Fish-eye lens	SD
PAR	Quantum sensor	SKP215[e]	Thermopile	2%
GBH	Tailor's tape/Callipers	-	Scale measurement	0.1/0.01
D_x	Thermal Dissipation Probe	Holburn-Brooks[c,i]	Visual interpretation	0.2
Fucover	Cross-wire sighting tube	-	Count intersections	SD

Manufacturers: (a) Kipp and Zonnen Ltd., (b) Exergen Ltd. , (c) Omega Engineering Ltd., (d) Vector Instruments Ltd., (e) Delta-T Services Ltd., (f) Environmental Monitoring Systems Ltd. Incorp Systems Inc., (g) Onsetcomp Inc., USA, (h) Skye Instruments Ltd., (i) built by author, (j) Campbell Scientific Ltd.

SD Denotes standard deviation

Table 2.2: Overview of measurement instrumentation manufacturer, model, mechanism, and accuracy for each variable measured in this study.

Hydrometeorological terms and the manner of their calculation or estimation are detailed below. Wherever it was not possible to make direct measurements of a given variable, this section states how values have been estimated from the literature or have been estimated for a particular transect position using measurements made elsewhere along the transect (see also Figure 2.8).

Net radiation and available energy

Measurements of incoming longwave ($L_{incident}$) and shortwave radiation ($S_{incident}$), canopy surface temperature (T*), reflected shortwave radiation ($S_{reflected}$) and emitted longwave radiation ($L_{emitted}$) are made or estimated at each transect location to describe the land surface energy balance (Figure 2.8). Incoming long and shortwave radiation is presumed homogeneous across the domain, and hence sampled only once (Figure 2.8). Net radiation (Rn) at the land surface can be calculated as follows:

$$Rn = S_{incident} - S_{reflected} + L_{incident} - L_{emitted} \qquad [W\ m^{-2}] \qquad (Equation\ 2.1).$$

Emitted longwave radiation is estimated from the surface temperature (T*, the 'surface' being either the swidden ground or forest canopy) combined with the Stefan-Boltzmann constant (σ), assuming an emissivity (ε) of 0.98 (following Gash &Shuttleworth, 1991):

$$L_{emitted} = \varepsilon\ \sigma\ T^{*\ 4} \qquad [W\ m^{-2}] \qquad (Equation\ 2.2).$$

Albedo (α) can also be calculated.

$$\alpha = \frac{S_{reflected}}{S_{incident}} \qquad [-] \qquad (Equation\ 2.3).$$

The available energy (A) to the land surface can be calculated where the ground heat flux (G), is known:

$$A = Rn - G. \qquad [W\ m^{-2}] \qquad (Equation\ 2.4).$$

Under forest canopies, soil heat flux (*G*) is considered not to be a large or important component of the energy balance and was assumed to be 10% of the net radiation (following Cox *et al*., 1998). However, in sparse canopy areas such as the swidden, this term becomes significant and must be measured (Figure 2.8). This was measured

using three heat flux plates (8cm depth) and three 'type E' thermocouples (4cm depth) wired in parallel in an equilateral triangular configuration.

Soil heat flux (G) is calculated by adding the measured differential of soil temperature(δT_s) at a fixed depth (d) over time (t) to the energy stored in the layer above the heat flux plates (S) for a given specific heat capacity of the soil (C_s). The heat capacity of the soil is calculated by adding the specific heat of the dry soil (C_d) to that of the soil water (C_w). The heat capacity of the moist is calculated as:

$$C_s = \rho_b \left(C_d + \text{\O}_m\, C_w \right) = \rho_b\, C_d + \text{\O}_v\, \rho_w\, Cw,$$ $[J\ kg^{-1}\ K^{-1}]$ (Equation 2.5),

where:

$$\text{\O}_m = \frac{\rho_w}{\rho_b \text{\O}_v}$$ $[cm^3\ cm^{-3}]$ (Equation 2.6).

The term (ρ_b) represents soil bulk density, (ρ_w) the density of water, ($\text{\O}_m$) soil water content on a mass basis, and ($\text{\O}_v$) soil water content on a volume basis. Gravimetric soil water content was calculated from measurements of volumetric soil moisture combined with measurements of bulk density (ρ_b) value:

$$\rho_b = \frac{Volume\ of\ dry\ soil\ \ x\ Volume\ of\ Rocks}{Mass\ of\ dry\ soil - Mass\ of\ Rocks}$$ $[g\ cm^{-3}]$ (Equation 2.7).

The storage term and soil heat flux are calculated as follows:

$$S = \delta T_s C_s\ \frac{d}{t}$$ $[-]$ (Equation 2.8),

and:

$$G = G_{8cm} + S$$ $[W\ m^{-2}]$ (Equation 2.9).

Partitioning of available energy: sensible and latent heat fluxes

The partitioning of available energy for each transect position was determined via recorded statistics of wet and dry bulb air temperature spectra sampled at 10Hz. These provide measurements for the estimation of sensible and latent energy exchanged between the land surface and atmosphere, respectively. Wind speed is measured at each station to permit the estimation of aerodynamic conductance.

Surface Renewal Analysis (SRA, Kyaw *et al.*, 1995) provides a low-cost, height-independent (Castellvi *et al.*, 2002) low-maintenance, robust, repeatable, versatile and mobile method of estimating sensible and latent heat fluxes (Duce *et al.*, 1997;

Snyder *et al.*, 1997; Spano *et al.*, 1997a, 1997b, 2000a, 2000b). SRA requires the high frequency measurement of the desired scalar at one point. As long as measurement frequency is of sufficient resolution to represent scalar spectra (2Hz measurements are sufficient over forest (Castellvi, 2004)), this method is independent of levelling and shadowing, and does not require repeated measurements at different heights. Importantly, it lends itself well to conditions where fetch assumptions are not met, owing to the physical basis of its temperature–ramp calculations (Castellvi *et al.*, 2006).

Using data obtained from spectra traces of temperature (T) and water specific humidity (q), latent (λE) and sensible (H) heat fluxes can be estimated as follows (Castellvi *et al.*, 2006; Snyder *et al.*, 1997):

$$H \; = \; (\alpha u \; z) \rho C \; p \frac{A_\lambda \; T}{\tau \; t} \qquad\qquad [W \, m^{-2}] \qquad\qquad \textit{(Equation 2.10).}$$

$$\lambda E \; = \; \lambda \, (\alpha u \; z) \; \frac{A_\lambda \; q}{\tau \; t} \qquad\qquad [W \, m^{-2}] \qquad\qquad \textit{(Equation 2.11).}$$

Terms (A_λ) and (τ) represent, respectively, the mean ramp amplitude and frequency of the given scalars. The term (αu) accounts for the uneven amount of the scalar from the measurement height to the ground. Determination of ramp parameters follows that of Van Atta (1977):

$$S^n_{(r)} = \sum^m_{i=1+j} (T_i\text{-}T_{i\text{-}j}) \qquad\qquad [\text{-}] \qquad\qquad \textit{(Equation 2.12),}$$

where *m* is the number of data points in the 30-minute interval measured at frequency (*f*) in Hz, (n) the power of the function, (j) a sample lag between data points corresponding to a time lag (r= j/f), and (T_i) the ith temperature sample. An estimate of the mean value for A_λ is determined by solving the following equation for real roots:

$$A_\lambda{}^3 = pA_\lambda + q = 0 \qquad\qquad [°C, K] \qquad\qquad \textit{(Equation 2.13),}$$

where:

$$p = \frac{10 \, S^3_{(r)} - \; S^5_{(r)}}{S^3_{(r)}} \qquad\qquad [\text{-}] \qquad\qquad \textit{(Equation 2.14),}$$

and:

$$q= 10S^3{}_{(r)} \qquad\qquad [\text{-}] \qquad\qquad \textit{(Equation 2.15).}$$

According to Chen *et al.* (1997), the relationship between the inverse ramp frequency (τ) and ramp amplitude is:

$$\frac{A_\lambda}{\tau^{1/3}} = -\gamma \left(\frac{S^3_{(rx)}}{r_x}\right)^{1/3} \qquad\qquad [-] \qquad\qquad (Equation\ 2.16).$$

The micro-front period (L_f) is given by:

$$L_f = \left(\frac{\gamma}{2}\right)^{1/2} r_x \qquad\qquad [Hz] \qquad\qquad (Equation\ 2.17).$$

(r_x) denotes the time lag (r) that maximises ($S^3_{(r)}/r$) and γ is a parameter that corrects for the difference between $A_\lambda/\tau^{1/3}$ and the maximum value of ($S^3_{(r)}/r$) $^{1/3}$.

2.6   PRECIPITATION, THROUGHFALL AND WET-CANOPY EVAPORATION

Precipitation (P) was measured with a tipping bucket gauge in the swidden. Total latent heat flux of a vegetated surface can be broken into 'wet' (evaporative, E_{wet}) or 'dry' (transpirative, $E_{transpiration}$) components:

$$\lambda E_t = E_{transpiration} + E_{wet} \qquad\qquad [W\ m^{-2}] \qquad\qquad (Equation\ 2.18).$$

E_{wet} can be estimated using Rn (i.e. available energy at the land surface, A) from the Penman (1948) open water equation:

$$\lambda E_{wet} = \frac{\gamma}{\Delta + \gamma}\ (A) \qquad\qquad [W\ m^{-2}] \qquad\qquad (Equation\ 2.19).$$

The influence of transpiration ($E_{transpiration}$) rates at forest edges upon λE_t could be negated by an equal and opposite response of the equivalent wet canopy evaporative component (E_{wet}). Klaassen *et al.* (1996) have already shown that the evaporative component of wet canopies is not affected by fetch at temperate forest edges, and this is supported by other studies (Neal *et al.*, 1993). No study has been conducted to confirm that this is the case for tropical humid forests. Wet canopy evaporation was estimated at the site by measuring throughfall and stemflow as a fraction of total incoming precipitation. Throughfall was monitored by roving homemade collectors and stemflow stations. 20 throughfall gauges were placed at distances of 30 (microplot BA), 50 (microplot BB), 80 (microplot CA), 100 (microplot CB), 150 (microplot DA) and 300m (microplot DB) into the forest from its boundary with the Wawasan Bentar swidden. The first letter (B-D) of each microplot name reflects the position of that microplot within the larger forest plots (B-D) detailed earlier, with the second letter (A or B) denoting which of the two microplots is closest (A) or furthest (B) from the forest edge. 20 gauges were deemed sufficient to capture the variation in *Macaranga spp.* - dominated forests (*cf.* Bidin & Chappel, 2003).

Throughfall measurements were made in a roving fashion, with collectors being moved within a 2m x 2m subplot after each collection. Measurements of precipitation were made in the adjacent clearing until 7th October 2007. A simple rainfall collection gauge was used thereafter, owing to the destruction of the tipping bucket gauge by elephants. Throughfall was measured between 1st January and 28th February 2008.

Wet canopy evaporation (E_{wet}) on a volumetric basis was determined as:

$$E_{wet} = P - (TF + SF) \qquad [mm] \qquad (Equation\ 2.20),$$

where throughfall (TF) was calculated based on the area covered by throughfall gauges (A_{TF}), ground area (A_{ground}), and the volume of water collected in the throughfall gauges (V_{TF}):

$$TF = \frac{A_{ground}V_{TF}}{A_{guages}} \qquad [mm] \qquad (Equation\ 2.21).$$

Stemflow (SF) was calculated using the volume of stemflow collected (V_{SF}) over a ground area (A_{ground}) for a number of trees (n) of given basal area (BA_{tr}) representing a proportion of the total stand basal area (BA_{stand}):

$$SF = \frac{BA_{stand}}{A_{ground}} \cdot \frac{V_{SF}}{\sum_{i=1}^{n} BA_{tr}} \qquad [mm] \qquad (Equation\ 2.22).$$

The basal area of the stand (BA_{stand}) and total ground area it occupies (A_{ground}) were also measured, as detailed in section 2.10.

Introduction

Latent heat fluxes from the canopy of a transpiring forest can also be derived from total stand sap flow. This is the bottom-up equivalent to SRA, which is top-down. Thus direct measurements of sap velocity in individual trees must be scaled by the area of water-conducting tissue (xylem) in an area of forest to estimate latent heat fluxes from the forest canopy as a whole.

Sap velocity was measured with Thermal Dissipation Probes (TDPs) built by the candidate, as described in Phillips *et al.* (1996, 1999, 2001), following the original technique of Granier (1985, 1987). This method is analogous to a hot wire anemometer, where the flow of a medium passing over a heat source is estimated by measuring the cooling effect that medium has upon the heated element when compared with an unheated counterpart at ambient temperature. In this case, probes were inserted into the water conducting elements of a tree (i.e. the xylem) to measure sap flow velocity (Figure 2.9).

To heat the upper probe of a TDP pair, a constant voltage was applied to a copper wire 'resistor' coiled around the upper of the two probes (Figures 2.9 & 2.10). Power was maintained at 0.2 W by a homemade voltage regulator (Horrowitz & Hill, 1964) also built by the candidate. A differential voltage measurement between a 'type-T' (relating to its millivolt response to temperature) thermocouple in each probe (separate to the copper heating coil circuit, Figure 2.9) was used to determine the rate of sap flow depending on how much the upper needle is cooled relative to its unheated, lower, counterpart. A direct measurement of how fast the medium (sap in this case) travels can be gained through appropriate calibration, detailed later in this section. Although it is possible to send bursts of voltage and measure the decay of each 'heat pulse', a constant voltage was preferred, since 'heat pulse' measurements can be highly unreliable, especially at low sap velocities (Green *et al.*, 2003; Hatton *et al.*, 1995).

 Thermal Dissipation Probes were installed in 21 'canopy' trees (defined as having a crown exposure > 4, Figure 2.15, section 2.10) to measure sap flow (i.e. transpiration) of 10 individuals per plot (B-D); i.e. < 50, 50-100 and >270m into the forest from its boundary with the Wawasan Bentar swidden. Positions of trees monitored for sap flow are shown in Figure 2.2.
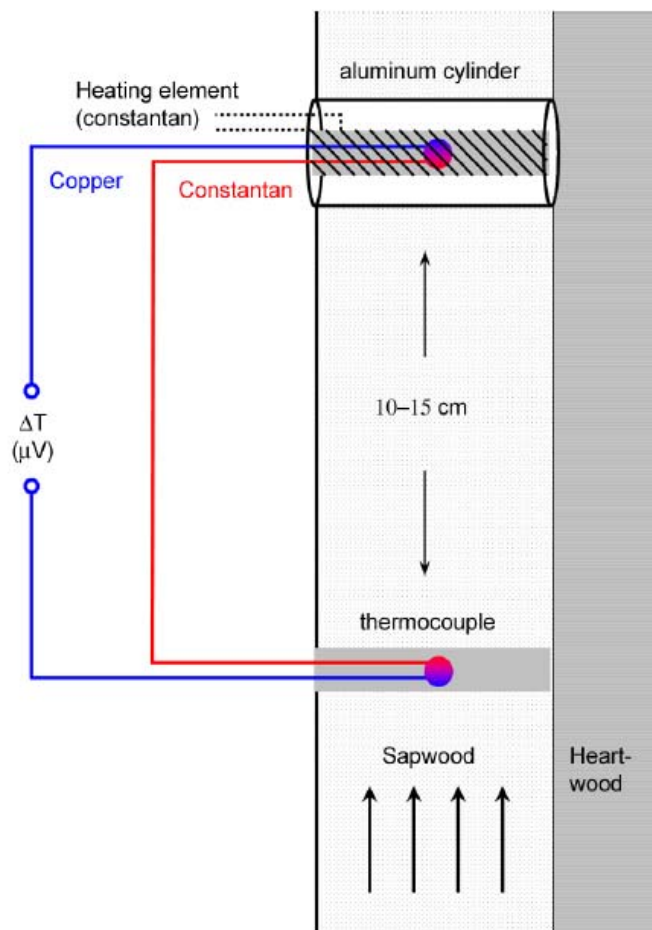
Figure 2.9   Schematic Representation of a Thermal Dissipation Probe pair, showing the insertion of a heated probed above a lower, unheated probe into the sapwood of a tree. The difference in temperature (δT, denoted ΔT in this figure) between the two probes is measured as a millivolt difference (μV) between two copper wires connected differentially via a constant/copper thermocouple junction (red-blue circles) in each probe (courtesy, Michael Clearwater, 2005).

Figure 2.10 A homemade Thermal Dissipation Probe set, comprising one heated (upper) and one ambient (lower) probe (courtesy, Michael Clearwater, 2005).

The relationship between sap velocity (v) and the measured temperature differential across a probe set described by Granier (1985) and confirmed by Clearwater *et al.* (1999) for tropical trees is as follows:

$$v = 0.0119\, k^{1.231} = 0.0119\, (\delta T_{max} \frac{-\delta T}{\delta T max})^{1.231} \qquad [cm\, dy^{-1}] \qquad \text{(Equation 2.23).}$$

(δT) denotes the difference in temperature between the two probes, (δT_{max}) is the value of δT when sap flow is zero (this is taken to be the average night time value of δT_{max}).

Two probe sets were installed in each monitored tree to account for circumferential gradients in sap velocity. To save on maintenance and wire costs, probe sets were connected in parallel (*cf.* Lu, 1997) to provide an average output across two circumferential positions. The necessity for wire maintenance prohibited more than two pairs of probes being installed per tree, but this is the recommended number of probes given the average diameter of measured individuals (Delta T systems, Cambs.): an excessive number of probes can severely affect sap flow (James *et al.*, 2002). Probes were covered in reflective bubble-wrap to minimize temperature effects on measurements resulting from radiation and moisture loading on the probes.

Experimental probe calibration

Although the sap-flow technique is the only practicable way to assess the variation in tree water use, in order to obtain the most accurate estimates of latent heat transfer from the canopy to overlying atmosphere, great care has to be taken in both the calibration of sap flow sensors and correcting flow measurements for azimuthal and radial variation.

In order to ensure accurate estimates of stand level transpiration and latent heat flux, the thermal dissipation probes measuring sap velocity were calibrated *in situ*. Clearwater *et al.* (1999) confirmed the original Granier (1985) calibration for various tropical tree species. It was necessary to recalibrate the probes specifically to the trees used in this study and also to account for slight differences between the probes built here and elsewhere: although the sensors were built to the exact specifications used by Clearwater *et al.* (1999) (Michael Clearwater, 2005, personal communication, University of Hawaii, USA), experimental calibration takes into account potential differences in wood and sap thermal properties typical of the study trees, and the

potential decalibration of thermocouple wire after it has been worked. Whereas Granier *et al.* (1990) asserted that the original calibration was independent of tree species. Smith & Allen (1996) have since shown that the calibration method is based on the empirical relationship between the temperature differential of the TDP and the sap flow rather than the heat transfer properties of the sap wood. Knowing this, and considering that no measurements of sap velocity have been made in *Macaranga* spp. previously, it was decided a specific calibration would be necessary.

Implicit in the design of the TDP is the integration of temperature and thus sap flow along its length. Clearwater *et al.* (1999) state that if sap velocity varies along the length of the probe, then the heat dissipation and probe surface temperature will also vary. Clearwater *et al.* (1999) proposed that the original calibration of Granier (1985) was only applicable over the sapwood area and that estimates of sap velocity should be scaled accordingly (Clearwater *et al.*, 1999):

$$\delta T_x = \delta T - \frac{A_i \delta T_{max}}{A_x} \qquad\qquad [°C, K] \qquad\qquad (Equation\ 2.24).$$

where (A_x) and (A_i) denote active and inactive xylem regions respectively. The corrected temperature difference accounting for the proportion of the probe in contact with sapwood (δT_x) is then used to calculate a corrected velocity (v_x). Sap flux can then be estimated for the whole-stand if the basal area (BA_{stand}) and ground area (A_{ground}) of the stand is known:

$$ET_{stand} = \frac{v_x \ X \ BA_{stand}}{A_{ground}} \qquad\qquad [cm^2 dy^{-1}] \qquad (Equation\ 2.25).$$

The aluminium sleeve used in the design of the TDP is used in conjunction with thermally conductive silicon lubricant to minimize temperature gradients along the probe profile and thus make the measured temperature differential between the heated and unheated probe (δT) equivalent to the mean value of the temperature profile along the probe. This is analogous to the use of heat sink chips and silicon lubricant in computer motherboards to ensure uniform heat conduction away from components. Thus, following Equation 2.24, if a portion of a probe is inserted into inactive xylem (A_i) and the remainder into active xylem (A_x) the measured δT is essentially a weighted mean of the temperature differential of the sapwood (i.e. the temperature difference caused by xylem, δT_x, Equation 2.24) and that in the non-conducting sapwood (which is assumed to be equal to δT_{max}), (Clearwater *et al.*, 1999).

The discrepancy between the actual sap flow and that calculated by a probe averaging temperature along its mean can be considerable. Clearwater *et al. (*1999) show that at moderate (0.05 mms^{-1}) and quite high (0.15 mms^{-1}) sap velocities errors can be between 8-15% and 35-52% for a= 0.9 and a= 0.5 respectively. There are two instances where the calibration of TDPS, and the sap flow measurements based upon them, can be affected by this source of error implicit in Equation 2.24. The first instance is in the calibration procedure whereby the probes are too long to be entirely in contact with active sapwood, and the second instance is in the measurement procedure where strong radial variations in sapwood velocity essentially render sections of the probe in contact with effectively active and inactive xylem regions. A third, but less likely, instance is when shallow sapwood depths mean that probes are not in full contact with sapwood *in vivo*, but this is most likely not to be the case given the great size of the trees measured in this study (Table 4.3, Chapter 4).

Heat dissipation probes were calibrated using stems from the two tree species measured in this study: *Macaranga hypoleuca* and *M. pearsonii*. Sections of stem were cut from branches with a pruning saw, brought to the laboratory, re-cut and smoothed with a razor blade. Bark was removed from near the upstream end and the stem connected to a reservoir of deionised water (rain water) using plastic tubing, hose clamps and motorcycle inner tube rubber. Two pairs of heat dissipation probes were installed on opposite sides of, and offs*et* along the length of, the stem. Probes were inserted to a depth of 20mm, with the proximal end of the heating element flush with the cambium. Power was supplied to the probes and δT_{max} recorded after reaching a constant temperature. Water was then passed through the stem by increasing the height of the water reservoir, or by applying a slight positive pressure to the reservoir for higher flow rates. Water flowing from the downstream end of the stem section was collected on a balance connected to the same data logger as the probes. The resolution of the balance was 0.01g. Mass flow through the stem was increased in steps to a high rate, and then decreased, with δT allowed to reach a constant value at each level. Flow was then stopped and δT_{max} compared with the starting value. Six probe pairs were selected at random from the full set (n = 120), and divided into two groups, with one group of three probes being tested on each excised stem. *Macaranga* species tend to have a hollow interior within both their trunks and limbs, within which ant colonies frequently nest. This was the case for the stems used in this calibration. To stop water running though this excised stem

section, a bolt was screwed into the hole, and then sealed with heavy-duty silicon sealant. Before measurements of mass were taken, water was allowed to run through for one minute to account for any capacitance associated with water filling the stem cavity initially.

For each of the 6 randomly selected calibration probes, the velocity of water (v) passing through each of the two excised stems (Table 2.2) was calculated as a function of the mass of water collected from each stem over a one-minute period divided by the area of active xylem (delineated by toluidine blue solution, which stains xylem cells blue) and δT was measured via a Campbell Scientific CR1000 data logger. δT_{max} is the temperature difference between heated and unheated probes when v = 0 and A_x is the proportion of the heated probe in contact with active xylem (Equations 2.23 and 2.24). Table 2.2 shows that both excised stems do not offer full probe contact with xylem; the theoretical influence of which upon the estimation of sap velocity is shown in Figure 2.11, which shows those proportions of A_x noted in Table 2.2, and how A_x influences the relationship between k and sap velocity to deviate from the original Granier (1985) calibration (i.e. where A_x=1). Shown in Figure 2.12 is the raw measured sap velocity (expressed as k= (δT_{max}-δT)/ δT) and the sap velocity calculated from mass flow measurements (Fd) divided by the sapwood cross sectional area (A_x, m^2) as derived from Granier (1985, 1987):

$$Fd = \frac{v}{A_x}$$ $[\ Ls^{-1}]$ (Equation 2.26)

Macaranga Species (*M.*)	Stem Diameter (mm)	δTmax (°C)	Depth of Sapwood (mm)	A_x (-)
M. hypoleuca	82	12.1	14.8	0.74
M. pearsonii	67	12.0	12.3	0.62

Table 2.3: Dimensions of excised stem segments used for the calibration tests of heat dissipation probes presented in Figures 2 and 3. δTm is the temperature difference between heated and unheated probes when v = 0 and A_x is the proportion of the heated probe in contact with active xylem (Equations 2.23 and 2.24).
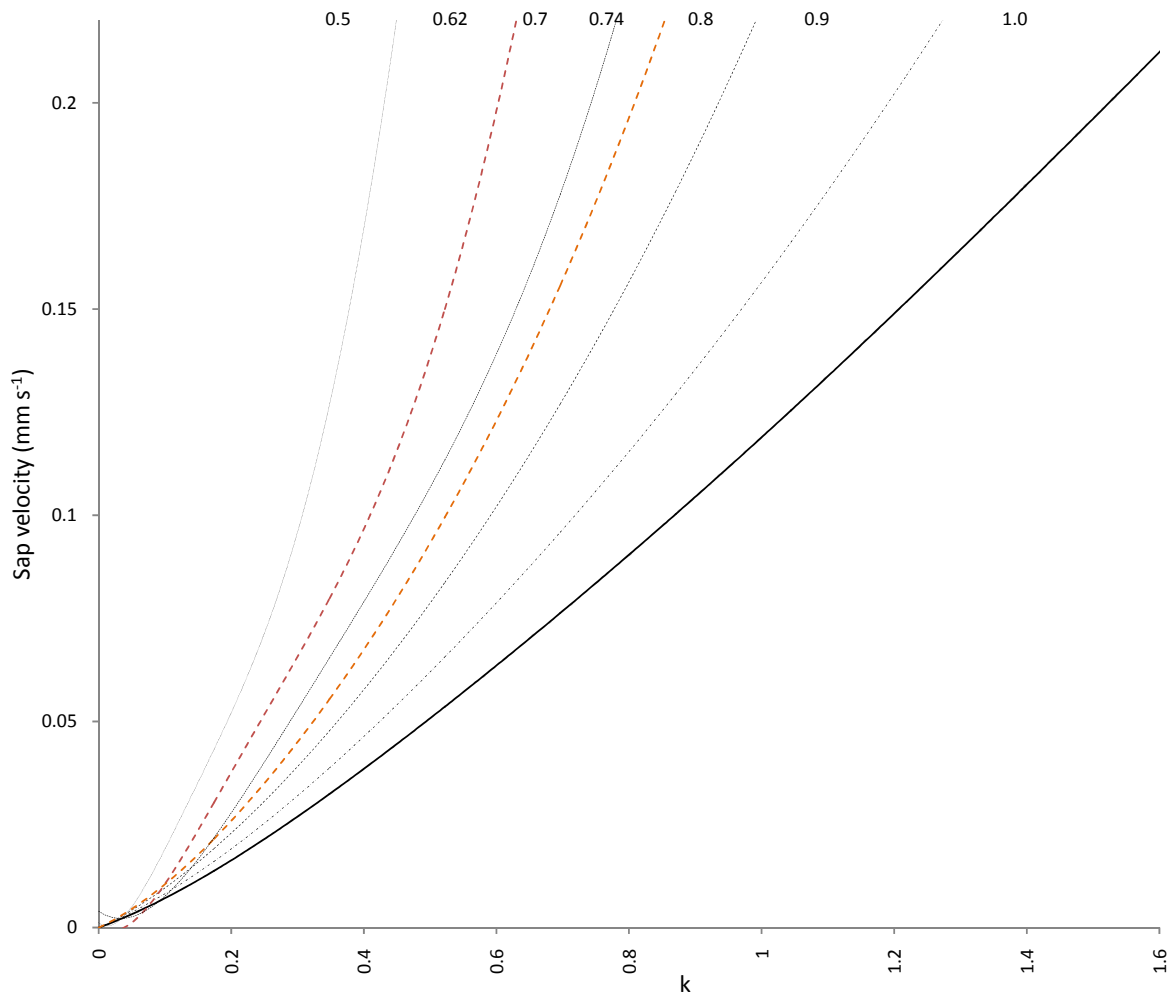
Figure 2.11 Sap velocity as a function of k (see further Equation 2.23), based on the Granier (1985) calibration and Equation 2.24, when the proportion of the probe in contact with active xylem is 1.0, 0.9, 0.8, 0.7 or 0.5. Sap velocity represents the mean value for the whole probe, including parts in non-conducting wood. Proportions calculated for those excised segments used in the calibration procedure (0.62, 0.74) are shown in red and orange respectively.
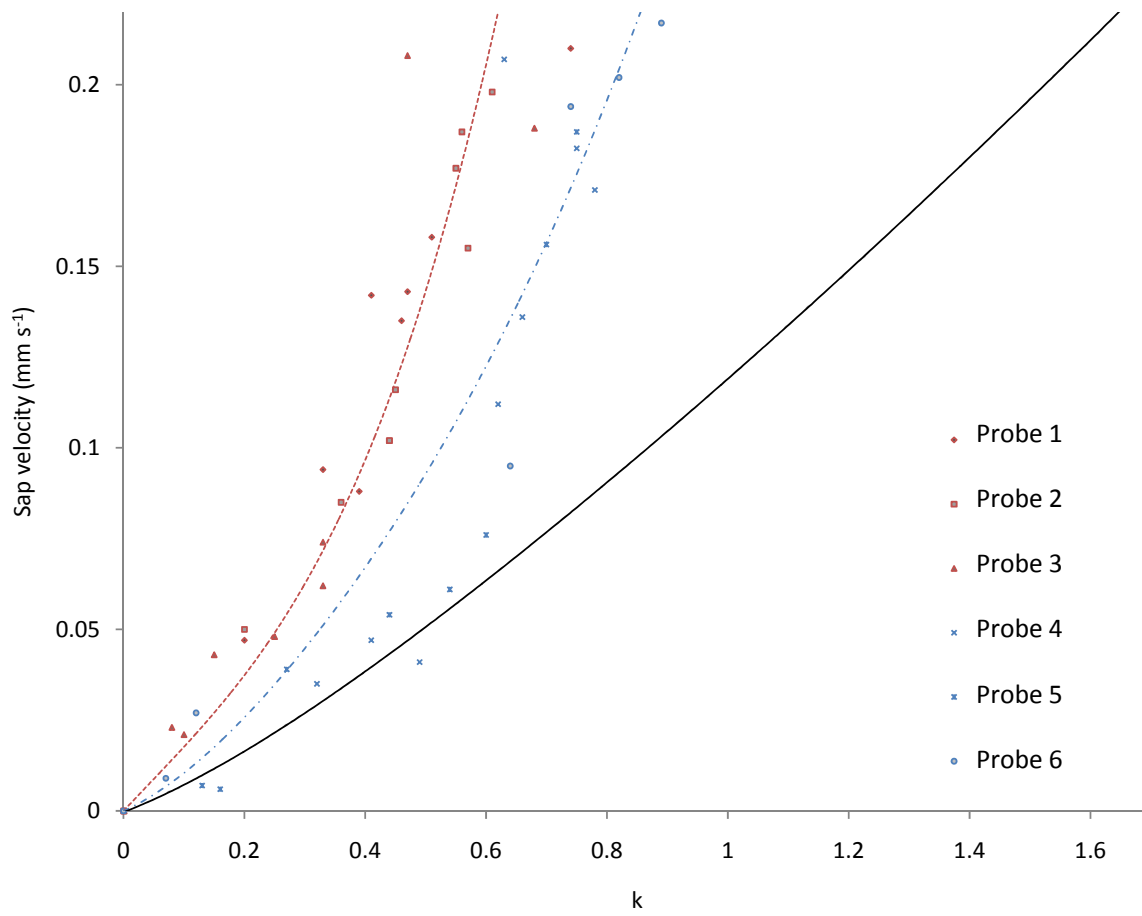
Figure 2.12 Estimation of k (see further Equation 2.23) from raw temperature data (dT) of 6 randomly selected probes (probes 1-6) as a function of actual (volumetric, following Equation 2.26) sap velocity (mm s^{-1}) for the two excised limbs used in the calibration (Table 2.3). The original Granier calibration is shown as a solid line and the expected rates for a given proportion of each probe in contact with sapwood for each limb are shown as dashed, following Equation 2.24. δTm = 12 °C.. Coloured lines represent the fit of k vs. sap velocity for those probes with data markers of the same colour.

Figure 2.11 clearly demonstrates the need to account for the proportion of each probe in contact with the sapwood in this calibration, as Table 2.2 shows the probes being calibrated are not in full contact with the xylem of each excised stem. Whereas superficially it seems that the probes do not conform to the Granier (1985) calibration (Figure 2.12), observing Figure 2.12 and Figures 2.13 a-d, it becomes apparent that the introduction of the Granier calibration as altered using Equation 2.24 to account for the proportion of TDP in contact with sapwood (dashed lines, Figure 2.12) indicates good agreement (Figures 2.13 a-d).
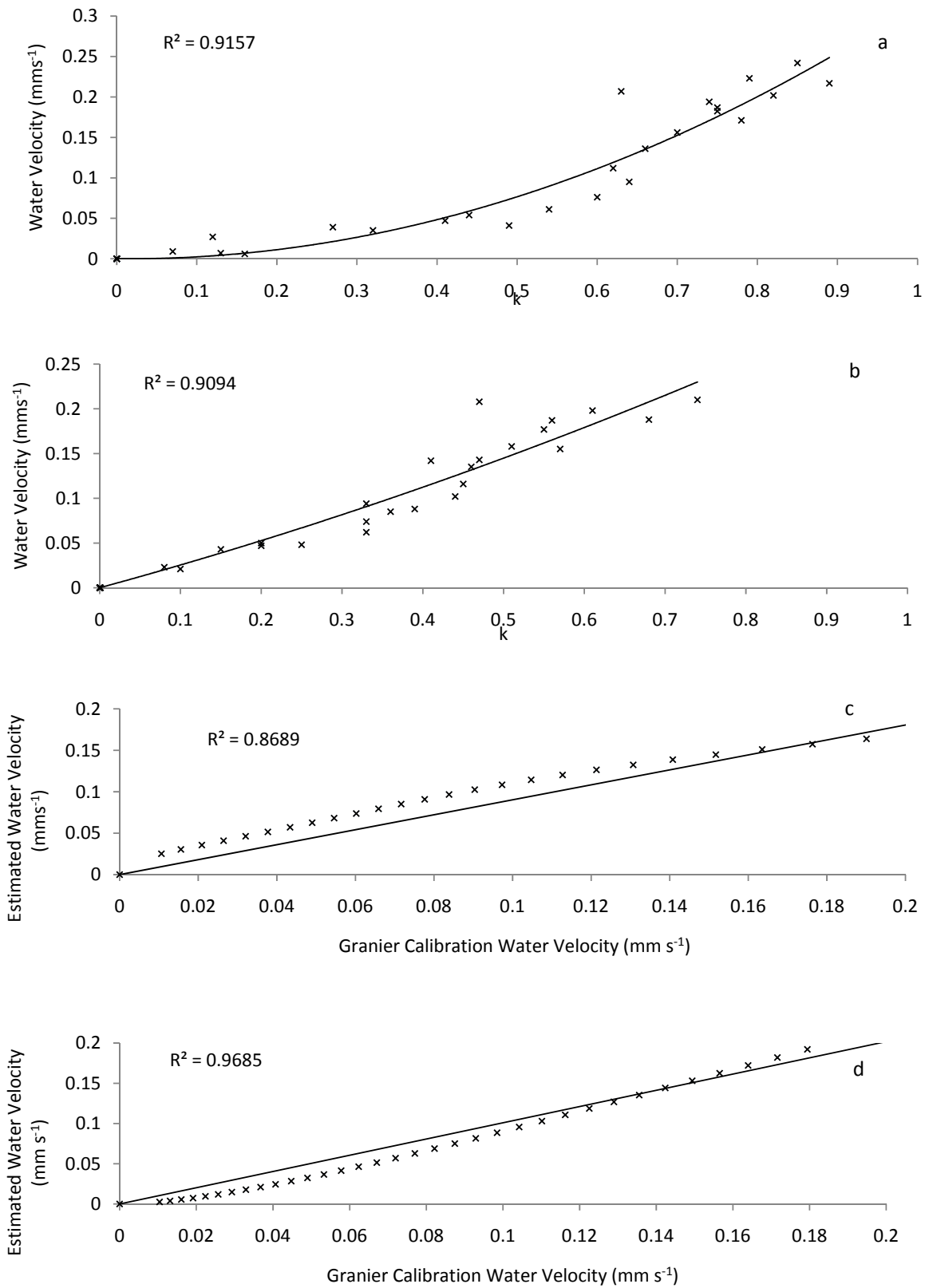
Figure 2.13 Grouped data of k (defined in Equation 2.23) as estimated from raw probe temperature (δT) vs. mass estimated sap velocity for three probes in excised a) Macaranga hypoleuca and b) M. pearsonii stems, and their respective fit with the original Granier (1985) calibration (c and d, for M. hypoleuca and M. pearsonii, respectively).

When data for each stem is grouped good repeatability is shown between probes (Figure 2.13), with tight residuals for both species (r^2= 0.92 for *M.pearsonii* and r^2= 0.91 for *M.hypoleuca* respectively). A similarly strong relationship is shown between the original Granier (1985) calibration (Figure 2.13, *M.pearsonii* r^2= 0.87, *M.hypoleuca* r^2= 0.97), and demonstrates that the calibration is indeed confirmed *when the proportion of the probe in contact with sapwood is accounted for by applying Equation 2.24*.

Given the rudimentary nature of the calibration procedure, the probes conform very well indeed to the Granier (1985) calibration. A more comprehensive calibration could have been achieved through the use of a specially-designed flow meter, but this approach (a) was unavailable and (b) would have not permitted *in situ* calibration with appropriate tree species specific to the site. A compromise was found by attaching the water reservoir to a tap to maintain the pressure in the reservoir and thus steady water velocity through the excised stem.

This analysis also demonstrates why the preference in this study was to use short probes that ensure complete contact with the sap wood. Similarly, an important point to be taken from this exercise is that it is essential to install the probes in a fashion so as that they do not make contact with the cambium of the tree. For most trees this was not a problem but some individuals had a thick cambium which was removed using a simple punch before probe installation.

Estimating sap flux density - accounting for xylem depth and radial profiles of sapwood velocity

In order to gain estimates of sap density from sap flow, the measured flow rate must be scaled across an appropriate area. This is called the 'sapwood area', which is the area of active xylem (A_X). Considering limitations associated with dyeing techniques (Clearwater *et al.*, 1999; Giambelluca *et al.*, 2003; James *et al.*, 2002), A_x was determined using a variable length probe inserted in the tree at sequential depths (5mm). Measurements of xylem depth were correlated with stem radius (SR) measurements, enabling the estimation of stand-scale transpiration (providing the total stand area is known), using the stem radius: sapwood area ratio (SR: A_{sw}). Measurements were taken throughout October 2007, in sixteen randomly selected individuals. Probes were inter-calibrated with those 2cm TDP probes used for the duration of the experiment.

However, the methodology outlined thus far assumes that sap flow density does not change with xylem depth. This has already been shown not to be the case (James *et al*., 2002). Zang *et al.* (1996) developed a correction coefficient (CC) to estimate the true sap flow velocity at each fixed sensor, which was calculated from the weighted average of the sap flow velocity ratios on the profile. Sap flow ratio (R) was calculated as the sap flow velocity measured by the moving sensors (v_m) divided by the sap flow velocity measured by the appropriate fixed sensor (v_s). For i = 1,2,3,... m, and j = 1,2,3,... ni:

$$R_{i,j} = \frac{v_m\ i,j}{v_s\ i,j} \qquad\qquad [-] \qquad\qquad \text{(Equation 2.27).}$$

where i is the position on the profile and j is an observation at that position. The average ratio at the ith position (Ri) is given by:

$$R_i = \frac{\sum_{1...ni}^{j} R_{i,j}}{n_i} \qquad\qquad [-] \qquad\qquad \text{(Equation 2.28).}$$

The data series of R_i is the profile of the sap flow ratio where n_i is the number of observations j at each position i. A correction coefficient (*CC*) to estimate the true sap flow velocity at each fixed sensor was calculated from the weighted average of the sap flow velocity ratios on the profile. The ratios were weighted by the areas (*Ai*) represented at each position. Because the distance (*d*) between positions on the profile was constant, *Ai* is half the area of a ring of radius $r_{p,i}$ measured to the centre of the stem. Thus:

$$A_i = 0.5p((r_{p,i} + 0.5d)^2 - (r_{p,i} - 0.5d)^2) = prp,\ id \qquad [mm^2] \qquad \text{(Equation 2.29),}$$

and the total conducting area *A* is calculated thus:

$$\sum_{i=1}^{m} A_i = \pi d \sum_{i=l}^{m} p,r_i \qquad\qquad [mm^2] \qquad\qquad \text{(Equation 2.30).}$$

The weighting factor (w_i) for each position on the profile was calculated as:

$$w_i = \frac{A_i}{A} = \frac{r_{p,i}}{\sum_{i=1}^{m} r_{p,i}} \qquad\qquad [-] \qquad\qquad \text{(Equation 2.31).}$$

Thus, the correction coefficient (*CC*) of the static sensor is expressed as:

$$CC = \sum_{i=1}^{m} (r_i w_i) \qquad\qquad [-] \qquad\qquad \text{(Equation 2.32).}$$

If v_k is the sap flow velocity observed at a static sensor k and n is the number of static sensors, during routine measurements, the average sap flux (v_a) in the sapwood is calculated as follows:

$$v_a = \frac{\sum_{k=1}^{n} C_k v_k}{n} \qquad\qquad [mm\ dy^{-1}] \qquad\qquad \text{(Equation 2.33).}$$

The use of a correlation coefficient is dependent on there being a consistent relationship between sap velocities measured by the reference probe and those measured in the profile. This has been demonstrated to be the case for a wide variety of tree species such as *Eucalyptus globulus* and *Pinus* spp.

Data pre-processing

Data pre-processing and analysis was conducted using MATLAB. Data were pre-processed to remove exceptionally low-rate readings and spikes, and to account for the effects of voltage drift. Voltage drift occurred as a result of the use of lorry batteries, which are not designed to cope with large discharges over a long period of time, and therefore gradually deteriorated, as it proved impractical to replace the batteries at a frequency that would avoid heavily discharging the batteries (called 'deep-cycling'). Batteries capable of 'deep-cycling' were not available in Malaysia and could not be shipped to the site. This problem is common, however, regardless of the batteries used, and a commonly-accepted practice is to adjust the value of δT_{max} to account for drift in the voltage. This was achieved by incorporating a section within the main analysis programme that recalculated δT_{max} automatically each day. Such a measure is sufficient since voltage drift tended to occur over a much longer period of time.

Data spikes were common and were removed using a simple filter that excluded any readings of sap velocity which increased by more than 0.1 mm s^{-1} 30 min^{-1}. Data points fitting this criterion were replaced with 'not a number' (NAN) markers and subsequent calculations were made ignoring such NANs.

Introduction

Under-storey evapotranspiration (Et_u) was estimated using bulk resistance values derived from closed flux chamber (CFC) measurements, owing to its increased practicality of use in dense jungle and rapid measurement nature when compared with open-chamber alternatives. Measurements were made during six days in September 2007, with measurements been made in a relatively dry and wet periods for three days each. A method of estimating the latent heat flux from short crops using closed flux chambers was proposed by Kohsiek (1981), combining meteorological and chamber-derived parameters to elucidate a surface resistance value from the Penman-Monteith (1965) equation.

Measurements were made on plots containing two types of ground cover: leaf litter and short plant communities (0.3-0.8m tall). These cover types were estimated to represent more than 70% of the ground cover. Each understorey plot covered an area of 0.64 m^2 with two replicates for each groundcover at each of the main measurement plots, giving a total of four circular plots per edge stratum. Measurements were made every hour from 10:00 to 16:00 hours to obtain representative day-time averages. The chamber used had a volume of 0.82 m^3 and consisted of a clear plastic sheeting body 0.65m diameter and 1.29m high, supported by four narrow PVC ribs. The chamber was axially tapered and housed four 12V computer cooling fans mounted midway up the chamber to encourage mixing of air. A Vaisala HM70 probe was mounted in the top of the chamber to measure specific humidity and air temperature. A schematic of the chamber is presented in Figure 2.14.

Chapter 2: The Hydrometeorology of a Humid Tropical Forest Patch –Methods

1.29 m
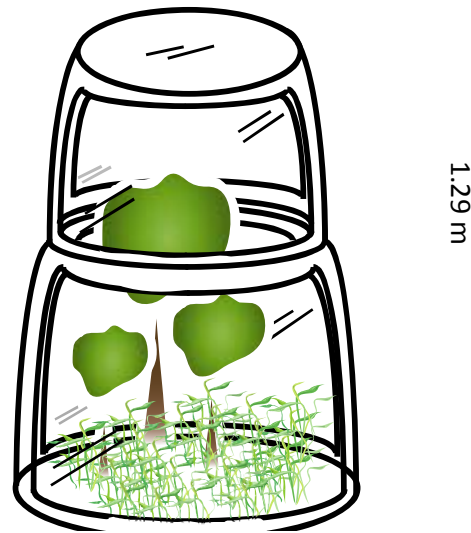
Figure 2.14   The Closed Flux Chamber (CFC) fits over small saplings and grasses.

After each measurement (3 min), the CFC was removed from the plot to prevent long-term changes to the microclimate of the plot. It is assumed that during the measurements the surface temperature is constant, and that both sensible and latent heat from the understorey is stored in the air inside the chamber. The temperature of the air as a function of time is then given by:

$$T(t) = T^* - [T_a - T^*] \, exp^{\frac{-t}{\tau_h}} \qquad\qquad [°C, K] \qquad\qquad (Equation\ 2.34),$$

Where:

$$\tau_h = r_h \frac{V_{chamber}}{A_{chamber}} \qquad\qquad [s] \qquad\qquad (Equation\ 2.35).$$

(r_h) represents the aerodynamic resistance for the heat transport from the leaf surfaces to the temperature sensor inside the chamber of volume ($V_{chamber}$) covering area ($A_{chamber}$). The absolute humidity as a function of time ($q_v(t)$) is:

$$q_v(t) = q_{vs}(T^*) - [T_a - q_v\, T^*] \, exp^{\frac{-t}{\tau_h}} \qquad [kg\ m^{-3}] \qquad (Equation\ 2.36),$$

where:

$$\tau_v = (r_v + r_{st}) \, r\frac{V}{A} \qquad\qquad [s] \qquad\qquad (Equation\ 2.37).$$

It was assumed that T* was equal to T_{air}, following those guidelines presented in Kohsiek *et al.* (1981). An estimate of surface resistance can be thus obtained from wet and dry bulb temperatures measured within the chamber, or alternatively the direct water flux can be obtained from integrating the absolute humidity curves. The method was compared with estimates of water loss from an evaporation pan, and a good agreement was found between the estimated and actual loss over a 1 hour period. PAR measurements were also made inside and outside the chamber, and it

was found that the light levels in the chamber were within 98% of those outside the chamber for typical under-storey light conditions.

2.10   FOREST VEGETATION STRUCTURE AND WITHIN-CANOPY MICROCLIMATE

Vegetation parameters were measured within 27 randomly located microplots of 5.5 x 5.5 metres each in each of the distance strata defined by plots B-D. This represents 2500 m^2 in each distance stratum. In each microplot the number and diameter breast-height (dbh, diameter at 1.3m) of all trees and lianas (>2cm dbh) were recorded. Vegetation less than 1.3m tall was not measured for DBH, as scaling for this vegetation type was conducted on a percentage basis by estimating the fractional coverage of three types of ground cover using the canopy scope as a cross-wire sighting scope (Hutley *et al.*, 2000, 2001). The communities measured were leaf litter, bare ground and vegetation (0.3-0.8m tall). The total basal area of a stand (BA$_{stand}$) can be estimated from diameter breast height (dbh) measurements used to derive tree radius (r):

$$BA_{stand} = \sum_{1...n}^{n} \pi r^2 \qquad\qquad [m^2] \qquad\qquad (Equation 2.38).$$

The total area of xylem for a stand of trees can be estimated if the total basal area of the stand is known, as Giambelluca *et al.* (2003) and Meinzer *et al.* (2001b) have shown for numerous tropical tree species that there is a constant, linear, relationship between the radius of a stem (r$_{stem}$) and its depth of active xylem (D$_x$). It thus follows that:

$$A_x = x + y\ r_{stem} \qquad\qquad [cm] \qquad\qquad (Equation 2.39).$$

To this end, a site specific calibration of equation 2.39 was made using a specially designed variable length thermal dissipation probe following the design of James *et al., (*2002).

Canopy illumination and gap fraction

A Canopy Illumination Index was also recorded for all trees using a modified version of that presented by Clark and Clark (1992), as defined in Figure 2.15.
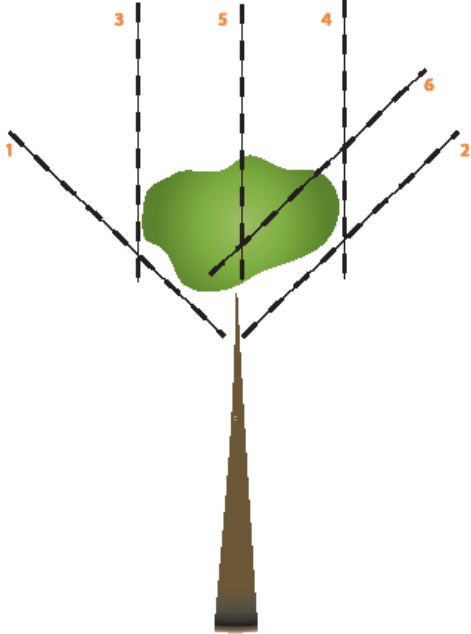
Index value	Definition of Canopy Illumination Class	Visual Reference
5	Completely exposed to light from that part of the sky circumscribed by a 45_ zenith angle **(1-2)**	
4	Full overhead light. Lateral light blocked within part of the sky circumscribed by a 45_ zenith angle **(1-6)**	
3.5	> 90% vertical light **(3-4)**	
3	Some overhead light (50-90 % exposed to vertical light) **(3-5)**	
2.5	High lateral light (from one major or multiple medium-sized gaps)	
2	Medium lateral light **(5-6)**	
1.5	Low lateral light (no large or medium-sized gaps) **(2-6)**	
1	No direct light	

Figure 2.15 A schematic defining the crown illumination index (following Clark & Clark. 1992). Red numbers in brackets under 'Definition of Canopy Illumination Classes' represent an illuminated canopy area between those same red numbers as marked on the 'Visual Reference', and are used to prescribe an 'Index Value' between 1 and 5.

Gap fraction was assessed within each 5.5x5.5m microplot, using a canopy scope also presented in Brown *et al.* (2000). The instrument follows a Moosehorn (Garison, 1949, in Brown *et al.*, 2000) redesigned as a transparent Perspex screen with a 20cm cord attached to one corner. The cord is used to ensure that the screen is always held at the same distance from the eye. The screen was engraved with 25 dots, approximately 1mm in diameter, spaced 3cm apart (centre to centre), in a 5x5-square array. Instead of being pointed at the zenith, the canopy scope is instead pointed at the largest gap visible anywhere in the canopy whilst standing at the point of measurement. The canopy scope was selected for its cheapness, robustness, speed and accuracy. Brown *et al.* (2000) have shown that the canopy scope has lower within- and between-observer errors than the other methods used. It had the highest correlation with canopy openness measured with hemispherical photographs, and Brown *et al.* (2000) propose this relationship is independent of forest type and canopy structure.

Different edge types and ages

Vegetation parameters were measured for three other edges to allow scaling for different edge scenarios typical of the region. These sites represent an 'old' degraded edge (DA2), a 'new' preserved edge (SL1), and an 'old' preserved edge (SL2), with the Wawasan Bentar (DA1) site representing a 'new' but degraded edge. An 'old' edge is here defined as being more than ten years and a 'new' edge as being less than five years since swidden creation. Degraded edges are defined as having had active anthropogenic disturbance with their forests, and preserved edges defined as having had limited or no anthropogenic disturbance.

Preserved forest edges that were not degraded were chosen along the perimeter of the Sungai Liang Recreational Park, Brunei Daresalaam (July 2008). The forest here is broadly similar to the secondary forest of Danum Valley, but is less disturbed as logging operations have long ceased here. Forest edges were chosen next to maintained swidden clearings, with a road running just before the forest edge. The presence of a public road (as opposed to a private logging road at Danum) seemed to discourage edge degradation due to the high public presence along the road. The forest is mixed Dipterocarp, and species include *Meranti*, Rubber, Myrtle and *Macaranga* trees intermingled with Palms, including the Spiky Nibong, rattans, Screwpines and lianas. Two edges were found where heavy disturbance had previously occurred, and *Macaranga hypoleuca* and *M. pearsonii* trees were present, along with *M.gigantea* and *M.winkereli* individuals. This broadly corresponds to secondary forest that has been moderately disturbed in the past. This was taken as evidence that the forest here broadly conforms to those secondary forests found throughout Sabah, Borneo, and Southeast Asia.

2.11   RELATIVE HUMIDITY AND TEMPERATURE GRADIENTS

11 Hobo dataloggers (H08-032-08, Onsetcomp Inc., USA) were used to monitor spatial gradients of relative humidity and temperature across the forest edge and within the canopy. Loggers were installed 4m above the ground and repositioned randomly within a 5x5m plot within distance strata defined as 5, 10, 15, 20, 30, 40, 60, 120, 180, 270 and 300 metres into the forest edge. These measurements were made to help characterise the forest in relation to more common below canopy measurements made at other forest edges.

CHAPTER 3 – THE FREQUENCY, DISTRIBUTION, AND SCALING PROPERTIES OF FOREST EDGES WITHIN THE TROPICAL HUMID BIOME-METHODS

This chapter details the methodology employed in this thesis to fulfil the following objectives (Aims and Objectives, Preface):

1) *"Ascertaining what proportions of tropical forests are under the influence of edge effects, and how this influences the estimation of a given parameter at the regional and global scale".*

2) *"Investigating whether a predictable relationship between patch perimeter and area is evident for tropical forest patches, and whether this pattern can be stratified by texture measures, nominal descriptors of fragmentation pattern, or by region".*

These aims were addressed by classifying 104 satellite images from across the tropical humid biome into 'forest' and 'non-forest' based on the Normalised Difference Vegetation Index (NDVI). Dominant patterns of tropical deforestation were measured by quantifying forest patch perimeter and area, and examined to determine whether they expressed a systematic relationship between different scales. To further clarify patterns of deforestation, texture measurements were made on satellite imagery of a reduced resolution (through a sensor simulation exercise) to stratify perimeter-to-area patterns. Texture measurements were based on wavelet coefficients, which isolate spatial patterns of deforestation on a scale-by-scale basis. This meant that the behaviour of deforestation pattern with scale, in addition to its pattern at a given scale, could be used to define texture. Forest perimeter and area data were used to inform a core-area model (*c.f.* Laurance & Yensen, 1991) that estimated the proportion of tropical forest expected to be under the influence of an edge effect of a given magnitude and extent (distance into the forest from its edge). This information was used to illustrate how different deforestation patterns combine with edge effects of different magnitudes and extents, and how ignoring these would affect regional and global estimates of a respective parameter. Results from the methodology detailed here are presented in Chapter 5.

Chapter 3 – The Frequency, Distribution, and Scaling Properties of Forest Edges within the Tropical Humid Biome-Methods

Owing to the unabated and unprecedented deforestation of tropical forest (Achard *et al.*, 2002a; Whitmore, 1984), the mapping of the tropical forest biome is now a paramount research focus (Achard *et al.*, 1998; Myers, 1996), yet there remains little knowledge of the spatial pattern of deforestation in the tropics despite the potential role of forest patch shape in tropical ecosystem function (Herbst *et al.*, 2007b; Imbernon & Branthomme, 2001; Laurance, 2004). Thus, there is a need to accurately measure the spatial pattern of deforestation and include these measurements in process-based analyses of fragmented regions (Defries *et al.*, 1997; de Ridder *et al.*, 2004; Drajeers *et al.*, 1994; Laurance & Yensen, 1991), to elucidate whether landscape pattern does indeed play an important role in ecosystem function at regional and global scales. As such, the need for including spatially explicit information from the tropical humid biome in regional and global climate models could be very important, as the tropical humid biome plays a key role in global climate (Chapter 1). The accurate measurement of landscape pattern is an essential part of determining whether spatially explicit phenomenon, such as edge effects, play an important role in ecosystem function at regional and global scales. The most common way of including spatially explicit phenomena in large scale analyses is to represent point measurements of these phenomena in a simple way for an entire region, in the process of regionalisation. A pertinent example would be a General Circulation Model (GCM), which must summarise spatially explicit calculations of small-scale processes, such as land surface atmosphere-interactions (LSAIs), within a 50km x 50km operational grid in a concise fashion to maximise computational efficiency.

In the fragmented tropics, the accurate representation of landscape pattern necessitates that it be measured in detail across small geographic extents (de Ridder *et al.*, 2004; Laurance *et al.*, 1998b), as deforestation is inherently a stochastic, fine-scale (Laurance *et al.*, 1998b) and spatially-complex (Gustafson, 1998) phenomenon. Deforestation and its associated responses (e.g. climatic feedbacks) occur throughout the tropics. As such, incorporating spatially explicit information of deforestation pattern, when regionalising processes within regional/global models for climate modelling/impact assessment, requires the measurement of spatially complex deforestation patterns over large geographic extents. This means that deforestation pattern must be measured at a high resolution and over a large area, making the assessment of landscape pattern a remote sensing science that relies heavily upon

information from satellite imagery (Mayaux *et al,*. 2005). Previous studies have used satellite imagery to classify regional/global tropical deforestation patterns on a nominal basis such as 'linear', 'diffuse' and 'massive' (e.g. the TREES project (CEC, 1991)), by modelling simple patterns representative of case-type scenarios (Laurance *et al.*, 1998b) , or by assuming all forest remnants are square in shape (Herbst *et al.*, 2007b). It is unknown, however, whether the assumptions and sampling systems upon which these aforementioned studies are based are appropriate for deforestation patterns throughout the tropics. This is because high resolution measurements of deforestation patterns have not been made for entire tropical regions. The only direct measurement of fragmentation across the tropics using high-resolution imagery (Landsat) was made by Skole & Tucker (1993), but this study only addressed deforestation from 1978-1988, and thus does not account for the last 20 years of ongoing forest fragmentation. There is also a strong need to ensure measurements of deforestation pattern can be readily incorporated into spatially explicit models, such as 'core-area' (Laurance & Yensen, 1991) or 'length-scale' models (de Ridder *et al.*, 2004), the information from which can then be integrated readily within other large-scale models such as Global Climate Models (GCMs).

3.2 BACKGROUND

Mapping tropical forests

Inconsistencies in the methods, legends and frequency of national forest surveys have led to the use of optical remotely sensed data (e.g. satellite imagery) to monitor tropical forests at the regional/pan-tropical scale (e.g. Achard *et al.*, 2002b; Skole &Tucker, 1993). Satellites produce a large number of digital images, and the large volume of subsequent data has lead to a workload that has outpaced the number of qualified remote sensing analysts to navigate, view, and interpret this data. Automated computerised analysis can offer help in dealing with large amounts of data. In particular, there is a need for the rapid and accurate elucidation of spatial data that describes the pattern of tropical deforestation and land cover change to permit the regionalisation of spatially explicit processes (e.g. LSAIs) operating in the tropics so as that they may be included in regional/global climate models/impact assessment.

There is an inherent trade-off between the geographic extent covered by a remote sensing platform (i.e. its instantaneous field of view, IFOV) and the temporal

frequency and spatial resolution (detail) it offers (Quattrochi & Atkinson, 1999). The coarsening of satellite image resolution associated with covering greater geographic extents leads to a loss of spatial detail at a rate that depends on the spatial structure of the landscape (Gervin *et al.*, 1985; Mayaux & Lambin, 1997; Woodcock & Strahler, 1987). This is particularly problematic for extracting spatial information from regions of fragmented tropical forest, as tropical deforestation forms spatially complex patterns owing to the aberrant nature of forest clearance, yet occurs throughout the tropics. This can be termed the problem of 'scale', or the 'Modifiable Areal Unit Problem (MAUP, Openshaw, 1984), whereby there is an associated bias of statistical interpretation arising from the necessary grouping of data into arbitrary units/scales (i.e. modifiable areal units, such as pixels, geographical regions, satellite images) by scientists for analysis.

The complete ('wall-to-wall') mapping of tropical forests and deforestation on a high-resolution basis at global spatial scales is clearly the best option to monitor landscape pattern, but requires the processing of large volumes of data at impractical acquisition rates (Achard *et al.*, 1998). Previous solutions were to map tropical forests across a large extent with coarse resolution imagery using higher resolution satellite data as a reference (Mayaux *et al.*, 1998). Following the success of these projects international efforts now attempt circumvent the problem of scale by assessing deforestation through sampling of representative strata with high resolution imagery (Achard *et al.*, 2002a, 2002b), or by calibrating (termed 'inverse calibration' by Brown (1982)) low-resolution imagery (such as Moderate resolution Imaging Spectrometer (MODIS) or Advanced Very High Resolution Radiometer (AVHRR) imagery) that is available across the pan-tropical extent of the phenomena. The calibration of low-resolution imagery is usually based on empirical relationships with high-resolution equivalents, and requires that there is a predictable behaviour of deforestation pattern between the two different resolutions of each sensor (de Ridder *et al.*, 2004; Mayaux & Lambin, 1995, 1997). For a pattern to be predictable across scales, it must express some degree of characteristic self-similarity (Mandelbrot, 1975). The exploitation of self-similarity in remote sensing studies is not new, and has already been used as the basis for imagery classification (Myint, 2003, 2006; Myint *et al.*, 2002, 2004; Sgrenzaroli *et al.*, 2002) and land surface modelling (Lindsay *et al.*, 1996; Neidermeier *et al.*, 2000). Despite the ubiquity of self-similarity in nature (Madelbrot, 1982), it remains unexplored for patterns of anthropogenic deforestation in the tropics. Given the complexity of deforestation patterns, it is also highly likely that

patterns uncovered would need stratifying to reduce the variance around the estimator (e.g. Mayaux & Lambin, 1997).

Forest fragmentation and edge effects

Deforestation is ubiquitous across the tropics and imposes different conditions upon forest remnants pre-adapted to the stable conditions that are typical of homogeneous forested land cover (Harper *et al.*, 2005; Murcia, 1995; Saunders *et al.*, 1991). Contrasting properties of non-forest cover have been shown to influence forest function at edges of adjacent forest remnants through the horizontal transfer of energy or biota. Recent studies all conclude that edge effects, and therefore patch shape and size, should be accounted for in the regionalisation of hydrometeorological (Ciencala *et al.*, 2002; Giambelluca *et al.* 2003; Herbst *et al.* 2007b; Klassen, 1992; Klaassen *et al.*, 2002), biological (Harper *et al.*, 2005; Murcia, 1995; Saunders *et al.*, 1991) and chemical (de Ridder *et al.*, 2004) parameters. This is often achieved on a core-area (Laurance & Yensen, 1991) or length-scale (Blyth, 1995; de Ridder*,* 2003) basis. Laurance & Yensen (1991) proposed a protocol for modelling the 'core-area' of forests *not* under the influence of edge effects based on estimating the area of forests that *are* under the influence of edge effects. Estimating the core-area of forests involves three steps: (1) identification of focal process (2) measurement of an "edge function" that describes the response of the focal process with distance into the forest from its edge, and (3) use of a "Core-Area Model" to extrapolate edge function parameters to existing or novel situations. An edge function incorporates a measure of the magnitude of a given property's divergence from its forest interior value (i.e. the Magnitude of Edge Influence, or 'MEI'), and distance into the forest edge over which that divergence is present (i.e. the Extent of Edge Influence, or 'EEI'). The core-area model of Laurance & Yensen (1991) calculates an edge enhancement factor (EFF) by incorporating the total area of a patch (TA) and a measure of its shape in the form of the Patton Shape Index (PSI, Figure 3.1) in the following manner:

EEF =   (EEI x MEI) x PSI x TA   [-]   *(Equation 3.1).*

The PSI (Patton, 1975, in McGarigal & Marks, 2002):

$$PSI = \frac{P}{(200(\pi TA)^{0.5})}$$ [-]   *(Equation 3.2).*

The Patton Shape Index (PSI) measures the complexity of patch shape compared to a circle of the same size (Figure 3.1) using measurements of perimeter (P) in addition to

TA. This alleviates the size-dependency problem of a simple perimeter-to-area ratio measurement.

Shape indexes such as *PSI* are one of many landscape pattern metrics, which include metrics such as fragmentation indices, patch shape indices, or proportion indices. Such metrics, like shape indexes, are usually based on a perimeter-to-area ratio. Length-scale modelling operates on a similar basis to the protocol of Laurance & Yensen (1991), but is simplified by only incorporating a typical edge frequency or length-scale of variation (Blyth, 1995; de Ridder *et al*., 2004), and thus does not include information of shape.
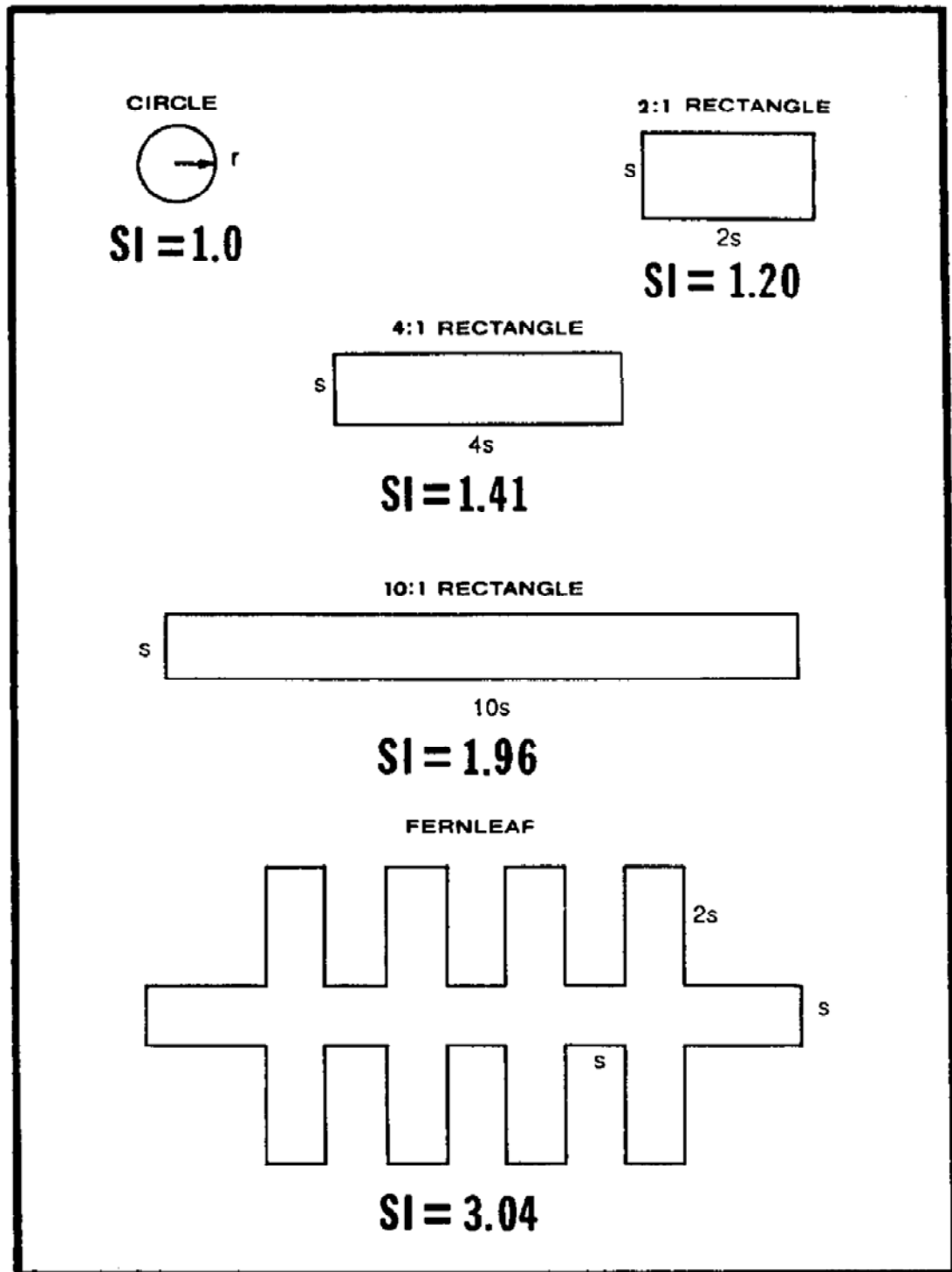
Figure 3.1   Six geometric shapes used as habitat fragmentation analogues by Laurance & Yensen (1991) and their respective Patton Shape Index (Equation 3.2, denoted 'SI' in this figure) values, which indicate the deviation of each shape from circularity. All shapes have identical perimeter-to-area ratios. 's' represents a unit length and values (n) before 's' identify the s: ns ratio, where n is a given number. Figure reproduced from Laurance & Yensen (1991).

Laurance & Yensen (1991) demonstrated empirically that the relationship between PSI and core-area (i.e. the area of a forest patch that is not under the influence of edge effects) is entirely predictable if the extent of edge effect (EEI) is known. Core area (CA) is calculated from the total patch area (TA) and the area affected by edge effects (AA):

$$CA = TA - A A \qquad\qquad [ha] \qquad\qquad (Equation\ 3.3),$$

where:

$$AA = 3.5\ EEI\ PSI\ \left(\frac{TA}{10000}\right)^{0.5} \qquad\qquad [ha] \qquad\qquad (Equation\ 3.4).$$

It was found that the relationship between PSI and CA was non-linear owing to the properties of various shapes. Laurance & Yensen (1991) applied a simple correction that rendered a highly accurate relationship between the adjusted AA (AA_{ad}) and CA (r^2 =0.999, p<0.001). AA_{ad} is calculated:

$$AA_{ad} = AA \left(1 - \left(\frac{\left(0.265\left(\frac{AA}{TA}\right)\right)}{PSI^{1.5}} \right) \right) \qquad\qquad [ha] \qquad\qquad (Equation\ 3.5).$$

Over 100 landscape pattern metrics can be calculated (McGarigal & Marks, 2002), but and many are correlated, and so the number of disparate landscape pattern metrics can, potentially, be low (Hargis *et al.*, 1998). This has lead recently to techniques which remove correlated landscape metrics via principle components analyses, whereby many pattern metrics are condensed into a single 'principal component' comprising a combination of non-correlated pattern metrics (Cain *et al.*, 1997; Cumming & Vernier, 2002; Hargis *et al.,* 1998; Imbernon & Branthomme, 2001; O'Neill *et al.*, 1988; Riitters *et al.*, 1995; Tinker *et al.*, 1998). For example, Imbernon & Branthomme (2001) aimed to describe the change in landscape pattern of six sites within the Brazilian Amazon. However it was unknown which of the 61 landscape metrics that could be computed best described landscape pattern in the tropics. Imbernon & Branthomme (2001) completed a variance analysis for 104 satellite images at sites across the humid tropical biome. The number of possible pattern metrics was reduced to a more manageable number by excluding metrics that co-varied: i.e. no more useful information of landscape pattern as a whole was gained by the additional use of a particular metric. Analysing the 12 indices that remained after the variance analysis proved more practical than analysing all 61 possible indices, and allowed a relatively concise description of fragmentation change at the six sites. The remaining variables after the variance analysis of Imbernon & Branthomme (2001) were:

1 Number of crop land patches	7 Fractal dimension of forest patches
2 Fractal dimension of all the patches	8 Forest patch size standard deviation
3 Total number of patches	9 Mean proximity between forest patches
4 Mean distance patches/nearest neighbour	10 Mean crop land patch size
5 % forest area	11 Mean forest patch size
6Fractal dimension of crop land patches	12 Landscape shape (Patton index)

Whilst the wide variety of possible landscape metrics can be reduced to a more manageable number using techniques similar to Imbernon & Branthomme (2001), landscape metrics can be calculated at a number of scales, or resolutions, depending on the satellite platform. Gustafson (1998) concludes that landscape pattern metrics are scale-dependent, rendering different values when calculated at different resolutions. This makes landscape pattern analysis highly problematic across scales or remote sensors (Uuemaa *et al.*, 2005). As such, measuring fragmentation across the tropical humid biome is greatly hampered by scale effects due to the need to use a variety of different sensors to cover the whole of the tropics at an appropriately (high) resolution, whilst ensuring that scale effects upon patch metrics are accounted for.

Texture

Texture is a commonly used feature in the analysis and interpretation of images. In image interpretation, pattern is defined as the overall spatial form of related features. Avery & Berlin (1992) define texture as the visual impression of coarseness or smoothness caused by the variability or uniformity of image tone or colour. Put another way, texture is the overall physiognomic impression given by pattern (or 'textons'). This is a somewhat simplistic definition, and does not reflect the almost infinite number of ways texture can be evaluated either nominally or numerically. Figure 3.2 demonstrates the wide variety of ways texture can be described, and draws attention to the subjective nature of assigning nominal descriptors to texture patterns in terms of being fine, coarse, smooth, rippled, molled, irregular, or lineated. Figure 3.2 also highlights those descriptors of deforestation pattern used in the TREES study, highlighted in red. Examples of typical deforestation patterns, their nominal descriptions, and the processes driving each pattern are also presented in Figure 3.2, to demonstrate the wide variety of deforestation patterns that could combine to form different textures at the landscape scale.

Texture examples

dusted | concentric/annular | linear | stripes/isotropic | gradient/anisotropic

branched | granular | stellate | radiative | shearing
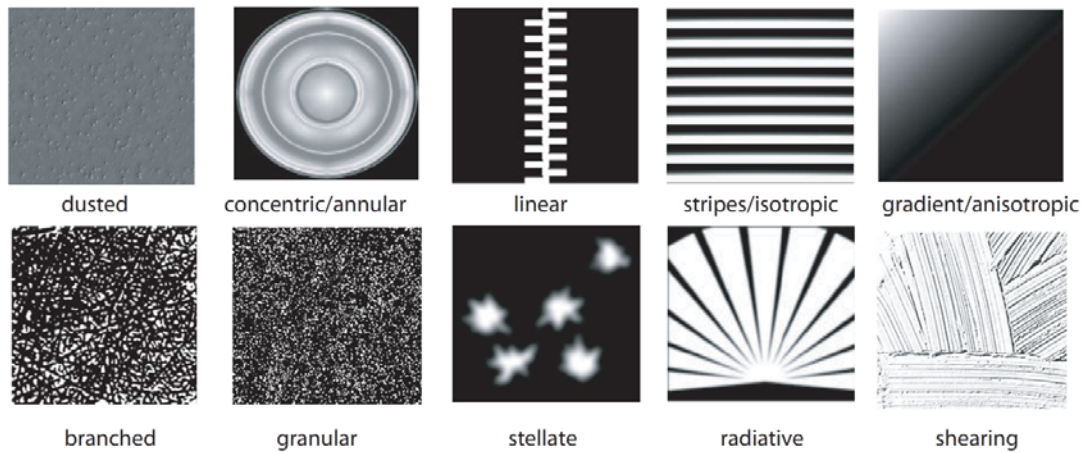
Typology of deforestation patterns

diffuse
shifting cultivation/small holdings

isolated/remnants
high population/extensive development

Island
perurban

massive
ranching

corridor
road-side colonisation

linear
systematic (government)
resettlement schemes
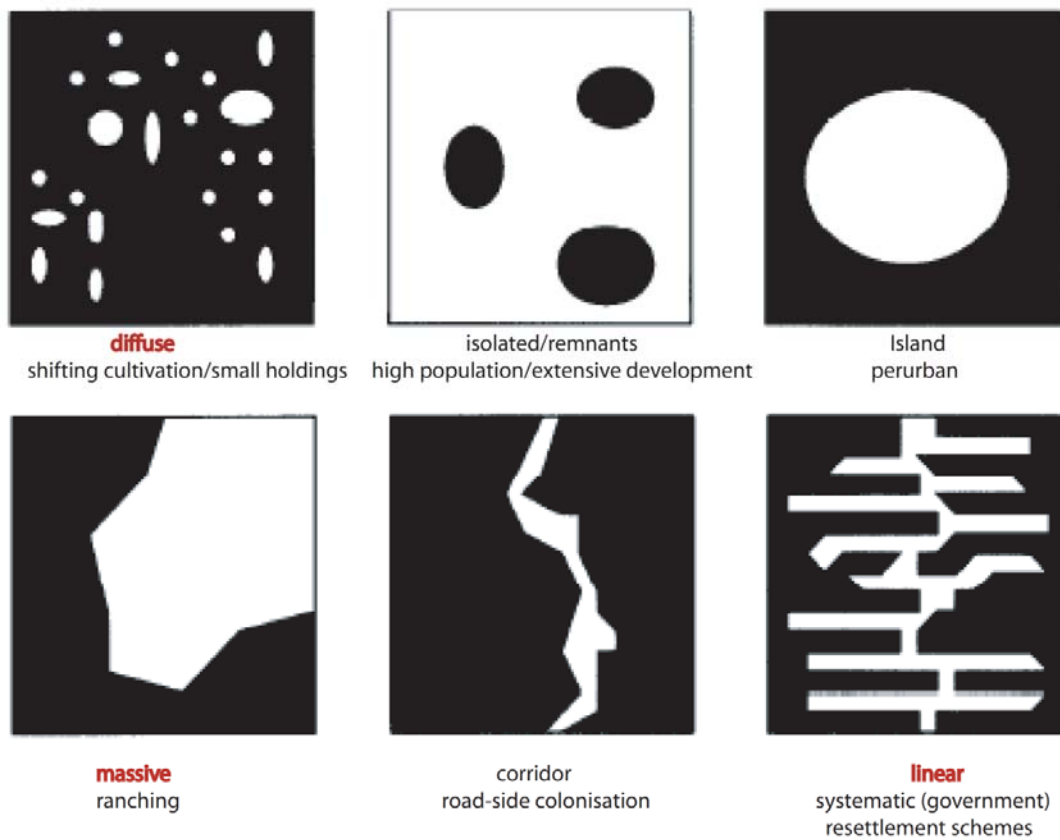
Figure 3.2   Examples of textures and their associated descriptions are presented. Also presented are six descriptors of typical patterns of deforestation, where three common descriptors of deforestation pattern in the tropics (Achard et al., 2002a, 2002b) are highlighted in red (i.e. linear, massive, and diffuse).

Despite difficulties in describing texture, the inclusion of spatial information in the form of texture measures still increases the power of analyses over that of those which have no spatial basis, as landscape pattern nearly always is linked to a process. The inclusion of texture measures usually greatly improves analyses such as land cover classification. Textural measures are employed routinely to supplement spectral components (i.e. pixel brightness values of an image for a given wavelength of light) of image classification, such as spatial feature discrimination in urban areas (Myint *et al.*, 2002, 2004) or forest classification (Hill, 1999; Sgrenzaroli *et al.*, 2002). Textural analysis has also previously been employed to classify strata for improved regression estimates from between coarse and fine resolution imagery (Mayaux & Lambin, 1995, 1997).

The complexity of texture means that it is impossible to define universally by a single mathematical descriptor, and that in reality the definition of a texture measure needs to be tailored to suit the end product of analysis. Thus, without an appropriate definition of texture the extraction of information for operational use remains problematic.

Satellite image texture is normally measured on a transform basis in which the variability of pixel digital number values is calculated within local 'windows' (pixel regions) via statistical and structural analysis. Statistical analyses, such as contrast between neighbouring pixels (Edwards *et al.*, 1988), standard deviation (Arai, 1993) local variance (Woodcock & Harward, 1992), and entropy (Zhu & Yang, 1998) can indicate the total variation of pixel values in a local area and can be computed easily, but lack information about spatial patterns (de Jong & Burrough, 1995). Structural analyses based upon co-occurrence matrices – which measure the spatial correlation between pixel values- are often used in texture analyses since they are able to capture the spatial correlation of gray-level values within an image. Just as pattern is scale-dependent, it stands to reason that texture and textural analysis also suffer from scaling effects.

Scale effects and fractals

The loss of spatial information with changing scale of satellite imagery is now widely documented (Friedl, 1997; Turner *et al.*, 1989). This occurs as the spatial resolution of remotely sensed data gets coarser, the image degrades and features become less detectable at critical thresholds as the size and shape of patches change (Gervin *et*

al., 1985).   This occurs as coarsening sensor resolution imposes an areal (i.e. discontinuous and spatially arbitrary) structure upon data (e.g. a square image pixel at different scales) and changes the information that is available at a particular resolution. Degradation of this nature means that information cannot be extracted directly across resolutions. In the case of course resolution satellite imagery, a calibration instead needs to be applied to correct for the effects of scale. Brown (1982) defined this as an 'inverse-calibration'. This requires investigation into the relationship between scale and the desired information to ascertain whether the information in question demonstrates a systematic (and thus predictable) relationship with itself as measured at different scales.

Previous studies have related empirically the relationship between scale and data via a scaling exponent (Cao & Lam, 1997). Approaches include geostatistics (Atkinson, 1993; Imbernon & Branthomme, 2001), scale variance (Townsend & Justice, 1988) semivariance, and fractal analysis (Cao & Lam, 1997; Lovejoy, 1982, Lovejoy *et al*., 2001). The use of a single scaling exponent relies upon there being a single constant relationship between the data and the scales over which it is measured. When such a relationship exists, the data is said to be self-similar and scale isotropically and exhibit 'fractal' properties (Mandelbrot, 1975). The Koch snowflake (Figure 3.3) expresses this, reflecting a constant relationship between the scale at which it is measured and the length of its perimeter. This attribute is a consequence of the self-similarity expressed throughout the structure sequence, whereby one sequence acts as the generator function for the next. In the sequence of Figure 3.3, the sole generator is a star, and the sequence has an exclusive fractal dimension of 1.26. Various techniques exist for calculating the fractal dimension (Pecknold *et al*., 1997). The initiator (a triangle in this instance) defines the translation sequence across which the generator multiplies. As a result, although the information within Figure 3.3 (perimeter and area) will change with scale, information can be characterized by, and extruded from, a singular scaling exponent (e.g. the perimeter-to-area ratio).

Initiator   **Generator**
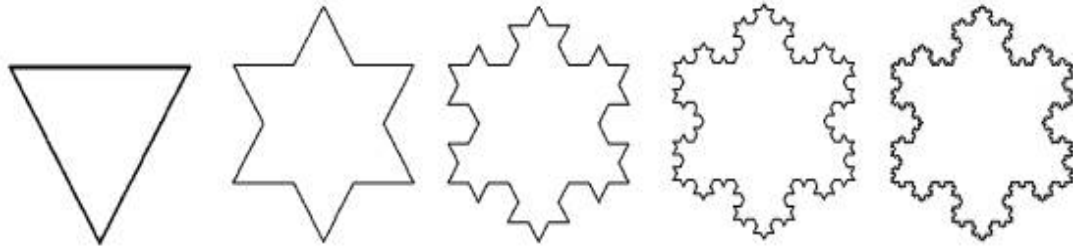
Figure 3.3   The Koch Snowflake

Mathematically, a perfectly self similar set contains a union of subsets which is simply a reduced copy of the full set (Mallat, 1989), implying each subset is neither redundant nor lacking in detail. Such a set is said to be complete. Thus under such circumstances an increase in scale would not reveal any more statistical knowledge. Self-similarity is not the only prerequisite of such conditions, but self-affinity also. That is, a self-similar pattern will not be self-similar if it is translated in an invariant manner. A set is said to be self-affine if it can be expressed as a union of non-overlapping subsets that linearly map into whole sets. Thus, scaling of a self-similar and self-affine series of subsets will not be uniform in coordinates but will be invariant under transformation (translation across scale). Although fractal geometry provides a consistent and hierarchical (Lindsay *et al*., 1996; Mallat & Zhong, 1992) mathematical framework for describing the pattern of structures, it is rarely the case that structures are self-affine (Parrinello & Vaughan, 2002) or self-similar (Pecknold *et al*., 1997). That is, natural systems have many 'initiators' and 'generators' and thus can be considered to be 'multifractal' (Pecknold *et al*., 1997). As an example, a Koch snowflake is a mono fractal, but many Koch snowflakes layered upon one another are multifractal. In simple terms, one expresses pattern and the other texture. This is likely to be the case for artificial edges delineating forests, which, although geometric, are aberrant and spatially complex (Achard *et al*., 2001; Ferriera & Laurance, 1997; Laurance *et al.,* 1998b). Importantly, the user has no *a priori* knowledge of the scaling pattern of natural systems. Consequently, a detailed analysis regarding ways of circumventing the break-down of self-similarity would be 'more than worthwhile' (de Ridder *et al.*, 2004). This is termed a multi-resolution analysis (Pecknold *et al*., 1997).

'Fractal' landscape metrics

The influence of scale upon perimeter-area relationships of a pattern can be measured by the fractal dimension (D). The perimeter-area method quantifies the degree of complexity of the planar shapes. For simple Euclidean shapes (e.g., circles and rectangles), Perimeter (P) ≈ √Total Area (TA) and D = 1 (the dimension of a line). As the polygons become more complex, the perimeter becomes increasingly plane-filling and P ≈ TA with D → 2. A correction of 0.25 is necessary to correct perimeter measurements for raster inputs (McGarigal & Marks, 2002):

D = 2ln (0.25P)/ ln TA   *[-]*   *(Equation 3.6).*

Traditional fractal analyses typically orientate around counting the number of pixels that contain 'perimeter' pixels and 'area' pixels within a m x n range of pixels defining a 'box', aptly named 'box-counting' (Voss, 1986), or by computing edge-detection transforms (such as the Canny transform (Canny, 1986)) over a known linear range of pixels (Lindsay *et al.*, 1996; Mallat, 1989).

The 'fractal' features of a set of objects can also be considered in a way which bears no conceptual relationship with that of the aforementioned traditional fractal analyses. Mandelbrot (1982) suggests that one could plot the logarithm of the perimeter length of individual objects viewed at different scales as a function of the logarithm of their surface area, or vice versa. Various researchers (e.g., Lovejoy, 1982) have observed that the resulting data points in the log–log plot often approximate relatively closely a linear pattern and therefore follow a power-law. Thus it has become customary in the literature to refer to the slope of the line on the log area–log perimeter plot as a 'fractal dimension'. This second perspective provides the conceptual basis for the definition of several 'fractal' indices based on the manipulation of simple area (a) and perimeter (p) values of (ij) pixels for a given number of patches (ni):

Mean Patch fractal dimension:

$$MPFD = \sum_{j=1}^{ni} \frac{2\,ln(0.25p_{ij})}{ln\,a_{ij}}$$ *[-]*   *(Equation 3.7),*

Area-weighted mean fractal dimension:

$$AWMPFD = \sum_{j=1}^{ni} \left[\left(\frac{2\,ln(0.25p_{ij})}{ln\,a_{ij}} \right) \left(\frac{a_{ij}}{\sum_{j=1}^{ni} a_{ij}} \right) \right]$$ *[-]*   *(Equation 3.8),*

Double log fractal dimension:

$$DLFD = \cfrac{2}{\cfrac{\left[n_i\left(\sum_{j=1}^{n}(\ln p_{ij} \ln a_{ij})\right)\right]\left[\left(\sum_{j=1}^{n}(\ln p_{ij})\right)\left(\sum_{j=1}^{n}(\ln a_{ij})\right)\right]}{\left(n_i \sum_{j=1}^{n} \ln p_{ij}^2\right) - \left(n_i \sum_{j=1}^{n} \ln p_{ij}\right)^2}} \qquad [\text{-}] \qquad \text{(Equation 3.9).}$$

Multifractal analysis

Although not perfectly self-similar (fractal), many patterns that cannot be characterised geometrically do express statistical self-similarity that is multifractal (Mallat, 1989). That is, numerous generator and initiator components unique to a multi-fractal data set may produce exclusive statistical properties if a systematic and contextual scaling structure is imposed upon data. Only when observations are made within this multifractal construct does a data's scaling behaviour indicate a phenomenon of interest (Bian, 1997; Mallat & Zhong, 1992; Openshaw, 1984). Such an understanding is gained through multifractal analysis (Lovejoy *et al.* 2001; Parinello & Vaughan, 2002; Pecknold *et al*., 1997; Tessier *et al.,* 1996), wherein the aggregation of single fractal sets and their signatures within a growing multi-fractal set is monitored with scale. This requires a series of localised (therefore, necessarily geometric, self-affine) fractal networks against which the behaviour of data can be monitored as they change in position with scale. This is simply a scale-invariant ruler.

As deforestation is both highly spatially localised and complex, it is unknown whether the spatial complexity of the deforestation 'signal' or the variation as it reaches an asymptote across scale will be predominantly due to: (i) scale (resolution) of the image, (ii) directionality of objects in a texture feature, (iii) spatial periodicity or size of objects which form a particular texture, and (iv) spatial variation of that texture (Myint *et al*., 2002). This necessitates analysing the variance of imagery on each basis via (i) aggregation and sensor simulation (e.g. de Ridder *et al*., 2004; Moody & Woodcock, 1994) (ii) directional analysis (e.g. Myint *et al*., 2002) (iii) application of different size windows (e.g. Pesaresi , 2000) and (iv) stratification based upon texture measure (e.g. Myint *et al*., 2002, 2004) , respectively. These five components would inform us as to the best (i) resolution, (ii) direction, (iii) size of window, and (iv) texture measure for stratification, to increase the accuracy of the estimator, respectively. This requires an analysis that captures (a) important signals (b) the location of these signals and (c) the scale at which these signals are discrete in magnitude and location. In measuring these three things, it can be seen which signals dominate a spatial series, and how their position and magnitude alters as they asymptote across scale with other proximal signals through the aggregation process until the desired level of degradation or resolution is arrived at. The scale at which

patterns are best characterised is called the 'operational scale' (Walsh *et al.*, 1997). The operational scale can be determined by examining the variance of a pattern or texture measure and how it decays/asymptotes with scale. This is called a variogram (Cao & Lam, 1997). Similarly, a scale- normalised variogram (semivariogram) would produce a peak at the operational scale (Cao & Lam, 1997).

Wavelets

Explicit analysis of pattern on a scale-by-scale basis has recently been made possible by wavelets, which have properties that can localise important signals well in both space and scale; as mentioned in the previous section (points a-b). The shape of a wavelet function means it can decompose a signal or an image with a series of averaging and differencing calculations- i.e. a wavelet is a filter. Wavelets compute average intensity properties as well as several detailed contrast levels distributed throughout the image. Wavelets can be applied according to various levels of resolution or blurring depending on how many levels of averages are calculated.

To analyze transient signal structures of various supports and amplitudes in space, it is necessary to use transforms with space-frequency spaces with different support sizes for different spatial locations. For example, in the case of high frequency structures, which vary rapidly in space, a higher spatial resolution is needed to accurately trace the trajectory of the changes; on the other hand, for lower frequency, a relatively higher absolute frequency resolution is needed to give a better measurement on the value of frequency. This requires bounded vectors that change systematically and constantly with scale, which are said to have compact support. Wavelets decay to zero at ±∞, so in order to cover the space of interest (the vector space, or Hilbert Space, **R**) they need to be moved sequentially along **R.** This is done in an integral fashion:

$\Psi(r-k)$, $k,l \in \mathbf{Z}$ [-]   (Equation 3.10),

where **Z = {...,-1,0,1,...}** is a set of integers. To consider different frequencies the wavelet needs to be dilated. This is achieved with a binary dilation in integral powers of 2:

$\Psi(2^l r - k)$, $k,l \in \mathbf{Z}$ [-]   (Equation 3.11).

The signal $\psi(2^l r-k)$ is obtained a mother wavelet $\Psi(r)$ by a binary dilation 2^j and a dyadic translation $k/2^j$. The function $\Psi_{k,l}$ is defined as:

$$\Psi_{k,l}(r) = (2^l r - k), \ k, l \in \textbf{Z}.$$ [-] (*Equation 3.12*).

Historically, the Fourier transform has dominated linear space-invariant signal processing. The associated basis functions are complex sinusoidal waves that correspond to the eigenvectors of a linear space-invariant operator. However, the Fourier transform is a global transform that cannot analyze local or transient properties of the original signal owing to its infinite support.

Wavelets provide a suitable framework by operating as a complete and stable signal representation provided by a wavelet frame, which acts as a multi-scale differential operator (Mallat, 1989, Mallat & Zhong, 1992) and provides compact support. Such an approach is powerful as it reduces greatly mathematical redundancy or incompleteness across scale, and has good signal-localisation properties (Lindsay *et al.*, 1996) -i.e. it is complete.

The energy spread of a transform basis (its function) is represented by a theoretical space called a Heisenberg rectangle- which helps the user visualise the spatial and scale resolution offered by a transform. Examples of spatial-frequency tiling with Heisenberg rectangles are shown in Figure 3.4. Notice that for a windowed Fourier transform, the shape of the time-frequency boxes are identical across the whole time-frequency plane, which means that the analysis resolution of a windowed Fourier transform remains the same across all frequency and spatial locations.

A wavelet is essentially a derivative of a smoothing filter, which itself is a derivative of a statistical edge (Figure 3.5), making wavelets highly applicable for detecting and localising in the space domain the abrupt changes in signal associated with forest edges. Mallat (1989) defined the first wavelet based on a Canny edge detector (Canny, 1986). Edge detection algorithms are essentially smoothing functions which converge to zero at infinity, and whose integral is equal to one, and are the first derivative of a Gaussian smoothing function.

A   B   C   D
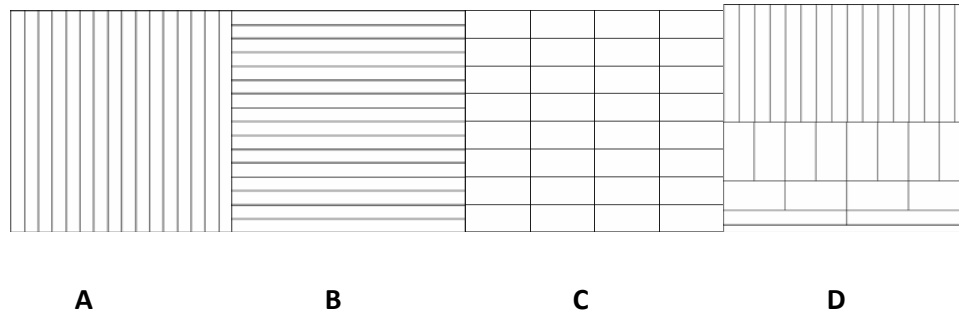
Figure 3.4 Spatial-frequency tiling of various transformations. x-axis: spatial resolution. y-axis: frequency resolution. (a) discrete sampling (no frequency localisation):e.g. Shannon. (b) Fourier transform (no temporal localisation). (c) windowed Fourier transform (constant Heisenberg boxes):e.g. Gabor filtering. (d) wavelet transform (variable Heisenberg boxes).
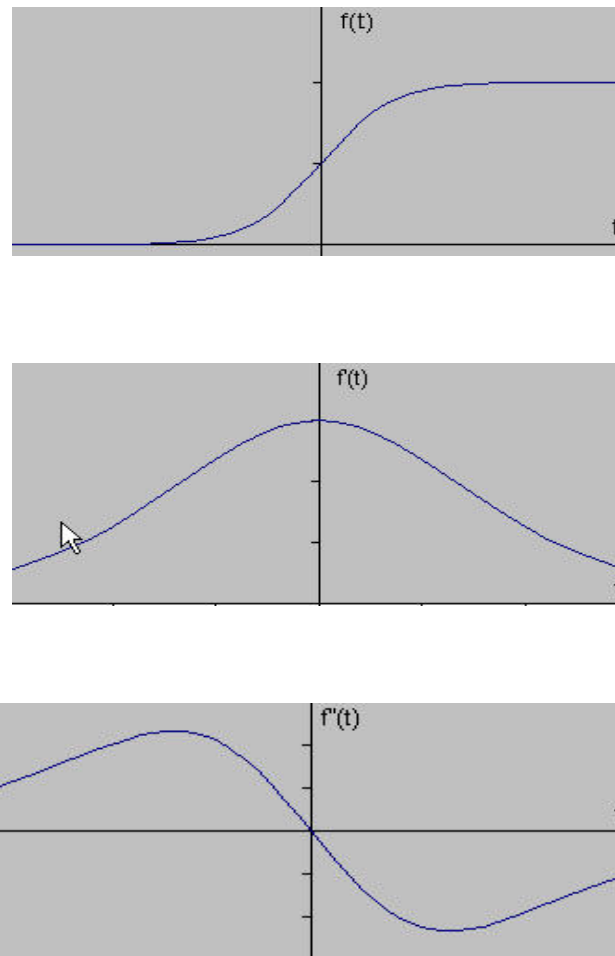
Figure 3.5 A statistical Edge (top), and its first (Gaussian, middle) and second (bottom) derivatives

A wavelet transform of a spatial series decomposes the signal into sets of coefficients: each set being derived from a spatial scale and each element within the set being assigned a particular location. The coefficients produced by wavelet transforms can then be used in conjunction with textural measures to define texture in a functional way that is highly localised in space and scale.

3.3 THE DISCRETE WAVELET TRANSFORM

Remote sensing imagery is discrete, and thus it is not necessary for wavelet analyses to adhere to a continuous scale parameter. Scale is made discrete through a dyadic scaling sequence imposed upon data (Mallat & Zhong, 1992). Importantly, this means the DWT permits fast numerical implementations, which is essential given the high data load of high-resolution satellite imagery. The DWT is achieved by the successive application of high pass and low pass filter corresponding to a single, dyadic, wavelet family (θ). Scale is accounted for by the insertion of 2j zeros between each response coefficient of the filter at each scale (j). The effect of inserting the zeros is to adjust the width and taper of the wavelet frame in a scale invariant manner- i.e. the representation is over-complete. Down sampling every other row/column after each filter pass accounts for the insertion of zeros and stops the analysis from being redundant. This process produces four coefficient sets at the next scale from the input (Ca_j): Horizontal, vertical and diagonal details (Hcd_{j+1}, Vcd_{j+1}, Dcd_{j+1}) and an approximation (Ca_{j+1}) that is equal to the sum of the details. Figure 3.6 describes the basic decomposition steps for matrices undergoing DWT.

3.4 WAVELET FAMILIES

Various functions satisfy the requirements of orthonormality and stability. This has resulted in the creation of many wavelet families. Wavelet bases derived from filters of order n are orthogonal to polynomials of order n-1. This means that trends in the spatial series of order n-1 are not represented in the output wavelet coefficients, i.e. they are not recognised or registered. Thus, to provide good characterisation of scale, it is important that many polynomial 'vanishing moments' are included in the wavelet function. However, to construct a wavelet that fulfils the requirements for mathematical completeness, it is essential that the increased number or vanishing moments in the filter are associated with an increase in the length of the wavelet window. This means there is a trade-off between a wavelet's ability to identify the spatial scale and the location of events in the spatial series. It is therefore important

to choose the appropriate wavelet family for the analysis (Torrence & Compo, 1998), as wavelets offering better approximation of high-pass filters offer poorer localisation properties. This is particularly an issue when there is no *a priori* knowledge of the pattern in question, and indeed this is often exactly the nature of the enquiry in hand.
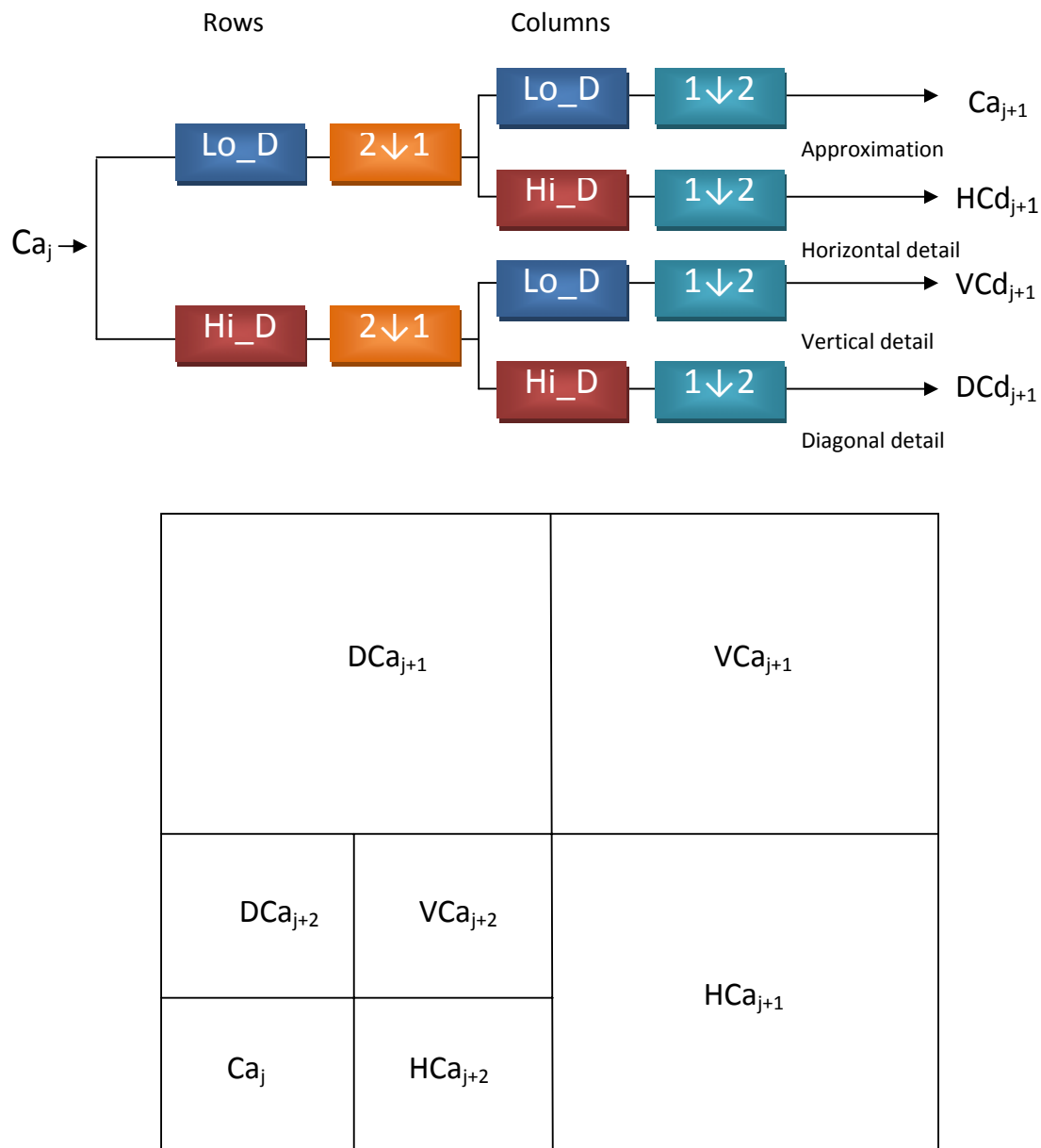
Figure 3.6   *Spatial and processing overview of a discrete wavelet transform in two dimensions for and input matrix $Ca_{j,.}$*

As an example, the Haar Wavelet offers good localisation properties as it comprises of only two elements, but is the worst high-pass approximation. Daubechies (1992) created a series of wavelet families having compactly supported orthonormal

wavelets to make discrete wavelet analysis practicable (Figure 3.7). The Haar wavelet has the same transform properties as the DB1 wavelet. The Haar wavelet (DB1) and other nine families representing the Daubechies (1992) wavelets are presented in Figure 3.7.

HAAR(db1)

db2 db3 db4 db5 db6

db7 db8 db9 db10
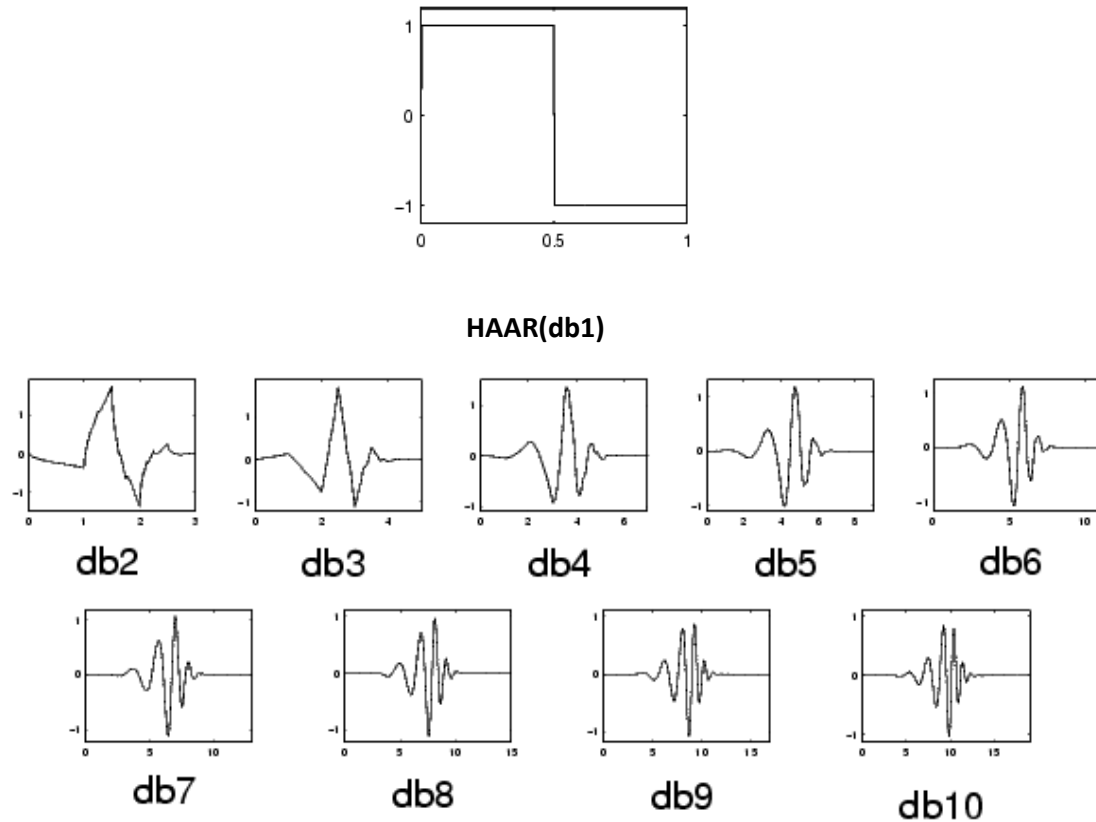
Figure 3.7   The Haar wavelet (DB1) and other nine families representing the Daubechies (1992) wavelets (from Matlab User's Guide: www.matlab.com *).*

3.5   WAVELETS AND TEXTURE

A sole wavelet analysis is good in localisation and scale, but not in providing anything but a highly localised textural measure. Texture analysis provides a synoptic texture measure within a local window, but lacks spatial information. By combining textural measures with wavelet coefficients, a wavelet-based textural measure provides both an indication of pattern at scale but retains the ability to be analysed in terms of local diversity, entropy, or energy.   This allows texture to be measured on a scale-by-scale basis whilst retaining as much spatial information as is possible.

As wavelets provide localised information in both scale and spatial domains, their combination with textural measures has recently received much attention. Zhu & Yang (1998) used information entropy as a measure to identify texture features in 25 types of aerial relief samples selected from remote sensing images. Albuz *et al.*

(1999) used the sum of squares of wavelet coefficients of each sub-band for their image retrieval system. Sheikholeslami *et al. (*1999) calculated the mean and variance of wavelet coefficients to represent the contrast of an image. Myint *et al.* (2002) used Log energy (LOG), Shannon's Index (SHAN), entropy (ENT) and angular second moment (ASM) to characterise texture of urban land use and land cover classes.

Despite the wide variety and application of both traditional and heuristic fractal analyses for single site studies, it has not been previously established as to whether these metrics express systematic, predictable scaling behaviours for multiple sites across the tropics. Given the inherent variability of pattern, it stands to reason that stratification on a textural basis would be expected to reduce variance of pattern estimators. Wavelets provide a means to calculate texture on a strictly scale-by-scale basis, meaning that scales expressing the greatest relevant information can be selected for stratification. Given the nature of wavelet functions, it would be expected that such wavelet-based texture measures will represent well the process of forest fragmentation. The discrete wavelet transform permits the rapid implementation necessary for the inherently large data sets considered representative of the tropical biome.

Introduction

Methodology employed in this chapter relies upon the established sampling system of the 'Tropical Rainforest Environment Observation by Satellite' (TREES) project (Achard *et al.,* 2002a, 2002b). As such, the TREES project is first introduced to describe the sampling system used in this chapter. Individual components of the methodology are then outlined thereafter, under the following headers:

1. Image selection and archiving

2. Sensor simulation

3. Patch metrics

4. Wavelet Analysis

5. Texture Measurement

6. Feature Reduction and Expectation Maximisation (EM) segmentation.

A flow-diagram is presented in Figure 3.9, which illustrates how components 1-6 (red, in bold, Figure 3.9), and their respective products (in green boxes, Figure 3.9), integrate with TREES metadata (blue boxes, Figure 3.9) and the core area model of Laurance & Yensen (1991) (purple boxes, Figure 3.9) to fulfil the aims and objectives of this study (Introduction, Table A, red boxes, under 'Aims and Objectives'):

A. *Estimate what proportion of tropical forest is under the influence of edge effects for different MEI and EEI values associated with common edge effects found in tropical fragmented forest, and how this influences the estimation of the respective parameter at the regional and global scale (orange box, Figure 3.9).*

B. *Determine whether a predictable relationship between patch perimeter and area is present for tropical forest patches, and whether this pattern can be stratified by texture measures, nominal descriptors of fragmentation pattern, or by region (orange box, italics, Figure 3.9).*

Chapter 3 – The Frequency, Distribution, and Scaling Properties of Forest Edges within the Tropical Humid Biome-Methods

The Tropical Rainforest Environment observation by Satellite (TREES) project

The 'Tropical Rainforest Environment Observation by Satellite' (TREES, http://www-tem.jrc.it/activities.htm) project was initiated in 1991 by the European Commission and European Space Agency. Research focussed on the development of techniques for global tropical forest mapping and monitoring active deforestation areas within this biome (identifying deforestation 'hotspots' of high deforestation levels), and the estimation of deforestation rates in the tropical humid domain in the 1990's.

The main product of the first TREES phase (1991-1995) was a baseline map of global tropical forest cover at 1km resolution (e.g. Eva *et al.*, 2004; Figure 3.8, in green). This was achieved using National Oceanic and Atmospheric Administration (NOAA) Advanced Very High Resolution Radiometer (AVHRR) satellite imagery covering the entire tropical humid biome at a resolution of 1km (i.e. producing maps at the 1:5,000,000). High-resolution Landsat TM images were selected for area-correction and validation of the coarser-resolution AVHRR imagery (Malingreau *et al.*, 1995; Mayaux & Lambin, 1995, 1997). From the global tropical forest cover baseline map, a statistical sampling strategy was developed to provide a reliable measurement of tropical forest change in a uniform, independent and repeatable manner. The baseline map was combined with a deforestation risk map identifying 'deforestation hot-spot areas' (Figure 3.8, in red), which had been constructed with knowledge from environmental and forest experts from each region (Achard *et al.*, 1998). This permitted the stratification of the tropical humid biome into five strata defined by 'forest' and 'hot-spot' proportions. A total of 104 sample sites were selected using a tessellated-hexagon spherical sampling grid (i.e. an icosahedron), whereby higher sampling probabilities were prescribed to strata containing a greater proportion of deforestation hotspot. Landsat images or quarter images were taken from selected sampling units (i.e. hexagons) and formed sample sites (Figure 3.8, blue boxes). The total area captured in the 104 Landsat images covered 6.5% of the humid tropical domain. Deforestation rates in the 1990's were estimated using Landsat imagery (30m resolution) at two dates closest to target years (1990 and 1997).
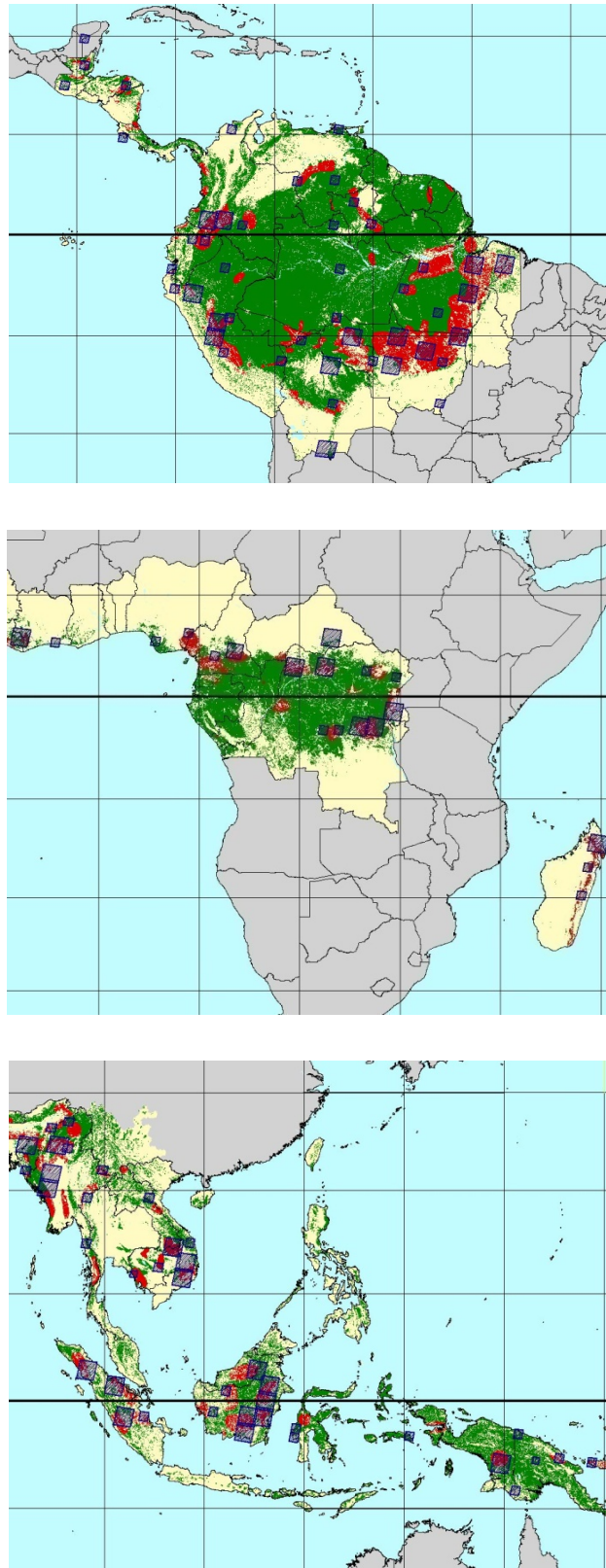
Figure 3.8   Locations of the 104 Landsat observation images (blue) around the tropics (Achard et al., 2002b). Deforestation hotspot areas as defined in the TREES study (following Achard et al., 1998) are shown in red, and tropical forest coverage in green (following maps produced by Achard & Estreguil (Southeast Asia), 1995; Eva et al., 2004 (South America); Mayaux et al., 1999(Central Africa)).
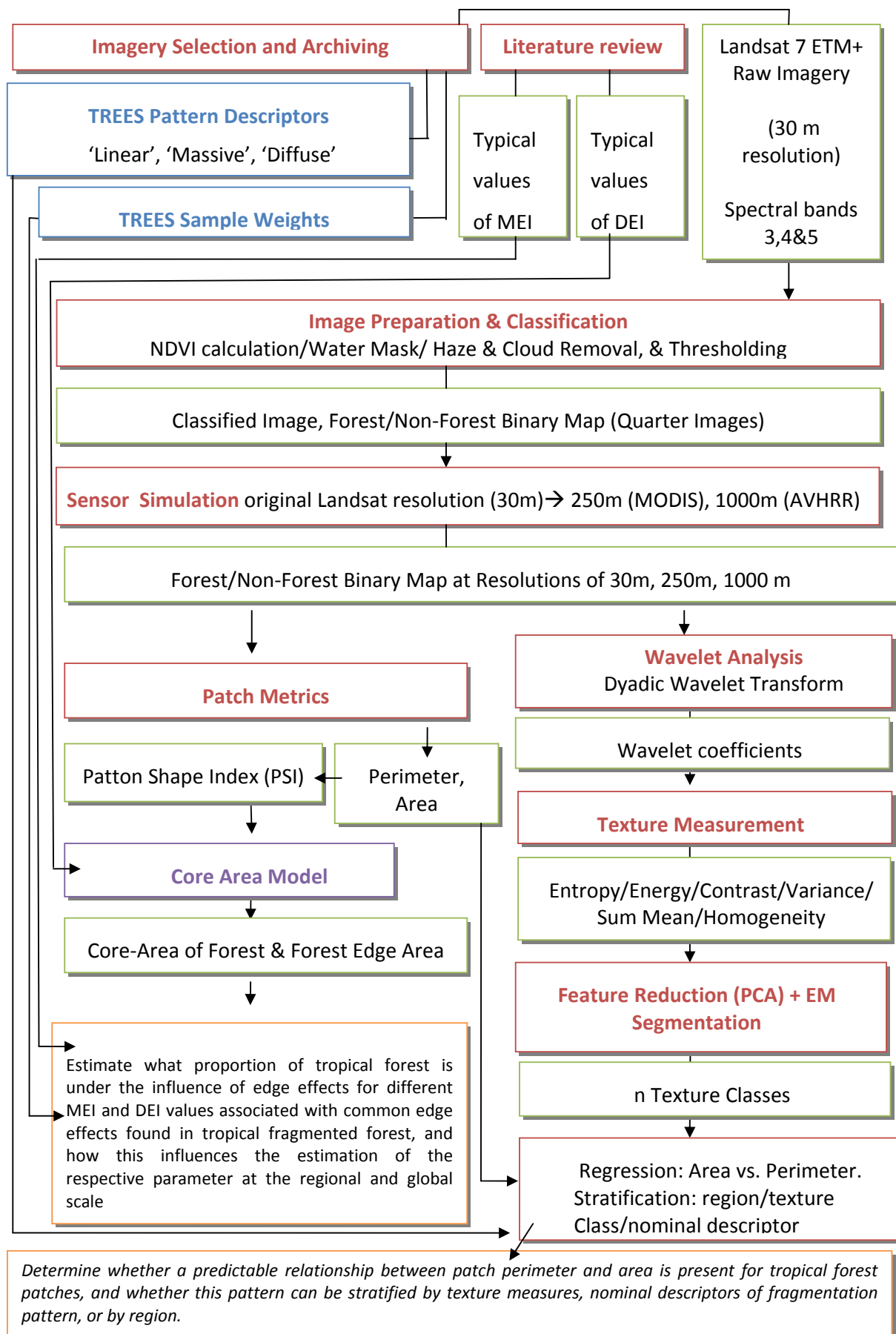
Figure 3.9   How TREES metadata (blue) & products (green) from methodology in this chapter (red)

integrate (arrows) into subsequent methodological components (1-6 in section), and into the Laurance

& Yensen (1991) core-area model (purple), to achieve aims A and B of the previous section (orange).

Imagery selection and archiving

The methodology described in this chapter makes use of 104 Landsat Enhanced Thematic Mapper (ETM+) full or quarter satellite images (30 meters resolution, covering a ground area of approximately 185km x 185km). Imagery was taken from the Landsat path and row position (whereby a path and row value defines a position and area on the earth's land surface within the instantaneous field of view of the Landsat sensor) defined by the TREES hexagonal sampling units (images marked as blue squares in Figure 3.8). The satellite images (also called 'scenes') chosen are representative of the wide variety of deforestation patterns found across the tropical humid domain (Achard *et al.*, 2002b). The TREES project classified forest fragmentation patterns into three primary classes on a nominal basis: 'linear', 'diffuse' and 'massive'. Mas *et al.* (2004) conclude that the relationship between fragmentation and local forest cover shows a much higher occurrence of deforestation for fragmented forest covers. This demonstrates that areas with greater deforestation rates are already fragmented, and confirms the suitability of the TREES sampling scheme to be used for the fragmentation study described in this chapter (confirmed by Javier Gallego, TREES primary statistician, 2008, personal communication). Sampling sites are shown in Figure 3.8 and the metadata (including the path and row positions of each Landsat image) for each sample scene presented in Table 3.1. By adhering to the TREES sampling scheme, it is also possible to use the TREES weighting system associated with each scene's sampling probability (Javier Gallego, TREES primary statistician, 2008, personal communication) to estimate, for the entire tropical humid biome, the total area influenced by edge effects based upon the shape of forest fragments.

Imagery for those paths and rows selected by the TREES projected were downloaded and archived from the Global Land Cover Facility (GLCF, www.landcover.org). Enhanced Thematic Mapper (ETM+) scenes were selected from the GLCF Landsat Geocover dataset (LGD). LGD is a collection of high-resolution satellite imagery (30m) provided in a standardized, orthorectified format, yielding map-accurate images tailored for the production of base maps. The orthorectification process for LGD (Tucker *et al.*, 2004) renders planimetrically corrected images to eliminate topographic effects. Orthorectification is essential for the accurate classification of satellite imagery (and thus the spatial analyses based upon it) covering the tropical humid biome, which commonly exhibits exacerbated terrain features such as mountains, valleys, plateaus, etc. Satellite images selected for the production of LGD

by GLCF were purposefully chosen a) to have minimal cloud cover (typically less than 10%), b) in the growing season (to highlight vegetation coverage) and c) to permit same-day successive acquisitions. Images selected for this study are as close to the year 2000 as possible. The reasons for this are that a) post-2003 imagery contains a 'striping' anomaly in the data b) more recent scenes incorporate as much information about the cumulative process of fragmentation as possible c) imagery for all study sites were mostly available around the year 2000. All images selected for LGD were pre-processed by EarthSat (www.Earthsat.com).

An overview of relevant metadata for each of the used scenes is presented in Table 3.1. Metadata is taken from the Global Environment Monitoring (GEM) Unit, Institute for Environment and Sustainability (IES), Joint Research Centre (JRC), European Commission, http://www-tem.jrc.it/activities.htm, and also from www.landcover.org.

Path Row		Region	Pattern Of Deforestation	Cause Of Deforestation	Deforestation/Degradation Rates(%)	

f= full scene used
#=number of quarter used

PNG=Papaya New Guinea
DRC = Democratic Republic of Congo

l=linear
m=massive
d =diffuse

sc=shifting cultivation
(i)lo=(illegal)logging
ae/ue=agricultural/urban expansion
plan=plantation
oil= oil drilling
ran=ranching
RIL=selective logging

Southeast Asia

Path Row		Region	Pattern	Cause	Rate	
129 058	f					
136 043	f	India/Maghalaya	d	sc	1.06	0.07
136 045	f	Bangladesh	l/d	sc	2.03	0.68
135 042	2	India/Naga Hills	d	sc	4.61	1.45
134 041	4	Myanmar/India	d/l	sc/lo	0.47	0.00
134 043	f	Myanmar Kachin	m/d	sc	0.19	0.08
134 045	f	Myanmar Safain	m a	ae/ran	3.05	1.96
134 046	f	Myanmar Rakhinem	l	sc/a	2.91	0.24
133 043	3	Myan Kachin East	l/m	ue/sc	1.58	0.17
131 045	2	China Yunan	d	ae/sc	0.85	2.33
131 047	1	Thailand/ChangMai	d	sc/ilo	0.28	0.10
131 050	2	Thailand/Kao Lem	d/m	sc	0.62	0.02
129 058	f	Sumatra/Lake Toba	m/l	ilo	0.70	0.13
127 047	1	-	m/l	lo /ae	1.77	0.00
127 052	1	Cambodia	l/m	ilo	0.25	0.21
127 059	f	Sumatra/Riau	m	ilo/plan	3.29	0.41
125 050	f	Cambodia/Ratanakiri	d/l	sc/ilo	0.23	0.01
126 051	4	Cambodia	d/m	sc ae	1.34	0.15
126 061	f	-		- -	-	-
124 050	f	Vietnam Quang Nai	d	sc/lo	0.67	0.20
124 052	f	Viet LamDon	m/d	plan	3.18	1.62

Table3.1 Metadata derived by the TREES initiative for the 104 Landsat sample scenes used in this study, indicating the path and row of each Landsat image, and whether the full (f) or quarter (quarters 1-4 are numbered clockwise from the top-left of a full scene) image is used in the analysis. Also shown for each image is the nominal descriptor of fragmentation described by trees, the cause of deforestation for that particular pattern, and the rate of deforestation and forest degradation (1990-1997) as estimated by TREES. Satellite images are grouped by continent (Latin America, Central Africa, and Southeast Asia), and the region an image covers is documented (continued on the following page).

Path Row		Region	Pattern Of Deforestation	Cause Of Deforestation	Deforestation/Degradation Rates(%)	

Southeast Asia

Path Row		Region	Pattern	Cause	Rate 1	Rate 2
125 061	f	Sumatra Jambi	m	plan/lo	5.93	1.88
120 061	1	Kalimantan/Sarawak	d	lo/sc	0.32	0.42
120 059	f	Danau Sentarum	d	ilo/plan	0.83	1.15
118 058	f	Sara	d/m	sc/lo	0.81	4.07
118 061	f	Kalinmantan Palank	l/m	plan	1.01	0.42
118 062	f	Kalinmantan Palank	m/l	plan	1.83	1.06
117 059	f	Kalinmantan	m	lo/plan	0.77	1.88
117 060	f	Makadam	d/m	plan	1.40	4.12
117 061	f	Gunung /Lumut	m/l	ae	2.67	3.71
115 062	4	Sulawesi	m	plan	1.41	0.06
107 062	3	Seram	d/m	ae	0.27	0.08
101 064	f	Irian/Jaya	d/l	ae	0.07	0.00
100 062	f	Irian/Jaya /PNG	d	a /lo	0.16	0.30
100 066	2	PNG/Kandarisa	d	a	0.30	0.41
099 064	2	PNG /Koroba/DOMA	d/l	sc	0.83	0.21
097 064	f	PNG /Madan	l/d	lo	1.07	0.00
095 064	f	PNG /New Britain	m	sc	1.52	1.20

Latin America

Path Row		Region	Pattern	Cause	Rate 1	Rate 2
020 050	1	Guatemala	d	sc	0.72	0.00
020 046	4	Mexico/Yucatan	d	sc	0.56	0.10
019 048	3	Guatemala/Belize	d	ae/sc	1.59	0.60
016 050	1	Honduras	d	sc/ae	0.86	0.12
016 053	f	Costa Rica	d	sc/ae	0.01	0.24
011 062	4	Ecuador/Tumbes	d	ae/sc	1.58	1.05
010 064	f	Peru/Piura	d	ae	0.30	1.90

Table 3.1 (continued)

Path Row		Region	Pattern Of Deforestation	Cause Of Deforestation	Deforestation/Degradation Rates(%)	

Latin America (continued)

Path Row		Region	Pattern	Cause	Rate	Rate
010 060	4	Ecuador/Latacun	d	sc	0.28	4.68
008 059	f	Colombia/Florencia	d	sc/ae	1.71	0.59
009 053	2	Colombia	d/m	ran	0.87	2.66
009 060	4	Ecuador/Napo River	d	ae/sc	1.37	0.94
009 064	f	Peru/Bagua	d	ae/sc	0.81	0.82
009 059	f	Colombia/ Florencia	d	sc/ae	1.71	0.59
007 059	4	Colombia/Amazon	n	n	0.00	0.00
007 062	3	Peru/Nanay	n	n	0.01	0.00
004 056	4	Venezuela/ Amazon	d	sc	0.38	0. 00
007 066	f	Peru/Tingo Maria	d	ae	0.61	0.41
007 067	f	Peru/Huanuco	d	ae/sc	1.19	0.17
006 066	1	Peru/Pucallpa	d	ae	0.77	0.40
001 056	3	Venezuela/Amazon	none	ae	0.01	0. 00
001 059	4	Brazil/Amazonas	none	none	0. 00	0. 00
233 058	2	Brazil/ Roraima	none	none	0.06	0. 00
001 067	3	Brazil/Bolivia/Acre	l		-	-
002 053	2	Venezuela/Amazon	d	ae	1.40	0.65
006 068	f	Peru/Huany	d/m	sc/ae	0.23	0.34
008 059	f	Colombia/Florencia	d	sc/ae	4.90	0.00
233 062	4	Brazil/Amazonas	none	none	0.03	0. 00
231 059	3	Brazil Roraima	l	ae	0.66	0.02
232 066	1	Rondonia/Portov.	d	ae	0.29	0.07
231 067	f	Brazil/Rondonia	l	a e	3.18	0.10
232 069	f	Bolivia/Rondonia	d-l	ae/ran	0.11	0.01
228 064	1	Brazil/ Para/Itaitu	n	n	0.04	0. 00
229 069	1	Mato Grosso	m	ae ran	0.56	0.01

Table 3.1 (continued)

Path Row		Region	Pattern Of Deforestation	Cause Of Deforestation	Deforestation/Degradation Rates(%)	

Latin America (continued)

231 072	1	Bolivia	d	ae	1.02	0.11
227 062	3	Brazil/Para/ Santa	d	ae	0.94	0.04
228 067	f	Mato Grosso/Apiacas	m	ae/ran	1.42	0.00
231 075	f	Bolivia	none	none	0.03	0.08
228 069	f	Mato Grosso	m	ae	0.34	0.35
226 065	4	Brazil /Para	none	none	0. 00	0.02
226 068	f	Mato Grosso/Cuiab	m	ae/ran	1.52	0.62
224 062	f	Brazil /Para/Tucur	l/d/m	RIL/ae	2.44	0.78
222 062	f	Brazil /Para/belem	l/d/m	RIL	2.44	1.02
224 064	f	Brazil Maramba	d/m	ran	1.33	0.11
224 067.	f	Brazil Mato Grosso	m	ae/ran	2.72	0.27
225 069	2	Brazil Mato Grosso	m	ae	0.52	0.04
224 072	1	Brazil /Mato Grosso	m	ae	1.39	0. 00
222 062	f	Brazil /Para belem	l/d/m	RIL	2.44	1.02

Central Africa

198 056	f	Ivory Coast/Liberia	d	oil	1.07	0.35
196 056	4	Ivory Coast	d	ue	2.91	1.66
189 056	3	Nigeria	d	oil	0.11	0.15
187 056	1	Cameroon	d	ae	0.82	0.06
185 342	f	Cameroon	m	ue	1.15	2.79
184 057	f	Cameroon	l/d	RIL/ae	0.21	0.03
180 058	f	DRC	d	ae/RIL	0.52	0.80
178 056	f	CAR/Bangasou	d	sc	0.01	0.00
178 058	f	DRC	d	ae/RIL	0.78	0.04
177 062	3	DRC	none	none	0.04	0.05
176 062	3	DRC	l/d	ae	0.81	0.19

Chapter 3 – The Frequency, Distribution, and Scaling Properties of Forest Edges within the Tropical Humid Biome-Methods

Table 3.1 (continued)

Path Row		Region	Pattern Of Deforestation	Cause Of Deforestation	Deforestation/Degradation Rates(%)	

f= full scene used   *PNG=Papaya New Guinea*   *l=linear*   *sc=shifting cultivation*

#=number of quarter used   *DRC = Democratic Republic of Congo*   *m=massive*   *d =diffuse*   *(i)lo=(illegal)logging*

ae/ue=agricultural/urban expansion

plan=plantation

oil= oil drilling

ran=ranching

RIL=selective logging

Central Africa (continued)

Path Row		Region	Pattern Of Deforestation	Cause Of Deforestation	Deforestation/Degradation Rates(%)	
175 058	3	DRC	d	sc	0.02	0.44
175 062	f	DRC	d	ae	0.46	0.13
174 062	f	DRC	l	sc	0.21	0.1
173 061	f	DRC	d	ref/ae/ran	1.42	.19
173 059	1	DRC	d	sc/ran	0.11	0.19
158 070	1	Madagascar	d	ae	1.37	0.57
158 072	1	Madagascar	d	ae	1.94	0.00
158 074	1	Madagascar	d	ae	4.73	0.00

Total: 104 scenes, covering 6.5% of the tropical humid biome, or 129,000km^2

Table 3.1 (continued)

Image preparation and classification

The Normalised Difference Vegetation Index (NDVI) was used to measure the amount of dense tropical forest in each image. This is possible as the chlorophyll of healthy, dense, water-replete vegetation has a higher NDVI value than drier or sparse canopies. Thus, NDVI measurements allowed the land surface to be classified into 'forest' (i.e. readily transpiring dense tropical forest and wet soils) and 'non-forest' (i.e. drier sparse forest/vegetation and dry soil). Whilst wet soils are not 'forest', wet soil is more similar to readily transpiring vegetation in terms of hydrometeorology as both are water-replete (Chapter 1). The same could also be said of rivers and water bodies, but these are removed from the analysis here for simplicity. As NDVI is a physically motivated measure based upon vegetation density and moisture status, the classification presented here is more relevant to energetic phenomena, such as land surface-atmosphere interactions, than arguably more subjective (i.e. nominal) 'forest'/'non-forest' classifications. Thus, the classification presented here is very different from that of the TREES classification, which describes the land surface in terms of its physiognomy rather than its energetic status. The strengths of the NDVI metric that facilitates the classification employed in this thesis are as follows:

1) NDVI offers good discrimination between dense forest and non-forest vegetation.

2) Soils which generally exhibit a near-infrared spectral reflectance somewhat larger than the red, and thus tend to also generate rather small positive NDVI values. This makes dry bare soil easily distinguishable from dense forest.

3) NDVI is the most commonly-used measure employed by remote sensing studies to indicate an amount or the abundance of vegetation, and is routinely used across remote sensing platforms. NDVI is therefore a well-established measure that can be used for comparative studies and to facilitate other such future work.

4) The use of NDVI makes it easy to identify free-standing water (e.g., oceans, seas, lakes and rivers). These targets need to be removed from the analysis as they are neither dense 'forest' nor 'non-forest' vegetation, and thus their identification using NDVI facilitates their removal.

5) The calculation of NDVI reduces the dimensionality and thus size of the data, making it more computationally efficient.

6) NDVI is a major component of surface energy balance algorithms (e.g. Batiaassenn, 1998a, 1998b), owing to its physically motivated derivation, that relates explicitly to land surface atmosphere-interactions as a function of the amount of vegetation present.

7) With a view for further work, NDVI can be used to calculate numerous other useful measures such as those found in surface energy balance algorithms, and also fPAR etc.

NDVI is calculated from the red and near infra red bands, i.e. bands 3 (bnd3) and 4 (bnd4) of the Landsat ETM+ thematic sensor:

$$NDVI = \frac{(bnd4 - bnd3)}{(bnd4 + bnd3)} \qquad [-] \qquad \text{(Equation 3.13).}$$

For optimal 8-bit storage, a scaled NDVI can be calculated also:

$$NDVI_{scaled} = (NDVI + 1) \times 127 \qquad [-] \qquad \text{(Equation 3.14).}$$

The following targets had to be removed from the classification as they are neither forest nor non-forest and therefore cannot be included in the calculation of pattern metrics:

1) Water bodies

2) Haze contamination

3) Cloud coverage

4) Shadow coverage

Haze and cloud cover greatly biases the derivation of land-based products from satellite imagery and is common in the humid tropics. Haze correction was applied using a modified NDVI index, which removes aerosols from images, appropriately named the Aerosol-Free Vegetation Index (AFVI (Karnieli *et al.*, 2001)). Attempts were made in this project to remove haze through more adaptive (and therefore accurate) haze removal algorithms, rather than the 'stock' calibration applied when calculating AFVI. Two packages were used, that both make use of a Haze-Optimised Transform (HOT), based on vector analysis between red and blue bands (Zhang *et al.*, 2002), whereby haze free areas of imagery are used to construct a 'clear sky' vector that spans many different land cover types. The first such approach was the Scene-

based Haze Removal (SHARE) (Dal Moro & Halounova, 2005) algorithm and code kindly provided by Dr. Giancarlo Dal Moro at the University of Trieste. The second was the ERDAS equivalent, found in the atmospheric correction (ACOR2.3) tool box, which again was kindly provided by Phil Cooper at INFOTERRA. However, due to the poor correlation between red and blue bands ($r^2 < 0.08$), a reliable clear sky vector could not be constructed for correction in either of these programs.

AFVI corrects imagery by replacing the blue band with the Middle Infra Red (MIR) band (Band 5) in the calculation of NDVI:

$$AFVI1.6 = \frac{(\rho MIR - 0.66\rho\ 1.6)}{(\rho MIR + 0.66\rho\ 1.6)}$$
[-]   (Equation 3.15).

Equations are taken from Karnieli *et al.* (2001), where ρ_i are the MIR top of atmosphere (TOA) reflectances, the calculations of which are provided in the appendices (under 'conversions'). The rationale behind the use of MIR is that MIR bands are transparent to most aerosols except for dust, as typical aerosol particle sizes are significantly smaller that the MIR wavelength (centred on 1.6μm). The MIR band, however, correlated strongly with the red band, making the calibration possible. AFVI has been demonstrated to be much more robust than other equivalent measures such as the Atmospherically Resistant Vegetation Index (ARVI (Kaufman & Tanre, 1992)). Furthermore, AFVI has the advantage of not reducing the useful dynamic range of NDVI, and having almost identical values. To estimate NDVI from its aerosol free analogue, a simple equation can be applied (Karnieli *et al.*, 2001):

$$NDVI = AFVI.*0.99+.01$$
[-],   (Equation 3.16).

Whereas this procedure removes haze from the imagery, dense cloud cover remains. Cloud is easily discerned from its characteristic NDVI values, and a cloud mask was created. The same can be said for water bodies, such as rivers and lakes. Both cloud and water bodies were removed post-hoc, using their masks to identify and replace cloud and water body pixels using a nearest-neighbour replacement algorithm that replaced pixels classed as 'cloud' or 'water' with a value from the nearest Cartesian 'forest' or 'non-forest' pixel. Small shadows were removed by nearest neighbour replacement also. The aim of this procedure was to remove targets that were not required for analyses in a fashion that would preserve the spatial structure of the underlying forest/non-forest patches that are the object of this study.

Whereas the removal of shadows, clouds, and water bodies could have been achieved more accurately via the use of Digital Elevation Models (DEMS, e.g. using

ERDAS ATCOR3), water masks etc, it was decided that given the quality of the images used in this analysis and the predetermined sampling scheme which avoided large water bodies, ice etc., a more simple series of methods could be used.

Unsupervised classification was processed by means of a simple series of thresholds to remove areas of water and differentiate between two simple classes: dense moist tropical forest and non-forest. Thresholding involved assigning a number to a given class by defining upper and lower NDVI value limits for that class. The choice of lower and upper limits of NDVI values for each class was guided by those values used in the production of the TREES tropical forest map (Achard & Estreguil, 1995 (Southeast Asia); Eva *et al.*, 2004 (South America); Mayaux *et al.*, 1999 (Central Africa))). Upper thresholds for water/cloud, non-forest and forest were chosen as NDVI values of 0.09, 0.3, and 0.8, respectively.

Whereas one would expect the effect of seasonality to be less in tropical areas due to a less pronounced seasonality, the spectral separability of dense moist forest from other land cover types (in particular vegetation mosaics) is particularly sensitive to seasonality. This occurs due to the deep-rooted nature of forest vegetation, which, unlike shallower-rooted mosaics/non-forest, can maintain transpiration through dry periods. The cumulative effect of this difference leads to a greater spectral contrast between these cover types at the end of the dry season(s)/beginning of wet season(s). Whereas GLCF maintain that image selection for their database is selected when forest is growing the most, data selection was checked again to ensure that scenes taken from the end of the dry season/early wet season were selected to ensure the greatest contrast between dense moist tropical forest and other cover types. With the exception of two scenes and some of the scenes expressing almost complete forest coverage, all scenes selected fitted in with this criteria, although it must be noted that exact dates for the seasons for each year were not available, and that selection was based on a general estimate of seasonal patterns.

Sensor simulation

To adhere to the sampling scheme imposed by the TREES initiative and to permit the fast implementation of image processing algorithms, images were processed as image quarters and split into quarters again (n=1065), essentially splitting each image into smaller units (Figure 3.10), referred to as 'subunits' from here on.
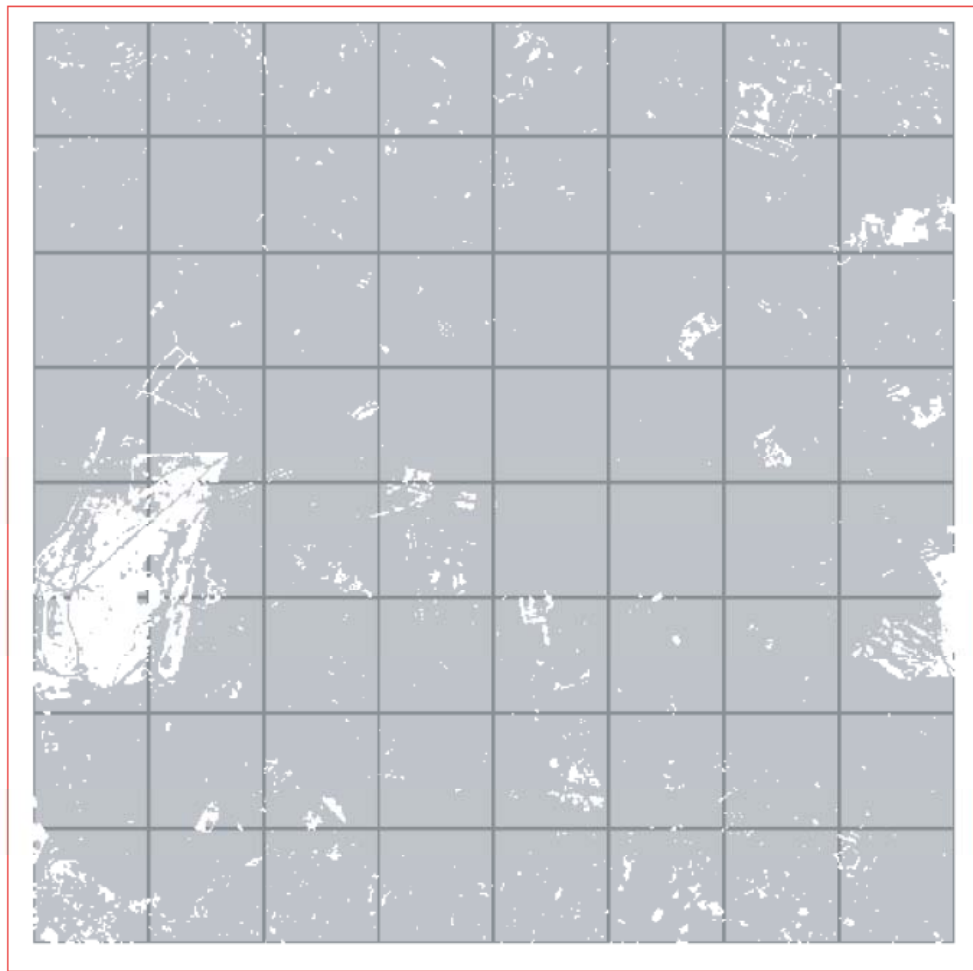
Figure 3.10   A classified image split into smaller 'subunits', with original image (red line) reduced in size by a clipping the image to account for Landsat scene overlap.

To address the influence of sensor resolution upon the calculation of statistics (which are addressed subsequently under headings 'Patch Metrics', 'Wavelet Analysis', and 'Texture Measurement'), an aggregation programme was written in MATLAB (www.mathworks.com) to average pixel values in sequentially larger pixels (double the size of the pixels at the previous resolution), thereby coarsening Landsat image resolution. Image resolution was coarsened in this fashion from its original resolution (30m) to model the effect of increasing sensor resolution typical of MODIS imagery (250m) and AVHRR imagery (1km) (Figure 3.9). Classification was performed before the aggregation exercise, and thus is a simulation exercise similar to those of Turner *et al.* (1989) and Woodcock & Strahler (1987). The simulation exercise presented here is thus employed to isolate the influence of scale on the size and shape of certain patches at critical thresholds of resolution (Gervin *et al.*, 1985), by eliminating effects of spectral aggregation that would be present in cross-sensor comparisons. Analysing resolution effects across sensor platforms (e.g. comparing Landsat imagery at 30m resolution to AVHRR imagery at 1km resolution) would not account for

spectral aggregation within sensors, which can influence the classification of satellite imagery (Markham & Townsend, 1981).

Patch metrics

For each of the 104 Landsat scenes classified into forest and non-forest, perimeter, area, and PSI were calculated for all forest patches within each of the subunits (Figure 3.10) of the classified image. Area-weighted mean patch fractal dimension (AWMPFD) and mean patch fractal dimension (MPFD) were also calculated for each of the subunits of each classified image. The calculation of each patch metric was repeated at each simulated sensor resolution, as described in the previous section. Measuring the perimeter, area and PSI constitutes a vector-based fractal analysis, whereby measurements are made by treating each forest patch as a vector target, i.e. a coherent shape made from many scalar pixels.

Wavelet analysis

Wavelet analysis in this study attempts to formalise operationally the link between vector (measuring the perimeter and area of a shape) and box counting (counting the number of perimeter and area pixels within a n x n pixel neighbourhood or 'box') fractal analysis. Whereas Millington *et al.* (2003) draw attention to the important division and differences between these two approaches, this study - whilst recognising both approaches as distinct - draws on their similarities to determine whether a combined approach improves scaling analysis.

Wavelet analysis represents the box-counting equivalent to the vector analysis of patch metrics. Three different wavelet families were used determine how the trade-off between the spatial and scale localisation of a signal (i.e. a forest edge) influences the textural analysis and its application to stratification of vector patterns (i.e. landscape metrics). This included using one wavelet family possessing good localisation properties (the Haar/DB1 wavelet) but offering poor scale-approximations, another family having poor localisation properties but offering better approximations (DB10 wavelet) wavelet, and one 'intermediate' family that represents a compromise between the two extremes (the DB5 wavelet). Wavelet analysis was programmed using the software Matlab (Mathworks Inc., USA) to analyse images through the multi-resolution decomposition with DB1, DB5 and DB10 wavelet families. Wavelet coefficients were stored as their respective matrices for textural analysis.

Wavelet degradations were applied to classified imagery at simulated resolutions only (for details of the simulated resolutions see 'Sensor Simulation'. This was done to provide a low-resolution proxy for each of the subunits within classified images to stratify the (scaling) patterns of their high-resolution, vector-based (i.e. landscape metric), counterparts. Degradation was applied at successively greater scales following a dyadic sequence, where each subsequent scale is twice that of the previous. When applying a discrete wavelet transform containing more than two scaling or wavelet function coefficients, typically either a mirror or periodic extension technique is applied to the wavelet filter. In this study a mirror extension was used. However, this is not entirely efficient and thus all scenes were clipped by 5%. Clipping in this nature also accounts for the 5% overlap of adjacent paths and rows by Landsat coverage (Figure 3.10).

Texture measurement

Texture analysis focussed on the phenomena of interest – i.e. forest edges as isolated by wavelet filters. Thus, texture calculations were based on the detail coefficients produced by the wavelet analysis outlined previously, representing the vertical, horizontal and diagonal structures within each of the image units as depicted in Figure 3.6. Texture measures represent 'features' of an image, and were repeated for wavelet coefficients produced for each direction (vertical, horizontal, and diagonal) at each scale of the dyadic wavelet degradation, for each wavelet family (DB1, DB5, and DB10).

Texture was calculated using co-occurrence matrices created for each image subunit. Co-occurrence matrices applied to wavelet details captures the spatial dependence of wavelet detail coefficients upon one another, i.e. the spatial dependence of forest edges in this case. A co-occurrence matrix C is an n × n matrix, where n is the number of gray-levels within the image. The matrix C (i, j) counts the number of pixel pairs having the intensities i and j. These pixel pairs are defined by specified distances and directions, which can be represented by a displacement vector d = (dx, dy), representing the number of pixels between the pair in the x and y directions. A co-occurrence matrix was calculated for the four cardinal directions. The detail coefficient matrices were absolute-valued since the averaging and differencing depend on the window structures, and in this case positive and negative contrast levels have the same meaning.

Traditional co-occurrence techniques also consider several distances between pixels. However, the texture descriptors are calculated based on multi-resolution wavelets, and the resolution levels act as distances. The following texture descriptors were then extracted from each co-occurrence matrix: energy, entropy, contrast, homogeneity, sum-mean, and variance, details of which are provided in Table 3.2.

Feature	Definition	Interpretation
Entropy	$-\sum_i \sum_j P[i,j] \times \log P[i,j]$	*Measures the randomness of a gray-level distribution*
Energy	$\sum_i \sum_j P^2[i,j]$	*Measures the number of repeated pairs*
Contrast	$\sum_i \sum_j (i-j)^2 P[i,j]$	*Measures the local contrast difference between gray-level values in pixel pairs*
Homogeneity	$\sum_i \sum_j (P[i,j] / (1 + |i-j|))$	*Measures the local homogeneity of a pixel pair*
Sum Mean	$(1/2)[\sum_i \sum_j iP[i,j] + \sum_i \sum_j jP[i,j]]$	*Provides the mean of the gray levels*
Variance	$(1/2)[\sum_i \sum_j (i-\mu)^2 P[i,j] + \sum_i \sum_j (j-\mu)^2 P[i,j]$	*Variance indicated how spread out the distribution of gray-levels is*

Table 3.2: The definition and interpretation of those texture measures (features) as calculated in this study from co-occurrence matrices of wavelet coefficients (Matlab Users' Guide). Definitions are computed on a grey level co-occurrence matrix of m x n pixels, relating each pixel (i) to its neighbour (j) for the number of m x n grey level co-occurrence matrices (p).

Feature reduction and EM segmentation

The texture measures outlined in the previous section are called features. A series of features representing different texture measures represents a feature vector. As texture measures were repeated for wavelet coefficients at different scales, for three different wavelet families, and in three directions (horizontal, vertical, and diagonal), a large feature vector was created for each of the subunits within each classified image.

Reduction of the feature vector is imperative to avoid over-fitting and to obtain a manageable feature space. Feature reduction was achieved by a Principal Components Analysis (PCA), to create a single feature comprising a linear combination of those texture measures (i.e. the feature vector) outlined in the

previous section. PCA feature-reduction allows the implicit selection of those scales, directions, and wavelet families used in the image degradation, in addition to removing redundant texture measures. The resulting principal component 'features' as calculated for each of the subunits of each classified image were segmented using an expectation maximisation (EM) algorithm, splitting the population of feature values into different 'texture' classes.

CHAPTER 4 – THE HYDROMETEOROLOGY OF A HUMID TROPICAL FOREST PATCH – RESULTS AND DISCUSSION

This chapter disseminates the results of the field methodology outlined in Chapter 2 that was employed to establish *"Whether forest edges transfer more water to the atmosphere than forest interiors"* (Aims and Objectives, Preface).

Various factors (including elephant disturbance, battery bank failure and diesel shortages) hampered the maintenance of a necessarily large array of sensors, meaning that the resultant dataset suffered from frequent interruptions. Once consequence was that simultaneous observations of clearing, forest edge and interior sites were rarely possible, and comparisons of forest-atmosphere water fluxes across sites had to be made on different days. Thus, analyses presented within this chapter were chosen to account for day-to-day changes in synoptic-scale variables that influence forest-atmosphere water fluxes and confound their comparison across different days.

Transpiration of trees in the forest interior was estimated to range from 1.8-2.5 mm dy^{-1} (657-890 mm yr^{-1}). Mean sap flux in trees within 50 meters of a forest-clearing boundary was found to be 73% greater than that in trees further into the forest interior. Evaporation from the forest canopy constituted a high fraction of annual rainfall (33%) at the Wawasan Bentar (DA1) site, but showed no edge effect similar to that of sap flux. The forest edge as a whole, however, expressed transpiration rates (228-794 mm yr^{-1}) 22% lower than forest interiors, owing to the lower basal area (and thus lower area of xylem) of trees within edge plots. One site, however, with a higher basal area, showed a much higher transpiration rate of 1335 mm yr^{-1} - 40.5% greater than that of the forest interior. Observations of increased sap flux in trees at the forest edge were corroborated by measurements of canopy temperature, which were lower a) at the forest edge, suggesting greater tree water use there and b) than that of air temperature over the forest canopy, suggesting a downward flux of sensible heat and concomitant increase in forest-atmosphere water flux. Gradients of air temperature, vapour pressure deficit, and wind speed from the adjacent clearing to the forest interior indicated that warm, dry air moving from the clearing to the forest was the most credible cause of increased sap flow of trees near the forest edge. This hypothesis was supported by a strong correlation between the vapour pressure deficit of air over the clearing and tree water use.

Chapter 4 – The Hydrometeorology of a Humid Tropical Forest Patch – Results and Discussion

The observation period was characterised by light winds and high humidity with overcast frequently reducing solar radiation. The reduction of incident (incoming) shortwave radiation ($S_{incident}$) leads to the diurnal pattern of $S_{incident}$ having a less-tapered appearance than commonly reported at other tropical sites (e.g. Ciencala *et al.,* 2000), with a plateau reaching about 450 Wm^{-2} (n = 65 days) from ~08:30 to ~16:30 hours (Figure 4.1a). A relatively low maximum value of 473 Wm^{-2} was recorded. Incident shortwave radiation deviated from and returned to zero at ~06:00 and ~18:00 respectively (Figure 4.1a). With a mean diurnal value of 405 Wm^{-2} (about 14.6 MJdy^{-1}), $S_{incident}$ here is comparable to that of other sites throughout Sabah and Southeast Asia. The mean incoming shortwave radiation presented here is higher than that reported at higher tropical latitudes (e.g. Giambelluca *et al.*, (2003) report $S_{incident}$ to be approximately 200 Wm^{-2} in Northern Vietnam) yet is lower than the values of Kumagai *et al.* (2004a) and Ciencala *et al.* (2000) who report values of ~650 Wm^{-2} (Lambir Hills, Sarawak) and ~500Wm^{-2} (Crocker Range, Sabah) respectively. The maximum value of 473 Wm^{-2} reported here is much lower than that reported by Ciencala *et al.* (2000) of approximately 970 Wm^{-2}.

As shortwave radiation tends to comprise the majority of net radiation (i.e. available energy to the land's surface for evapotranspiration, Figures 4.1a, 4.2 and 4.3), it is expected that transpiration rates would be relatively low at this site (Figure 4.3). The main observation period (31st March- 14th July, 2007) straddles the onset of the south-westerly monsoon, which itself follows the drier months of March and April. The high cloud cover (and thus reduced incident shortwave radiation) at this time is typical not only of lowland tropical humid forest before the onset of a period of increased rainfall. The apparent rapid ascent and decent of shortwave radiation values at sunrise and sunset (Figure 4.1 a) may be compounded by the measurement period coming just after the equinox. Observing Figure 4.1a, it can be seen there is a slight but notable depression of incoming shortwave radiation in the mid afternoon at about 14:00 hours, with higher values coming before noon. It is presumed that the depression occurs due to cloud formation in the late afternoon following evapotranspiration earlier in the day. As rainfall at the site over the study period was frequent and light the depression in incoming shortwave radiation is not very pronounced.

Diurnal Incident Shortwave Radiation (Wm^{-2})

Diurnal Surface Temperature (°C)
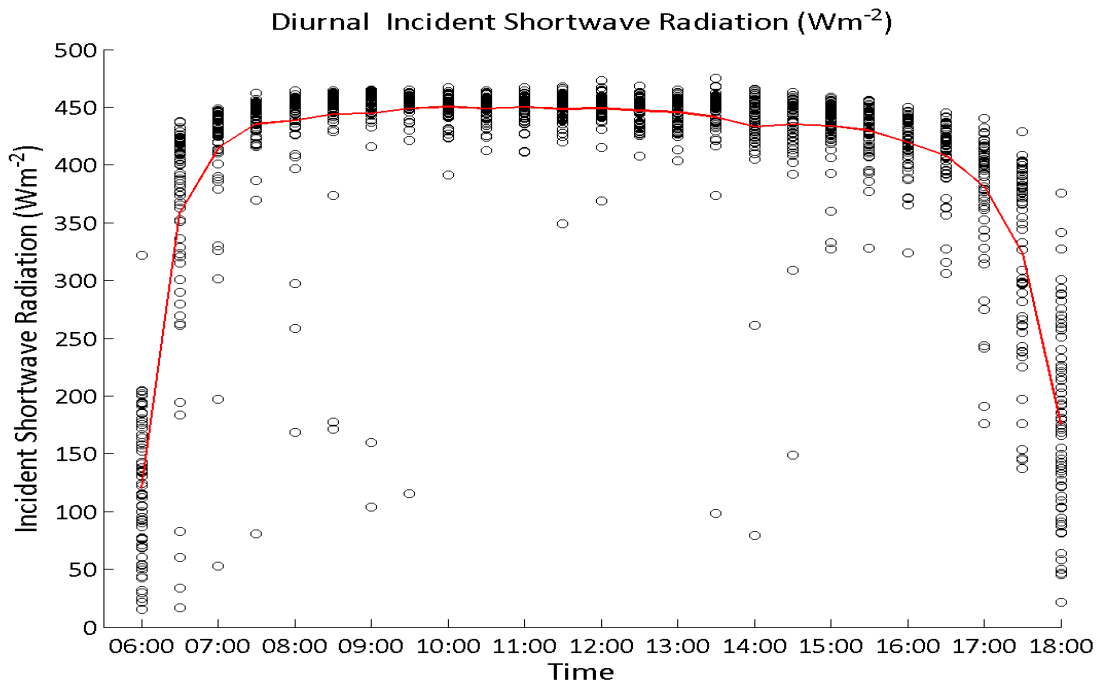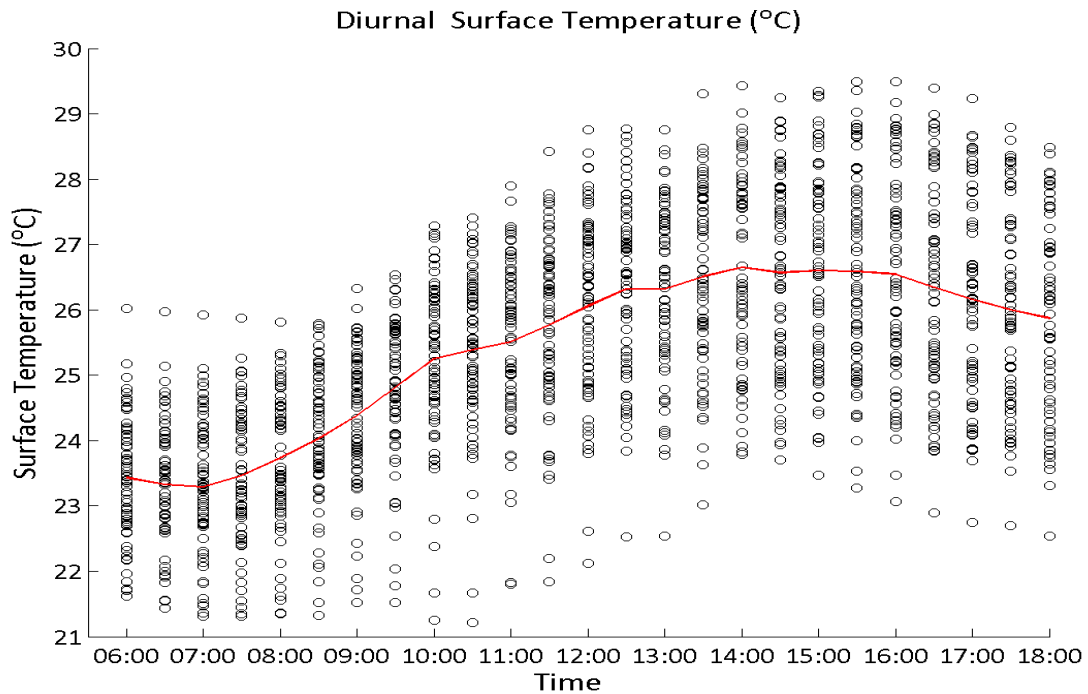
Figure 4.1   Diurnal patterns of a) incident shortwave radiation (Wm^{-2}) and b) canopy surface temperature (°C) between 06:00-18:00 hours inclusive, as measured within plot D (forest Interior).Red lines represent the mean of all data points, which are daily replicates of 30-minute averages at a given (24-hour clock) time, represented by circles (n=65 and n=63 days, for shortwave radiation and canopy surface temperature, respectively).

Chapter 4 – The Hydrometeorology of a Humid Tropical Forest Patch – Results and Discussion

Diurnal Net Longwave Radiation (Wm^{-2})
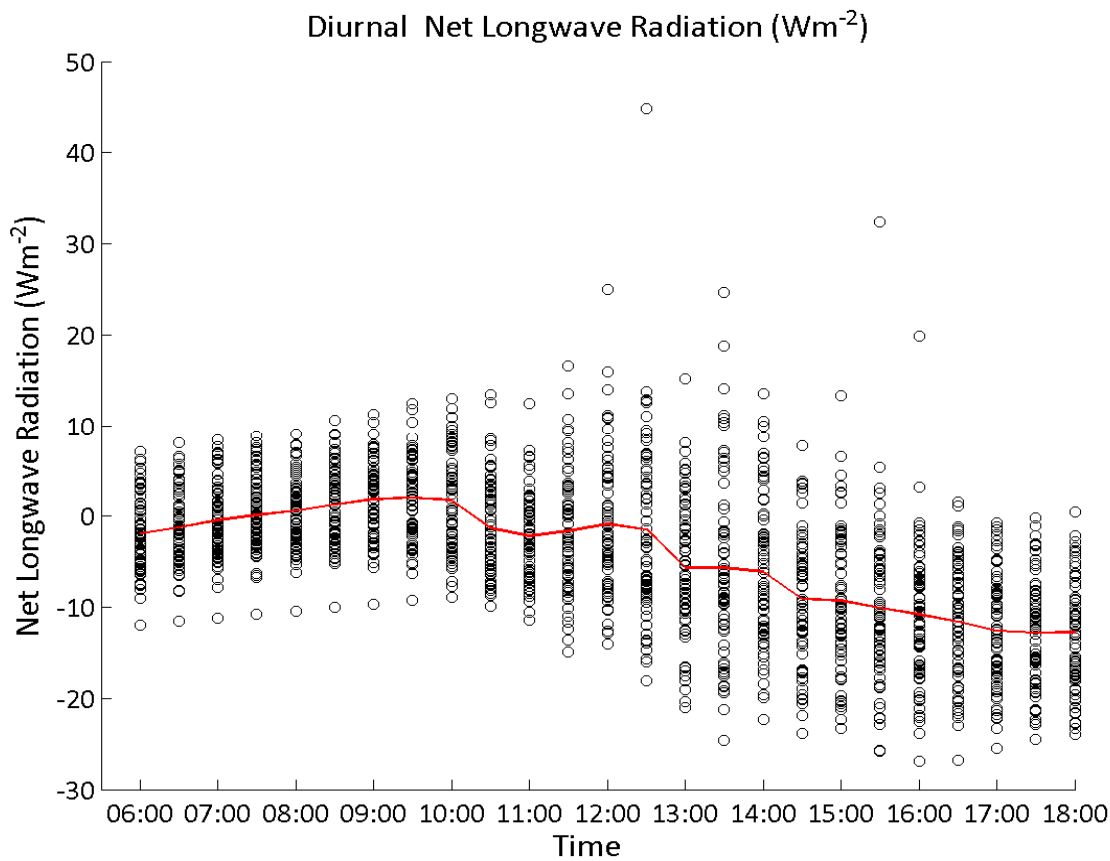
Figure 4.2   Diurnal patterns of net longwave radiation as measured at station D. Solid red line is the mean of n=63 daily replicates of 30-minute averages at a given time (expressed in 24-hour clock units), which themselves are represented by circles. A dotted red line is also presented to show where net longwave radiation is zero.

Mean diurnal (06:00h-18:00h) net longwave radiation was - 4.40 Wm^{-2} (ranging -12.8 – 2.0 Wm^{-2}, n= 63 days) - indicating an overall flux of longwave radiation away from the land's surface (Figure 4.2). This is a slightly higher (less negative) value compared to values reported elsewhere (-28.90 Wm^{-2}) under relatively high cloud (84%) conditions (Shuttleworth *et al.*, 1993, Reserva Ducke, Brazilian Amazon). The value reported here is less negative than reported elsewhere for continental tropical humid forests (-28.90 to - -54.03 Wm^{-2}), and exceeds zero for a short period around 08:00-10:30h (Figure 4.2). However, good agreement is found with other tropical humid maritime lowland forests such as Puerto Rico (11Wm^{-2}), under similarly cloudy conditions (Rn = 13.5 MJ dy^{-1}). It would appear that the combined effect of increased tree water use and resultant high humidity act to suppress the conversion and transfer of longwave energy from the canopy to the atmosphere. This concept is supported further by the steady reduction of outgoing longwave radiation at night, which suggests the land surface does not store as much longwave radiation- possibly as a result of its substantial water use during the day. Net longwave radiation is not

as constant across the day as reported in other studies, and varies by approximately 10 Wm^{-2}, although this is still a modest amount of variation in comparison to the total energy budget of the land surface.

Net longwave radiation steadily increases until its slight positive peak at 10:00h (Figure 4.2), and then gradually falls into the evening. The point at which net radiation becomes least negative is immediately after the longest period of incident shortwave radiation in the morning (Figure 4.1a). A theoretical link between an increase in transpiration, the consequent cooling of the canopy and cloud creation, and a decrease in outgoing longwave radiation offers a possible explanation for this.
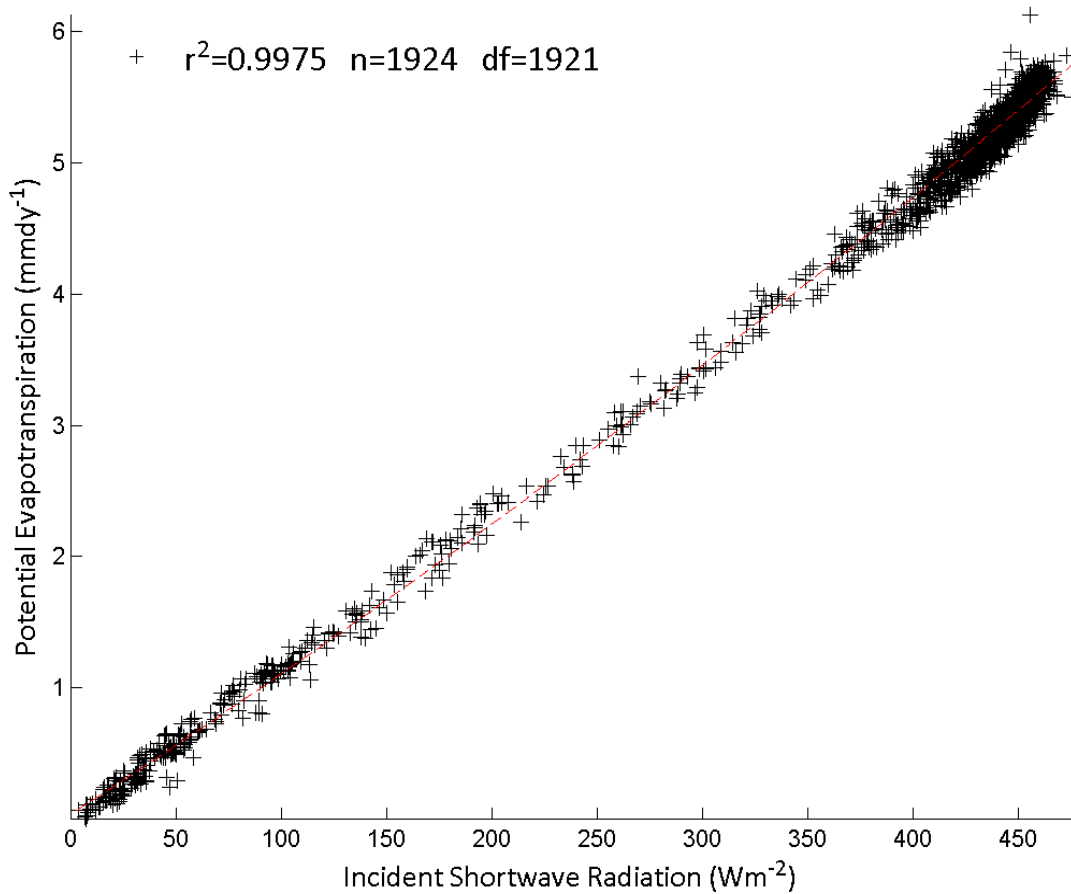
Figure 4.3 The influence of net longwave radiation, when combined with incident shortwave radiation of a much larger magnitude, upon estimated potential evapotranspiration (PE, Equation 1.10, Chapter 1), as derived from the available energy (A, Equation 2.1, Chapter 2) at the canopy surface of plot D. The red line represents a linear regression fit between S$_{incident}$ & PE, showing how the negligible influence of net longwave radiation renders a strong linear relationship between incident shortwave radiation and estimated PE.

Because the shortwave contribution is much greater than that of longwave radiation it is highly correlated with the net radiation and thus the available energy available to the land surface for evapotranspiration (Figure 4.3). For this reason, the difference in albedo (see further Chapter 2, Equations 2.1 and 2.3) between the swidden and the forest determines to a large extent the difference in available energy to the land surface and thus the transpiration/latent heat flux from it. That is, the higher albedo of the swidden will lead to it having less available energy in comparison to the rougher forest. Comparing incoming shortwave radiation to net radiation over the forest, it can be seen this is indeed the case, with a tight correlation between the two variables. This means that patterns such as the early afternoon depression of incoming shortwave radiation are mirrored in net radiation patterns. Observations of mean midday albedo (n=10) are presented in Figure 4.4, as calculated following Equation 2.3, Chapter 2.

Albdeo of Plots A-D
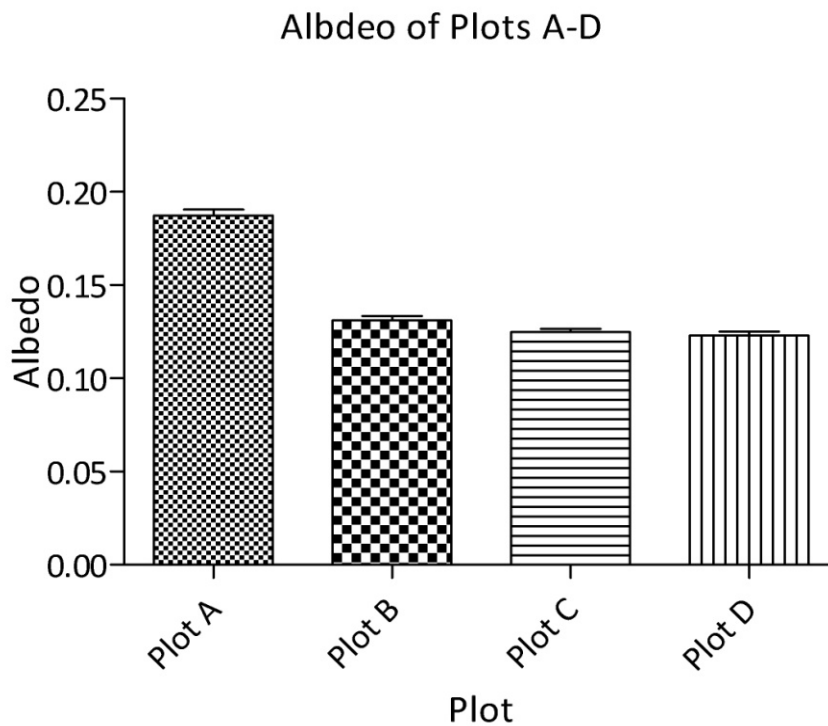
Figure 4.4   Mean midday albedo (α, dimensionless) for plots A-D (swidden to forest interior), as calculated following Equation 2.3, Chapter 2. Error bars represent standard error.

Albedo of the swidden (plot A, $\bar{x}$ = 0.19, n=10, σ= 0.010) is significantly higher (unpaired one-tailed t-test, P<0.001, n=40, df = 38, t = 20.82) than that of the forest ($\bar{x}$ = 0.126, n=30, σ= 0.007, all forest stations B-D) owing to its lighter colour and smoother physiognomy (Figure 4.4). The forest edge (plot B, Figure 4.4) is appears to be slightly rougher ($\bar{x}$ = 0.13, n=10, σ= 0.007) than that of plots C ($\bar{x}$ = 0.12, n=10, σ=

0.006) and D ($\bar{x}$ = 0.12, n=10, σ= 0.007) (Figure 4.4), a significant difference being observed between the albedo of plots B and C, (unpaired two-tailed t-test, P<0.05, n=20, df =18, t= 2.28), and B and D (unpaired two-tailed t-test, P<0.05, n=20, df =18, t= 2.71), which may result from the considerable amount of disturbance observed in plot B (light logging and a small skid trail). Data here were measured at midday on ten randomly selected days for each plot. Ideally a diurnal course of albedo measurements should be taken. It can be expected that following rainfall the swidden could have a much lower albedo owing to its darker colour when wetted.

Swidden-forest gradients

The effect of proximity to the forest edge, and comparisons between the forest and swidden can be made using various synoptic variables. I here focus on air temperature, relative humidity, vapour pressure deficit, wind speed and surface temperature; mean diurnal patterns of which are presented in Figures 4.8-4.10, with average diurnal values presented in Figure 4.6. Figure 4.5 demonstrates that wind was blowing into the forest the majority of the time.

It was only possible to make simultaneous observations of wind speed to compare across sites. For other variables (vapour pressure deficit, air temperature, and surface temperature), days having precipitation of less than 2mm dy^{-1} were selected to compare different sites whilst controlling for the influence of rainfall (i.e. moisture status of the land surface, the importance of which is addressed in Chapter 1, section 1.2) upon thermodynamics of the system. Comparisons are made between days by calculating the mean diurnal value of a given variable using 30 minute averages between 06:30-18:00h (Figure 4.6).

wind rose in swidden

wind rose at forest edge
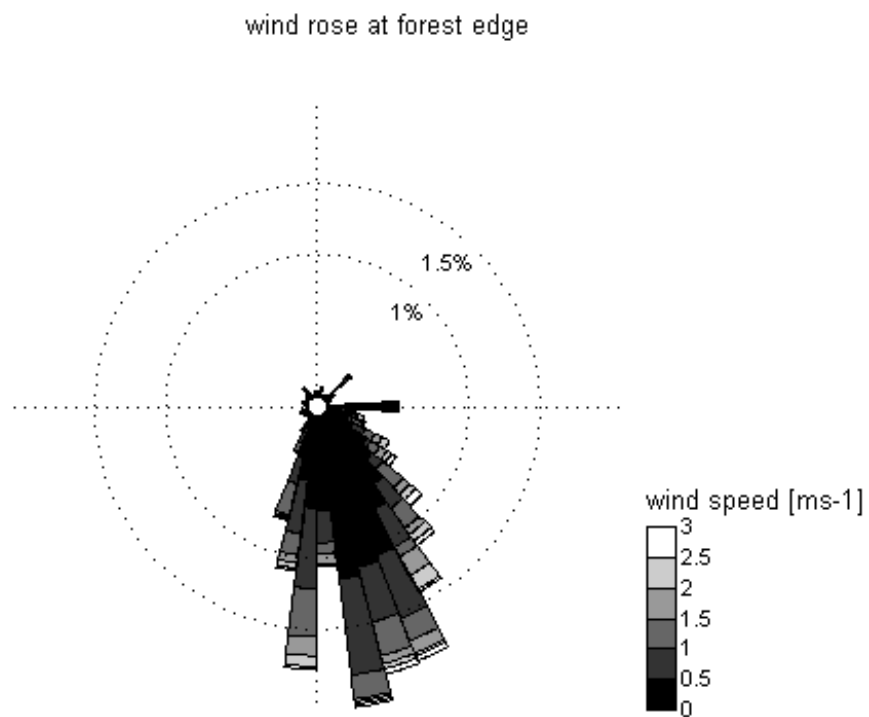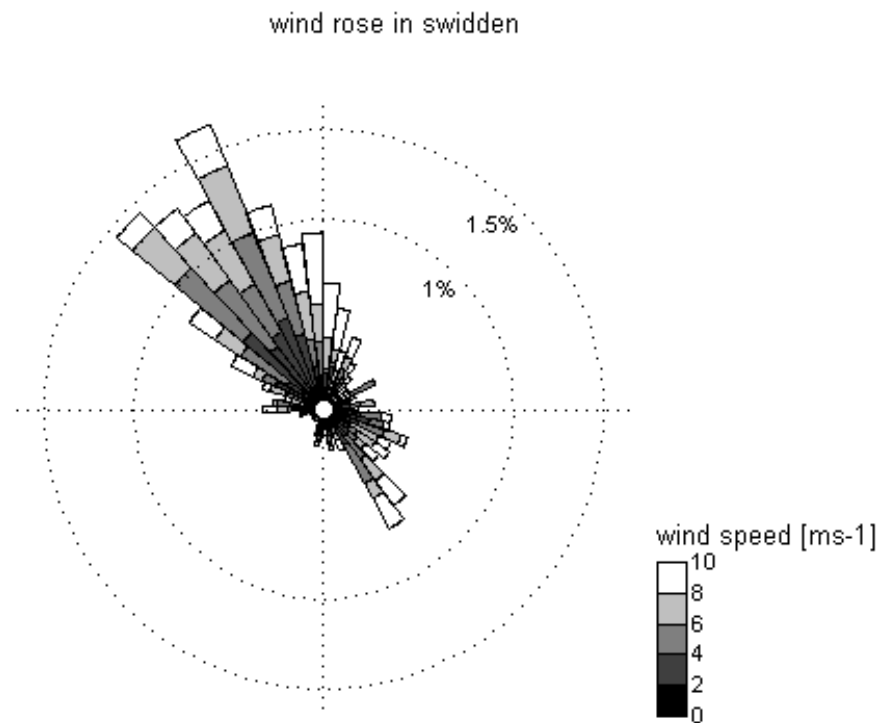
Figure 4.5   Wind roses showing wind speed and direction at a) plot A (swidden) and b) plot B (forest edge). Line represents relative orientation of the forest (f) – swidden (s) boundary to the wind direction.

c

d

e

f
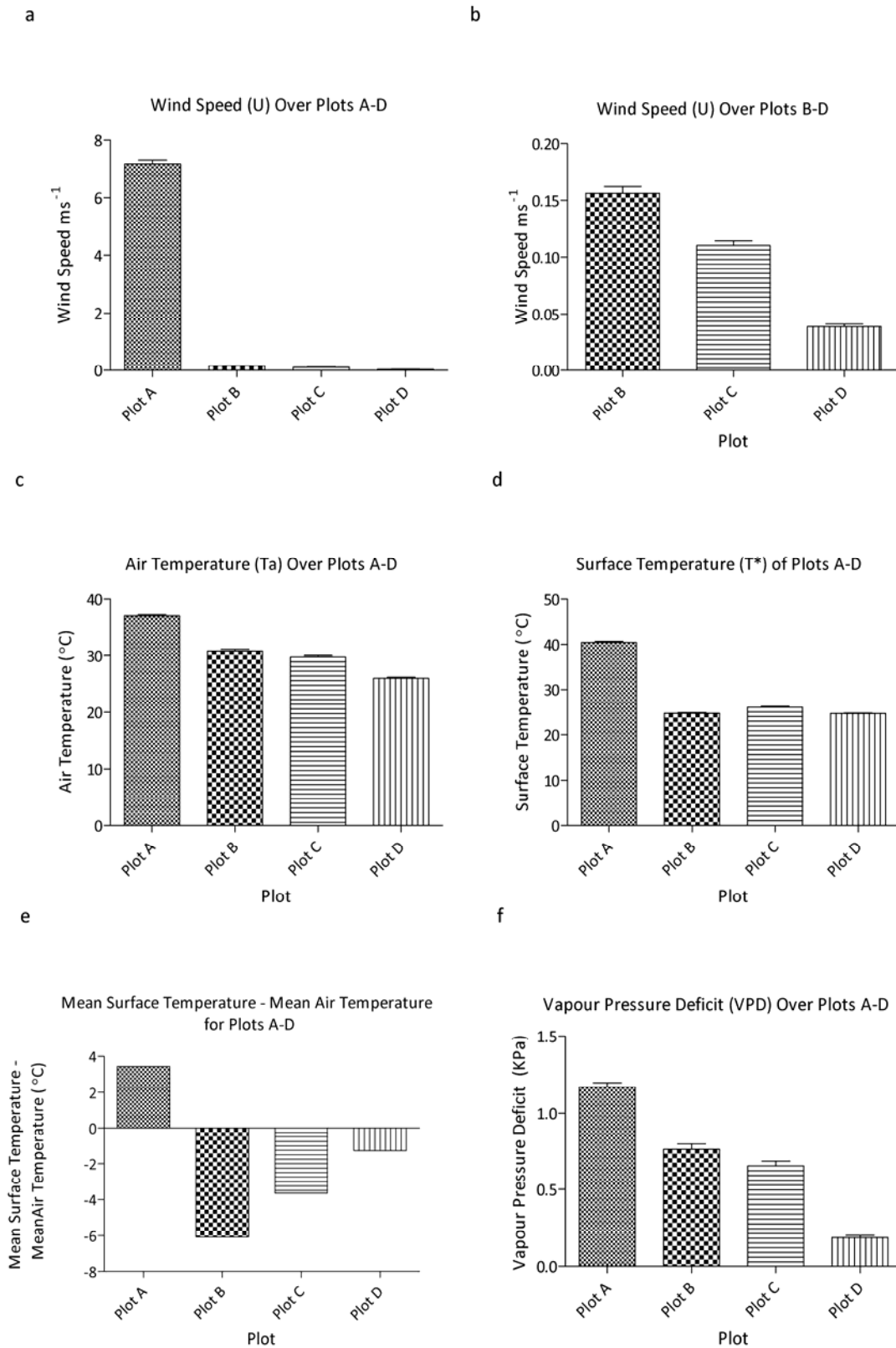
Figure 4.6   Mean diurnal values (taken as the mean of all 30-minute average values between 06:30 and 18:00 inclusive) of a, b) wind speed, c) air temperature, d) surface temperature, e) (mean surface temperature – mean air temperature) and f) vapour pressure deficit measured over plots A-D for days where precipitation was less than 2mm dy^{-1}. Error bars show standard error.

To compare wind speed, mean wind speed at each height was adjusted to a common reference height 3 m above the respective zero plane displacement height (d). Roughness length (z0) was taken to be 0.1 vegetation height, and d was set to be 0.67 vegetation height. The wind speed at a given height (z2) can be computed from a measured wind speed measured at height (z1):

$$\frac{U2}{U1} = \frac{[ln(z2 - d) - ln(z0)]}{[ln(z1 - d) - ln(z0)]}$$ [-]   *Equation 4.1,*

where U1 and U2 are mean wind speeds at elevations z1 and z2, respectively (ms^{-1}). Note that strictly speaking this relationship only applies to neutral atmospheric conditions and stability corrections should be applied for unstable and stable conditions (Rosenberg *et al.,* 1983). However this requires temperature profile measurements and thus corrections were not possible, though the uncorrected wind speeds are acceptable for these purposes (Thomas Giambelluca (2008), personal communication, University of Hawaii, USA).

A significant pattern in mean wind speed between plots A-D (repeated measures ANOVA, P<0.0001, df=3, n= 792 (33days), F = 2552) shows higher wind speeds in the swidden ($\bar{x}$ =7.17 ms^{-1}, n=792, σ= 3.96, Figure 4.6a) than over forest sites B ($\bar{x}$ = 0.16 ms^{-1}, n=729, σ= 0.17, Figure 4.6b), C ($\bar{x}$ = 0.11 ms^{-1}, n=792, σ= 0.11, Figure 4.6b) and D ($\bar{x}$ = 0.04 ms^{-1}, n= 792, σ= 0.07,Figure 4.6b), as the swidden surface is much smoother than the aerodynamically rough forest. Mean swidden wind speed peaks at 10:30h ($\bar{x}$ = 8.89 ms^{-1}, σ= 3.58, n=33, Figure 4.9a), whereas wind speed in the forest is lower at this time(unpaired one-tailed t-test, P<0.0001, df = 129, t= 24.64) and averages 0.089 ms^{-1} (σ= 0.09, n=99) across stations B-D; peaking much later in the day (0.19 ms^{-1} average across sites at 17:00h, σ= 0.17, n=99). Upon transition from the swidden to the forest, wind speed abruptly drops an order of magnitude (Figure 4.6a), and an influence of fetch reduces wind speed further (repeated measures ANOVA, P<0.0001, n= 792, F= 485.2) to its lowest point at the forest interior (plot D, Figure 4.6b). This is in fitting with the concept of forest edges being high flux environments, where a net downward flux of momentum (i.e. a change from a high wind speed to a low wind speed) at the forest edge is theoretically expected to produce an increased upward flux of latent and/or sensible heat depending on the moisture status of the land surface. Wind speed follows a diurnal pattern, with higher values coming during the day and peaks in the late morning to early afternoon. Mean wind speed in the swidden is quite high, possible due to day time valley winds travelling the length of the slight valley upon which Wawasan Bentar was positioned.

Significant differences in surface temperature (T*, Figure 4.6d) across plots A-D (Kruskal-Wallis Test, P<0.0001, df= 3, H= 1291) and B-D are present (Kruskal-Wallis Test, P<0.0001, df=2, H=1291). The swidden has the highest mean diurnal surface temperature ($\bar{x}$ = 40.43^{o}C, σ= 5.60, n= 552 (23 days), Figure 4.6d), possibly due to the higher bulk density of the soil there and its reduced ability to hold as much accessible water (section 4.3, this chapter). This, along with the sparse vegetation in the swidden, indicates that even though the swidden has less energy available to it by virtue of its higher albedo (Figure 4.4), the energy received by the swidden is predominantly converted into sensible rather than latent heat.

Air over the forest however is much cooler (Figure 4.6c), owing to the cooling of the canopy by transpiration. Indeed, surface temperate is a good proxy for the rate of transpiration, with tree crowns (and thus, *en masse,* the canopy) behaving in a similar fashion to wet bulbs (Pereira *et al.*, 2009) by cooling as increased water loss acts as a sensible heat sink. It can be seen that there is a lower surface temperature at the forest edge (plot B, $\bar{x}$ = 24.77^{o}C, σ= 2.90, n= 648 (27 days), Figure 4.6d) than further into the forest (plot C, $\bar{x}$ = 26.12 ^{o}C, σ= 3.66, n= 552 (23 days), Figure 4.6d), although the plot furthest into the forest (plot D) has a similar mean surface temperature to that of plot B (plot D, $\bar{x}$ = 24.75 ^{o}C, σ= 1.85, n= 744 (31 days), Figure 4.6d).

Of particular importance is that at all forest sites (Plots B-D) mean air temperature (Tdb) exceeds mean surface temperature (Figure 4.6e) This is indicative of heat advection, and is quite sizeable – i.e. there appears to be a so-called 'oasis effect' (Oke, 1983) occurring within this forest patch. Following the rationale of Pereira *et al.* (2009), it seems quite possible that if a tree crown acts as a wet bulb and cools under advective forcing then the same could be said for the canopy as a whole. This differential is greatest at the forest edge (T*-Tdb = -5.65^{o}C, plot B, Figure 4.6 e), and is least at the second forest edge plot (T*-Tdb = -2.98^{o}C, plot C, Figure 4.6e). This is a stark comparison to the positive swidden value (T*-Tdb ≈ 6°C, plot A, Figure 4.6e).

Clear trends are expressed at stations A-D in air temperature (Kruskal-Wallis Test, P<0.0001, df= 3, H= 574.7, Figure 4.6c), which decreases from Plot A to Plot D, and also vapour pressure deficit 4m above the canopy (Kruskal-Wallis Test, P<0.0001, df= 3, H= 344.5, Figure 4.6f), which increases from Plot A to Plot D. These trends demonstrate a significant influence of fetch (distance from the forest edge) for both mean diurnal air temperature (Kruskal-Wallis Test, P<0.0001, df= 2, H= 143.1) and

vapour pressure deficit (Kruskal-Wallis Test, P<0.0001, df= 2, H= 155.3) 4 m above the forest canopy (i.e. in plots B-D, Figures 4.6c and 4.6f, respectively).

The air over the forest edge is generally hotter (plot B, x̄ = 30.86 °C, σ =5.14, n = 288 (12 days), Figure 4.6c) and drier (i.e. a higher VPD, plot B, x̄ = 0.76KPa, σ= 0.59, n= 288 (12 days), Figure 4.6f) than that of those plots further into the forest, and indeed the plot with the lowest vapour pressure deficit and lowest air temperature is that of plot D (with x̄ = 26.02 °C, σ= 2.85, and x̄ = 0.19KPa, σ= 0.24, for air temperature and vapour pressure deficit, n= 11 days) at about 300 meters into the forest (Figures 4.6 c and 4.6f).

Daily mean relative humidity over the forest canopy at its edge (x̄ = 76.43, σ = 19.97, n = 288 (12days)) and over the swidden (x̄ = 50.06%, σ = 25.54, n = 288 (14 days)) are much lower than reported at the Danum Valley field site (74% and 95% at 14:00h and 08:00h respectively). Given the nature of the swidden cover (highly compacted mineral soil), and the high surface temperature there, it stands to reason that the relative humidity will be much lower than the Danum site which is over grass situated immediately adjacent to a large river (Sungai Segama), and is furthermore sheltered by surrounding trees (Marsh & Greer, 1994).   The diurnal pattern of relative humidity is similar to that reported at the Danum site however, with a similar differential (24.07% vs. 21% at Danum) in the swidden between 08:00h (62.66%) and 14:00h (38.59 %). It should be noted that all sites here report the lowest relative humidity not at 14:00h but at 12:30h and a direct comparison is not possible with the Danum site as measurements are only made at 08:00h and 14:00h. Accounting for the canopy height explains the difference in relative humidity values over the canopy. As near canopy values of relative humidity and temperature are very rare, it is very easy to make the mistake of assuming that those values above the canopy will be comparable to those measured elsewhere at ground level.

Values of relative humidity measured in this study (minimum mean relative humidity = 59.34% (σ= 17.29, n= 12days), 59.91% (σ= 17.16, n= 14 days), and 91.10% (σ= 9.01, n= 11 days) for stations B-D respectively) are comparable to those measured under similar conditions. For example, Madigosky & Vatnick (in Lowman & Rinker, 2004) report above canopy (32m and 24 m) relative humidity to reach a minimum (15:00h) of about 62% and 67% respectively at the Amazon Conservatory for Tropical Stuides (ACTS, Iquitos, Peru). Given the similar latitude (S3° 14' W72° 55') and position of this tropical site, and the relatively undisturbed nature of the forest at ACTS (and thus

lower sensible heat within the region as a whole) the values of relative humidity reported here seem reasonable considering the proximity to the swidden and also the degraded and patchy nature of the forest in the Yayasan Sabah logging concession as a whole.

It is interesting to note that Giambelluca *et al.* (2003) report an *increase* in relative humidity at a forest edge measured in Vietnam. An increase in relative humidity is indicative of increased latent heat flux, but also of the formation of a boundary layer, which would act to decouple the land surface from advective edge effects. The strong gradient of relative humidity presented here suggests that should an increased latent heat flux be present at the forest edge then the gradient of vapour pressure deficit is maintained there.

Regressions (first order polynomial) between the mean diurnal patterns of relative humidity at each station are presented in Table 4.1. It can be seen that there is a high correlation between plot A and B ($r^2= 0.88$), and that the correlation between the swidden weakens with distance in to the forest edge ($r^2= 0.81$ and $r^2= 0.71$ for sites C and D). The same pattern is reflected in vapour pressure deficit (Table 4.1 and Figure 4.7). This can be taken as support for the advection of drier air from the swidden into the forest gradually adjusting to the underlying surface as it travels into the forest.

	r^2	n	df	Slope	Intercept
Vapour Pressure Deficit (KPa)					
Plot A vs. Plot B	0.89	24	22	1.67	-1.22
Plot A vs. Plot C	0.86	24	22	1.41	-0.99
Plot A vs. Plot D	0.61	24	22	0.27	-0.12
Relative Humidity (%)					
Plot A vs. Plot B	0.88	24	22	0.72	39.45
Plot A vs. Plot C	0.81	24	22	0.62	47.01
Plot A vs. Plot D	0.71	24	22	0.10	89.05

Table 4.1: Regression coefficients between the mean diurnal pattern of vapour pressure deficit and relative humidity at station A and those of stations B-D (n= means of half-hour periods between 06:30-18:00 for 12 days when precipitation < 2mm dy^{-1}).
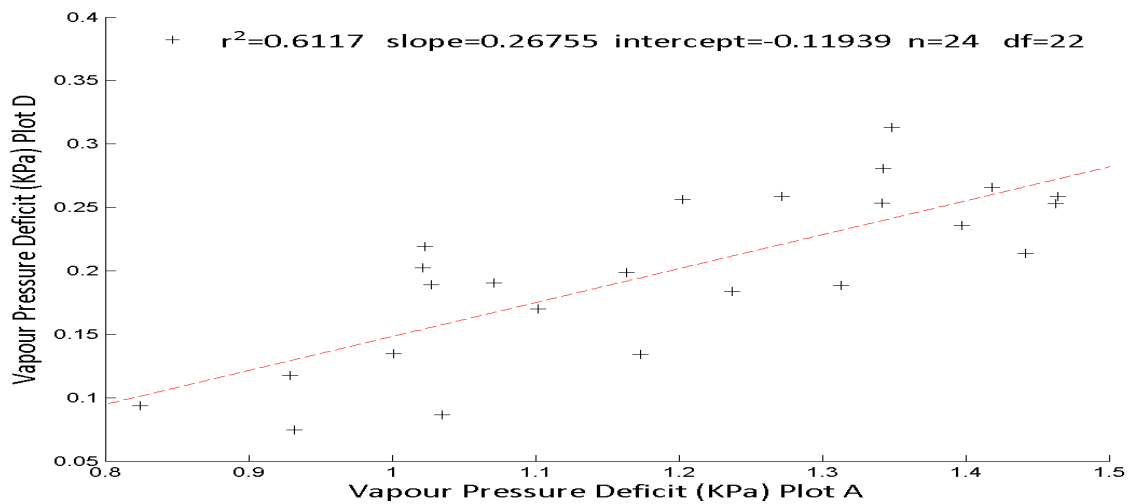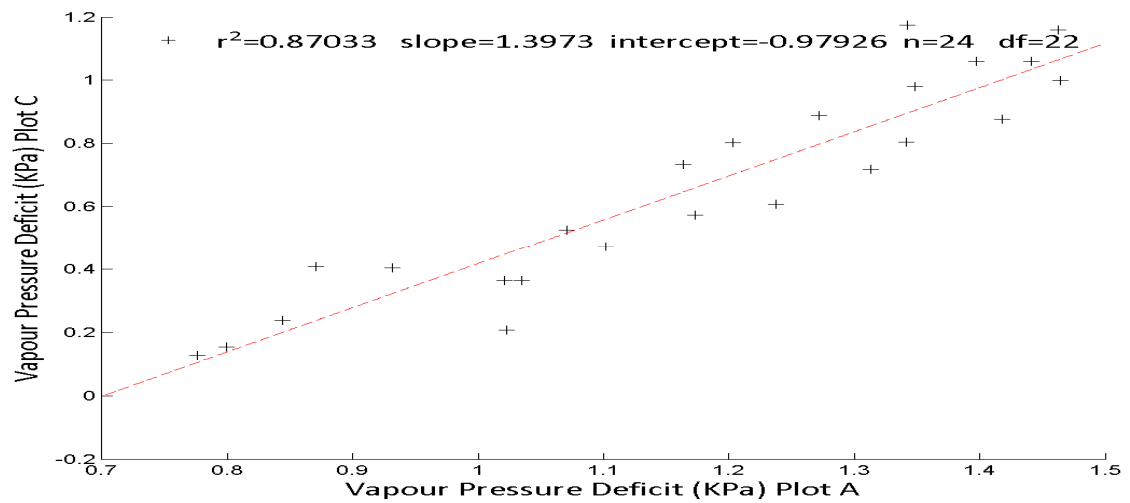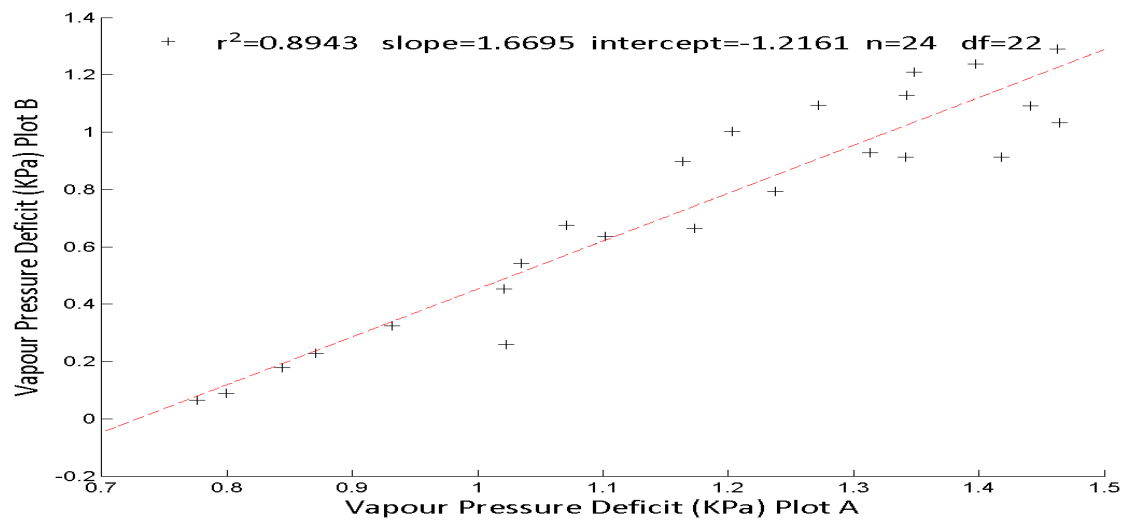
Figure 4.7   Regressions between mean diurnal patterns of vapour pressure deficit as measured in swidden (Plot A) and forest plots (Plots B-D) (top to bottom) for days when precipitation < 2mm dy^{-1}.
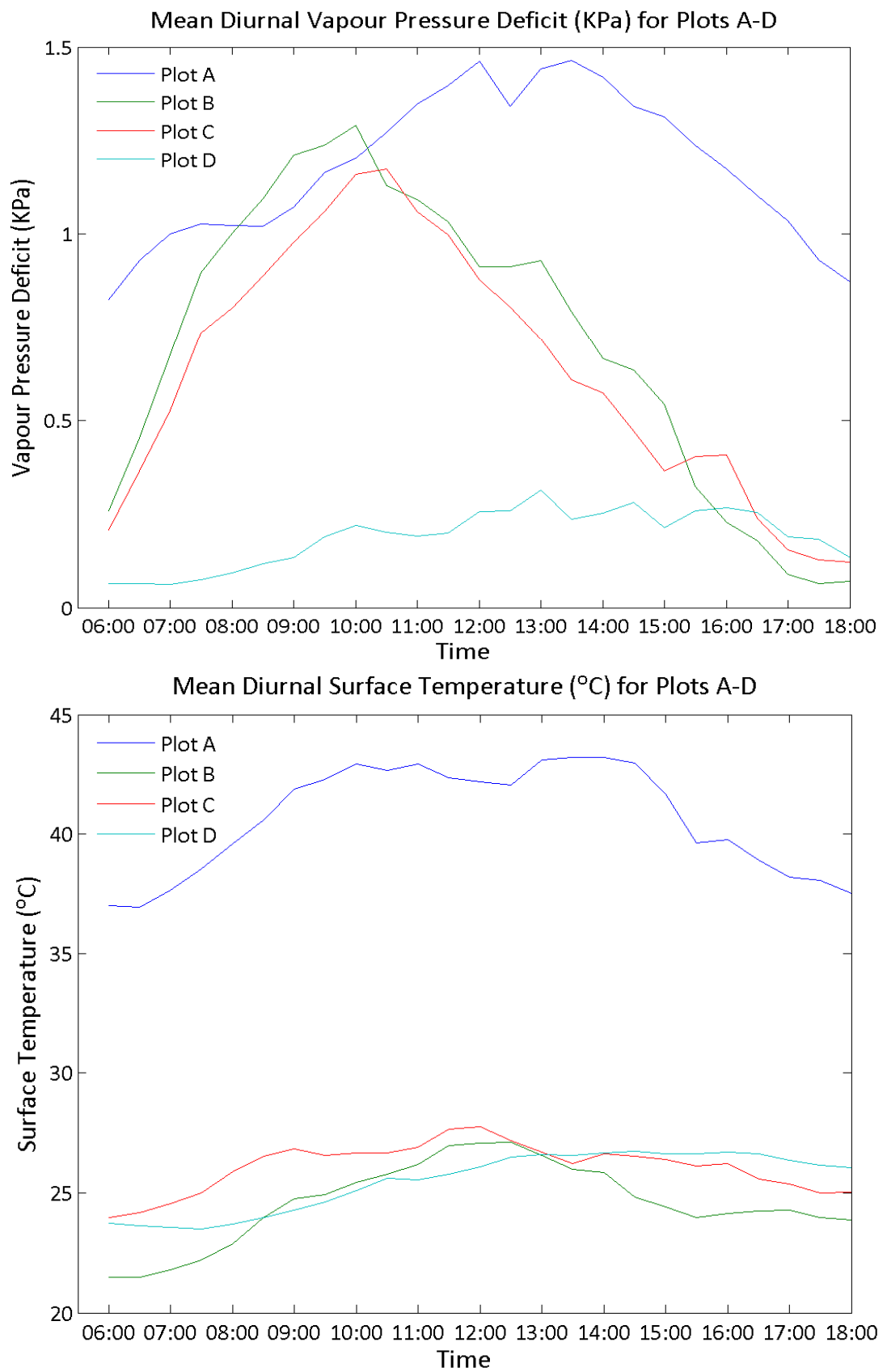
Figure 4.8   Mean diurnal patterns (06:00-18:00) of vapour pressure deficit (top) and surface temperature (bottom) as measured over plots A-D when precipitation < 2mm dy^{-1}.
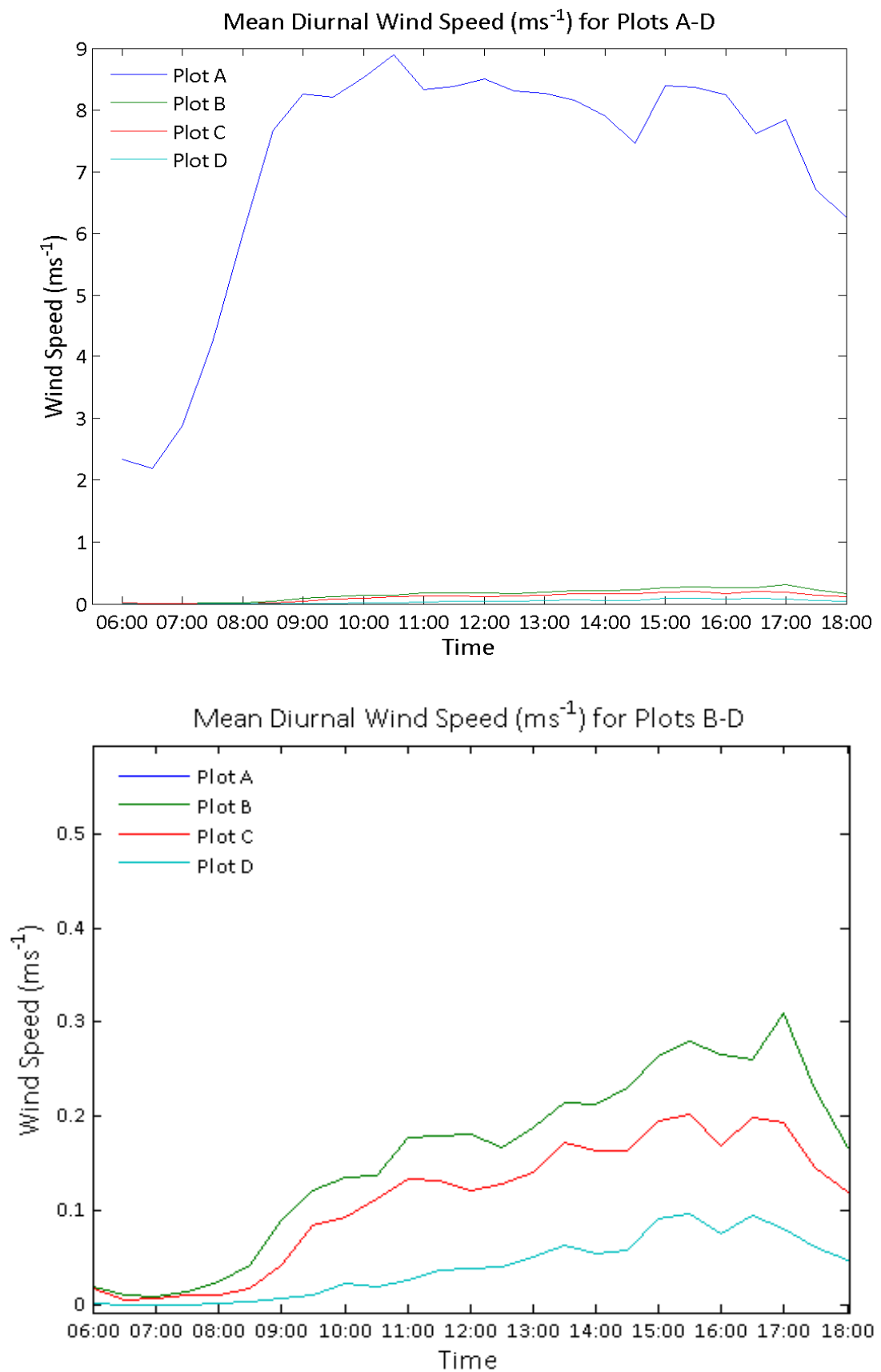
Figure 4.9   Mean diurnal patterns (06:00-18:00) of wind speed as measured over plots A-D when precipitation < 2mm dy^{-1}.
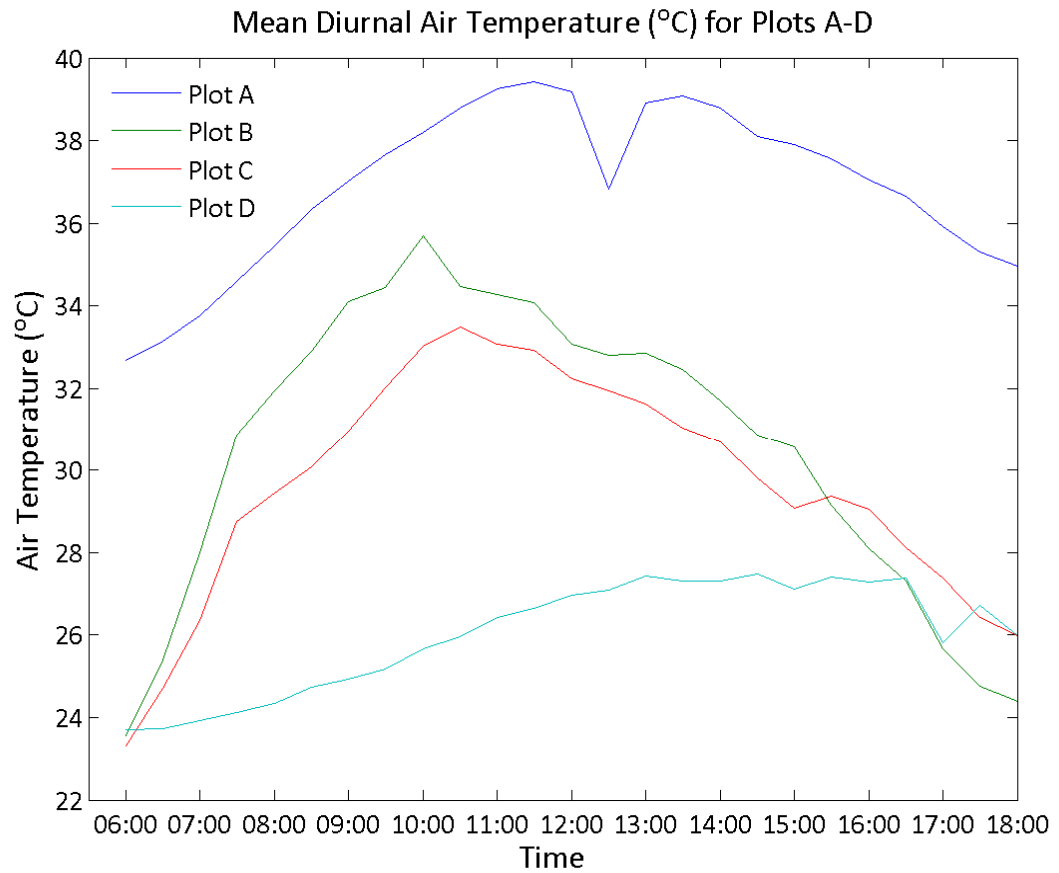
Figure 4.10 Mean diurnal patterns (06:00-18:00) of air (dry bulb) temperature as measured over plots A-D when precipitation < 2mm dy^{-1}.

The mean heat flux (H) from the swidden can be estimated using the resistance method:

$$H = \frac{(\rho\ Cp\ T^{*} - Tdb)}{r_a} \qquad\qquad [Wm^{-2}] \qquad\qquad Equation\ 4.2$$

Mean aerodynamic resistance (ra), as derived from mean wind speed and the average vegetation height (0.3m) near the automatic weather station, was estimated to be 34.57   sm^{-1}. The estimated aerodynamic resistance here is indeed the typical value for short grass (Oke, 1983). Patterns of diurnal heat flux are presented in Figure 4.11. Net longwave radiation of the swidden, like that of the forest, was fairly constant throughout the day, but at the swidden was much more negative (-110.98 Wm^{-2}) and showed slightly greater variation (44.56 W m^{-2}). Mean heat flux was 117.62 Wm^{-2}, which represented 55% of estimated net radiation (253.3 Wm^{-2}) at this site. It should be noted that estimates of net radiation require an estimation of soil heat flux which was estimated to be 40 Wm^{-2} at this site. These figures are highly comparable to those presented by Giambelluca *et al.* (2000) for unused pasture in

Igarapé-Açu, Brazil (Rn =313 Wm^{-2}, H= 166 Wm^{-2}, H/RN =0.54). The mean diurnal patterns of calculated parameters are shown in Figure 4.11.
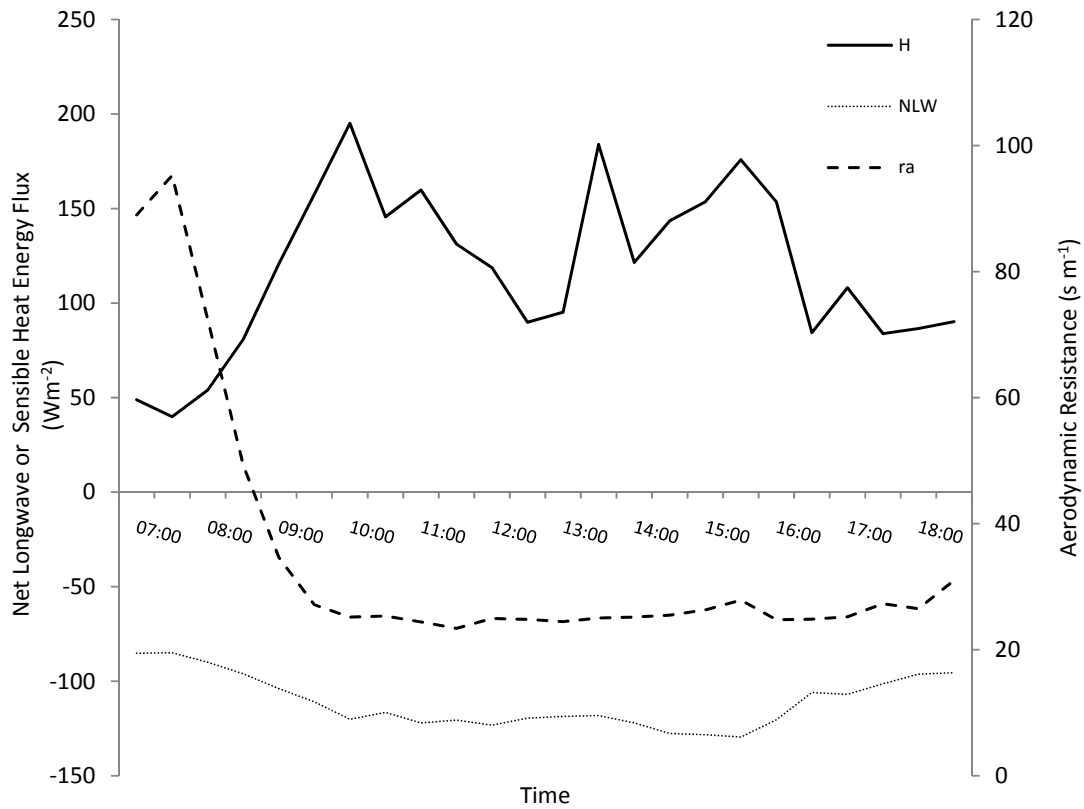
Figure 4.11   Mean diurnal patterns of sensible heat flux (H), aerodynamic resistance (ra) and net longwave radiation (NLW) over the swidden.

There is also an edge effect below the canopy as demonstrated by averages of relative humidity and temperature measured at 4m (i.e. below the canopy, Figure 4.12). Due to the mass failure of loggers, only four distances into the forest are presented here: 10, 60 and 40 and 120 meters into the forest edge. It can be seen that in fitting with previous studies there is a clear pattern of decreasing relative humidity with distance into the forest from its edge (Figure 4.12), although four measurement points is hardly conclusive. As expected, the relative humidity above the forest is much lower than that measured at approximately the same fetch lower below the forest.

The synoptic variables presented here are highly consistent with the depiction of forest edges as high flux environments (Veen *et al.*, 1996), suggesting a zone which actively absorbs thermal energy and momentum from surrounding areas and transfers this energy into an increased latent heat flux from its readily transpiring canopy.
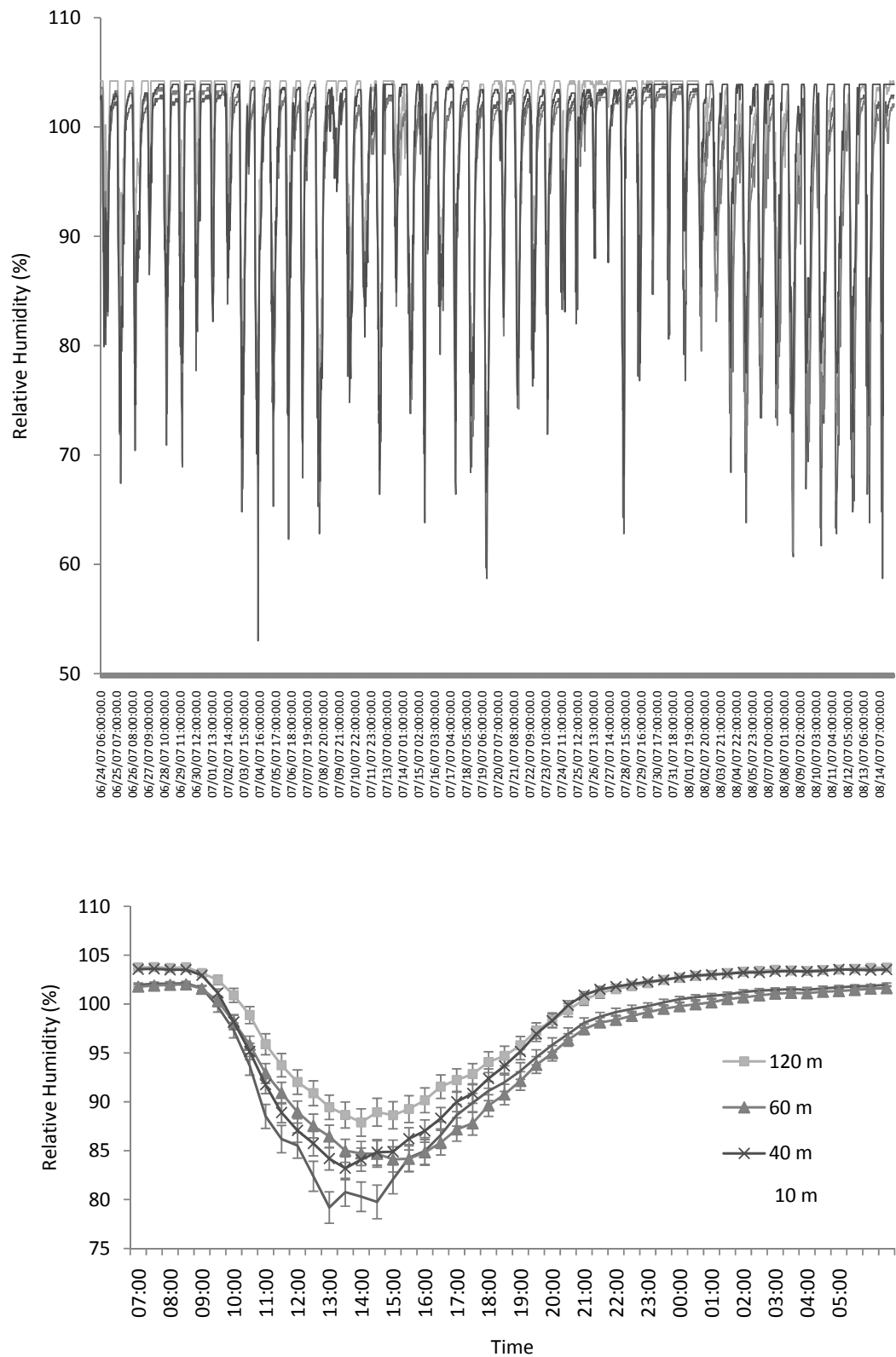
Figure 4.12   Diel patterns of relative humidity (4m height) at four distances into the forest edge (10m, 40m, 60m and 120 m). Mean diel pattern (07:00 – 06:30 h) shown in bottom panel, where error bars denote the standard deviation.

Bulk density

Bulk density at the swidden was much higher (paired one-tailed t-test, P<0.01, n=20, df =9, t= 3.724) than that in the forest ($\bar{x}$ = 1.60 gcm^{-3}, σ= 0.256, and 1.14 g cm^{-3}, σ= 0.211, for forest and swidden, respectively, n =10). Standard deviation for the forest is slightly higher than that of the stamping ground. The higher bulk density value in the swidden is to be expected owing to the compaction of the soil by heavy machinery in the process of creating the stamping ground. Indeed, most of the organic top layer had been removed, exposing the much denser mineral soil below the surface. Judging by the difference in height between the cleared area and adjacent forest, it appears that the organic soil layer was relatively thin, and certainly wouldn't have been more than 2 metres deep. Bulk density values for disused log landings taken shortly after abandonment are typically 1.8-2.0g cm^{-3} (Nussbaum, 1991). Disturbance at Wawasan Bentar is not as extreme as this, as the site has yet to be used. It would be expected that the compaction of soil at this site is somewhere in between that of used stamping grounds and lesser-used skid trails. This is confirmed by the slightly lower value of bulk density for this site than reported by Nussbaum (1991), conforming to 'category B' disturbance typical of compacted skid trails (Brooks & Spencer, 1997). The highly compact nature of the soil in the swidden suggests a resultant decline in total pore space, which means that the soil needs a lower moisture input to become saturated and for run off to occur – something particularly pertinent to the available moisture for evaporation on this sloping site. The reduction in total pore space also results in water being harder to extract from the ground either by plants or through evaporation. After time, runoff forms rivulets in the ground (clearly visible at this site), meaning that water is either locked in the soil or immediately redistributed away from the area by the rivulets. As this site is on a slope such a scenario is highly likely.

Bulk density of the forest is slightly higher than values reported for primary forest, owing to the disturbance of the surrounding forest associated with the process of tree removal and clearing the stamping site. Owing to the higher bulk density of soil in the swidden it is expected that what water is held in the soil is likely to be inaccessible to plants owing to the increased tension at which it will be held by the smaller pores there. This means that a decreased latent heat flux can be expected from the swidden.

Xylem depth

Both Meinzer *et al.* (2001b) and Giambelluca *et al.* (2003) have shown there to be a consistent and linear relationship between tree size (radius) and xylem depth, independent of species. This is particularly important for the stand scale estimation of tree water-use (Equations 2.24 and 2.25, Chapter 2). Data from this study show a similar relationship for those trees (n=16) at Wawasan Bentar, and are presented alongside those found of Meinzer *et al.* (2001b), Ciencala *et al.* (2000) and Giambelluca *et al.* (2003) in Figure 4.13.
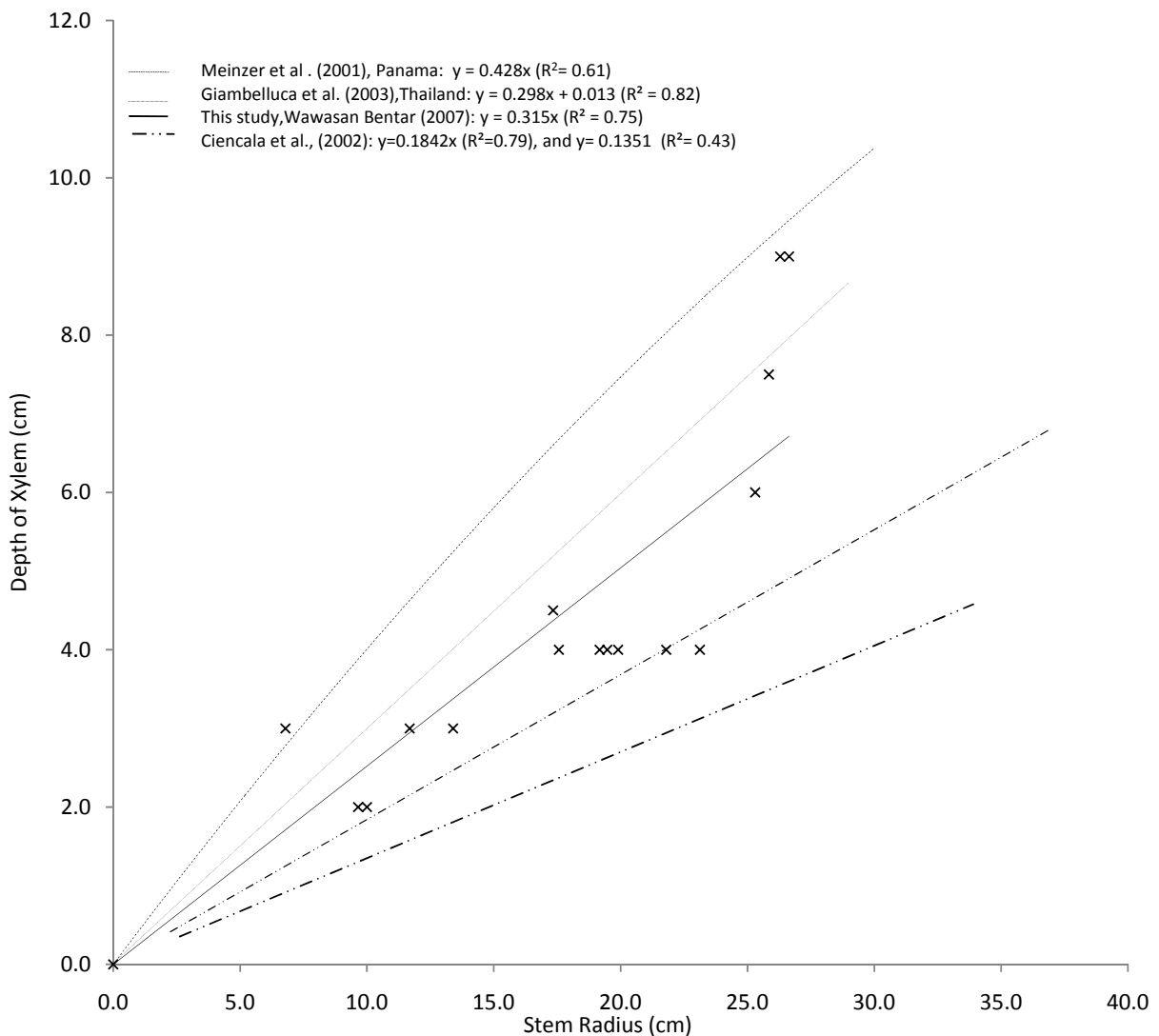
Figure 4.13 Relationship between stem radius (sr) and xylem depth (dx) for 16 individual trees at Wawasan Bentar expressed alongside relationships for other tropical sites. Raw data shown in Table 4.2.

Chapter 4 – The Hydrometeorology of a Humid Tropical Forest Patch – Results and Discussion

Macaranga Species	Xylem Depth (cm)	Stem Radius (cm)	Correction Coefficient (-)
M.hypoleuca	4.0	17.6	0.857
M.hypoleuca	4.0	19.5	0.813
M.pearsonii	6.0	25.3	0.895
M.pearsonii	4.0	23.1	1.286
M.pearsonii	3.0	11.7	0.705
M.hypoleuca	3.0	13.4	0.843
M.hypoleuca	2.0	9.6	0.899
M.pearsonii	4.5	17.3	0.757
M.pearsonii	4.0	19.2	0.747
M.pearsonii	2.0	10.0	0.893
M.hypoleuca	3.0	6.8	0.763
M.pearsonii	4.0	19.9	0.660
M.hypoleuca	4.0	21.8	1.305
M.hypoleuca	9.0	26.3	0.820
M.hypoleuca	9.0	26.6	0.727
M.pearsonii	7.5	25.8	0.731
		Mean	0.856
		Standard Deviation	0.186
		Standard Error	0.046

Table 4.2: Relationship between stem radius (sr) and xylem depth (dx) for 16 individual trees at Wawasan Bentar, and the associated correction coefficient (CC, Equation 2.32, Chapter 2) calculated from area weighted sap flux measurements at 0.5 centimetre increments into sapwood from cambium.

All four studies shown in Figure 4.13 express a similar pattern. The relationship in this study is also apparently species-independent (r^2=0.75), although only *Macaranga hypoleuca and M. pearsonii* individuals are measured. The fit presented here includes an assumed (0, 0) 'measurement', without which the r^2 falls to 0.67. This pattern lies between that measured by Giambelluca *et al.* (2003) for a site in northern Vietnam (*Vernicia montana*, *Alphonsea tonkinensis*, and *Garcinia planchonii*.) and those of *Acacia mangium* measured by Ciencala *et al.* (2000) in the Crocker range. All species measured by Giambelluca *et al.* (2003) and Ciencala *et al.* (2000) are diffuse-porous tree species and thus the pattern presented here is consistent with those of other studies.

The site-specific relationship elucidated here for Wawasan Bentar was used to correct stand-scale estimates of water-use for xylem depth (using the correction coefficient, CC, Table 4.2, following Equations 2.27 – 2.32, Chapter 2) to ensure sap flux estimates were as accurate as possible. This relationship also demonstrates that

for the range of tree sizes in which sap flow was measured, it can be expected the entirety of each relatively short probe was in contact with sapwood, and consequently that corrections for incomplete probe contact are not necessary.

Radial profiles of sap velocity

For each of the 16 trees measured in the previous section (Table 4.2), the radial profile of sap velocity is expressed as a fraction of the speed measured by a standard 2cm probe at a depth from the cambium (d) in Figure 4.14.
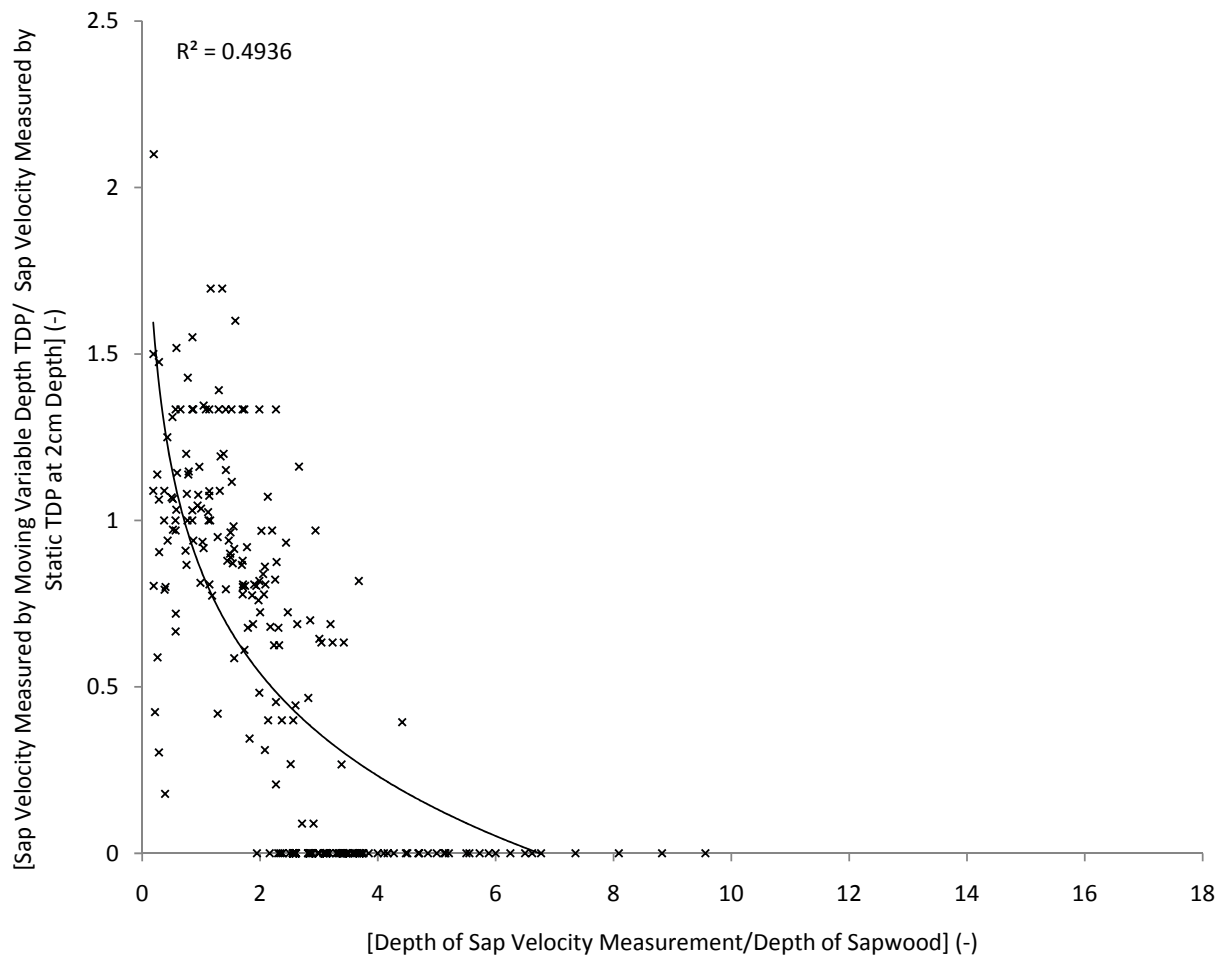
Figure 4.14 The ratio of sap velocity measured by a thermal dissipation probe moving ($_m$) in 0.5 cm increments into the sapwood and that measured by a 2cm static ($_s$) probe (Vm/Vs) (Equation 2.27, Chapter 2) plotted against xylem depth normalised by stem diameter (i.e. the depth of the Vm sap velocity measurement/ depth of the sapwood in which Vm was made) for 16 trees at the Wawasan Bentar forest.

Whereas initially there seems to be only a weak pattern for all trees when the velocity ratios, R_{ij} are expressed as a fraction of total xylem depth (f_{xd}) the pattern becomes somewhat more defined and renders a strong (r^2= 0.49) regression with a logarithmic function (Figure 4.14). The approach of normalising by total xylem area is particularly useful for a mixed-species analysis (Ford *et al.*, 2004a, 2004b). Radial profiles of sap velocity show that there is a general trend for all trees of decreasing sap speed with increasing distance into the xylem from the cambium. This leads to an overall correction coefficient (CC, defined in Equation 2.32, Chapter 2) of CC= 0.856 (σ = 0.19, Table 4.2) that is used as multiplier to correct sap flow estimates (i.e. there is a need to reduce the sap velocity estimates of trees in the stand measured here, see further Equations 2.27-2.32, Chapter 2). Details of the correction coefficient as derived for each of the 16 trees measured are shown in Table 4.2, along with their corresponding measured xylem depth.

When trees are genetically and ontogenetically similar, radial profiles of sap flux can be similar from tree to tree (Zang *et al.*, 1996). As both *M.hypoleuca and M.pearsonii* are typical of the same level of forest disturbance (see Slik (20050, Davies (1998), and Davies (2001), for a full definition of 'disturbance') it seems plausible that their ontogenetic development will be quite similar. Whereas such a pattern is more typical of plantations, the trees studied here were from the same genus and diffuse-porous (i.e. not having 'tree rings' consisting of densely packed xylem elements, but instead having constant, but relatively lower, xylem element density when compared to species with 'tree rings'), both of which tend to generate more consistent radial profiles (Clearwater *et al.*, 1999, Zang *et al.*, 1996).

These data should, however, be treated with some caution. It should be noted that this relationship was based on measurements that were not made at the same time. It has been widely reported that the radial variation in sap velocity changes both diurnally and with differing climatic conditions. To best account for such differences, measurements were taken at the same time in the day (between 10:00am and 13:00pm) and all within one week. However, without a more comprehensive analysis the radial profiles measured here should be treated with caution despite suggestion on their convergent properties.

Data are presented for each tree measured at stations B, C and D below. The main data collection period was from March 31st 2007 to July 14th 2007; although the data were often broken due to the sheer physical effort needed to maintain the probes.

Whereas the number of tree and days measured in this study (701 tree days) is in the mid range of previous studies (e.g. Taylor *et al.* (2001), Giambelluca *et al.* (2003) Herbst *et al.* (2007b) measure approximately 392, 648 and 2744 tree days respectively), this is the first study to make these measurements within the tropical humid biome.

Due to the limited number of days when sap flux was measured simultaneously (17 days), attempts are made in this section to define a control with which sap flux measurements can be standardised with via normalisation. In analysing the controls acting upon the trees and how the influence of these controls change with distance from the forest edge it is possible to deduce what is driving any altered transpiration rates at the forest edge.

Sap velocity

Data for sap flux the whole period are presented in Figure 4.16, along with those data for a few select days in Figure 4.17. The magnitude of observed flux densities (Fd) did not differ significantly between the two species ($\bar{x}$ $\approx$ 0.04 kg m s^{-1}, unpaired t-test assuming equal variance, P<0.05)*. Sap flux density here is similar to fluxes reported for other diffuse-porous species (i.e. being typically an order of magnitude lower than that of ring-porous species) under similar net radiation loads (Ciencala *et al.*, 2000; Herbst *et al.*, 2007b,) and are typical for their respective tree sizes (Meinzer *et al.*, 1993, 1997, 2003; Wullshleger *et al.*, 1998). Examining mean diurnal patterns of Fd (Figures 4.15 and 4.17b) it can be seen that there is often a clear depression of transpiration rate in the late morning or early afternoon. Examining Figure 4.15 (trees 5b, 6c and 32 d) this pattern is clear although some variation is experienced in the time and extent of the depression (occurring for trees 5b, 6c and 32d at ~12:00h, ~14:30h, and ~13:00h, respectively). A peak in Fd usually occurred one to two hours before this depression, and in some cases a series of smaller peaks and troughs occur before a more significant peak and depression. Where a less significant depression is present this gives a diurnal transpiration profile very similar to that of net radiation

(for example, tree 9b, Figure 4.15).   These patterns are typical of tropical trees (Goldstein *et al.*, 1998) and similar patterns have been reported in Lambir Hills, Sarawak (Kume *et al.*, 2006).

Comparing Figures 4.15 and 4.17 with Figure 4.1a, it can be seen that the peak of Fd in trees occurs after or during the longest unbroken load of incident shortwave radiation ($S_{incident}$). The onset of Fd is matched by a corresponding and gradual decrease in outgoing longwave radiation, wherein the greatest decreases are associated with the highest values of Fd in some trees. This is associated with a decrease in $S_{incident}$ and then Fd immediately thereafter.

Sap velocity rarely exceeded 0.15 mms^{-1}, confirming the velocity measured *in vivo* was within the calibration parameters set *in vitro* and indeed that the accuracy percentage of probes used in this study can be considered to render only low absolute differences in water flux measurements of the stand as a whole.
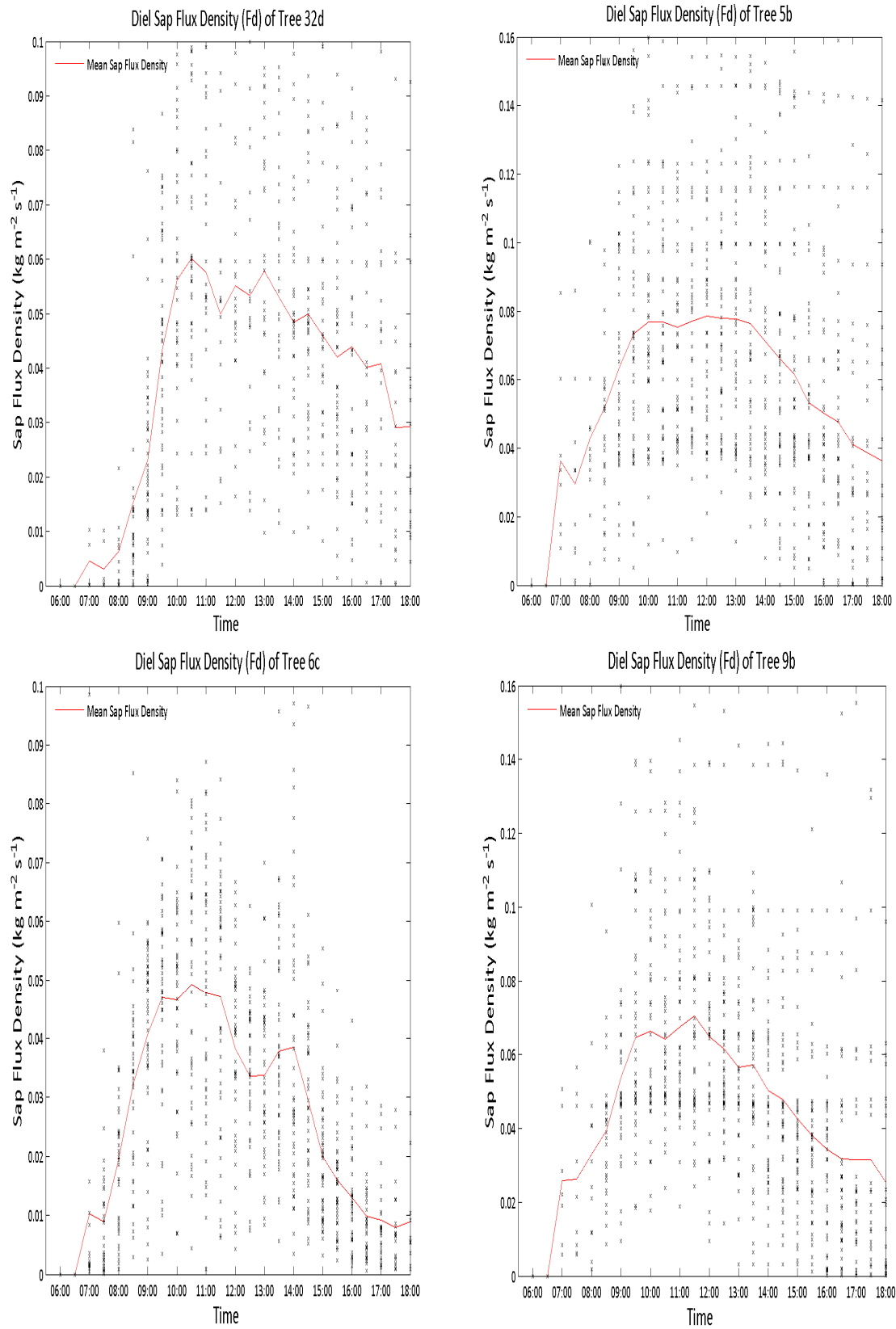
Figure 4.15 Mean diurnal patterns of sap flux density (Fd) in selected trees (red lines) for individual daily replicates of 30 minute averages at a given half hour period. Note the depression in sap flux density for trees32d, 5b, and 6c in the late afternoon/early morning.
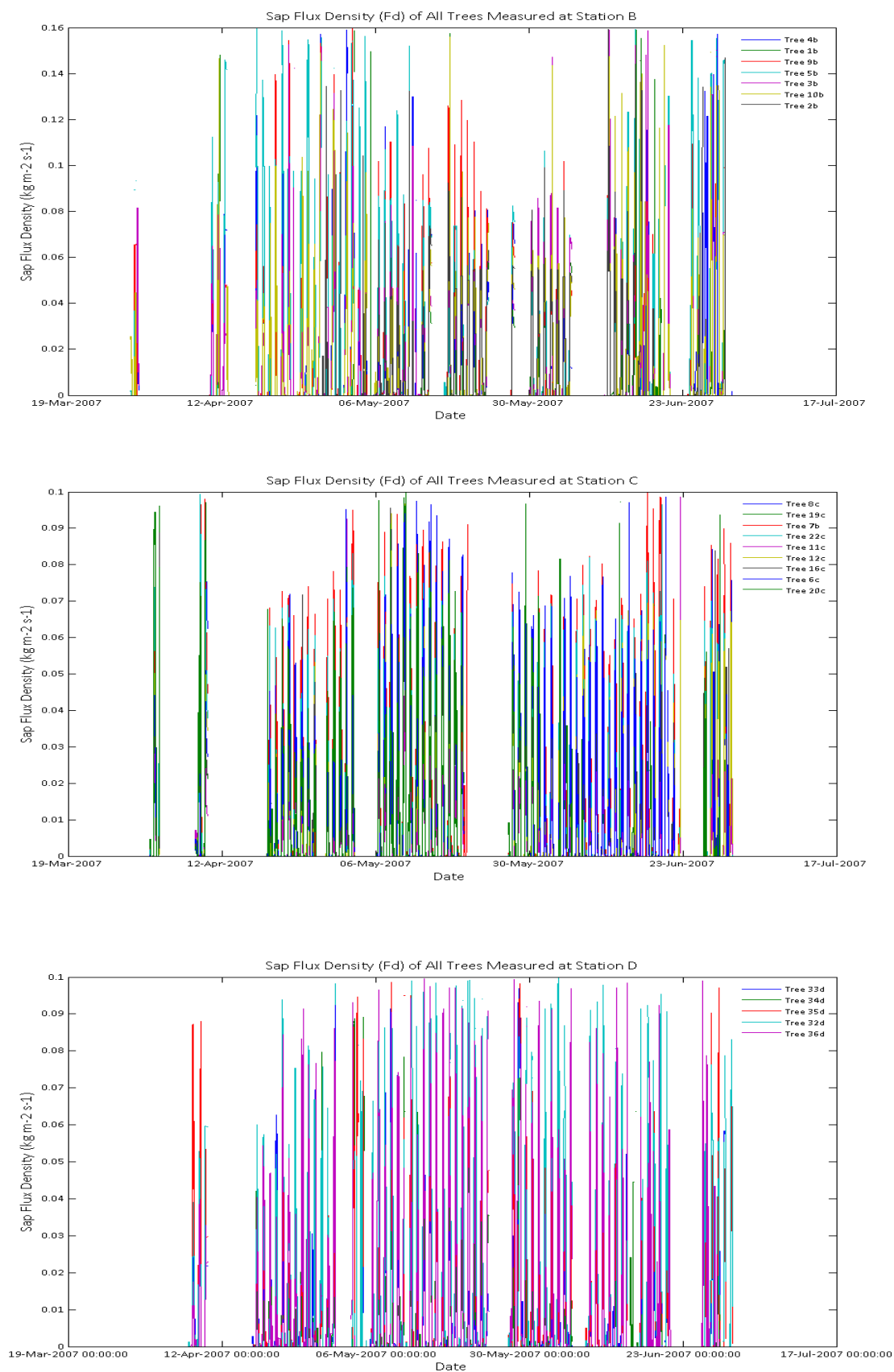
Figure 4.16 Sap flux (kg m^{-2} s^{-1}) data collected for all trees over the study period at stations B-D (top to bottom respectively).
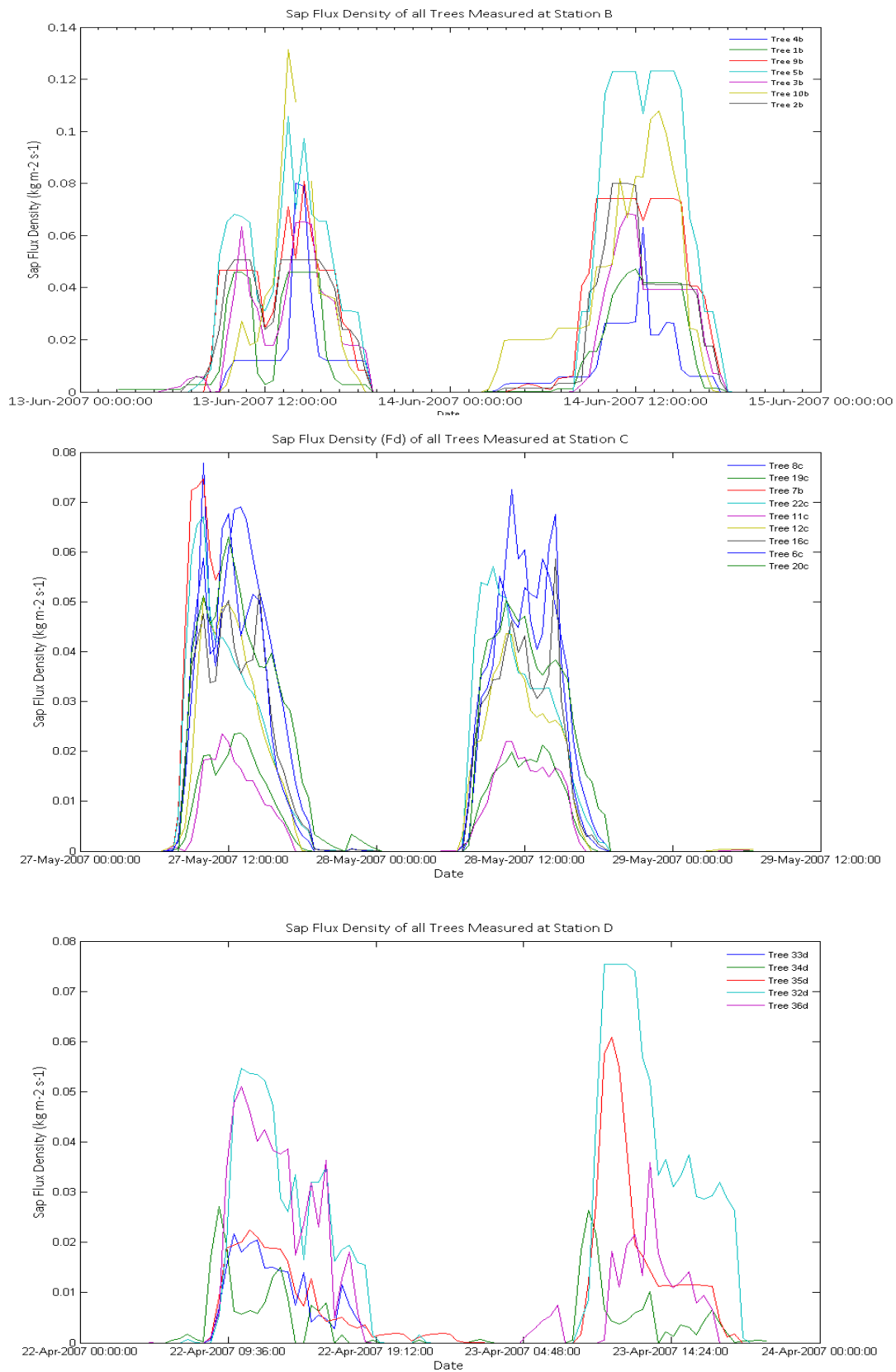
Figure 4.17 Data for all trees at stations B-D (top to bottom respectively) for select days during the study period.

Correlation between sap flux density and shortwave radiation

The correlation between 30-minute averages of sap flux density and shortwave radiation was best described by a first-order exponential fit (Figures 4.19-4.22). This contrasts to other studies, which report linear or parabolic saturation function-type fits (Ciencala *et al.*, 2000; Herbst *et al.*, 2007b; Komatsu *et al.*, 2006a). Close correlation was found in most trees but with considerable variation (r^2= 0.24 – 0.77 , $\bar{x}$ = 0.54 for all trees), with correlations appearing similar to those presented in Herbst *et al.* (2007b) at a mixed deciduous forest edge in Wytham Woods, Oxford, UK; although the r^2 is not presented by Herbst *et al.* (2007b). Correlations here are weaker than those presented by Giambelluca *et al.* (2003) and Ciencala *et al.* (2000) (r^2= 0.83 and r^2= 0.79 respectively). Weaker correlations are to be expected under the advective conditions commonly thought to drive forest edge effects and also the low variation of solar radiation expressed over the period in which sap flux measurements were taken. When grouped, trees in plot D had the lowest r^2 (0.35), those in plot C the highest (r^2= 0.68), with trees in plot B between the two (r^2= 0.46). Variation between r^2 is 0.0096, 0.0077 and 0.0099 for plots B-D respectively, i.e. those trees with the weakest correlation to shortwave radiation (plot D) express the greatest variance (Figure 4.18).
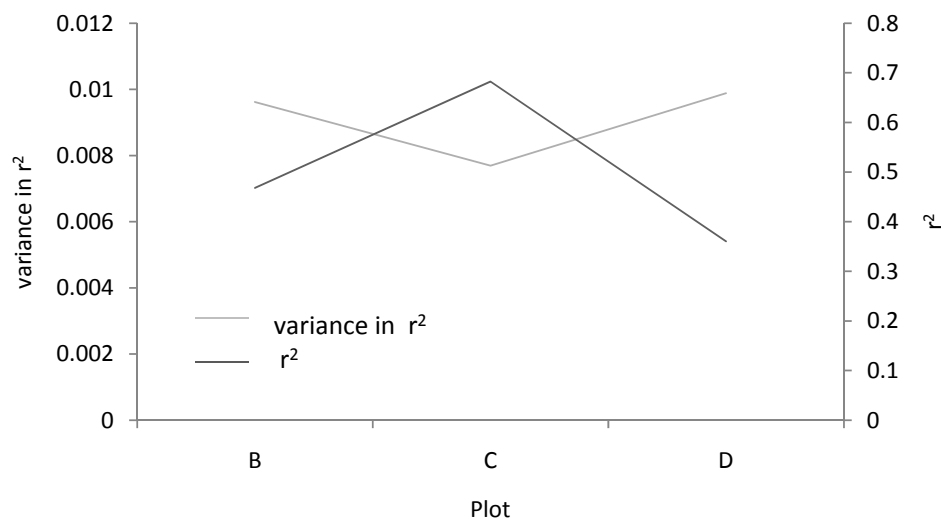
Figure 4.18 Mean r^2 (dark line) for sap flux (Fd) of all trees in plots B-D and the respective arithmetic variation in r^2 (light line) between trees, when regressed against incident shortwave radiation ($S_{Incident}$).

Figures 4.19- 4.22 show that sap flux became independent of shortwave radiation (and thus potential evapotranspiration, PE) at >450 Wm^{-2} (PE equivalent of >5 $mmdy^{-1}$), corresponding to sap flux densities of 0.060, 0.050 and 0.040 kg m^2 s^{-1}, when trees were grouped within plots B-D. At >450 Wm^{-2} sap flux became independent of radiation, with values of Fd after this point ranging by 0.075, 0.050 and 0.060 kg m^2 s^{-1} for trees within stations B-D, respectively. This is in fitting with those ranges reported by Herbst *et al.*(2007b) for *Quercus robur* and *Fraxinus excelsior* trees (Wytham Woods, Oxford, UK) at a forest 'edge' (~0.55 kg m s^{-1}) when accounting for the diffuse-porous nature of the trees here (i.e. that the sap flux is an order of magnitude lower).
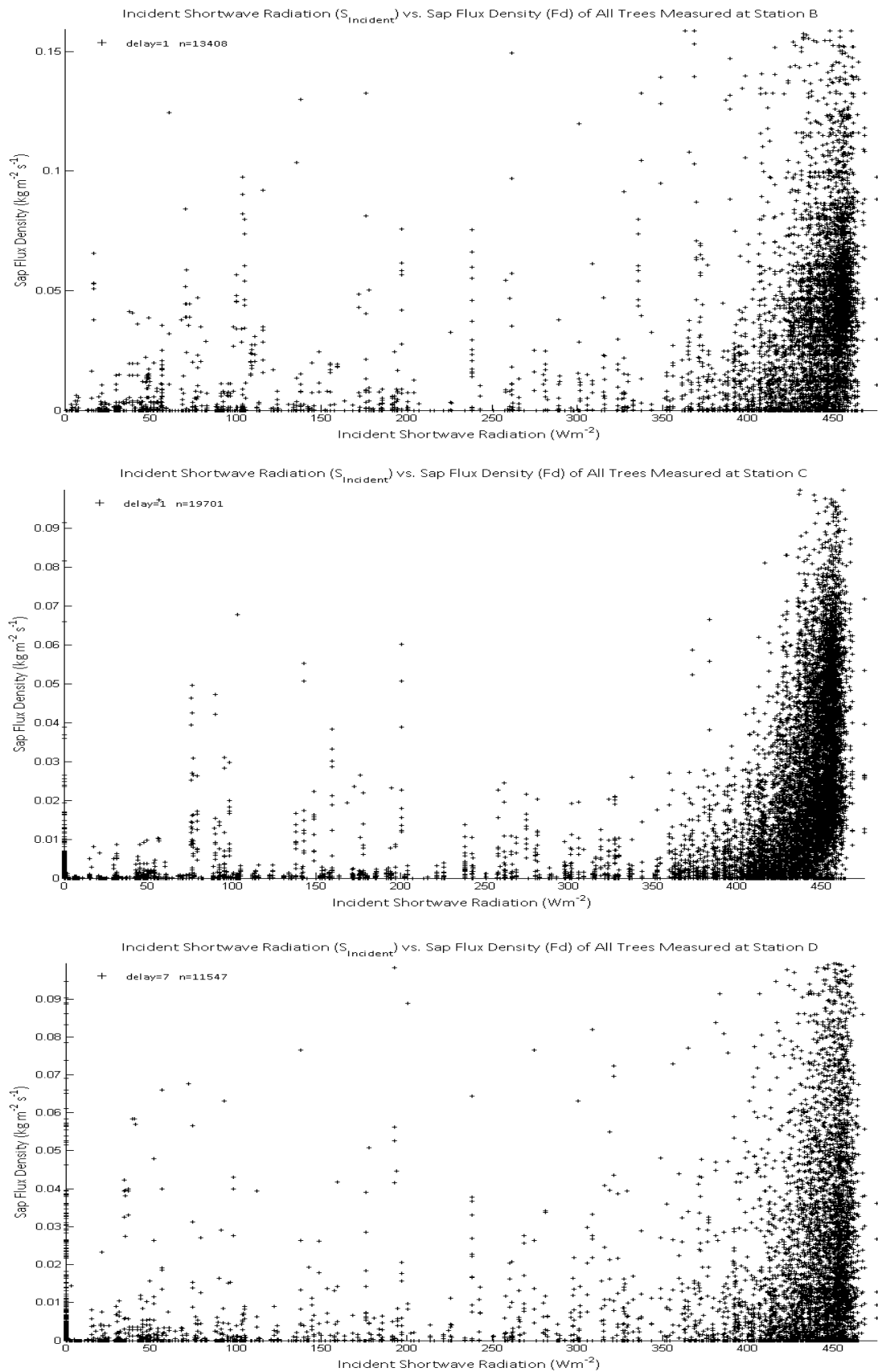
Figure 4.19 Regressions of sap flux against incoming shortwave radiation for all trees at stations B-D (top to bottom respectively) during the study period.

Incident Shortwave Radiation (S$_{Incident}$) vs. Sap Flux Density (Fd) for Tree 10b

delay=10 n=1996

Sap Flux Density (kg m^{-2} s^{-1})

Incident Shortwave Radiation (Wm^{-2})

Incident Shortwave Radiation (S$_{Incident}$) vs. Sap Flux Density (Fd) for Tree 7b

delay=13 n=2221

Sap Flux Density (kg m^{-2} s^{-1})

Incident Shortwave Radiation (Wm^{-2})
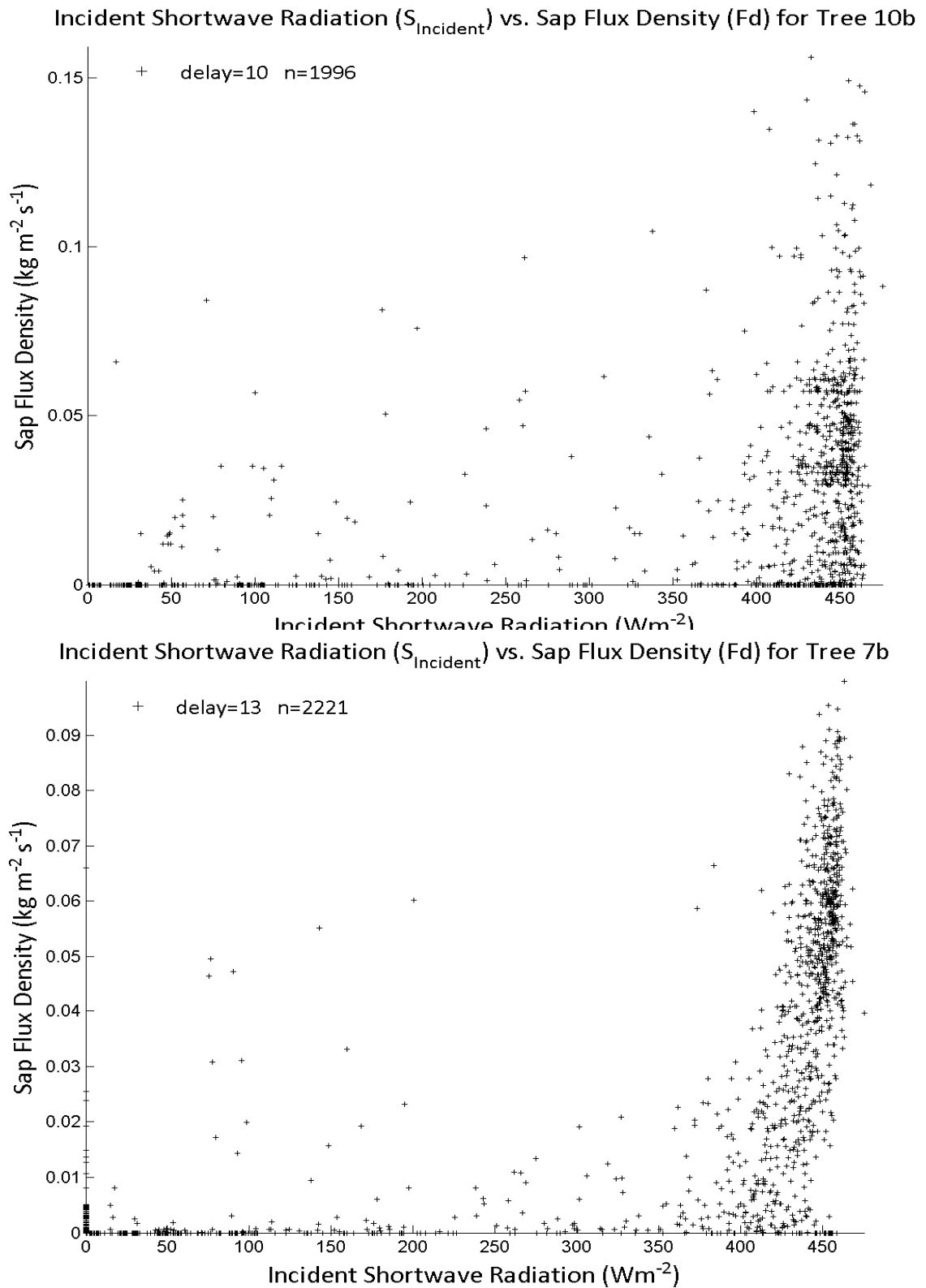
Figure 4.20 Regressions of sap flux against incoming shortwave radiation for selected trees representing a 'poor'(top) and 'good' (bottom) correlation within plot B. Delay denotes the number of 30-minute periods required to offset variables and optimise the relationship between them.

Incident Shortwave Radiation ($S_{Incident}$) vs. Sap Flux Density (Fd) for Tree 19c

delay=10   n=2253

Incident Shortwave Radiation ($S_{Incident}$) vs. Sap Flux Density (Fd) for Tree 6c

delay=10   n=2269
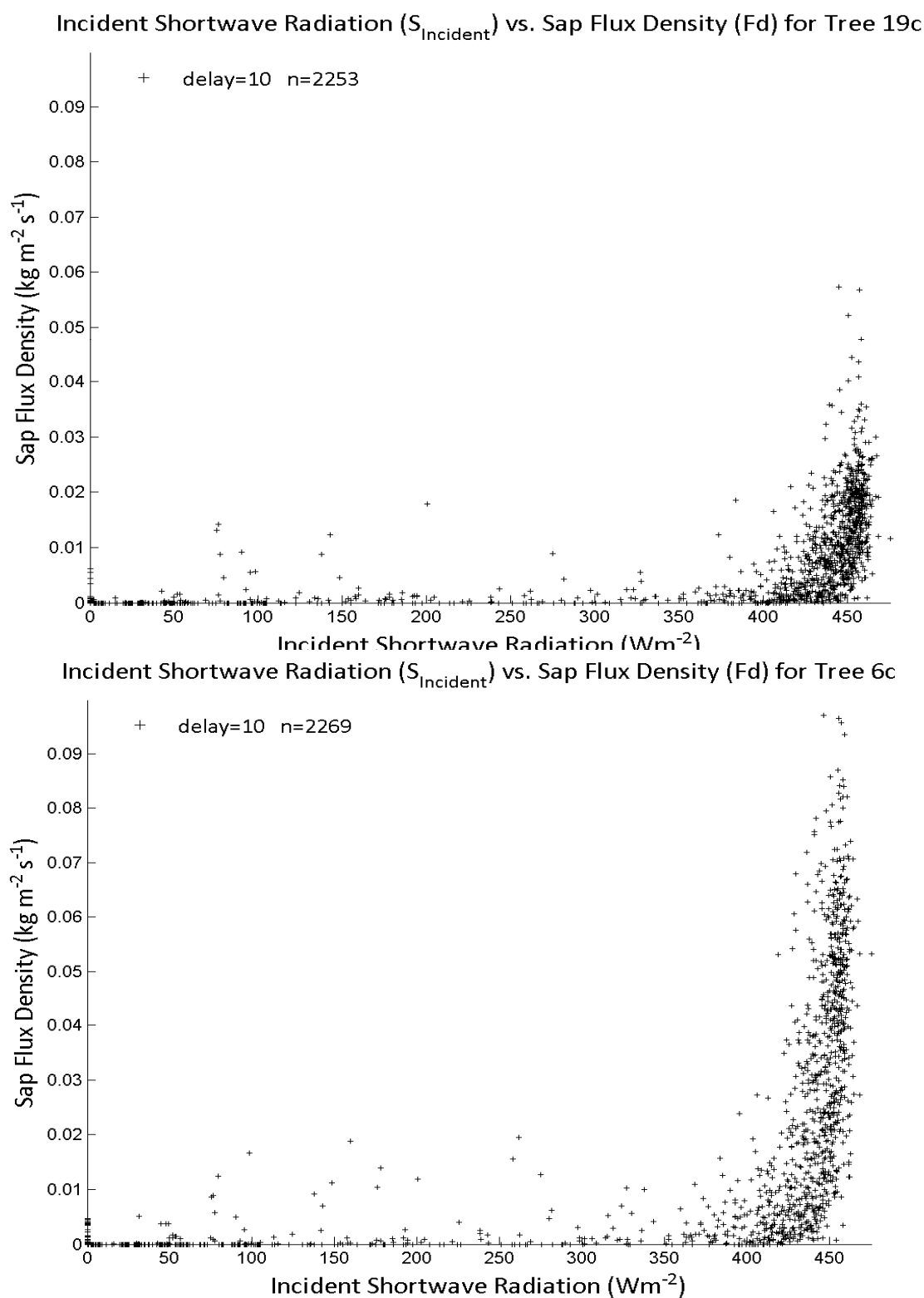
Figure 4.21 Regressions of sap flux against incoming shortwave radiation for selected trees representing a 'poor' (top) and 'good' (bottom) correlation within plot C. Delay denotes the number of 30-minute periods required to offset variables and optimise the relationship between them.

Incident Shortwave Radiation ($S_{Incident}$) vs. Sap Flux Density (Fd) for Tree 34d

Incident Shortwave Radiation ($S_{Incident}$) vs. Sap Flux Density (Fd) for Tree 32d
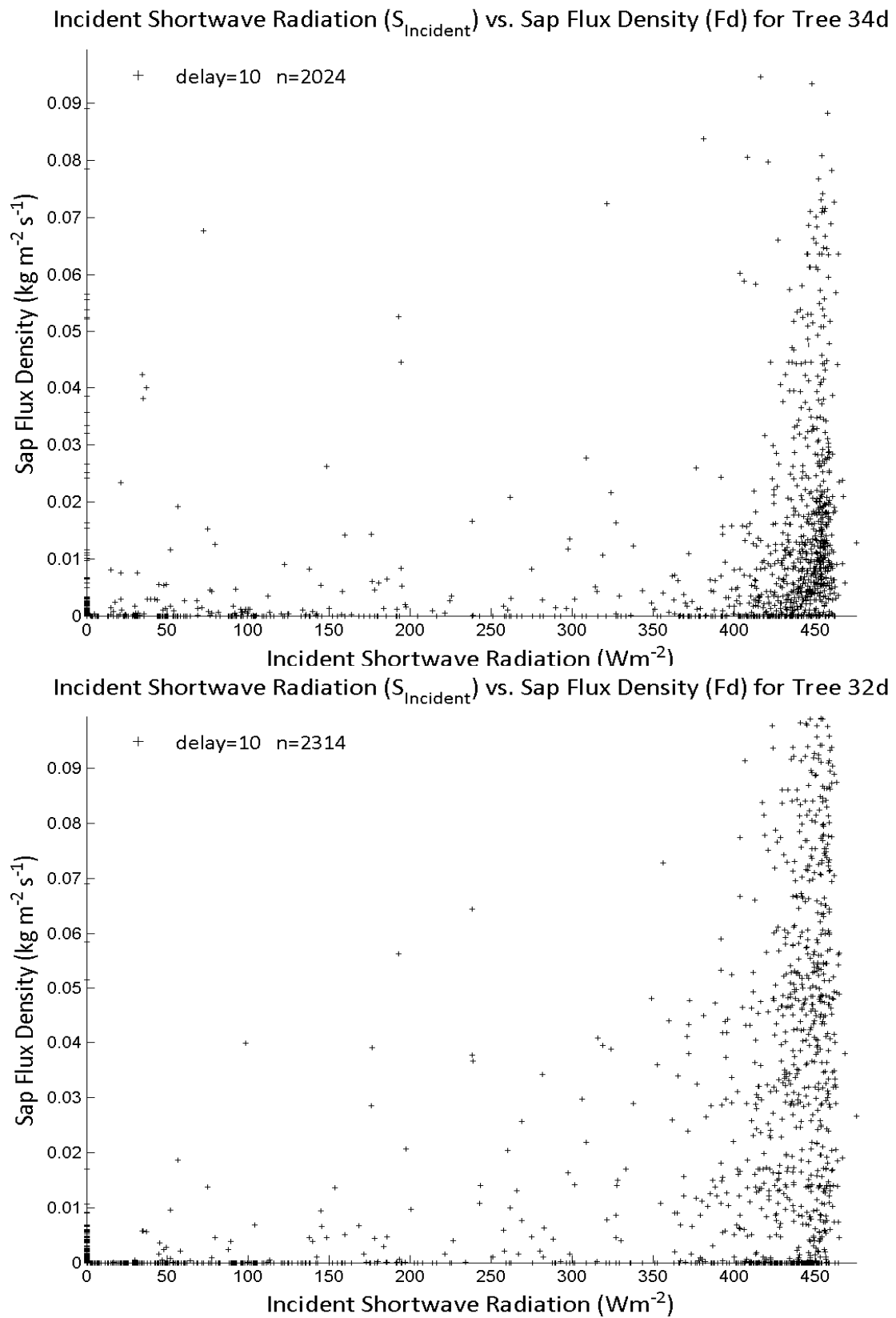
Figure 4.22 Regressions of sap flux against incoming shortwave radiation for selected trees representing a 'poor' (top) and 'good' (bottom) correlation within plot D. Delay denotes the number of 30-minute periods required to offset variables and optimise the relationship between them.

Correlation between sap flux density and vapour pressure deficit

Regressions between 30-minute averages of sap flux density and vapour pressure deficit (VPD) in the swidden were made between the 20th and 28th of May 2007. VPD for the period of regression is shown in Figure 4.23. VPD over this period averaged 0.96 kPa during the day, with a maximum of 1.86 kPa, which is comparable to ranges reported by Ciencala *et al.* (2000) and Kumagai *et al.* (2004b) who report maximums of 1.9 and 2.6 KPa, respectively.

Plant-soil resistance may limit water uptake under conditions of high evaporative demand (represented mostly by VPD) regardless of soil water conditions. Reasons for this are numerous and include embolism of conductive tissues (Tyree *et al.*, 1986), soil water (matric) potential and stomatal resistance. If this limitation occurs, then the canopy becomes decoupled (represented by a high decoupling coefficient value, Equation 4.5) as canopy conductance increases.
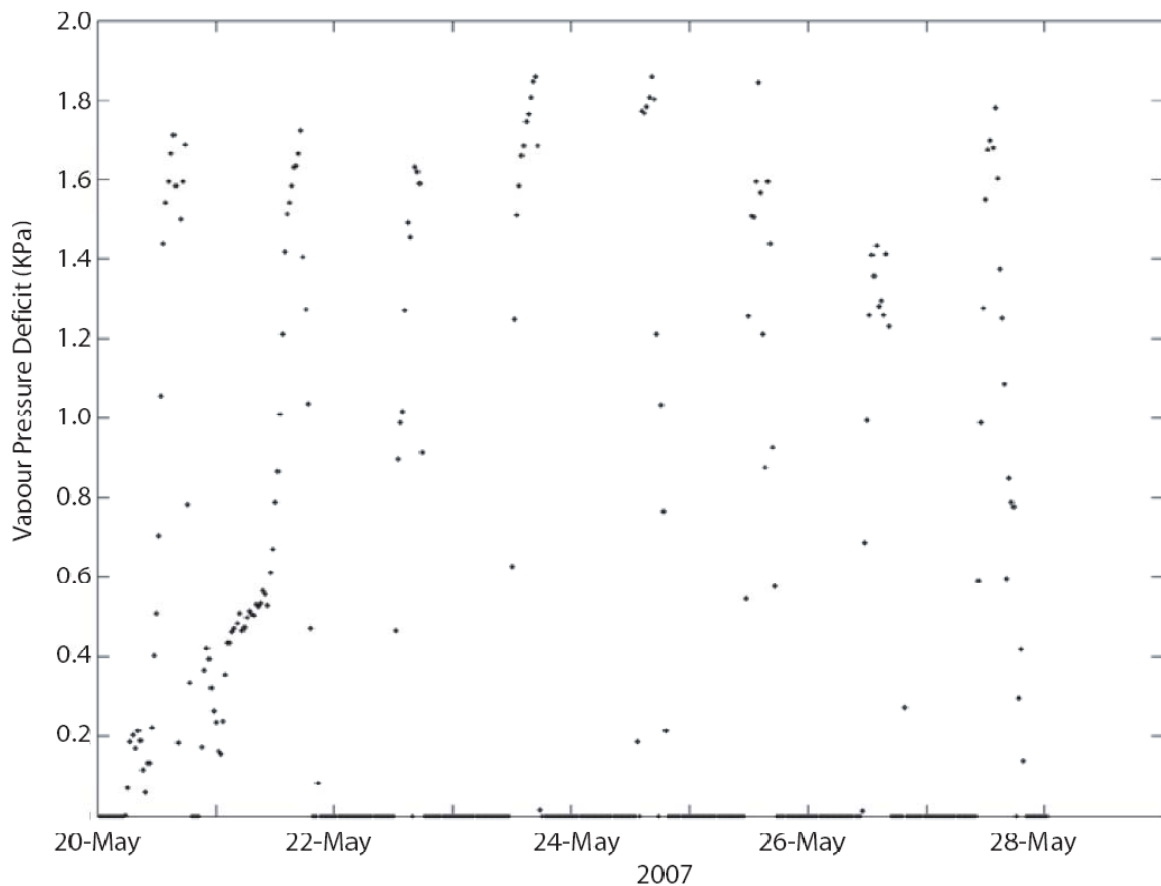
Figure 4.23 Vapour pressure deficit (VPD) from station A (swidden) used for regression with sap flux density (20th-28th May 2007), in 30 minute averages (black dots, n=400).

A first-order exponential fit best described the relationship between VPD and sap flux density for trees in plots C and D (Figures 4.24-4.27). Trees in both plots C and D do not show saturation with VPD. Although trees at plot B showed a similar exponential trend between VPD and sap flux density, there was a visible tapering of sap flux response for VPD>1.67 kPa. This suggests that some trees within plot B become decoupled from the atmosphere under relatively high evaporative demand.

Time lags

In order to maximise the correlation between driving factors and sap flux density it is sometimes necessary to put a time lag between variables (Herbst *et al.*, 2007b). Generally, the lower the time lag the more closely coupled the canopy is considered to be to the atmosphere above it. Significant delays between the driving and response variable are to be expected if there is significant resistance to water transport (e.g. low water content and high matric potential) or similarly if there is significant capacitance in the rhizosphere-xylem-leaf pathway (e.g. the sideways movement of stored water within xylem elements). The formation of a significant boundary layer over the canopy would also act to delay the response sap movement to climatic variables. Given the relatively small size of the trees in this study it is unlikely that significant water storage capacitance is present in these trees, and even so the water storage capacity of even large trees represents a small fraction (9-15%) of daily tree water use (Goldstein *et al.*, 1998). Consequently any delays in transpiration response to net radiation are likely to be due to poor canopy coupling or soil water limitation. Lags necessary for good correlations between sap flux density and VPD were typically less than 1.5 hours (Figures 4.25-4.27) although some notable delays occurred of approximately 4 hours in some individuals. When canopies are well coupled to the atmosphere and there is no limitation to water transport in either terms of diabatic and adiabatic energetic inputs or resistance to the hydraulic pathway responses to driving variables can be immediate (Komatsu *et al.*, 2006a, 2006b). Thus water transport of trees in plots B-D at Wawasan Bentar appears to be limited in a number of ways given the variety of responses to VPD, $S_{incident}$, and the consequential lags in responses of Fd to them.
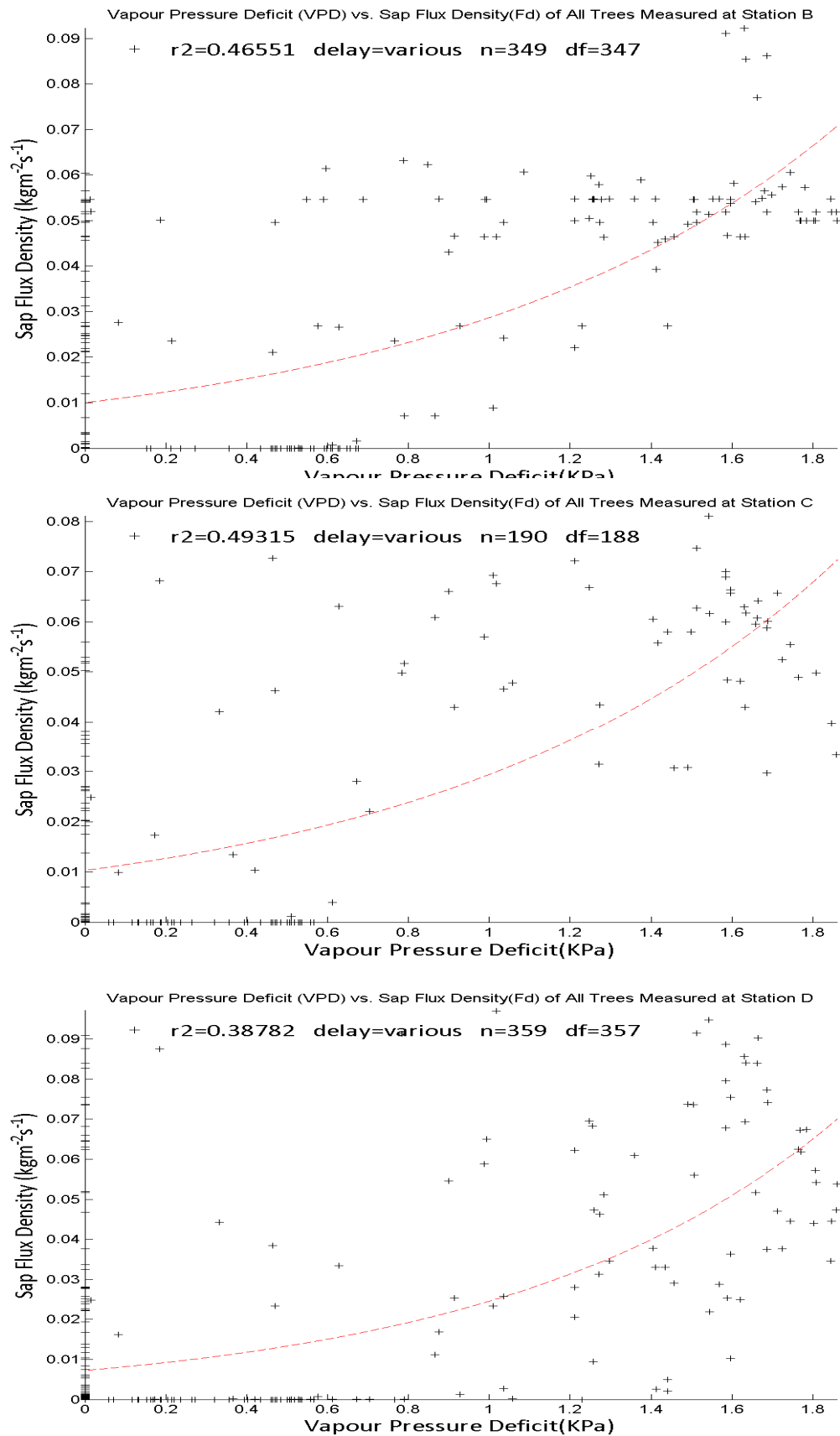
Figure 4.24 Regressions of sap flux against vapour pressure deficit for all trees at stations B-D (top to bottom, respectively) during the period 20th-28th May 2007.
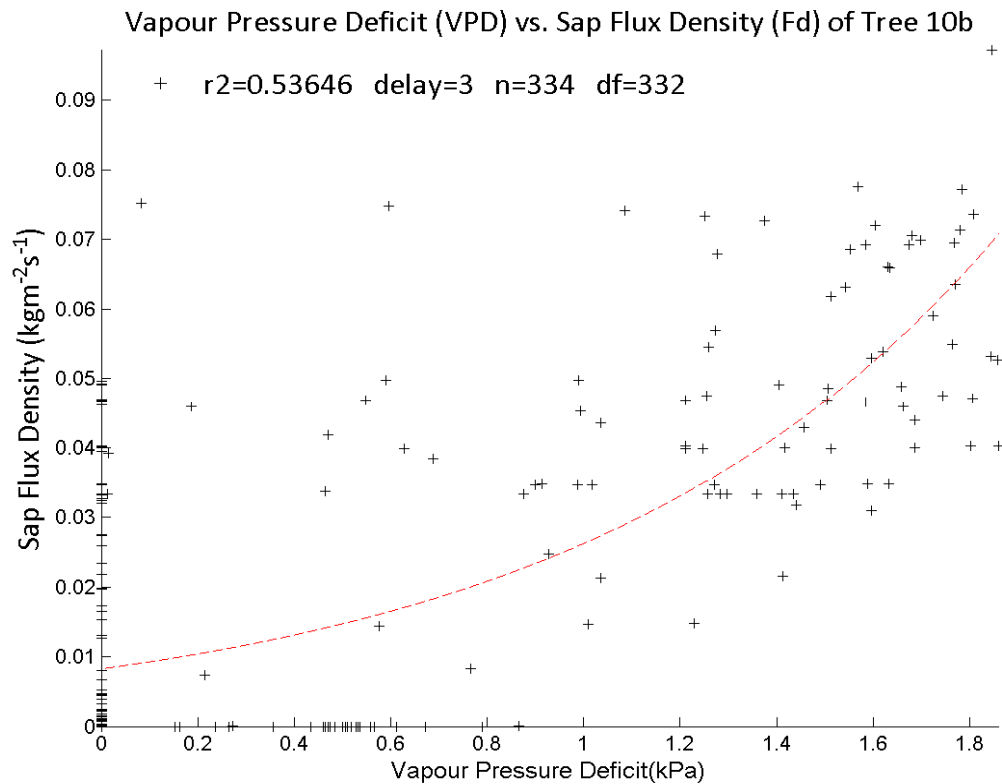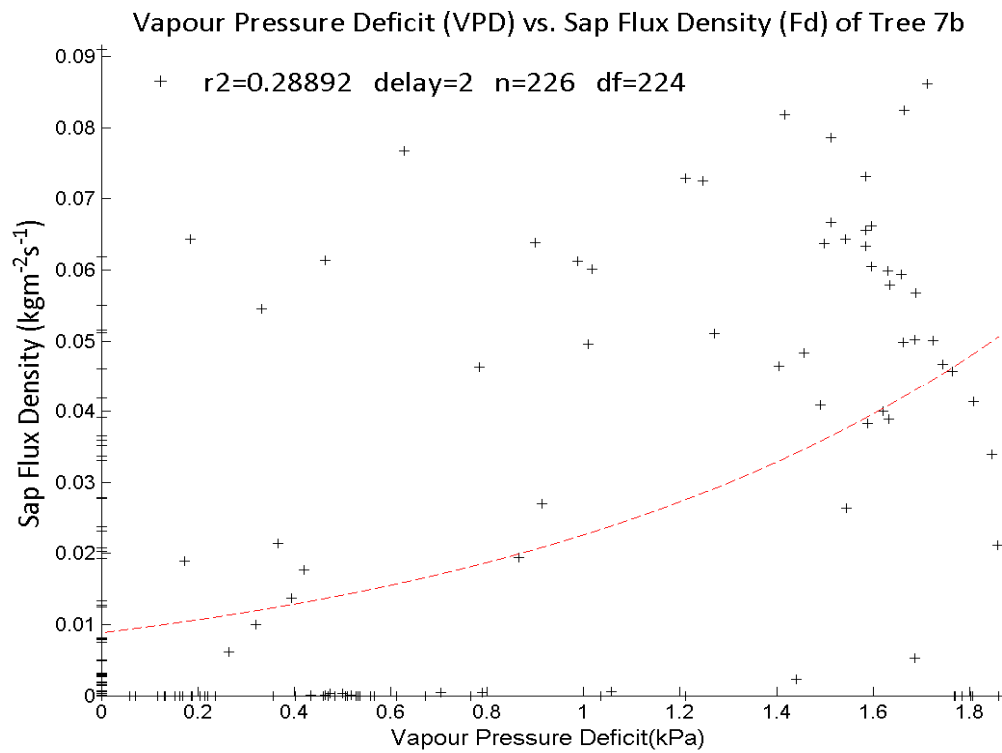
Figure 4.25 Regressions of sap flux against vapour pressure deficit for selected trees within plot B representing a 'poor' (top) and 'good' (bottom) correlation (20th -28th May 2007). Delay denotes the number of 30-minute periods required to offset variables and optimise the relationship between them.

Vapour Pressure Deficit (VPD) vs. Sap Flux Density (Fd) of Tree 22c

r2=0.496   delay=2   n=193   df=191

Vapour Pressure Deficit (VPD) vs. Sap Flux Density (Fd) of Tree 19c

r2=0.58496   delay=4   n=191   df=189
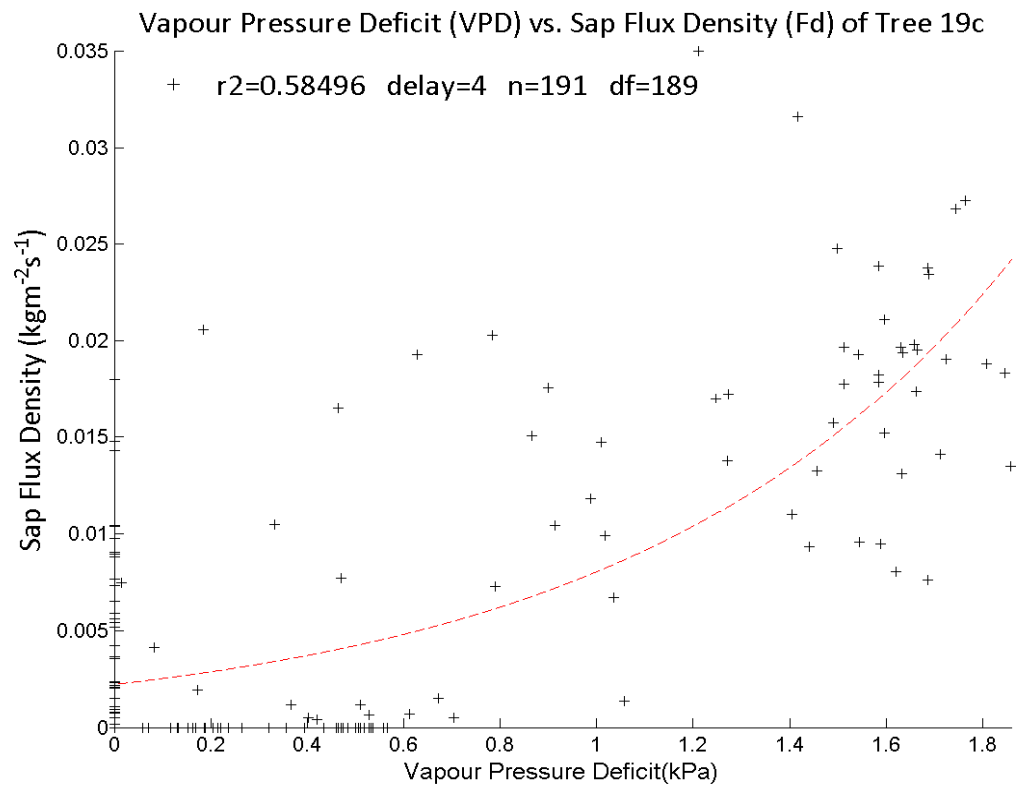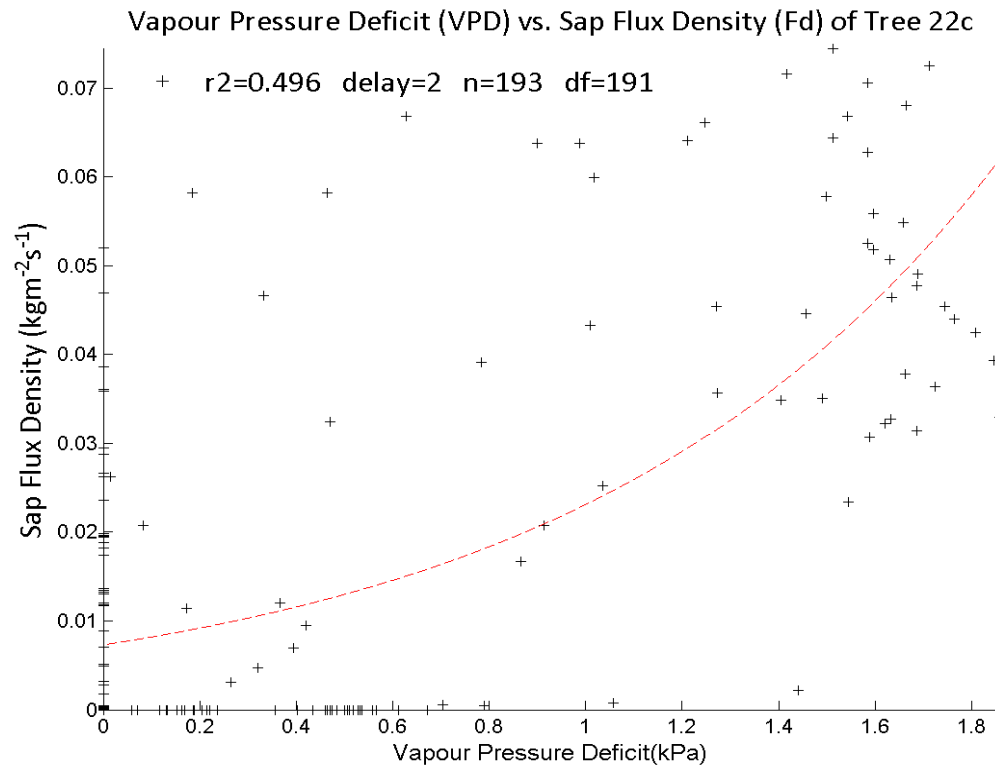
Figure 4.26 Regressions of sap flux against vapour pressure deficit for selected trees within plot C representing a 'poor' (top) and 'good' (bottom) correlation (20th -28th May 2007). Delay denotes the number of 30-minute periods required to offset variables and optimise the relationship between them.
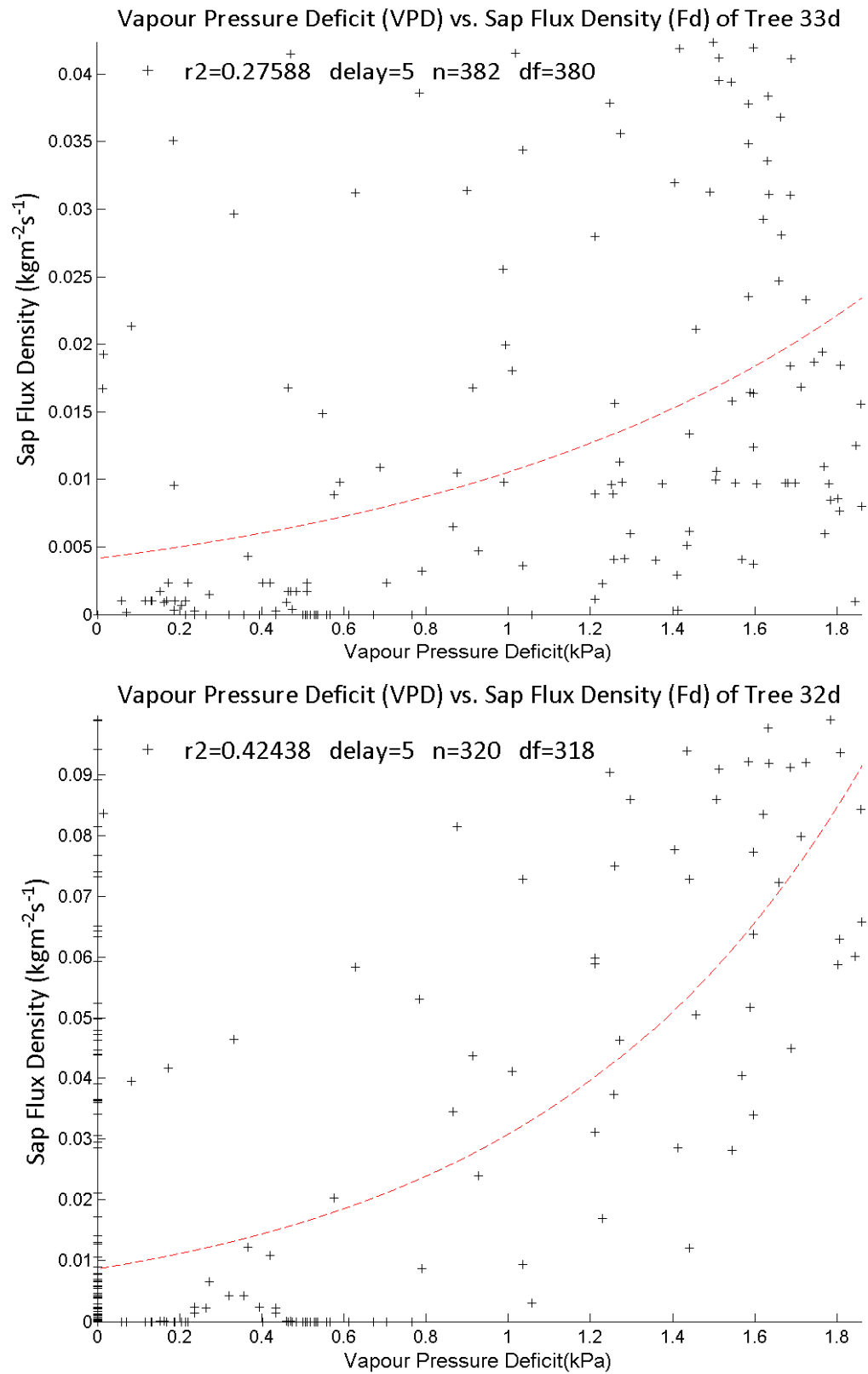
Figure 4.27 Regressions of sap flux against vapour pressure deficit for selected trees within plot D representing a 'poor' (top) and 'good' (bottom) correlation (20th -28th May 2007). Delay denotes the number of 30-minute periods required to offset variables and optimise the relationship between them.

As with shortwave radiation and sap flux density, close correlation was found between vapour pressure deficit and sap flux density in most trees, but with considerable variation (r^2= 0.23 – 0.73, $\bar{x}$ = 0.46 for all trees, Figures 4.24-4.27). For all trees, this represents an overall greater range and poorer fit with vapour pressure deficit when compared to incoming shortwave radiation. Correlations here are weaker than those elsewhere (Ciencala *et al.* (2000) report values of r^2= 0.85).

When grouped, trees in plot D had the lowest r^2 (0.36), those in plot C the highest (r^2= 0.52), with trees in plot B between the two (r^2= 0.47). Variation between r^2 is 0.0059, 0.0089 and 0.0040 for plots B-D respectively. This, as shown in Figure 4.28, means that unlike correlation with shortwave radiation, regression with vapour pressure deficit does not render those trees with the weakest correlation as a group with lower arithmetic variances in r^2 between trees, and actually the opposite pattern is present.
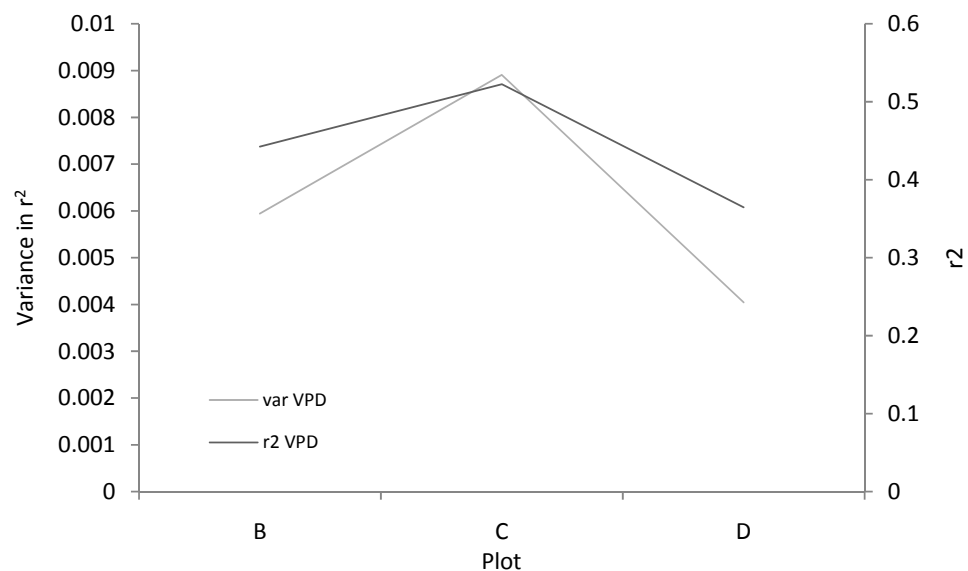
*Figure 4.28 Mean r^2 for the sap flux of all trees in plots B-D and the respective arithmetic variation in r^2 between trees within each plot, when regressed against vapour pressure deficit (20th -28th May 2007).*

Statement a: If there were a response of sap flux density to $S_{INCIDENT}$ and VPD consistent with the assumptions of the Penman-Monteith (Monteith, 1965) equation then plots with higher correlations between sap flux density and $S_{INCIDENT}$ would have lower correlations between sap flux density and VPD, and vice-versa (following Equation 1.5, Chapter 1).

Statement b: Under conditions of heat advection, the relationship described above would be expressed as a better correlation between sap flux and $S_{INCIDENT}$ with fetch, and an opposite, lower correlation between sap flux and VPD with distance into the forest (following Equation 1.5, Chapter 1).

Both statements a) and b) are violated, as shown in Figure 4.29, which plots r^2 values for the sap flux densities of all trees grouped at stations B-D when regressed against VPD (Figures 4.24-4.27) or $S_{INCIDENT}$ (Figures 4.19-4.22).
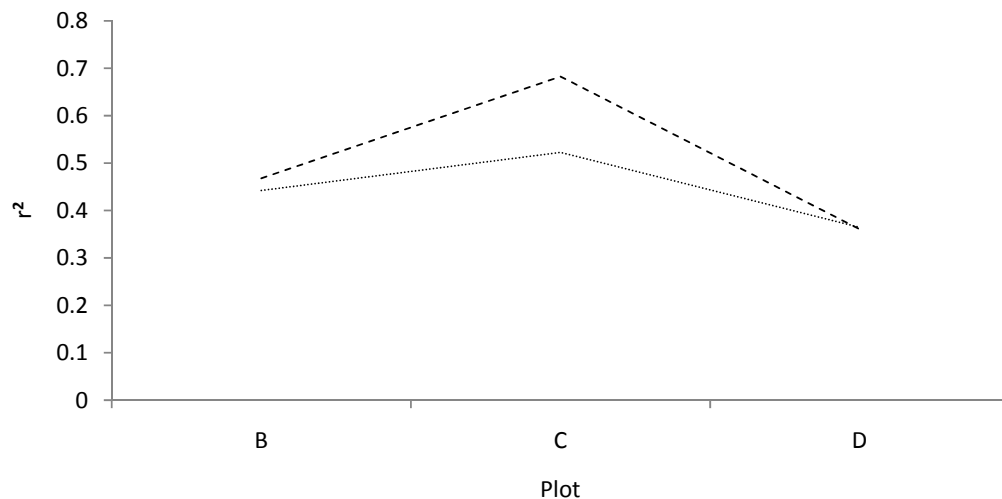
Figure 4.29 Mean r^2 for all trees in plots B-D and the respective arithmetic variation in r2 between trees, when regressed against vapour pressure deficit (dotted line) and shortwave radiation (dashed line) over the period 20th -28th May 2007.

Comparisons between regressions of incoming shortwave radiation (adiabatic) and vapour pressure deficit (diabatic) of the nature presented so far implicitly assume that only factors above the ground influence sap flux density. This assumption is in fitting with the Penman-Monteith (Monteith, 1965) equation, which essentially assumes that resistance to water movement in the soil-rhizosphere-xylem pathway is

not in any way limited. Within the tropical humid biome it is tempting to conclude that this assumption is met by virtue of the high precipitation in the biome.

However, the clear violation of *statement a)* suggests that other controls may be acting upon the trees at Wawasan Bentar asides from those present at the land surface. Furthermore, there is also a clear violation of *statement b)*, and thus assumptions of an edge effect running from plot B→C→ D is not necessarily the case.

Observing Figure 4.29, it can be seen that sap flux of trees within plot D show the weakest correlation to both VPD (r^2= 0.365) and $S_{INCIDENT}$ (r^2= 0.30) with sap flux of trees within plot C having the strongest correlation (r^2_{VPD}=0.552 and $r^2S_{INCIDENT}$=0.682). The correlation between driving variables and responses of those trees at the forest edge (plot B) lay in between those of trees within plots C and D (r^2_{VPD}=0.462 and $r^2 S_{INCIDENT}$ = 0.468). It would therefore appear that trees within plot D are greatly limited by soil-rhizosphere-xylem resistances, trees within plot B less so, and trees within plot C not limited very much at all. Those trees that are limited by resistance in the soil-rhizosphere-xylem pathway violate *statement a.*

As explained in Chapter 1, controls within the soil-rhizosphere-xylem pathway (e.g. soil moisture) which also influence, and confound the influence of vapour pressure deficit and radiation upon, sap flux are numerous and hard to measure. To implicitly account for these controls, I here compare the relative improvement in r^2 between the adiabatic and diabatic (RN and VPD respectively) fits for each tree by computing r^2_{VPD} - $r^2 S_{INCIDENT}$. The influence of distance from the forest edge on r^2_{VPD} - $r^2 S_{INCIDENT}$ is shown in Figures 4.30 and 4.31.

When comparing stations B and C it is clear that although station C has the higher correlations for both regressions with shortwave radiation and vapour pressure deficit, the relative improvement for those trees at the forest edge (station B) by regressing with VPD is much greater than those trees ~50 metres further in from there (i.e. station C). This is expressed by a weak (r^2=0.284, P<0.01, df = 15, Figure 4.30) relationship with r^2_{VPD}-$r^2 S_{INCIDENT}$ and fetch (Figure 4.33). However, introducing data from plot D (Figure 4.31) it becomes apparent that trees in the forest 'interior' also show considerable improvement. The introduction of data from plot D renders a much weaker r^2 (r^2 = 0.033, P>0.05, df = 20, Figure 4.31).
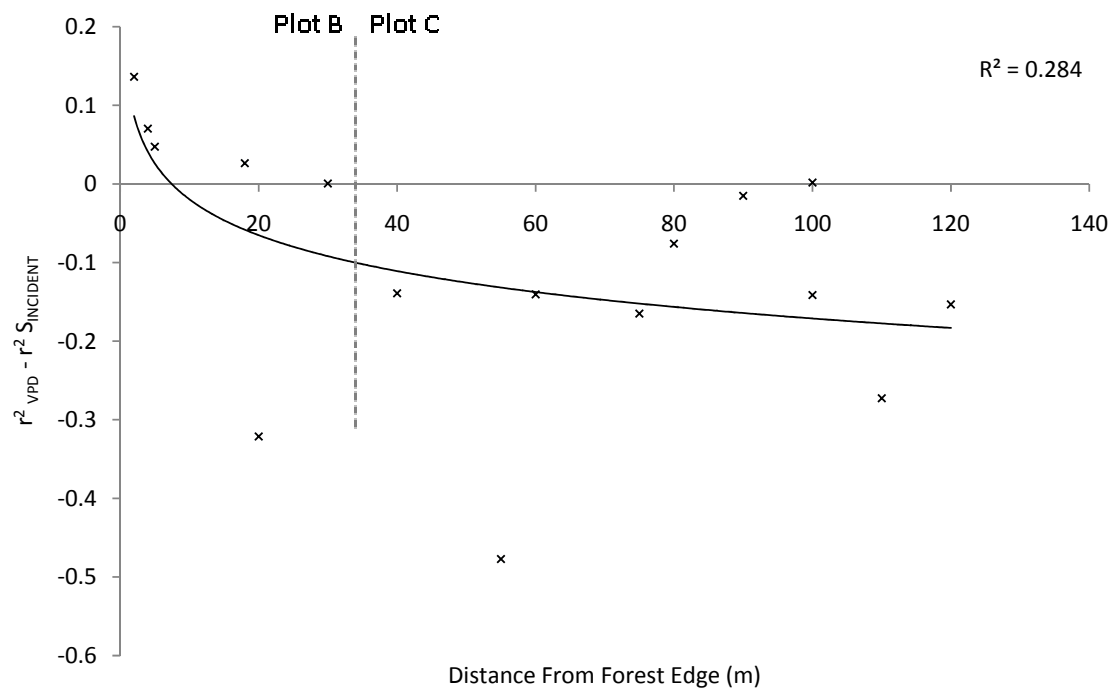
Figure 4.30 $r^2{}_{VPD}$-$r^2S_{INCIDENT}$ *plotted with distance from the forest edge for all trees in plots B and C. Individual trees within plots B and C are delineated by a dashed vertical line.*
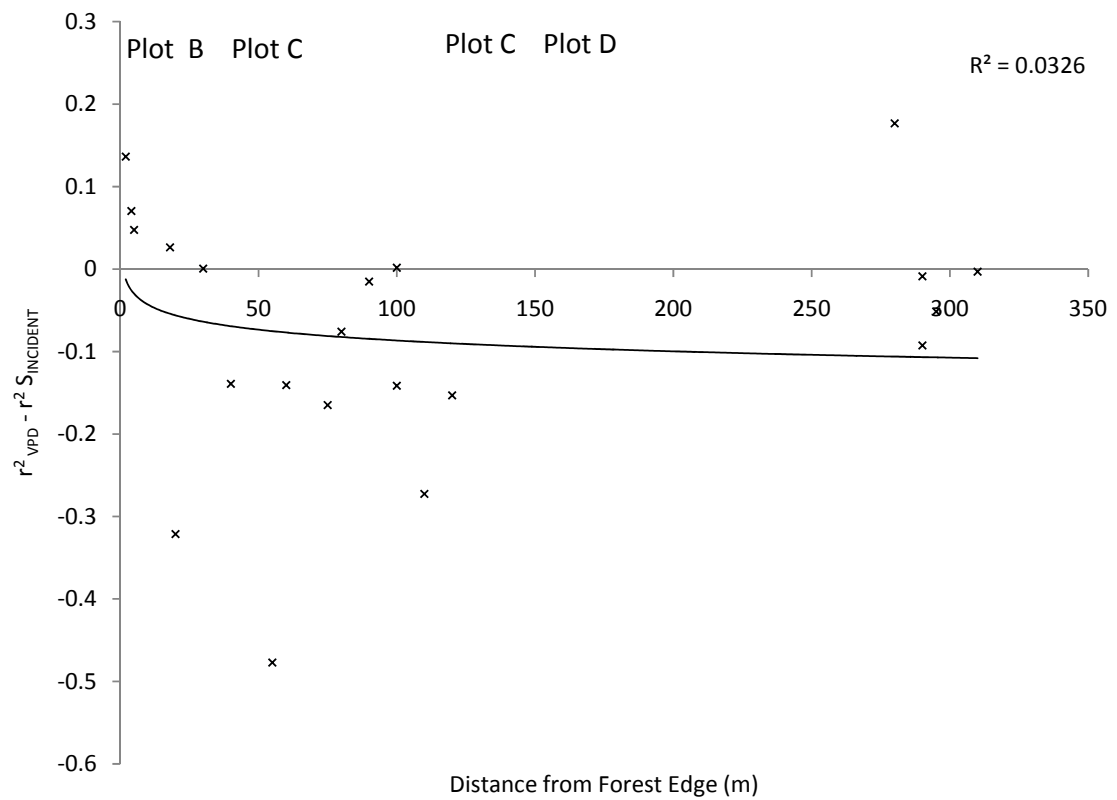
Figure 4.31 $r^2{}_{VPD}$-$r^2S_{INCIDENT}$ *plotted with distance from the forest edge for all trees in plots B-D. Individual trees within plot B-D are delineated by a dashed vertical line.*

Plotting the average values of r^2_{VPD} - r^2 $S_{INCIDENT}$ for trees in plots B-D (Figure 4.32), it can be seen that both plots B and C render a better correlation with shortwave radiation over that of VPD than those trees of plot D (i.e. negative values of r^2_{VPD} - r^2 $S_{INCIDENT}$ for stations B and C, and a slightly positive value for plot D). Thus, despite the presence of some trees within plot B showing an improved relationship to VPD over $S_{INCIDENT}$, those trees in the interior plot (D) show the greatest overall improvement. This is in clear violation of *statement b).*
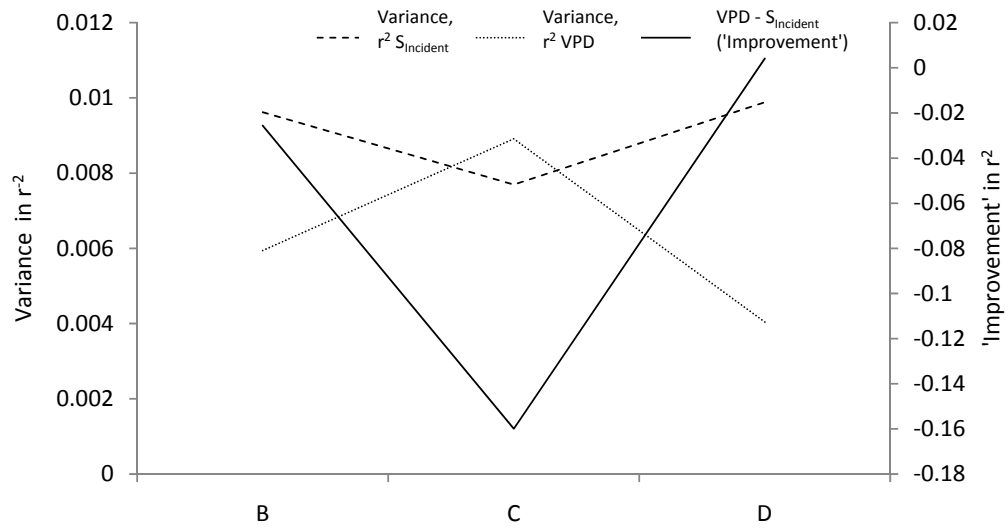
Figure 4.32   Variance in r^2 of sap flux density in all trees within plots B-D when regressed with vapour pressure deficit (dotted line), incoming shortwave radiation (dashed line), and the improvement offered by regression with vapour pressure deficit over that of regression with incoming shortwave radiation (solid line).

Viewing the control of sap flux density as a response to VPD or $S_{INCIDENT}$ whereby the two are antagonistic explains the difference in variation in r^2 between stations, which in turn clarifies the residuals at each station for regressions with VPD or $S_{INCIDENT}$. Those trees which show the greatest improvement of fit when grouped against $S_{INCIDENT}$ show the least variation between fits of $S_{INCIDENT}$, and the greatest variation between fits of VPD (Figure 4.32). This is the case for those trees in plot C. On the other hand, those trees in plot D show the same pattern acting in the opposite direction, demonstrating better relative improvement of r^2 with VPD than $S_{INCIDENT}$. These trees have a lower variation between fits with VPD than $S_{INCIDENT}$.

Thus comparing residuals directly does not elucidate a pattern, but comparing residuals when accounting for other controls such as matric potential through standardisation provides a clear and coherent pattern. This is because those trees at station D appear to express an edge effect (i.e. be predisposed to advection) similar

to those trees at station B. Whereas individual trees in plot B show the greatest improvement of fit when correlated with VPD over $S_{INCIDENT}$, the response of those trees at station D show a more consistent improvement in response. Given that trees in plot D show a weaker but more consistent response to advective (VPD) quantities, it would appear that trees at this site are limited by soil-rhizosphere-xylem resistance in a consistent fashion. Trees in plot B are less limited, but in a more variable fashion. The great variation in response of trees in plot B actually makes the average improvement (r^2_{VPD}-$r^2S_{INCIDENT}$) for the plot negative. As plot D was positioned on the apex of a hill it is likely that the trees in plot D would be more predisposed to advective influences. A similar pattern was described by Giambelluca *et al.* (2003), who note that exposed trees in forest interiors show considerable increases in transpiration.

Forest edge – interior gradients in sap flux density

Sap velocities are here normalised by potential evapotranspiration as derived from net radiation (calculated following Equation 2.1, Chapter2) for each tree within each plot, and then compared to ascertain patterns in sap velocity and tree water use with fetch. The standardisation of sap flux data using potential evapotranspiration to obtain a spatially and temporally complete data record is somewhat controversial. Shuttleworth & Calder (1979) draw attention to this explaining that if the vegetation and atmosphere are closely coupled then diabatic surface factors rather than the adiabatic energy input to the land surface determines water loss. Indeed, the presence of edge effects is usually *assumed* to be due to adiabatic advection and it is this which will lead to a lower decoupling coefficient and weaker correlation between sap flux and net radiation. Despite this, numerous researchers have employed the Priestley Taylor coefficient to compare sap flux rates across sites (Komatsu *et al.*, 2006a, 2006b) and between edge and inner trees (Giambelluca *et al.*, 2003, Herbst *et al.*, 2007b, Taylor *et al.*, 2001), and have shown that even when not measured simultaneously groups can be distinguished through standardisation with potential evapotranspiration. Herbst *et al.* (2007b) state that "neither the uncertainties in the calculation for the [sap flux] data and their relation with [potential evapotranspiration] nor the variability in [sap flux] weaken any statements made about the magnitude (and spatial extension) of the edge effect, since all trees, inner and edge, are effected in the same way". Whereas the nature of using thermal dissipation probes means that normalisation by net radiation/potential evapotranspiration is convenient or even necessary, Shuttleworth & Calder (1979) point out that "the laws of physics do not change to suit the need for a mathematically simple computation of [water use]". Although standardisation such as that presented by Herbst *et al.* (2007b) does indeed produce comparable transpiration rates it is arguable whether all trees are affected in the same way.

Given the relationships between r^2_{VPD}-$r^2_{Sincident}$ values of trees in plots B-D are consistent in terms of statements (a) and (b), the lack of VPD data, and the relatively good correlation between sap flux and $S_{INCIDENT}$ when compared to other studies answering similar questions, it was decided that normalisation of sap flux density by $S_{INCIDENT}$ is appropriate for this study. The relationship between tree size and average normalised sap velocity (Figure 4.33) was insignificant (r^2= 0.0023 P>0.05, df = 20) as

there was little variation in the size of those trees measured. Grouping trees into sizes was therefore deemed unnecessary.
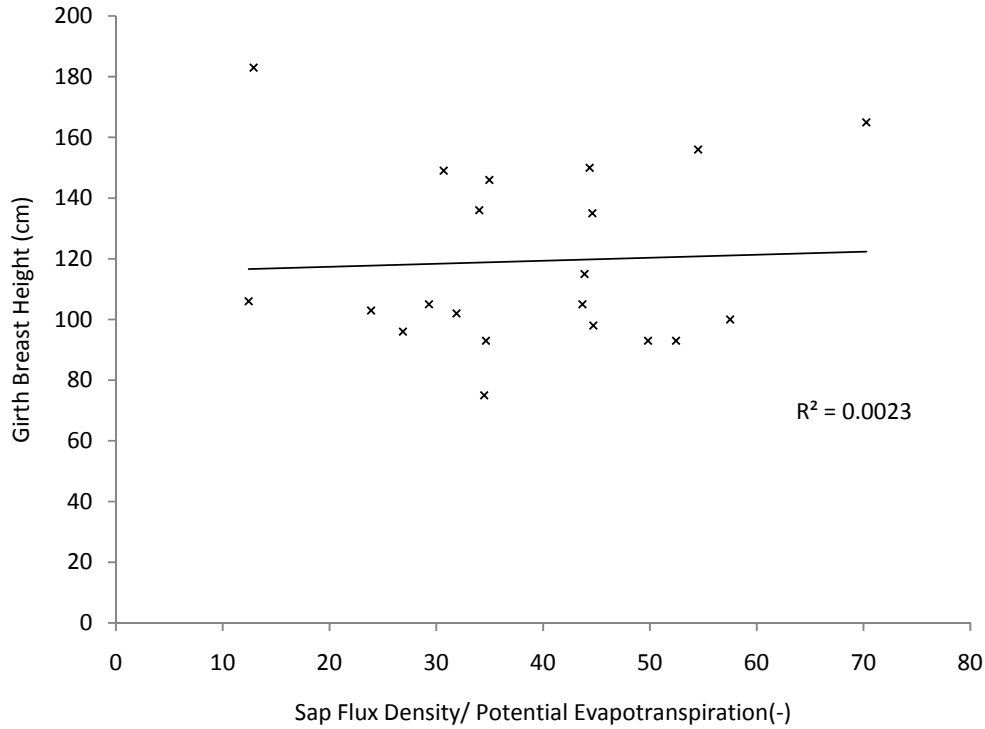
Figure 4.33 Sap flux density normalised by potential evapotranspiration (Fd/PE) vs. girth breast height (GBH) for those trees from which sap flow data was recorded(r ^{2}=0.0023).

Comparisons are made for tree water use and transpiration by extracting relative sap velocities from their mean normalised components with potential evapotranspiration using an assumed day length of 10 hours and the mean potential evaporation rate across the study period (4.4 mm dy^{-1}) and are presented in Table 4.3.

Tree water use (WU) is estimated using the integrated (trapezoidal numerical integration) daily sap velocity (v) and estimated area (m^2) active xylem (A$_x$,) as derived from Equation 2.39 (calibrated) and measurements of tree diameter breast height (DBH).

*WU = v * A$_x$*   *[kgdy^{-1}]*   *Equation 4.3.*

Transpiration (Tr) is estimated using the projected crown area in m^2 (A$_c$), (Giambelluca *et al.*, 2003):

Tr = $\frac{WU}{Ac}$ *[mmdy^{-1}]*   *Equation 4.4.*

Plots B and D possess trees of larger girth (x̄ = 128.29 cm, σ = 30.77, and x̄ = 129.00 cm, σ = 20.99, respectively, Table 4.3) and greater crown area (x̄ =54.05 m^2, σ = 12.50

and x̄ =72.76 m², σ = 8.08, respectively, Table 4.3), whilst plot C has the lowest crown area and tree girths (x̄ = 34.20 m², σ = 12.17 and x̄ =106.78, σ= 30.09 cm, respectively, Table 4.3).

Sap velocity and tree water use

For simplicity and comparison with previous studies (Laurance & Yensen, 1991) a logarithmic function *y = a ln(x) + b* was fitted to model gradients of sap flux density normalised by potential evapotranspiration (Fd /PE) across plots B-D.

Ratios of sap flux density to potential evapotranspiration are purposefully made here to allow comparison to the work of Herbst *et al.* (2007b). Values presented here show a greater range (12.44 − 70.26) but similar mean (38.67) to those values presented for diffuse porous species by Herbst *et al.* (2007b) (range=10-40, x̄ ≈ 30).

When comparing trees within plots B and C, normalised sap flux (Figure 4.34a) expresses a clear relationship with distance (r^2=0.38, P<0.01, df = 15) from the forest edge, with the highest values recorded very close to the boundary (<20m). Introduction of standardised sap flow from trees within plot D (x̄ = 42.33) renders a much weaker correlation (r^2=0.12, Figure 4.34b), although the trend is still significant (P<0.01, df =20). Mean normalised sap flux at plot B (49.87) is 79% greater than that of trees within plot C (27.90).

Given the distribution of canopy and stem sizes, it can be seen that an increase in sap flux density leads to greatly increased transpiration and tree water use rates in those individuals under the influence of the forest edge (Table 4.3). This can lead to huge daily water uses for a given tree size, with trees 3b and 5b using 217 kg and 313 kg of water in a day. Although a large amount of daily water use for their respective sizes, values here are still comparable to those reported by Vertessy *et al.* (1995, 1997) for a 15 year old *Eucalyptus regans* stand and indeed water usage of this magnitude is not uncommon (Wullschleger *et al.*, 1998). Usually, however, such large water use values are present in larger trees such as a 102 cm in diameter *Anarcadium excelsum* reported by Goldstein *et al.* (1998) to use 379 kg of water per day.

Tree #	Fetch (m)	Girth (cm)	A_c (m^2)	Macaranga species	Fd/PE (-) $\bar{x}$	σ	σM	Tree Water use (kg dy^{-1}) $\bar{x}$	σ	σM	Transpiration (mm dy^{-1}) $\bar{x}$	σ	σM
Plot B													
4b	5	150	36.51	M.hypoleuca	44.36	77.25	2.27	164.10	285.74	8.39	4.49	7.83	0.23
1b	18	136	67.83	M.hypoleuca	34.01	28.27	0.86	103.70	86.20	2.62	1.53	1.27	0.04
9b	40	93	45.29	M.pearsonni	52.45	73.24	2.04	75.81	105.84	2.95	1.67	2.34	0.07
5b	20	165	49.30	M.hypoleuca	70.26	88.09	2.44	313.71	393.30	10.89	6.36	7.98	0.22
3b	4	156	49.32	M.hypoleuca	54.51	100.71	2.86	217.86	402.49	11.41	4.42	8.16	0.23
10b	2	93	58.86	M.pearsonni	49.83	96.97	2.75	72.01	140.13	3.97	1.22	2.38	0.07
2b	30	105	71.24	M.hypoleuca	43.68	26.85	0.84	80.07	49.23	1.54	1.12	0.69	0.02
Plot C													
8c	75	102	33.23	M.hypoleuca	31.88	23.52	0.63	55.21	40.76	1.10	1.66	1.23	0.03
19c	80	183	29.04	M.hypoleuca	12.90	16.30	0.44	70.66	89.29	2.40	2.43	3.07	0.08
7b	55	98	45.74	M.pearsonni	44.70	32.16	0.88	71.57	51.51	1.42	1.56	1.13	0.03
22c	110	75	14.80	M.hypoleuca	34.47	24.02	0.65	32.72	22.81	0.62	2.21	1.54	0.04
11c	90	106	33.39	M.pearsonni	12.44	20.56	0.56	23.23	38.42	1.04	0.70	1.15	0.03
12c	120	96	33.05	M.hypoleuca	26.87	19.54	0.52	41.32	30.05	0.80	1.25	0.91	0.02
16c	100	103	30.02	M.pearsonni	23.90	18.59	0.51	42.19	32.82	0.90	1.41	1.09	0.03
6c	60	105	58.86	M.pearsonni	29.30	2.97	0.60	53.72	40.28	1.10	0.91	0.68	0.02
20c	100	93	29.70	M.pearsonni	34.64	19.68	0.60	50.06	28.44	0.87	1.69	0.96	0.03
Plot D													
33d	310	149	73.83	M.hypoleuca	30.69	62.35	1.74	112.02	227.59	6.34	1.52	3.08	0.09
34d	280	100	76.24	M.pearsonni	57.52	574.76	16.63	95.82	957.53	27.71	1.26	12.56	0.36
35d	290	146	76.24	M.pearsonni	34.95	61.86	1.68	122.57	216.94	5.90	1.50	2.66	0.07
32d	295	115	72.31	M.hypoleuca	43.88	41.69	1.23	96.19	91.37	2.70	1.33	1.26	0.04
36d	290	135	59.77	M.hypoleuca	44.61	69.81	1.99	134.05	209.79	5.97	2.24	3.51	0.10

Table 4.3: Sap flux density (Fd) / Potential evapotranspiration (PE), daily water use (kg dy^{-1}), and transpiration (mmdy^{-1}), for all trees in plots B-D, indicating the standard deviation (σ) and standard error (σM) of each mean value ($\bar{x}$) , presented alongside the crown area (A_c, m^2), girth (cm), distance from the forest edge (fetch, m), tree species (belonging to the Macaranga genus) and identification number (Figure 2.2, Chapter 2) of a given tree. Crown area calculated using the mean of four diameter measurements and assuming a circular crown projection onto the ground.

The contrast in water use by trees at a forest edge is seen by comparing the mean values of plots B and C with the edge plot yielding a much higher mean ($\bar{x}$ = 146.75 kg dy^{-1}) than the 'interior' ($\bar{x}$ = 48.97 kg dy^{-1}). Those trees in plot D yield a value in between of 112.13 kg dy^{-1}. Similar patterns in transpiration are shown, with three trees at the forest edge exceeding the potential evapotranspiration of 4.4 mm dy^{-1}.

Whereas the main scaling component for estimating water use at the scale of the canopy is the sap flux density (kg m^2 s^{-1}), estimations of transpiration and tree water use have important physiological implications at the scale of the individual tree/rhizopshere. Trees using more water are more likely to cause localised soil moisture depletion and are also more prone to cavitation in their conductive elements. Thus trees at a forest edge appear more likely to decouple themselves from land surface effects (i.e. VPD and $S_{INCIDENT}$) by virtue of their increased sap velocity. This is remarkably consistent with the previous section, as those plots using the most water (B and D) are indeed the plots most limited by soil-rhizosphere-xylem resistance, and furthermore those trees under the greatest advective (station B) influence show the greatest variation in response to VPD. Such feedbacks have indeed been hypothesised but measurements to support this are non-existent.
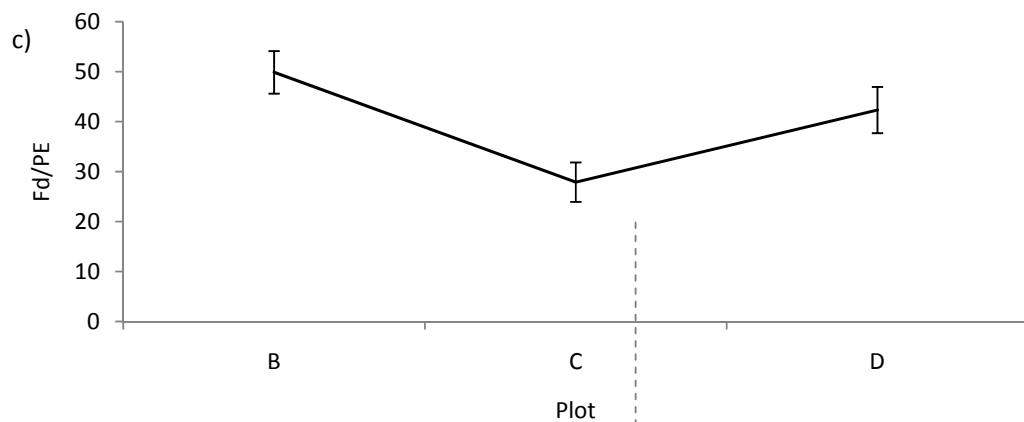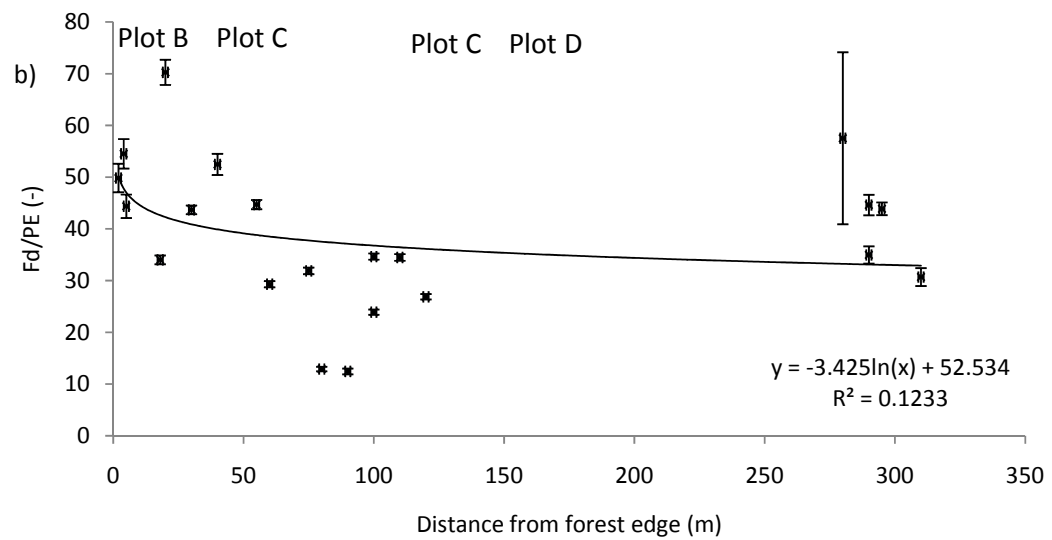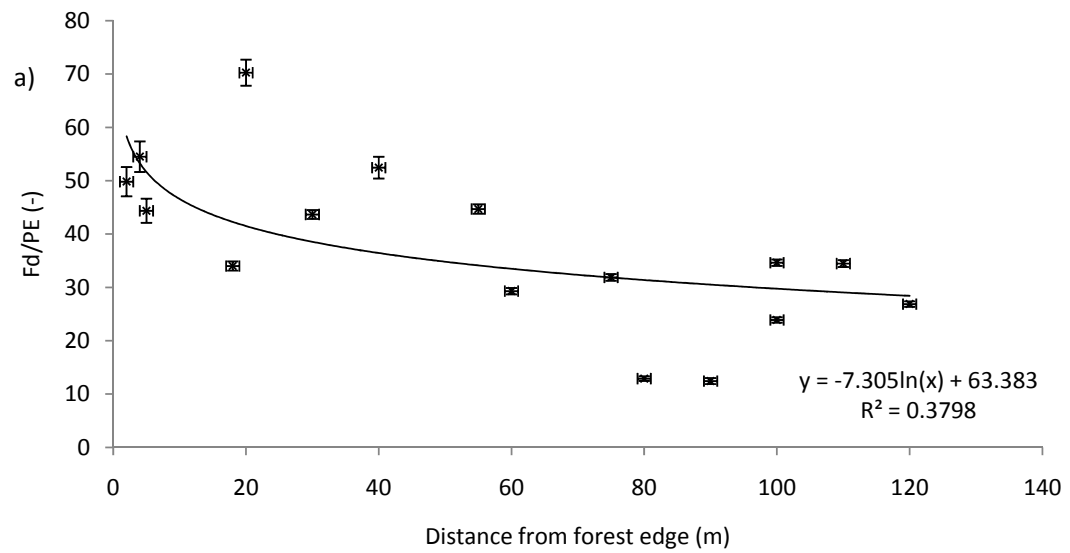
Figure 4.34   Sap flux density normalised by potential evapotranspiration (Fd/PE) in relationship to distance from the forest edge for a) those trees in plots B and C, b) all trees in plots B-D and c) mean values of Fd/PE for all trees in each plot B-D. Individual trees within plots B-D are delineated by dashed vertical lines in parts a) and b). Error bars denote standard error.

Soil moisture

Whereas the implied effect of increased tree water use upon cavitation of conductive elements and soil water limitation is well documented (Tyree *et al.*, 1986, Sperry & Tyree, 1988), this study does not make direct measurements of this nature.

However comparing daily soil moisture patterns (Figures 4.35a and 4.35b) taken at 10cm below a single tree in station B (tree 5b, Figure 4.35a) and station D (tree 34d, Figure 4.35b) to diurnal patterns of sap flux (Figures 4.15-4.17) it is apparent that water use by the tree at station D is immediate and much more considerable than that at station B. Both trees remove water to a volumetric content below the wilting point, although accounting for the use of the nominal probe calibration and its associated accuracy may account for this discrepancy. The tree at station B however shows a greater delay in water uptake that is much lower in magnitude (Figure 4.35a).

Soil moisture follows a diurnal pattern consistent with patterns of transpiration and thus can act as an indicator as to the nature of water use. Da Rocha *et al.* (2004) suggest that the pattern of water withdrawal reflects the distribution of root activity. Water content decreased during daytime and recovered fully during the night at both sites. The nocturnal redistribution of water is well documented (da Rocha *et al.*, 2004, Lopes, 2001) and occurs by either flow through hydraulic lift (Caldwell *et al.*, 1998) or capillary action.

Using nocturnal and diurnal means a daily withdrawal of 0.004 m^3m^{-3} is present under tree 34d, whereas the volumetric soil moisture under tree 5b decreases by only 0.0002 m^3m^3. This corresponds to 0.4mm under tree 34d and 0.002 mm under tree 5b in the top 10cm of soil. Thus it seems a significant amount of soil moisture for evapotranspiration is drawn from the top 10cm of soil at site D (6.36%), but only 0.05% of evapotranspiration comes from the same depth at site B.

Should the pattern of water withdrawal reflect the distribution of root activity, it stands to reason that it is possible that the roots of those trees in plot D are physically constrained by the amount of water they can withdraw from the soil, by being, for example, confined to more shallow soil than those trees in plot B. Although this is conjecture, such a hypothesis is consistent with the patterns of sap flux magnitudes and responses presented here. As tree 5b uses less water in the top 10cm that tree 32d it is within the realms of possibility that trees at station B have

the option of sourcing the water they need from either deeper soil (as is common at the bottom of a hill) or by the expansion of rooting systems into the numerous gaps at the forest edge or the swidden itself. The larger volume of water extracted at plot D indicated that trees in plot D do not appear to have this option, and therefore are greatly limited in their water extraction options. These two statements would also explain the greater variability in responses to advection within plot B as opposed to advection in plot D. Given the potential for huge water use of individual trees in plot B (as demonstrated by micrometeorological measurements and supported by estimates of individual tree water use in the same plot) it could be possible that a feedback is occurring between increased tree water use at the forest edge and an increased resistance in the soil-rhizosphere-xylem pathway.
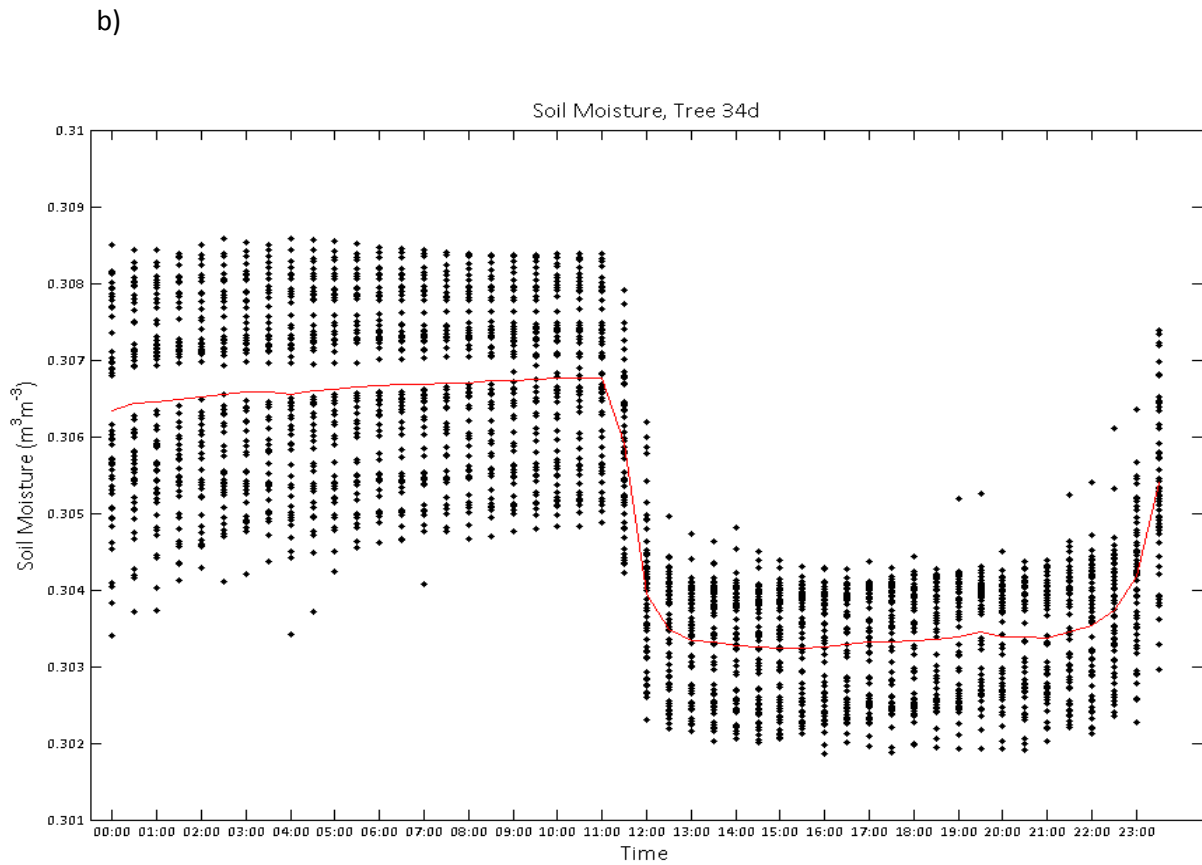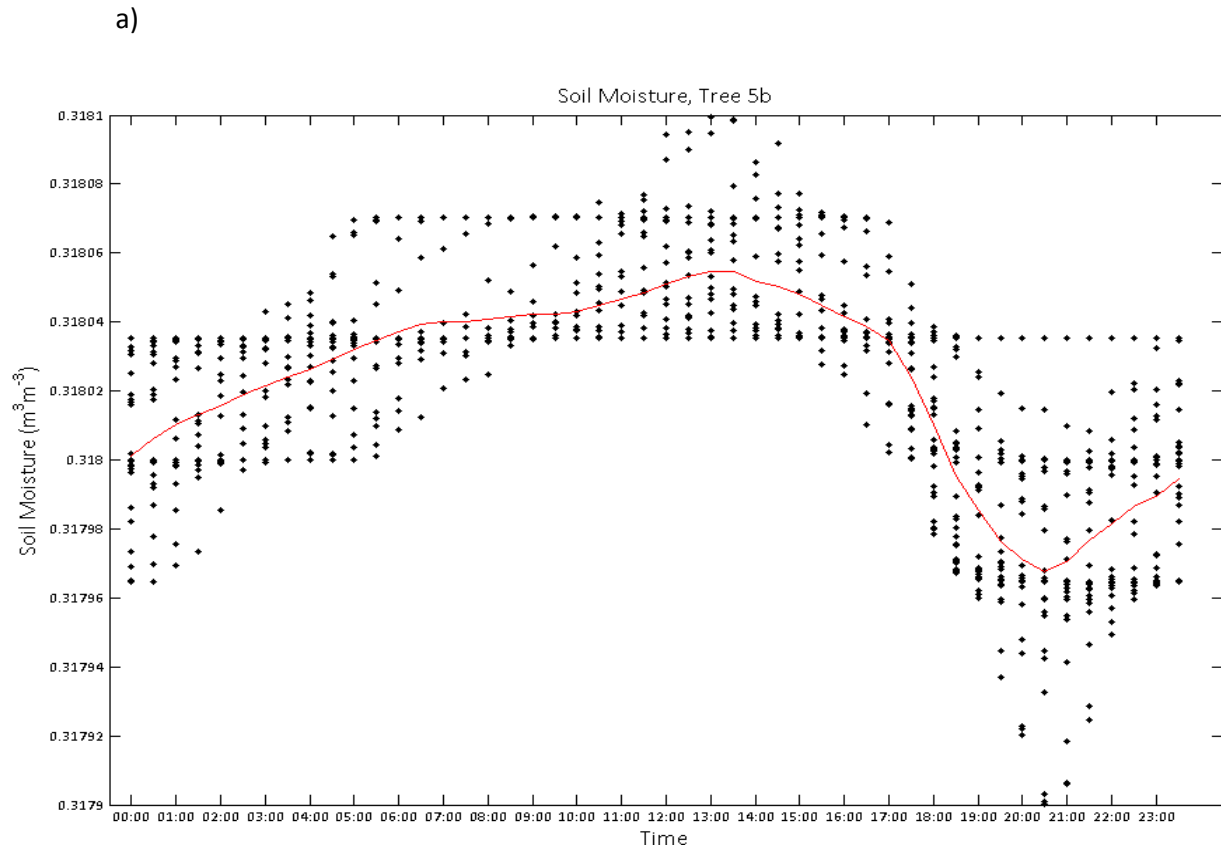
Figure 4.35 Diel patterns of volumetric soil moisture (m^3m^3) at 10cm depth under a) tree 5b and b) tree 34d. Red lines represent the average soil moisture values for n= 88 and n= 98 days, measured under trees 5b and 34d, respectively, which are represented by black dots for a given half hour period in the diel cycle.

Decoupling coefficient

Another measure of the partitioning between advective (diabatic) and radiative (adiabatic) controls is the decoupling coefficient. McNaughton & Jarvis (1983) quantitatively defined the degree of coupling between transpiration and the saturation deficit of the air in the boundary layer by the decoupling coefficient as:

$$\Omega = 1 + \frac{s+\gamma}{\gamma}\frac{ga}{gc}$$
[-]   *Equation 4.5*

The decoupling coefficient is essentially the ratio of aerodynamic to canopy conductance, which ranges from 0 to 1. Larger values thus indicate that the forest is less coupled to the atmosphere above it, and that the chances of advection are lower, something that is seen by considering the decoupling coefficient is inversely related to the Priestley-Taylor α coefficient (Pereira, 2004). If ga>>gc then gc can be calculated:

$$gc = \frac{\gamma \lambda Ec}{cp \, \rho VPD}$$
[ms^{-1}]   *Equation 4.6*

Aerodynamic conductance was estimated from Phillips & Oren (1998) following the method of Thom & Oliver (1977):

$$ga = \frac{0.212*1+0.54\,U}{\left(ln\left(z-\frac{d}{zo}\right)\right)^{\wedge}2}$$
[ms^{-1}]   *Equation 4.7*

As mean aerodynamic conductance above the forest of plots B and C exceeded canopy conductance by an order of magnitude (Figure 4.36) then the application of Equation 4.5 was deemed appropriate. However, this assumption was not met for the respective conductance of plot D (Figure 4.36). The analysis thus focuses on a comparison between plots B and D to examine the theoretical partitioning of adiabatic and diabatic controls by the canopy.

VPD was not available over the forest for those days when transpiration was measured. VPD was therefore estimated for each station using the regression coefficients from average diurnal patterns of VPD over each station as presented in section 4.2. Canopy evapotranspiration was estimated by scaling tree sap flux density (kg m^{2}s^{-1}) by the area of active xylem (m^2) within each plot as measured in section 4.7.
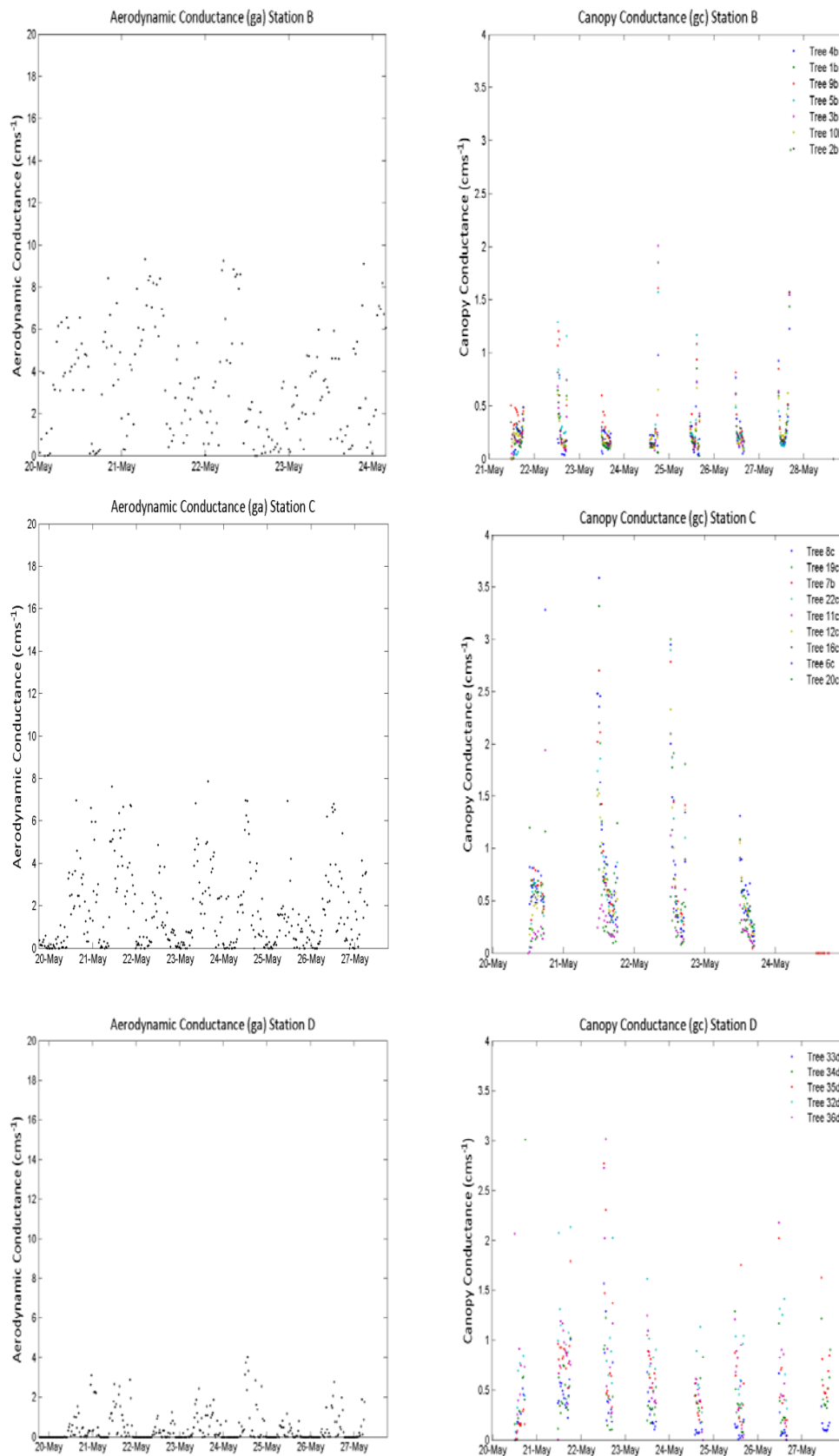
Figure 4.36   Available data of (right) diurnal canopy conductance and (left) diurnal aerodynamic conductance for all trees in plots B-D (top to bottom) during the period 20th-28th May 2007. Note the change in scale between canopy conductance and aerodynamic conductance.
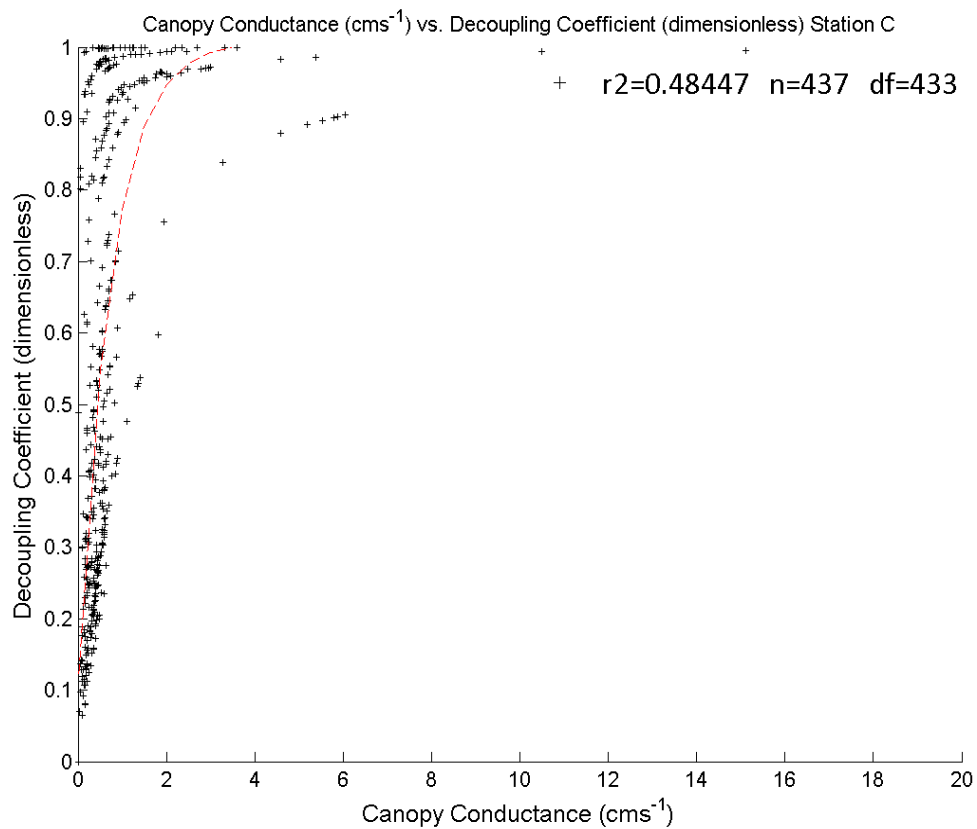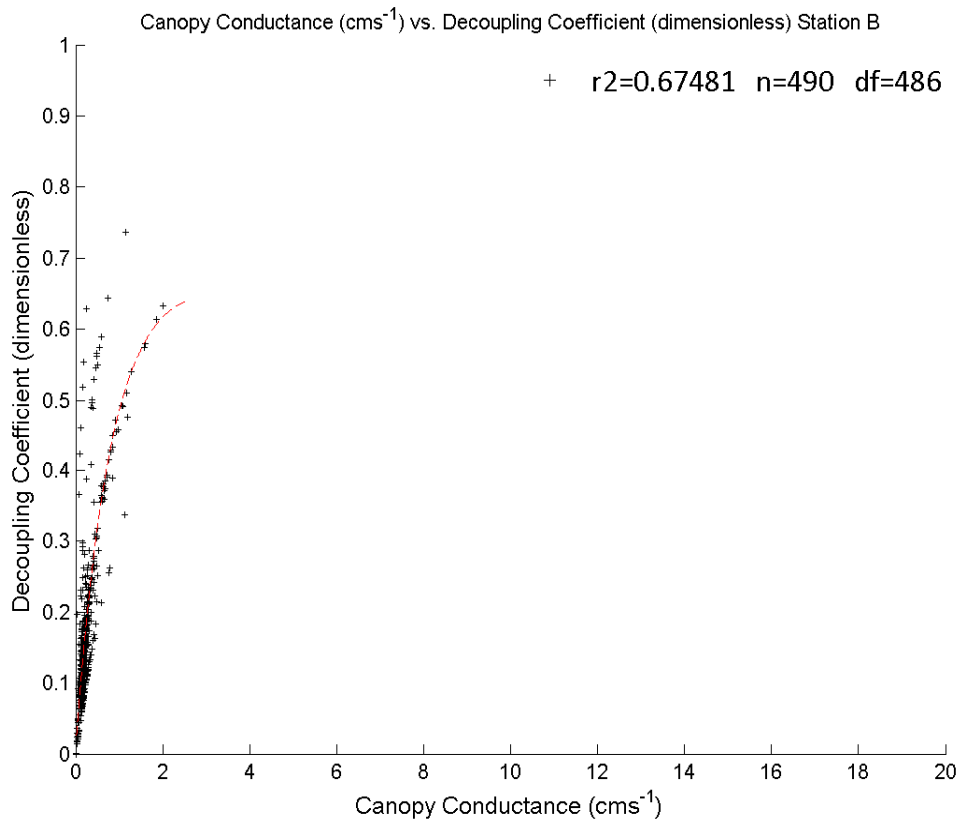
Figure 4.37   The relationship between canopy conductance and decoupling coefficient for all trees in plots B (top) and C (bottom).

It can be clearly seen that an increase in canopy conductance over plot B leads to a more gradual decoupling of the land surface that reaches lower levels of decoupling when compared to plot C (Figure 4.37). This is expressed as a shallower curve that reaches its asymptote at a lower decoupling coefficient: i.e. the canopy of plot B is better coupled to advection in a more stable fashion. It would therefore appear that the increased tree water use at the forest edge site is due to a better coupled canopy there. The decreased canopy conductance that acts to decouple the canopy in plot B is strongly influenced by the much lower total area of active xylem in the stand (i.e. a lower stand basal area). However, recalculating the decoupling coefficient with the sap flux densities of those trees in plot B with the estimated area of active xylem in plot C still renders a shallower curve that is less decoupled from the advective controls when compared to plot C (Figure 4.38). Thus it appears that under replete soil moisture conditions an advective edge effect is still possible for tree densities and sizes similar to those found in forest interiors.

Canopy Conductance (cms^{-1}) vs. Decoupling Coefficient (dimensionless) Station B

+ r2=0.70992 n=490 df=486
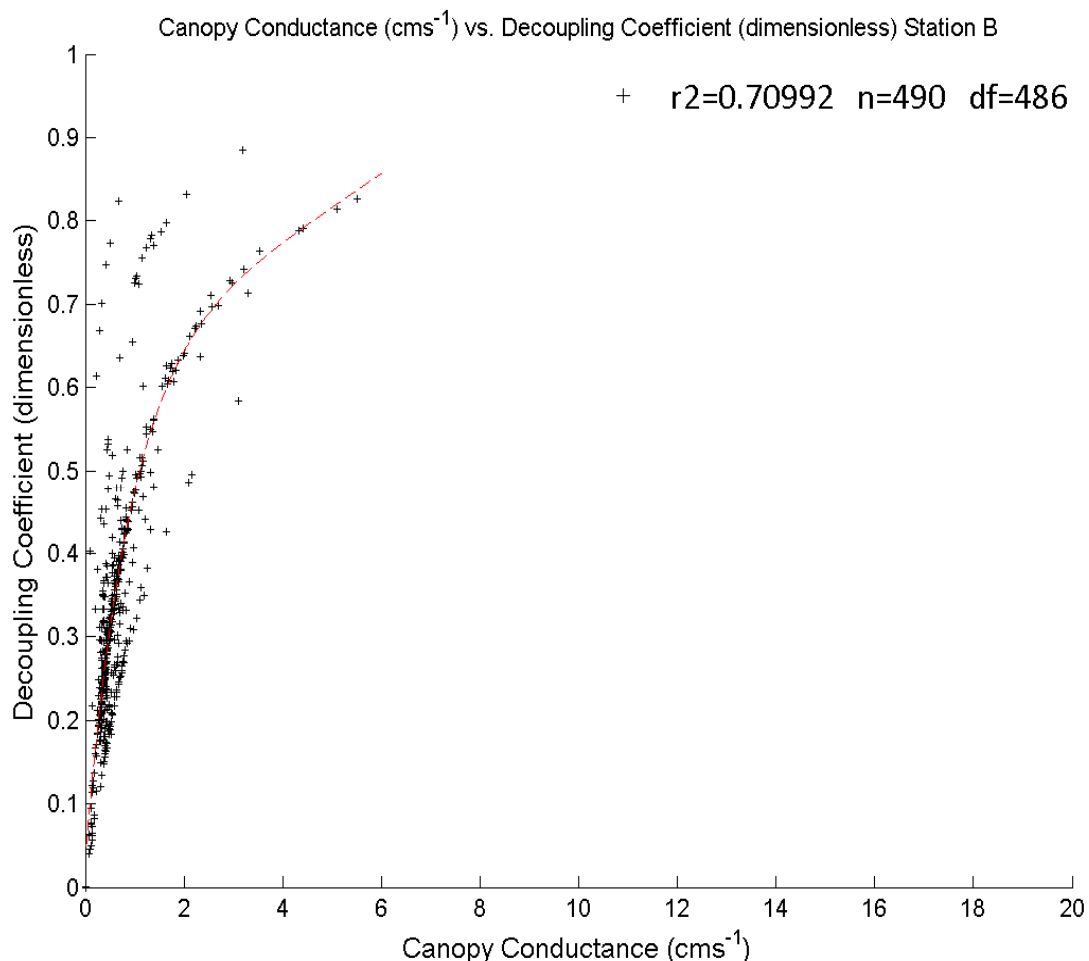
Figure 4.38   The relationship between canopy conductance and decoupling coefficient for all trees in plot B given the same total stand xylem area (Ax) value as station C.

Understorey evapotranspiration

Understorey evapotranspiration (mm dy^{-1}) is presented in Figure 4.39, where data are grouped into 5 canopy openness categories numbered 1-5, representing 0-19%, 20-39%, 40-59%, 60-79%, 80-100% canopy gap fractions, respectively.

When evapotranspiration measurements in all canopy openness categories were grouped, mean evaporation from leaf litter (0.42mm dy^{-1}) was lower (P<0.001, t-test for equal variances, n=102) than that of vegetation evapotranspiration (0.97 mm dy^{-1}). Although means for both leaf litter and vegetation covers were significantly across canopy openness categories (P<0.01, one-way ANOVA, df=4) there is a much more prominent influence of gap fraction (and therefore presumably light levels below the canopy) on vegetation that leaf litter. This is to be expected in understorey conditions where light is limiting. A decrease in the influence of canopy openness upon evapotranspiration from both litter and vegetation is seen after category 3 (Figure 4.39), expressed as a greater variability around the mean. Insignificant patterns were found between evapotranspiration, soil moisture and vapour pressure deficit.
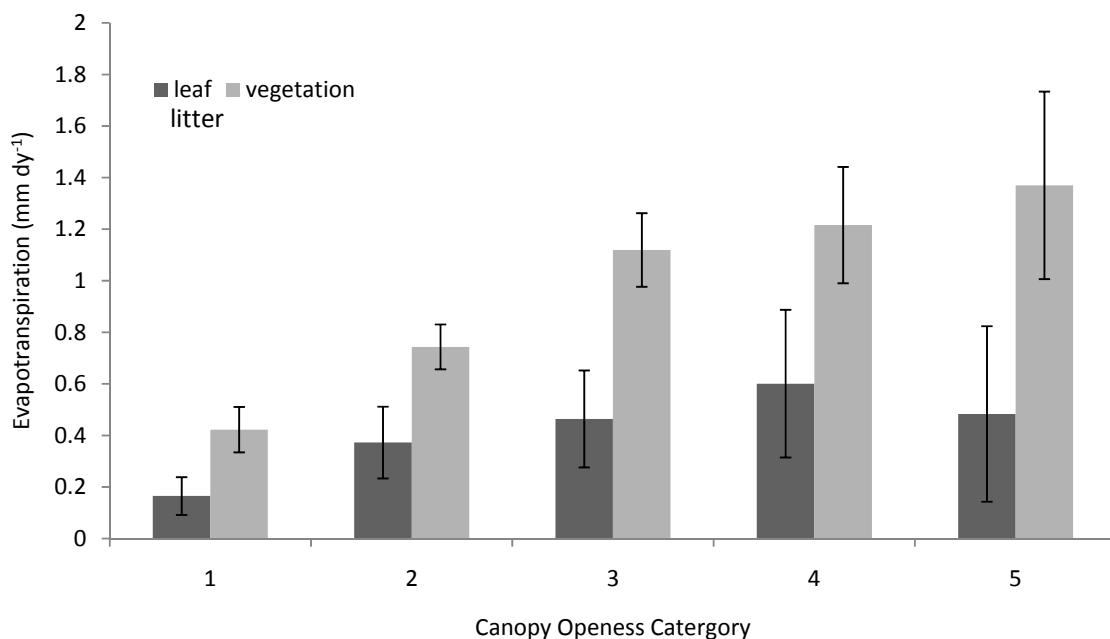
Figure 4.39   Estimated evapotranspiration (mm dy^{-1}) of leaf litter and vegetation understorey ground covers for 5 canopy openness categories representing 0-19%, 20-39%, 40-59%, 60-79%, 80-100% gap fractions, respectively. Canopy openness measured with a canopy scope (Chapter 2, section 2.10).

Chapter 4 – The Hydrometeorology of a Humid Tropical Forest Patch – Results and Discussion

Precipitation, throughfall and wet canopy evaporation

Wet canopy evaporation (E_{wc}), which was assumed to be equal to rainfall interception, was estimated following Equation 2.20, Chapter 2. E_{wc} was significantly different between plots (P<0.05, one-way ANOVA, df =5). Relevant throughfall data for each plot are presented in Figure 4.40, and total precipitation is addressed below.

Rainfall during the throughfall collection period (January and February 2008) was 194.3mm in January and 175.8 mm in February, totalling 370.1 mm (i.e. 6.27 mm dy^{-1}). Precipitation over this period is considerably lower than the average at Danum (310.7 mm January and 235.8 mm in February, or 10.5 mm dy^{-1} averaged across the two months). This is however consistent with the observed lower rainfall at Wawasan Bentar (6.24 mm dy^{-1}, n=188 days) than at Danum during in the 2007 study period (7.99 mm dy^{-1}). Estimated annual rainfall at this site was estimated to be the ratio (0.781) of rainfall at Wawasan Bentar to that at Danum over the study period multiplied by the total rainfall received at Danum that year (3021.7 mm) = 2359.9 mm.

The agreement between rainfall collected during the 2007 and 2008 study periods means that the estimation of wet canopy evaporation (E_{wc}, %) differs little using precipitation of either periods. E_{wc} was therefore estimated using the precipitation measurements taken at the same time as the throughfall measurements.

Estimated wet canopy evaporation, as calculated following Equation 2.20 (Chapter 2), averaged 33.60% of total precipitation across all sites. This value is much higher than recorded elsewhere in the Danum region (Bidin & Chappel (2003) report values between 13.6-14.0%) but is still comparable to those similar forests in Puerto Rico and west Malaysia where E_{wc} = 39% (Scatena, 1990) and E_{wc} =27% (Nik *et al.*, 1979) have been reported. Indeed, increased proportions of E_{wc} are often associated with more disturbed forests (Bidin & Chappel, 2003) which are inherently more aerodynamically rough and thus increase wet canopy evaporation and thus there is a strong case for an increased evaporative fraction at this site.

Grouping data from microplots (BA, BB, CA, CB, DA, DB) into their corresponding vegetation plots (B-D) - e.g. 'BA' + 'BB' = 'B', following section 2.6, Chapter 2, mean estimated wet canopy evaporation was 33.32, 33.21 and 34.04 % for plots B-D. That is, forest edges do not have a significantly higher throughfall fraction that leads to a decreased amount of wet canopy evaporation.

Stemflow was measured but data were considered unreliable as many of the trees chosen for stemflow measurements were growing at such a rate that stemflow conduits were twisted to a point of not being able to channel water into their collectors.
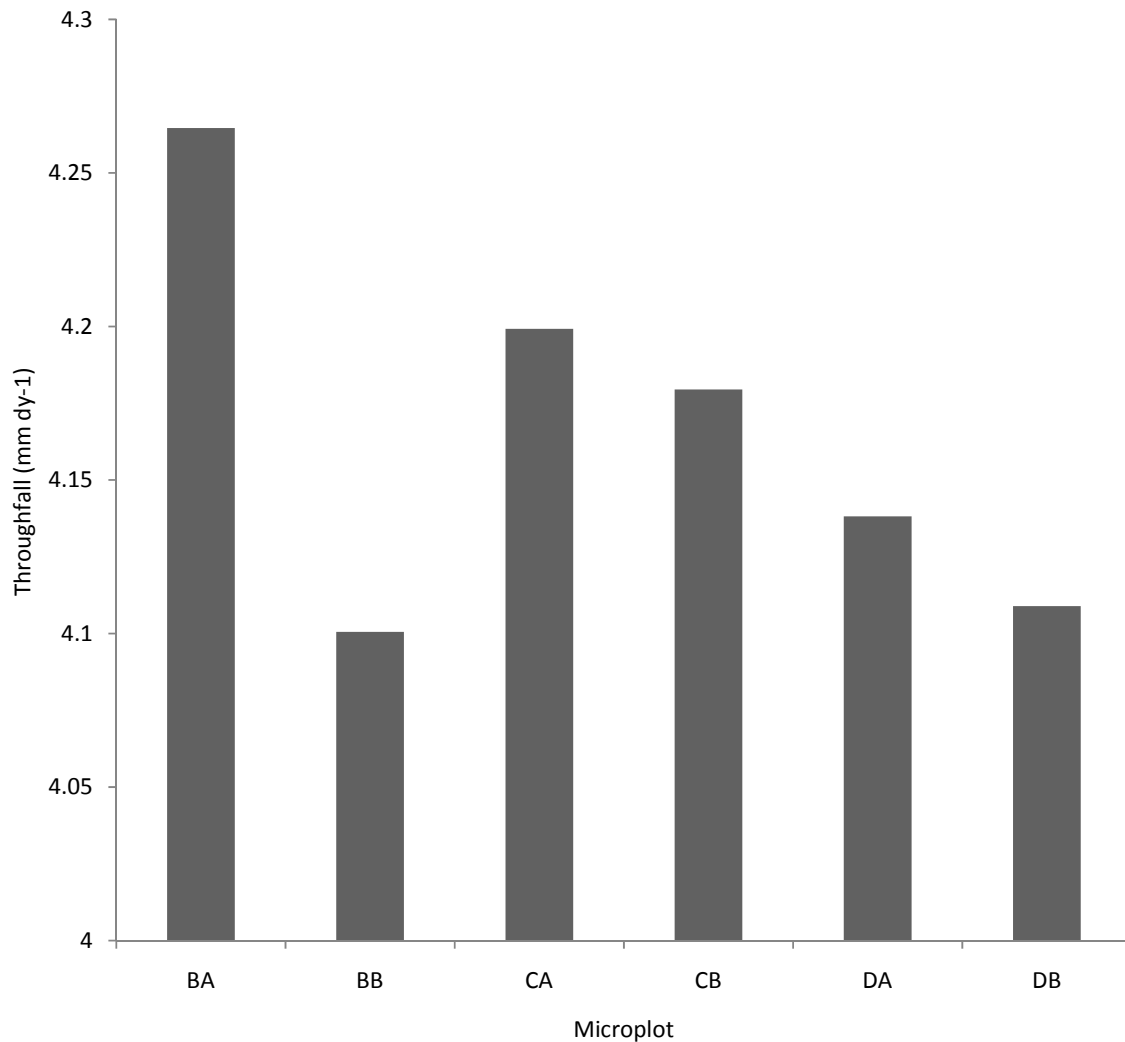
Figure 4.40 Mean throughfall (mmdy^{-1}) for plots BA –DB as measured in the period 1st January -29th February 2008.

Introduction

A water budget is estimated for four different edge scenarios using the hydrometeorological data reported previously. Vegetation parameters (total stand basal area, ground cover fraction, canopy openness, crown exposure) measured at two edges within Danum Valley (DA) and Sungai Liang (SL) forest sites, representing four different edge scenarios are presented and used to scale fluxes to the stand scale. These sites represent an old degraded edge (DA2), a young preserved edge (SL1), and an old preserved edge (SL2), with the Wawasan Bentar (DA1) site representing a relatively new, but degraded, edge. These four scenarios are stereotypes of not only Sabah and Borneo, but also have been reported in other edge effect studies. For example, Laurance *et al.* (2000) report the death of large trees in Manaus, Amazonia, at forest edges which is consistent with the 'degraded edge' stereotype. Whereas this pattern lead to a decrease in biomass of 10% (Laurance *et al.*, 1998b), Herbst *et al.* (2007b) and Ciencala *et al.* (2002) report increases of basal area at preserved forest edges conforming to the 'preserved' or 'sealed' edge stereotypes described by Harper *et al.* (2005) and Murcia, (1995).

As water fluxes were measured only measured at the Wawasan Bentar forest (DA1), estimations of water fluxes at each other site (DA2, SL1, SL2) in this section are derived using their respective vegetation parameters and are compared to the estimated water budget at Wawasan Bentar. Thus this exercise is essentially a crude sensitivity analysis of the effect of age upon two broad edge categories: 'disturbed' and 'preserved' *in terms of vegetation parameters only.* Although crude, this approach represents a much needed sensitivity analysis using appropriate parameters. As shown in section 4.5, decoupling is still possible for even high tree densities given the values of vapour pressure deficit and canopy water use measured at a forest edge.

Tree transpiration is scaled on a basal area (m^2 ha^{-1}) basis using Equation 2.25, Chapter2. Sap velocities are derived for the means presented for each distance strata of plots B-D as in the field study. Wet canopy evaporation is estimated using the mean daily precipitation from each site (2359.9 mm at Wawasan Bentar and ~3000mm at Sungai Liang) and the proportions of wet canopy evaporation (E_{wc}) as derived from throughfall measurements reported in the section 4.6. Wet canopy

evaporation was taken to be 17% at Sungai Liang in fitting with typical reported values of E_{wc} in the literature.

Understorey evapotranspiration is estimated using chamber measurements from the field campaign weighted by the fractional area coverage of three understorey covers associated with each site. As shown in the previous section understorey water flux is dependent on the openness of the canopy. Understory flux estimates are thus made accounting for the openness of the canopy as measured with the canopy scope.

A major limitation of this study is that transpiration measurements are only made for exposed trees and so it is hard to say whether estimates of edge effects should be made by scaling the basal area of all trees within the stand or only those trees that are exposed. Two estimates are made then with one scaling the edge effect by the basal area of all trees in the stand and the other scaling the edge effect by only exposed trees. This is mediated with the use of the canopy index as outlined in the methodology.

An overview of the raw vegetation parameters at each of the four edge sites is presented below. Water budgets for each stand are then created to estimate the net edge effect upon evapotranspiration of tropical forest.

Basal area

Basal area (>10cm DBH) of both the disturbed sites is much lower than that of their interiors, or of the equivalent plots B-D of preserved sites (Figure 4.41). This is unsurprising as plots were chosen for their similarity of forest type and their expression of a highly stereotyped pattern of edge structure.

The older disturbed edge shows a great penetration of effect upon basal area (Figure 4.41) with very low basal (plot B = 8.56 m^{2}Ha^{-1}, plot C=8.56 m^{2}Ha^{-1}) areas being present even at a considerable distance into the forest patch (i.e. plot C). Similar values are present at site DA1 within plot B (7.48 m^2 Ha^{-1}). These values are about 30% of those values typical of well regenerated secondary forest and are typical of values presented by Sagar & Singh (2006) for disturbed dry forest in Vindhyan, India, which averaged 7.7 m^2 Ha^{-1} (range 1.3-13.8 m^2 Ha^{-1}) over five different plots.

Basal area of trees >10cm DBH in interior plots at SL1 (31.21 m^2 Ha^{-1}) and SL2 (32.05 m^2 Ha^{-1}) compare well to values found in the literature although the same plots at sites DA1 (23.65 m^2 Ha^{-1}) and DA2 (23.87 m^2 Ha^{-1}) are quite lower than those values

reported for secondary forests in the region. For example, Brearley *et al.* (2004) report values of 25.72 m^2 Ha^{-1} for old growth secondary forest in Barito Ulu, Kalimantan. Okuda *et al.* (2003) showed similar values to this of 27 m^2 Ha^{-1} in Pasoh, Penninsular Malayisa, and Giambelluca *et al.* (2003) values range from 24.1-24.3 m^2 Ha^{-1}. Although sites SL1 and SL2 are slightly higher than values reported in secondary forest this is nowhere near as high as the primary forest estimates of Proctor *et al.* (1983, 1988) or Ashton (1964) whose estimates were (57, 42.2 and 35.2 m^2 Ha^{-1} respectively), although others report lower values of ~27 m^2 Ha^{-1} (Newberry *et al.*, 1992; Pinard & Putz, 1996).

The pattern of forest degradation and its associated lower basal area is much more pronounced in both magnitude and distance of edge influence than reported by Laurance *et al.* (1997) for other tropical forest edges in Amazonia, because the disturbance reported here is subject to the active anthropogenic degradation of forest edges. The study by Laurance *et al.* (1998b) was specifically made within a specially fragmented reserve to look at a solely biological feedback (see Laurance *et al.*, 2002). The pattern of basal area loss presented for forest edges at sites DA1 and DA2 is similar to those present throughout the Yayasan Sabah logging concession. This is especially the case along logging roads where considerable lengths of the road side have very few trees and high vegetation coverage. A slight influence of distance from the forest edge is expressed in basal area at site SL2 (B=22.98 m^2 Ha^{-1}, C= 26.48 m^2 Ha^{-1} D =39.79 m^2 Ha^{-1}).

Ground coverage, canopy openness and crown exposure

The lower basal area of edge plots for sites DA1 (i.e. plot B) and DA2 (i.e. plots B and C) is reflected in a more open canopy, and higher incidence of vegetation within these plots (Figure 4.42). This effect is greatest in the highly degraded edge plots of site DA2, where the exceptionally low basal area leads to high canopy openness and very high vegetation coverage (74% and 72% for plots B and C respectively). This represents a great increase in the vegetation coverage when compared to the younger DA1 site (46% vegetation coverage). It can be expected that the understorey contribution to evapotranspiration is greater than in interior plots or those plots of the 'undisturbed' (SL1 and SL2) sites. There is a similar relationship between canopy openness and vegetation proportion for all sites.

There was little change in the contribution of exposed trees to stand basal area with distance from the forest edge (Figure 4.43). This can be resolved by considering that large trees will be exposed in either degraded or non-degraded forest, owing to uneven canopy levels typical of Bornean tropical forest in the latter case and the removal of vegetation leaving larger trees better exposed in the former case. As expected smaller trees were more exposed at the edges of site DA2 (plots B and C), although this was not the case for site DA1- presumably because of the sheltering of smaller trees by larger ones. The inconsistencies of these patterns are to be expected given the aberrant nature of anthropogenic disturbance and its consequent impact upon patterns of regeneration.
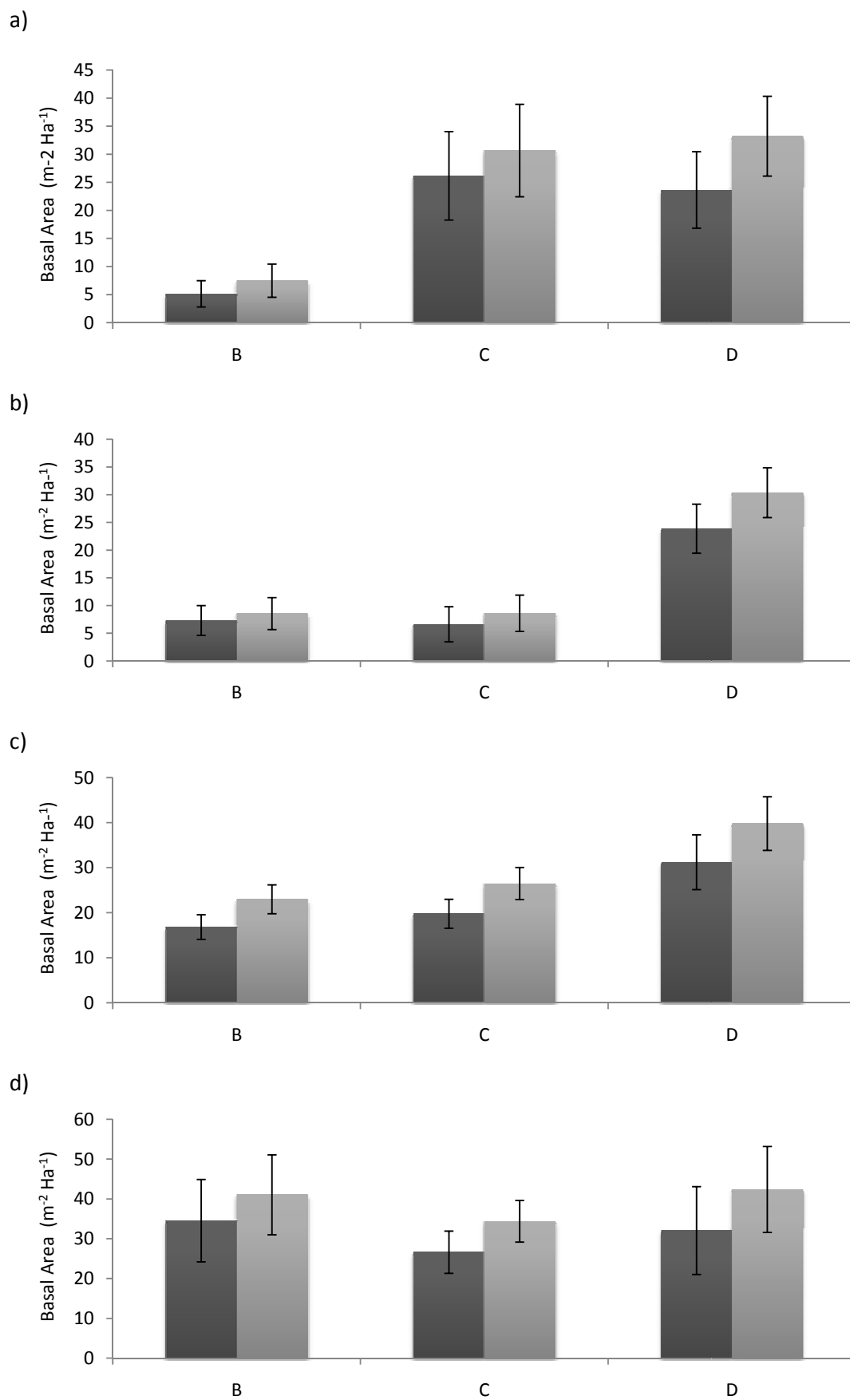
Figure 4.41 Basal area of large trees (dark grey) and all trees (light grey), for forest plots (B-D) at a)

a)

b)

c)

d)

a)

b)

c)

d)

e)

f)

g)

h)
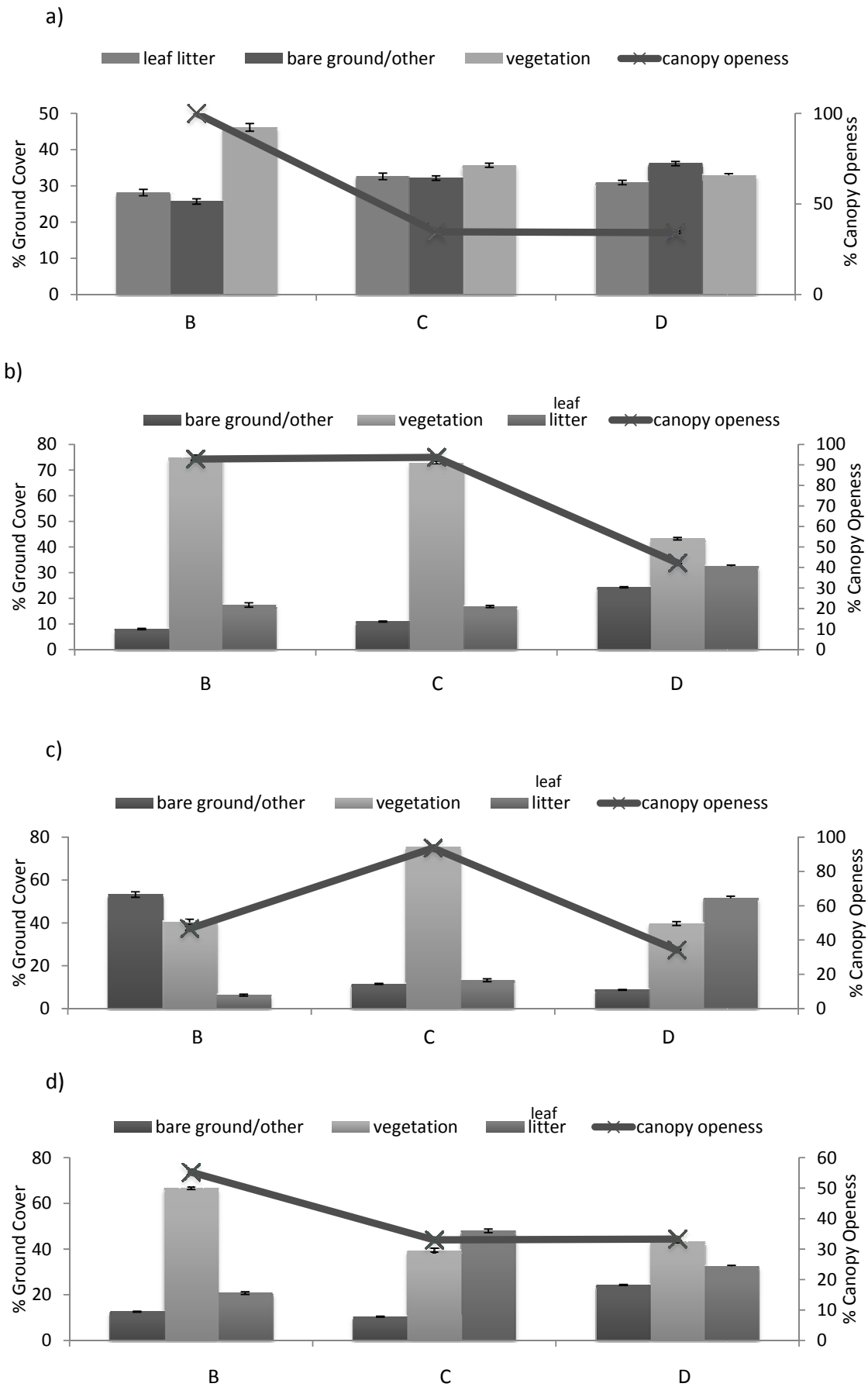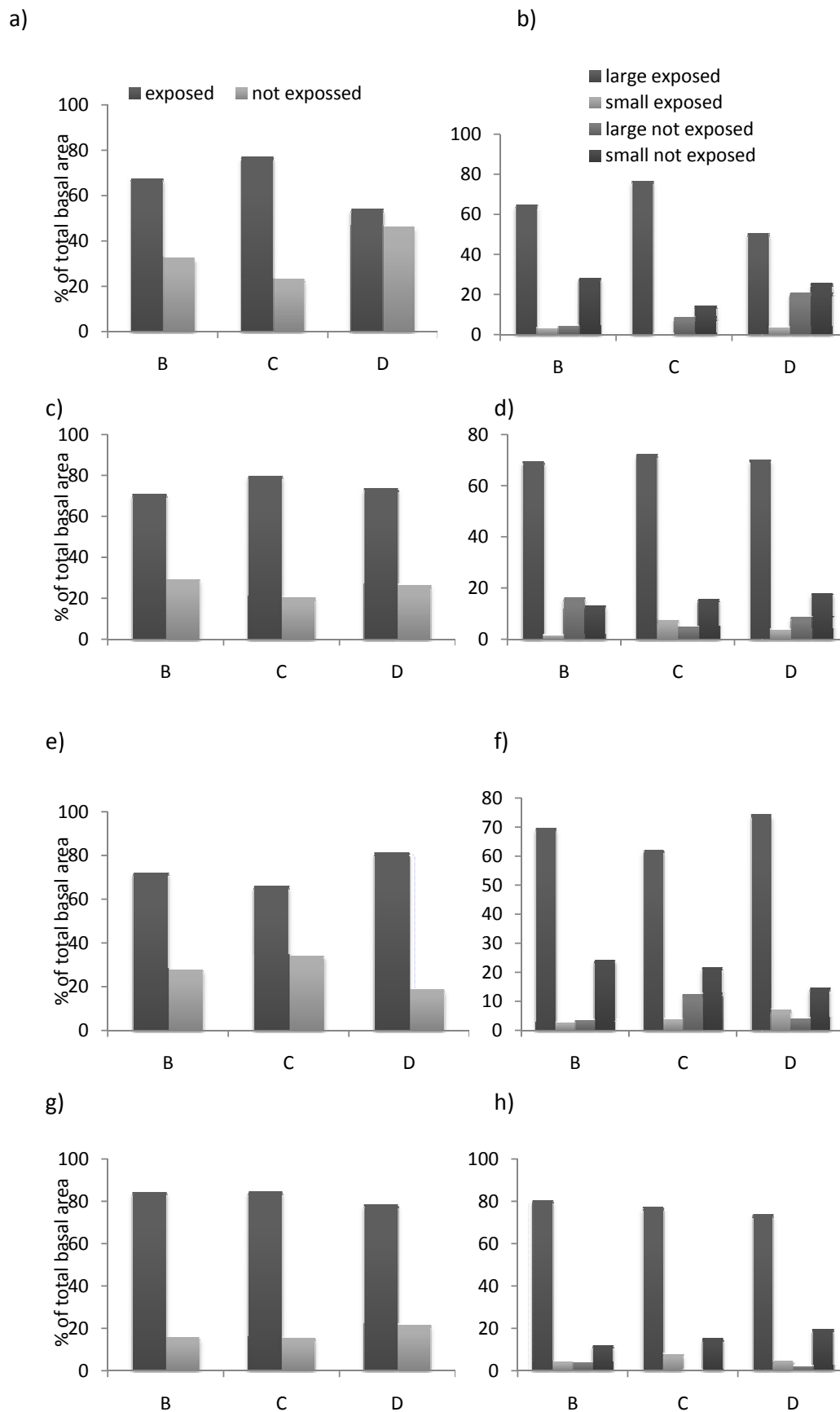
Figure 4.43 % of total stand basal area contributed by exposed trees for (left) trees > 10cm diameter breast height within forest plots (B-D) at a) DA1, c) DA2, e) SL1 and g) SL2 sites, and (right) % of total

Evapotranspiration estimates

Transpiration was scaled using basal area data of all trees combined with the findings of section 4.5 (Table 4.3) to estimate the area active xylem in each plot (B-D) and correct for radial variations in sap velocity. An edge effect was introduced for those trees in plot B by increasing the mean sap flux density (taken as 0.04 kg m^{-2} s^{-1}) by 73% in fitting with the findings of section 4.5.

Daily transpiration of trees in interior plots (D) of all sites (DA1, DA1, SL1, SL2) is estimated to range from 1.8-2.5 mm dy^{-1} which equates to a yearly estimate of 657-890mm yr^{-1} (Figure 4.44) The addition of understorey evapotranspiration renders values of 877-1091 mm yr $^{-1}$ (Figure 4.45). Bruijnzeel (1990) reviews the literature and reports values of yearly transpiration 885-1285 mm yr^{-1} ($\bar{x}$ = 1045 mm yr^{-1}, n= 9) for various lowland humid tropical forests with evapotranspiration measurements generally converging around 1225 mm yr^{-1}. Thus transpiration estimates of interior plots compare well to those presented tropical lowland forest and also for a variety of forests within Southeast Asia.

Estimates of total evapotranspiration from interior plots at Danum plots (DA1, DA2) are 1656 mm yr^{-1} and 1668 mm yr^{-1} respectively (Figure 4.46a and 4.46b). Sungai Liang plots are lower (1525-1553 mm yr^{-1}, Figure 4.46c and 4.46d) owing to the assumption of lower E$_{wc}$ there (17%). In Malaysia, forest evaporation was estimated to be 1251- 1536 mm yr^{-1} in the Tekam basin. Danum Valley evaporation rates were similarly estimated to be 1089 mm yr^{-1}. Given that estimates of evapotranspiration using the methods in the aforementioned studies are about 15% inaccurate, the results presented here compare well.

Transpiration rates are within the lower bounds of the typical range for the region and this makes good sense in context of the lower incoming shortwave radiation during the field campaign. Overall evapotranspiration rates are however towards the higher end of the expected range owing to the considerable fraction of precipitation that forms wet canopy evaporation.

Edge plots of disturbed forest (DA1 and DA2) and also of site SL1 express lower tree transpiration rates (228-794 mm yr^{-1}, Figure 4.44) owing to their lower basal area (Figure 4.44). SL2 shows a much higher transpiration rate of 1335 mm yr^{-1} (Figure 4.44d). Where edge effects in disturbance lead to lower basal area of plots an edge effect in transpiration response of trees to a certain extent reduces the impact of the

lower basal area upon stand estimates of evapotranspiration (Figures 4.44-4.46). For disturbed edges this counteraction never leads to an overall increase in either the transpiration or evapotranspiration at the forest edge (Figures 4.45 and 4.46). The influence of an edge effect upon transpiration is estimated to be greatest in scenario SL2 (Figure 4.44) owing to the slightly increased basal area there and the relatively low fraction of E_{wc}. In Danum plots DA1 and DA2 the proportional influence of diverging transpiration rates is reduced due to the considerably higher fraction of E_{wc}.

The highest value of evapotranspiration estimated at the forest edge of site SL2 (2208 mm yr^{-1}) is comparable to values of Tanaka *et al. (*2008), who review evapotranspiration estimates for Thailand and adjacent regions and report ranges from 219-2153 mm yr^{-1}. Whereas those forests from which the lower estimates are derived can be considered irrelevant for comparison, the maximum value reported for evergreen forest is still comparable to the ranges of evapotranspiration here and indeed the high estimates there were attributed to advection. Loescher *et al.* (2005) report values of 1892, 2292 and 2230 mm yr^{-1} (1998-2000 respectively) at La Selva in Costa Rica under similar radiation regimes (incoming solar radiation averaging 14.9 MJ dy $^{-1}$) , although mean precipitation (4000 mm yr^{-1}) at this site is much greater than that estimated at Wawasan Bentar.

The overall influence of an edge effect upon transpiration can be compounded by a variety of hydrological processes that either act in concert with or against transpiration rates. The four scenarios (new degraded, old degraded, new preserved, old preserved) here highlight the need to account for other hydrological processes and also the danger of drawing simplistic assumptions made based on estimates of transpiration alone. Under conditions of low disturbance where it is possible for the forest to develop in physiognomy at its edges increased transpiration rates relative to those of the forest interior can lead to a large increase the total water lost from the forest (a 49.5 % increase, Figure 4.47). However this influence can easily be negated by the increase of wet canopy evaporative fraction which can become the dominant hydrological process in degraded forests under low radiation loads. Furthermore anthropogenic disturbance in the form of tree removal renders such a low basal area that the stand does not possess enough conductive tissue to afford high transpiration at the canopy scale. This is demonstrated at Wawasan Bentar (DA1) where even if all trees at the forest edge show an increased transpiration of 73% there is still a net decrease in evapotranspiration of 22.3% (Figure 4.47).
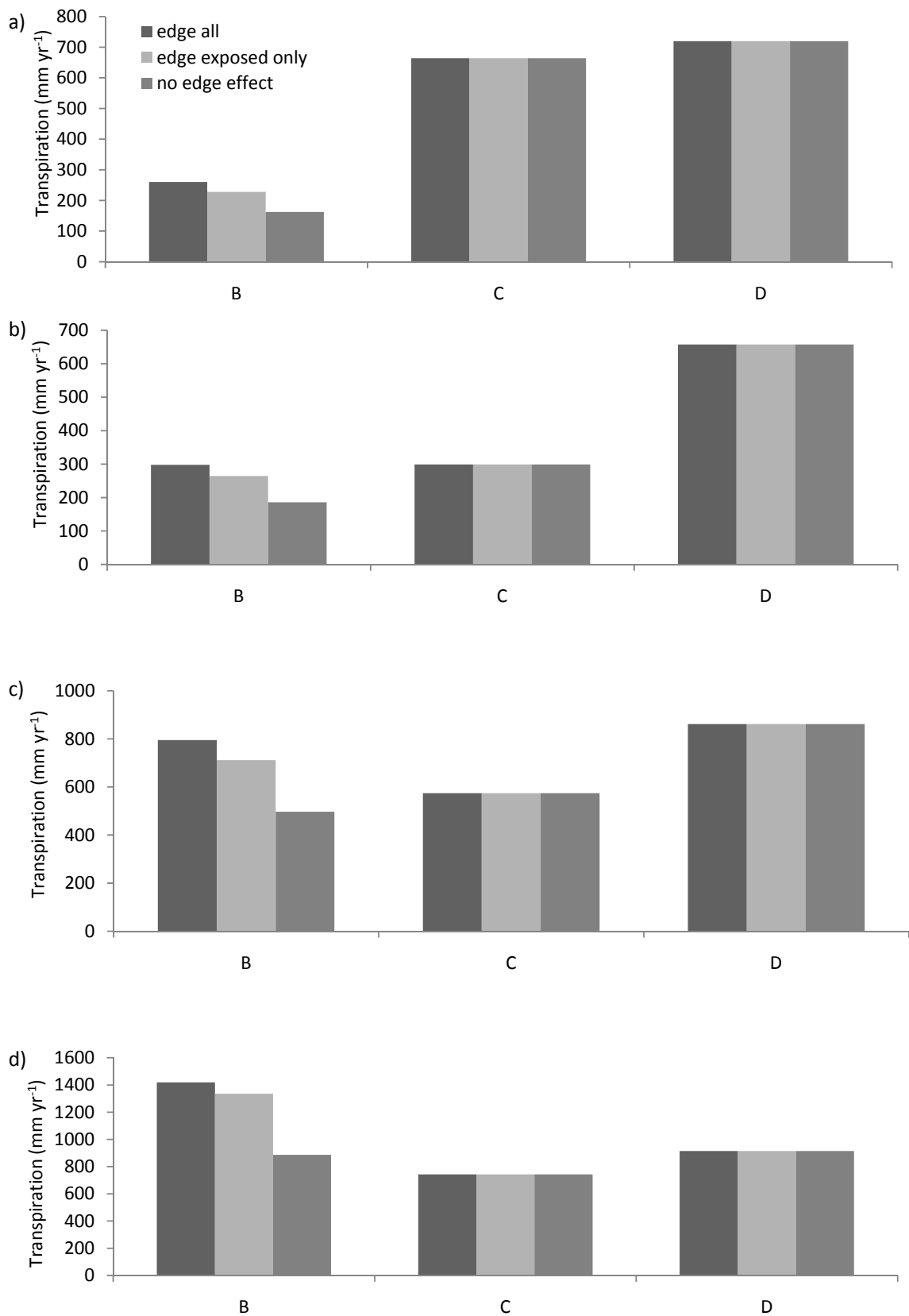
Figure 4.44 Estimated transpiration (mm yr^{-1}) of from all trees in plots B-D for sites a) DA1, b) DA2, c) SL1 and d) SL2 sites, based on their respective values of stand basal area (m^{2}ha^{-1}, Figure 4.41) and contributions of exposed trees to total basal area within each plot and site (Figure 4.43), combined with the mean sap flux densities estimated for sites B-D at Wawasan Bentar (section 4.5). Differences between edge-affected plots are denoted.
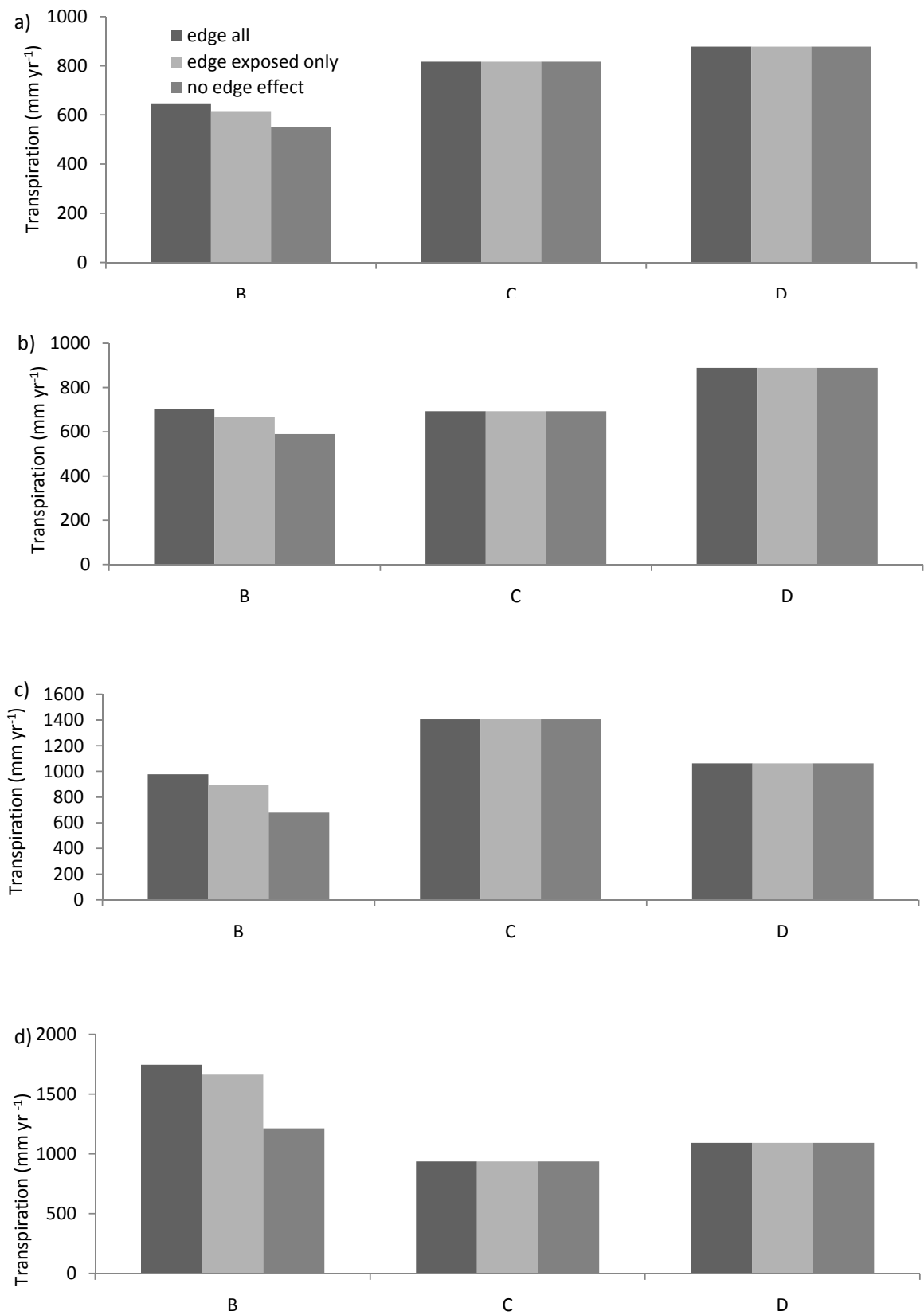
Figure 4.45 Estimated transpiration (mm yr^{-1}) of forest and understorey in plots B-D for a) DA1, b) DA2, c) SL1 and d) SL2 sites, based on those transpiration estimates in Figure 4.45 combined with understorey water flux estimates detailed in Figure 4.39, weighted by ground cover proportions and according to canopy openness categories presented in Figure 4.42. Differences between edge-affected plots are denoted.
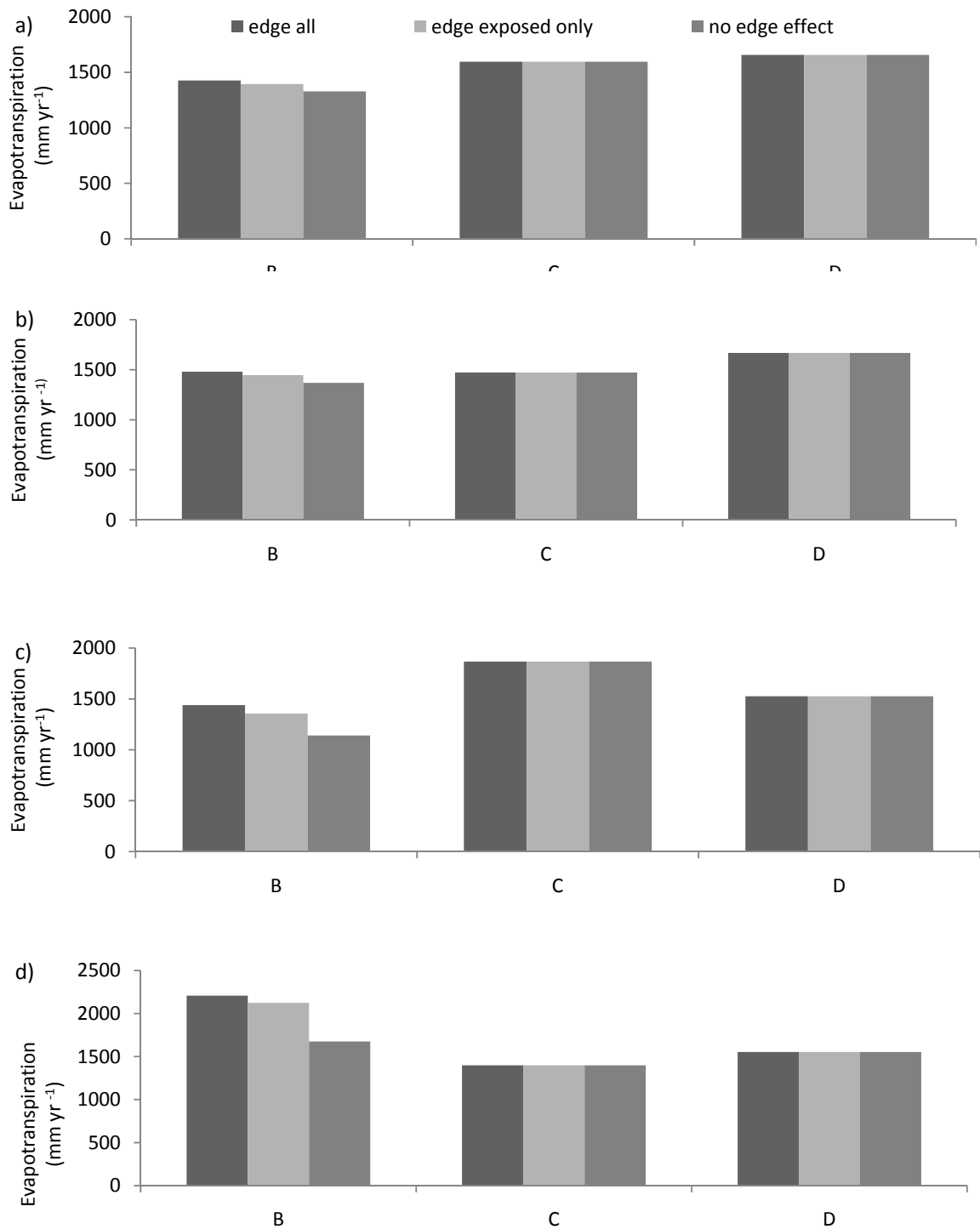
Figure 4.46   Estimated evapotranspiration (mm yr^{-1}) in plots B-D for a) DA1, b) DA2, c) SL1 and d) SL2 sites, based on the transpiration of forest and understorey components of transpiration (Figure 4.45) combined with estimates of E_{wc} detailed in Figure 4.40 for sites DA1 and DA2. For sites SL1 and SL1, E_{wc} is derived from mean annual precipitation and a prescribed throughfall fraction from the literature (17%).
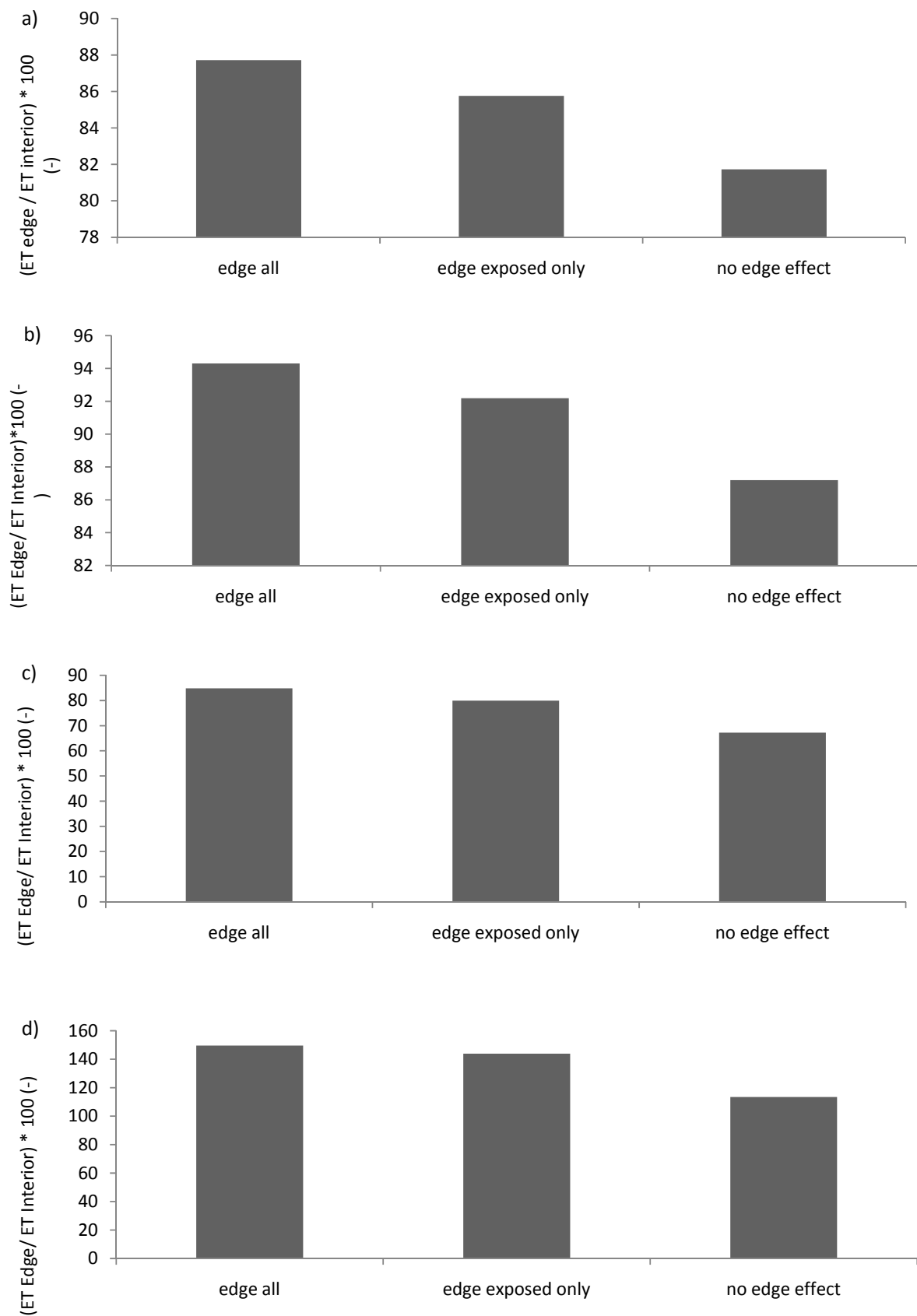
Figure 4.47   Percentage difference in estimated evapotranspiration (ET) for a) DA1, b) DA2, c) SL1 and d) SL2 at their edges (plot B) when compared to the mean of plots C and D (interior sites) for an edge effect upon the transpiration of i) all trees, ii) exposed trees only and iii) no edge effect.

A method utilising thermal dissipation probes made with cheap and easily accessible components has been shown to provide a good ground-based method of estimating canopy-level processes at a tropical forest edge.

Calibrations of sap velocity to probe temperature response have been performed confirming values commonly used in the literature for two species of tropical tree not measured previously. A top-down meteorological scheme is shown to be in good agreement with bottom-up probe measurements. Meteorological measurements show the forest edge to be a site of high fluxes owing to the rapid change in momentum expressed over the forest edge. Although there is apparent contradiction between the overall lower evapotranspiration level at the forest edge and a lower skin temperature this discrepancy can be resolved by accounting for the relatively small footprint of the infrared thermometer measuring skin temperature.

Attention is drawn to the influence of physiological controls acting upon tree water use such as high resistivity in the soil-rhizosphere-xylem pathway. A theoretical feedback between advection, high water use, and increase roles of physiological controls at forest edges is propounded and to a certain extent supported by soil moisture measurements. Under such conditions the boles of trees using the most water would be under great tension. Individuals under great tensions would be more likely to snap under high momentum loads. This concept would certainly support the greatly increased number of snapped boles reported at forest edges in large exposed trees that are particularly susceptible to advective influences (D'Angelo *et al.*, 2004).

Transpiration rates divergent from a forest interior are expressed at a forest edge in the form of greatly increased transpiration rates. The extent of edge influence is shown to be approximately 50 meters and the magnitude of edge effect to be about 73% greater than that of the forest interior. Trees expressing an influence of distance to the forest edge upon their transpiration rates show a better correlation with vapour pressure deficit than incoming shortwave radiation. This represents the first attempt to qualify exactly what influences are causing an increased transpiration on trees at forest edges. Although an edge effect is shown in this study, in fitting with previous work it is noted that a more exposed plot (site D, Wawasan Bentar) can render transpiration rates comparable to a forest edge even if that plot is a considerable distance from the forest edge.

Chapter 4 – The Hydrometeorology of a Humid Tropical Forest Patch – Results and Discussion

CHAPTER 5 – THE FREQUENCY, DISTRIBUTION, AND SCALING PROPERTIES OF FOREST EDGES WITHIN THE TROPICAL HUMID BIOME - RESULTS AND DISCUSSION

Results are presented and discussed following the methods and aims detailed within Chapter 3. Finally, the main aim of this thesis is answered: "*Whether edges of tropical forest patches contribute significantly to climate and need to be included in regional and global climate models*" (Aims and Objectives, Preface).

The question of accurate Landsat image classification (see Chapter 3) is addressed by comparing examples of Landsat images classified by this study into 'forest' and 'non-forest' with existing classifications. A broad agreement is observed between the forest/non-forest classification of this study (the 'Aggregated Fluxes in Fragmented Forested Tropical Ecosystems' study, denoted 'AFTE') and that of 'The Tropical Rainforest Environment observation by Satellite' (TREES) project. Following the AFTE classification, estimates of total forest coverage in Latin America, Central Africa, and Southeast Asia are found to be comparable to those estimates of TREES and FAO.

In agreement with the literature, this study concludes that Southeast Asia has the most numerous and smallest forest patches of each continent, yet in agreement with Rudel & Roper (1997), this study finds Central Africa to be the most fragmented continent. This is attributed to a concomitant reduction in forest patch complexity with the extensive deforestation present throughout Southeast Asia. A consistent relationship between perimeter and area of all tropical forest patches in the humid tropical biome is demonstrated, the nature of which alters when more than 50% forest has been removed. However, this relationship is multifractal, and cannot be stratified into its fractal components. Integrating measures of forest patch size, shape, and number into a core area model (Laurance & Yensen, 1991), global estimates including edge effects of transpiration, microclimate, and biomass loss are not expected to deviate from area-weighted average estimations by more than 0.25%, and this deviation would not exceed 4% for edge effects of greater magnitude and extent.

A statistical classification accuracy assessment was not practicable, as is commonly the case for broad-scale mapping exercises (see further the accuracy assessments of Achard & Estreguil (1995) (Southeast Asia); Eva *et al.* (2004) (Latin America); Mayaux *et al.* (1999) (Central Africa)). Broad scale mapping exercises do no permit a statistical classification accuracy assessment, as they cover such a large geographic extent that *in situ* ground-surveys to confirm remote sensing classifications (i.e. 'ground-truthing') would be too labour-intensive. Furthermore, the classification system imposed here bares only limited similarity to previous classification schemes, and therefore a direct comparative statistic such as a Kappa score would lack sufficient subjective interpretation.

Therefore, in fitting with previous studies that have had similar restrictions by virtue of large-scale mapping, I here address the similarity between my classification and those of other maps through subjective interpretation. The comparison here is made with the TREES classification system, in a manner following that of Mayaux *et al.* (1999), who faced similar issues when mapping vegetation cover for Central Africa using AVHRR imagery. I here compare representative regions expressing contrasting and similar vegetation classifications as classified under the TREES classification protocol and the classification system presented in this thesis (hereafter assigned 'AFTE', denoting the 'Aggregated Fluxes in Fragmented Tropical Ecosystems' classification of the author). To ensure an appropriate comparison, images selected from the TREES data base are done so to ensure:

1) they are reasonably close in acquisition date (<5 years) to those images used in this study

2) Little or no 'no data' (cloud cover) pixels exist

3) There is a clear distinction between 'Dense Tropical Forest' and 'Other' classes as defined by the TREES classification scheme.

It should be noted that there are other differences in the classification systems in terms of number of classes, classification method, and also the effective resolution at which classification is conducted. Due to limitations in computational power, analyses here were modified from the previously detailed methodology in the following manner:

a) Resolution was set to 140.5 meters.

b) Aggregation had to be performed on separate spectral bands and was not performed post classification, but rather before the classification took place.

Whereas there will be information loss due to aggregation, it has been noted that classification based upon separate spectral bands, whilst not ideal, is both acceptable and pragmatic for broad classifications given such limitations (Hill, 1999). Examples from Latin America (Figures 5.1 and 5.2) are taken from Landsat paths and rows 001/067 and 226/068 (whereby a path and row value defines a position and area on the earth's land surface within the instantaneous field of view of the Landsat sensor). Examining figures 5.1 and 5.2, it can be seen that the AFTE classification captures very well the shape and distribution of patterns for two areas which express a stark contrast between 'forest' and 'non-forest' cover types, and that if both classifications are grouped into 'dense tropical forest' and 'other', that classes match very well indeed. Areas of forest and re-growth alike are classified as 'forest' in the AFTE scheme, whereas many areas classified as 'non-forest vegetation' in the TREES scheme are classified as 'forest' with the AFTE approach. This demonstrates how classifying forest on a physiognomic basis may not agree with physical measures such as NDVI and thus might not be appropriate for physically-motivated applications (*sensu* Jupp & Twiss, 2006).

Examples from Southeast Asia are taken from Landsat paths and rows 134/043 and 135/042 (Figures 5.3 and 5.4). The influence of effective resolution is seen comparing classifications of position 134/043, whereby smaller patches are not delineated by the TREES scheme. This is due to the size of the minimum mapping unit employed by the TREES scheme, which is 50 ha, corresponding to an effective pixel size/resolution of 700m. The AFTE classification at a resolution of 140m, however, can classify smaller patches due by virtue of its higher resolution. Comparing images of position 135/042, the AFTE classification expresses clear geometric patterns embedded in the larger diagonal pattern running across the image. These correspond to the red areas on the TREES image, which most likely are hill-side clearances. The agreement in these regions demonstrates the AFTE scheme works well for stark contrasts such as recent deforestation.

Examples from Africa are taken from paths and rows 180/058 and 158/074 (Figures 5.5 and 5.6). Observing products for position 180/058 it is clear that the AFTE scheme delineates riparian corridors of forest cover embedded within a 'non-forest' region. It

is apparent that for some scenes 'non-forest vegetation' as defined by the TREES scheme is sometimes classed as 'forest' and sometimes classed as 'non-forest' within AFTE. This is because the broad category 'non-forest vegetation' will certainly include vegetation covers that sometimes have a high NDVI value, and sometimes have a low NDVI. The AFTE classification system is similarly broad but is purposefully biased towards including both 'non-forest' and 'forest' covers, as defined by TREES, in the same class based upon their similar NDVI responses. This approach makes the classification more relevant for climatic quantities, but at the cost of offering a poor agreement with the TREES classification system. The same can be said for the site at position 158/074 where a similar disagreement between the classification schemes exists. Note however that the distribution of 'forest' (defined as 'dense tropical forest' by TREES) patches again is in broad agreement with the TREES scheme, and that stark areas of deforestation (in red) are also captured well.

Sample site: Mato Grosso / Cuiab Processed by Ecoforca

Landsat TM (Path 226, Row 68)

Land cover change from 1992 to 1998

- Deforestation 1
- Deforestation 2
- Degradation
- Reforestation

Land Cover Classes

- Forest
- Mosaic
- Non-forest vegetation
- Non-vegetated
- Water
- Clouds,No data

Back to sample site

0   80   160   Kilometers
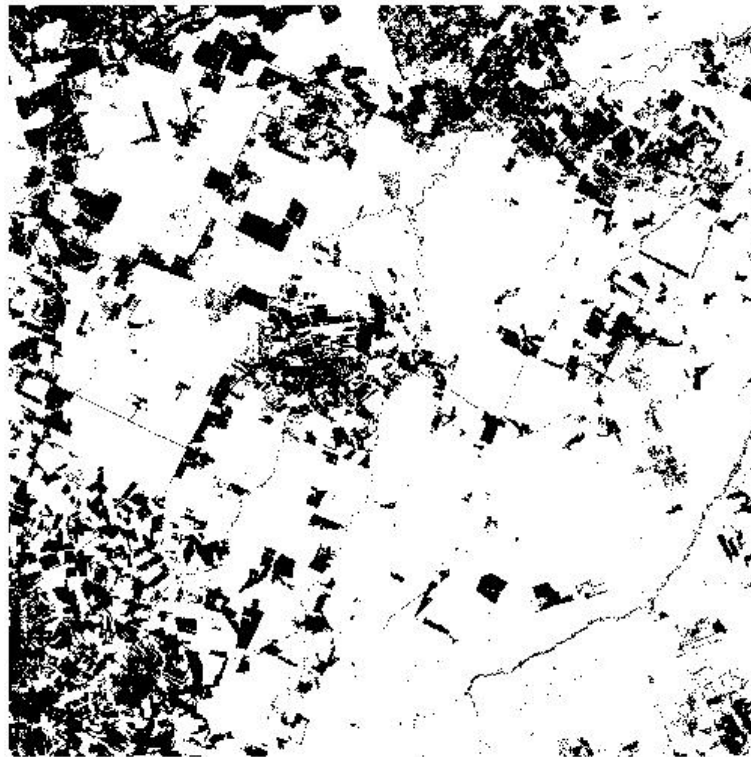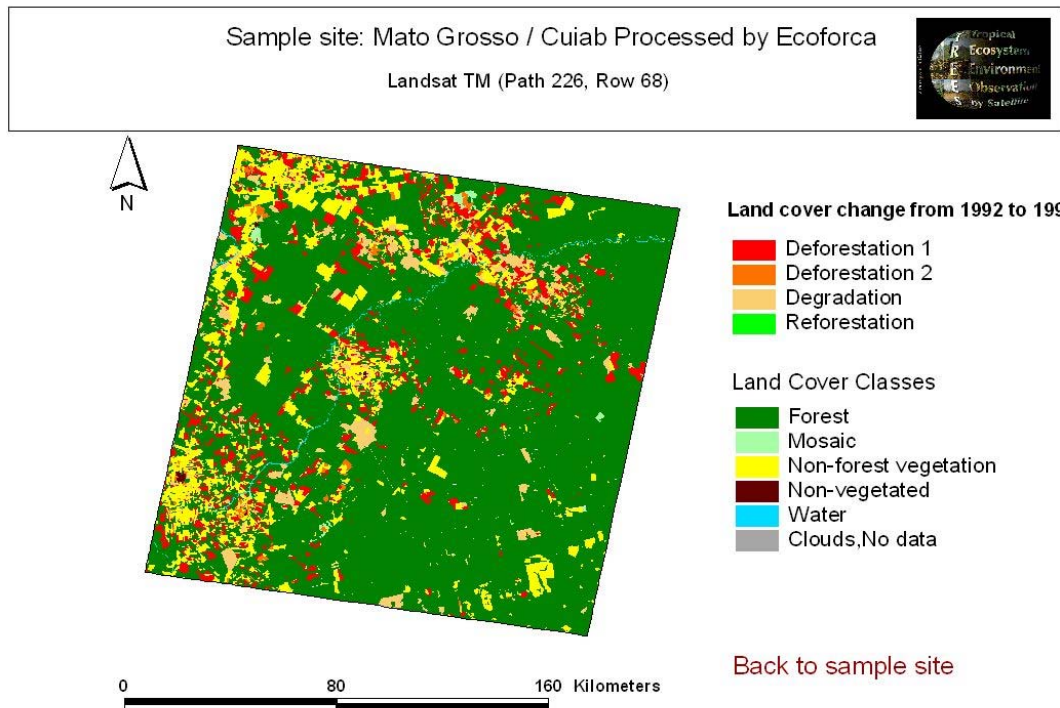
Figure 5.1   Comparison of the AFTE forest (white) non-forest (black) classification with that of TREES

for Landsat path 226 row 068.

N

Land cover change from 1992 to 1998

- Deforestation 1
- Deforestation 2
- Degradation
- Reforestation

Land Cover Classes

- Forest
- Mosaic
- Non-forest vegetation
- Non-vegetated
- Water
- Clouds,No data

Back to sample site

0   30   60 Kilometers
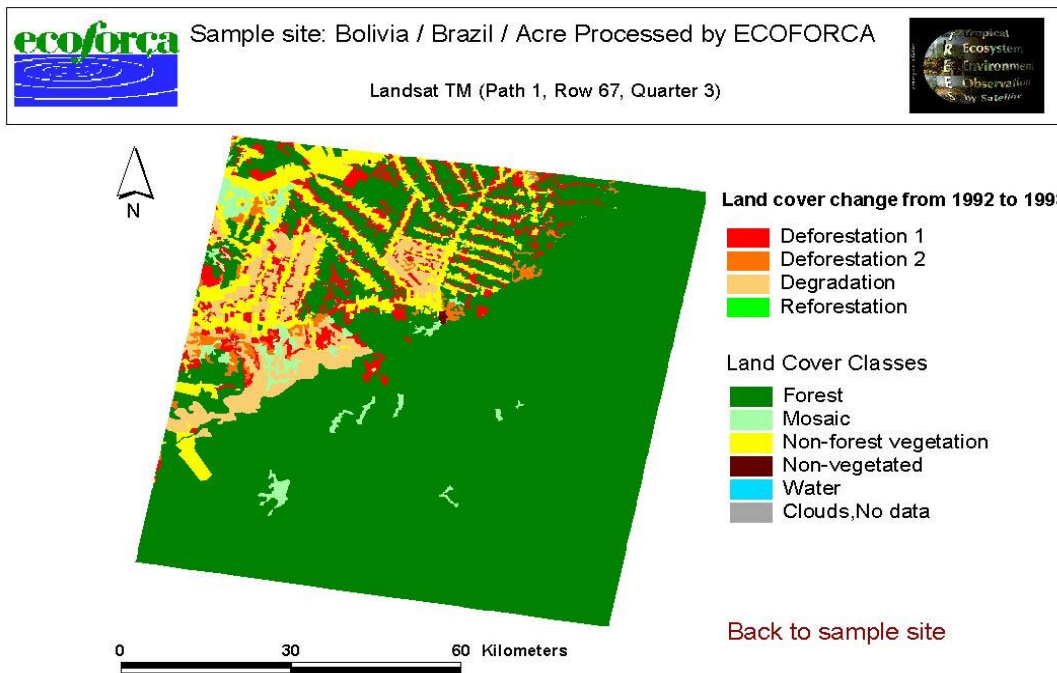
Figure 5.2   Comparison of the AFTE forest (white) non-forest (black) classification with that of TREES for Landsat path 001 row 067.
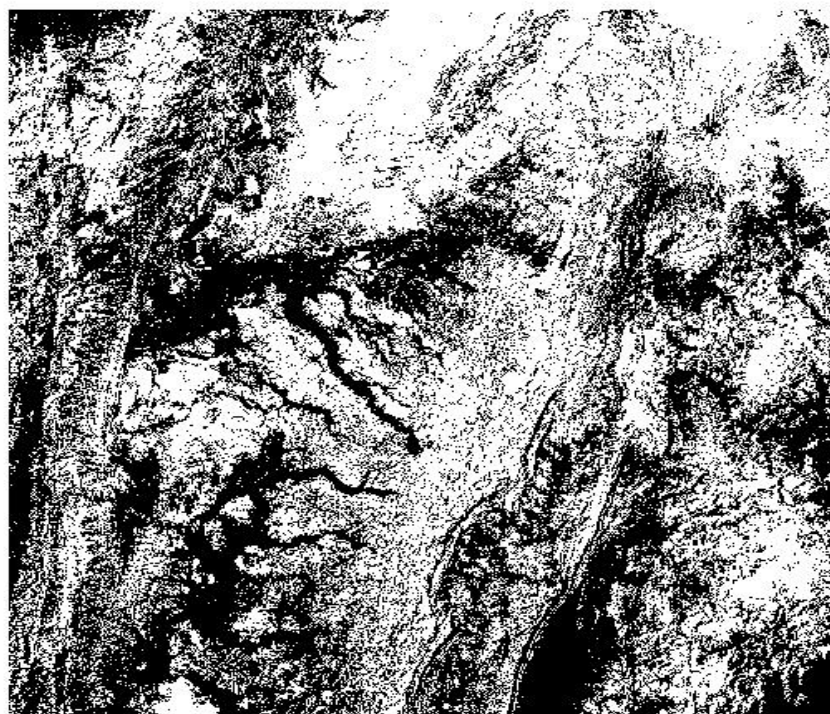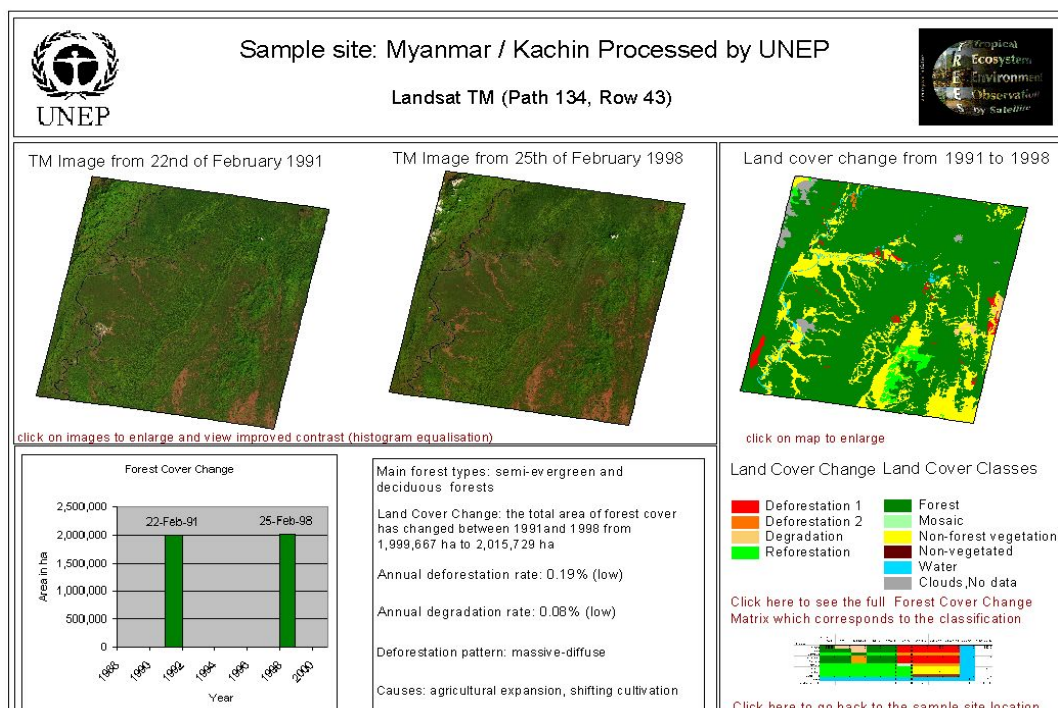
Figure 5.3   *Comparison of the AFTE forest (white) non-forest (black) classification with that of TREES for Landsat path 134 row 043.*

Indian Institute of Remote Sensing (IIRS)

Sample site: India / Naga Hills Processed by IIRS

Landsat TM (Path135, Row 42, Quarter 2)

Tropical Ecosystem Environment Observation by Satellite

TM Image from 28th of January 1991
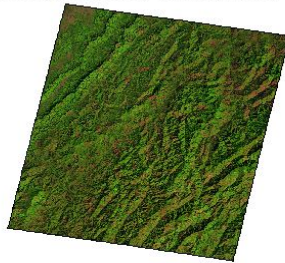
TM Image from 11th of February 1996
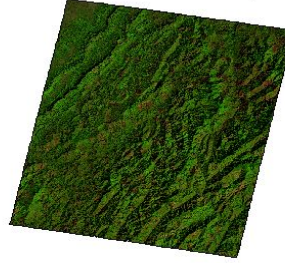
Land cover change from 1991 to 1996

click on images to enlarge and view improved contrast (histogram equalisation)

click on map to enlarge

Forest Cover Change

Area in ha

600,000

450,000

300,000

150,000

0

28-Jan-91   11-Feb-96

1988 1990 1992 1994 1996 1998 2000

Year
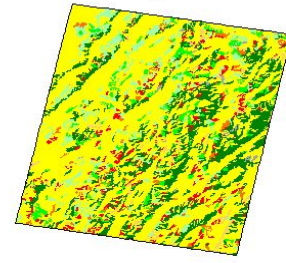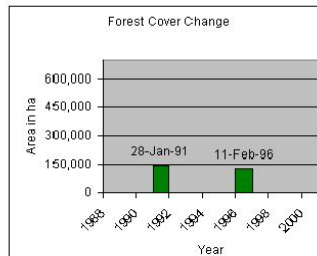
Main forest types: evergreen and semi-evergreen upland forests

Land Cover Change: the total area of forest cover has changed between 1991 and 1996 from 247,363 ha to 131,693 ha

Annual deforestation rate: 4.61% (very high)

Annual degradation rate: 1.45% (very high)

Deforestation pattern: diffuse

Causes: shifting cultivation

Land Cover Change Land Cover Classes
1991 - 1996

Deforestation 1   Forest
Deforestation 2   Mosaic
Degradation   Non-forest vegetation
Reforestation   Non-vegetated
                     Water
                     Clouds,No data

Click here to see the full Forest Cover Change
Matrix which corresponds to the classification

Click here to go back to the sample site location
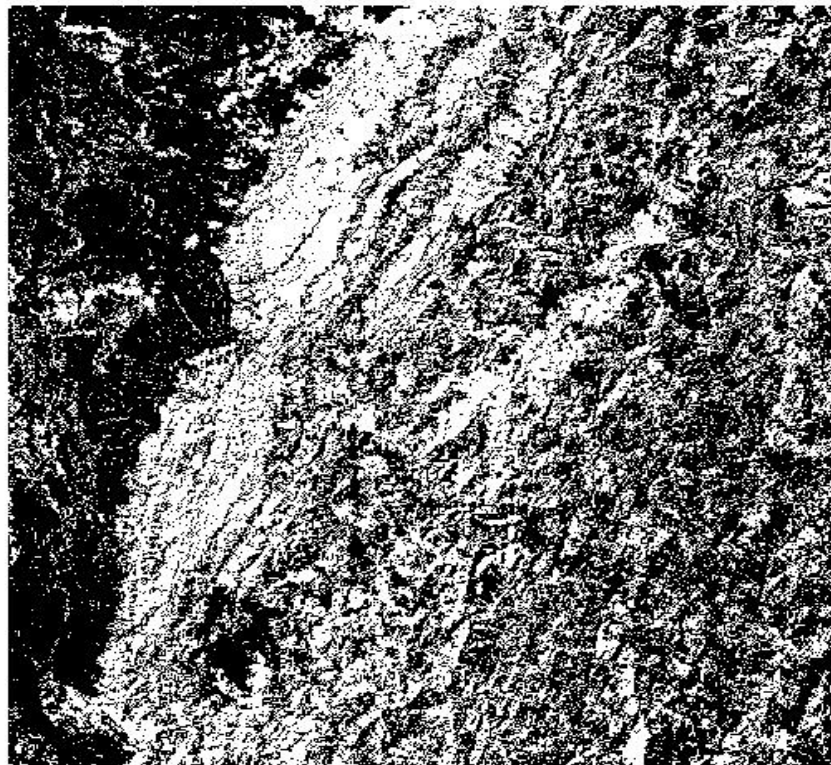
Figure 5.4   Comparison of the AFTE forest (white) non-forest (black) classification with that of TREES for Landsat path 135 row 042.

Sample site: D.R. Congo Processed by I-MAGE

Landsat TM (Path 180, Row 58)

Land cover change from 1986 to 1994

- Deforestation 1
- Deforestation 2
- Degradation
- Reforestation

Land Cover Classes

- Forest
- Mosaic
- Non-forest vegetation
- Non-vegetated
- Water
- Clouds,No data

Back to sample site

0   80   160 Kilometers
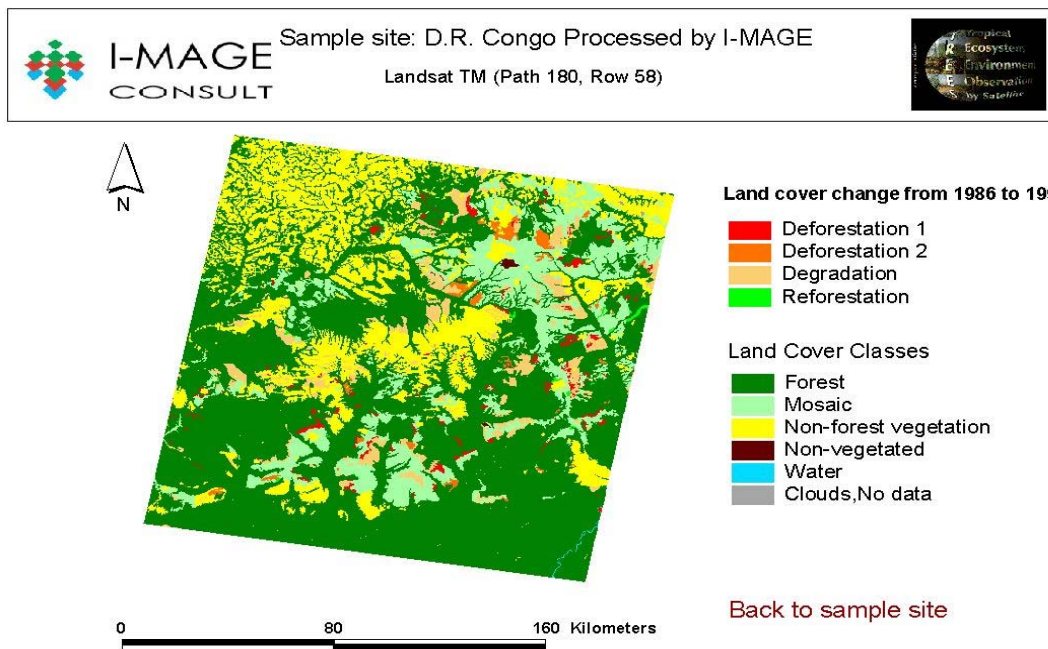
Figure 5.5   Comparison of the AFTE forest (white) non-forest (black) classification with that of TREES for Landsat path 180 row 058. This example demonstrates the classification of only quarter 1(red box) to show the quarter units defined by the TREES sampling scheme (Figure 3.8, Chapter 3), and also the 5% clipping of the image to account for Landsat imagery overlap (Figure 3.3, Chapter 3). Quarters units are numbered 1-4 inclusive in a clockwise fashion from the top left of the image).

Sample site: Madagascar Processed by FTM

Landsat TM (Path 158, Row 74, Quarter 1)

TM Image from 30th August 1993

TM Image from 8th May 1998

Land cover change from 1993 to 1998

click on images to enlarge and view improved contrast (histogram equalisation)

click on map to enlarge

Forest Cover Change

Area in ha

600,000

450,000

300,000

150,000

0

1986 1988 1990 1992 1994 1996 1998

Year

30-Aug-93

08 May 98

Landscape: Upland Forest

Land Cover Change: the total area of forest cover has changed between 1993 and 1998 from 254,213 ha to 212,268 ha

Annual deforestation rate: 4.73% (very high)

Annual degradation rate: 0%

Deforestation pattern: Diffuse

Causes: Agricultural Expansion

Land Cover Change Land Cover Classes

Deforestation 1
Deforestation 2
Degradation
Reforestation
Forest
Mosaic
Non-forest vegetation
Non-vegetated
Water
Clouds,No data

Click here to see the full Forest Cover Change Matrix which corresponds to the classification

Click here to go back to the sample site location

Figure 5.6   Comparison of the AFTE forest (white) non-forest (black) classification with that of TREES for Landsat path 158 row 074.

The analysis here follows closely that of Ewers & Laurance (2006) to allow comparison between this study and theirs, the two of which represent the first–ever investigations into the scaling properties of forest/clearing patterns and processes pan-tropically and within the Legal Amazon, respectively. Due to the large sample size (n= 248, 248) all perimeter-to-area regressions calculated in this chapter were highly statistically significant. Selected model regressions were done so on the basis of the adjusted r-squared statistic (from here on denoted ASR), which accounts for the number of parameters required to fit a model and therefore ensures models do not 'over-fit' data in a redundant fashion.

Standard and double log plots (corresponding to the DLFD metric) of perimeter to area are shown in Figure 5.7 for all patches within the 104 sample sites across the tropical humid biome. The total number of patches analysed by continent at maximum resolution were 79,408 patches within Latin America, 54,552 in Africa, and 146,288 in Southeast Asia. It can be seen that there is a distinct breakpoint in the data whereby an increase in forest area no longer relates to a similar increase in perimeter, but instead the perimeter associated with areas of forest beyond that point actually decreases. This break point occurs at approximately 500km^2, with the largest areas of forest measuring up to 1300km^2.

Chapter 5 – The Frequency, Distribution, and Scaling Properties of Forest Edges within the Tropical Humid Biome - Results and Discussion

Area (m²)

Log10 Area (m²)
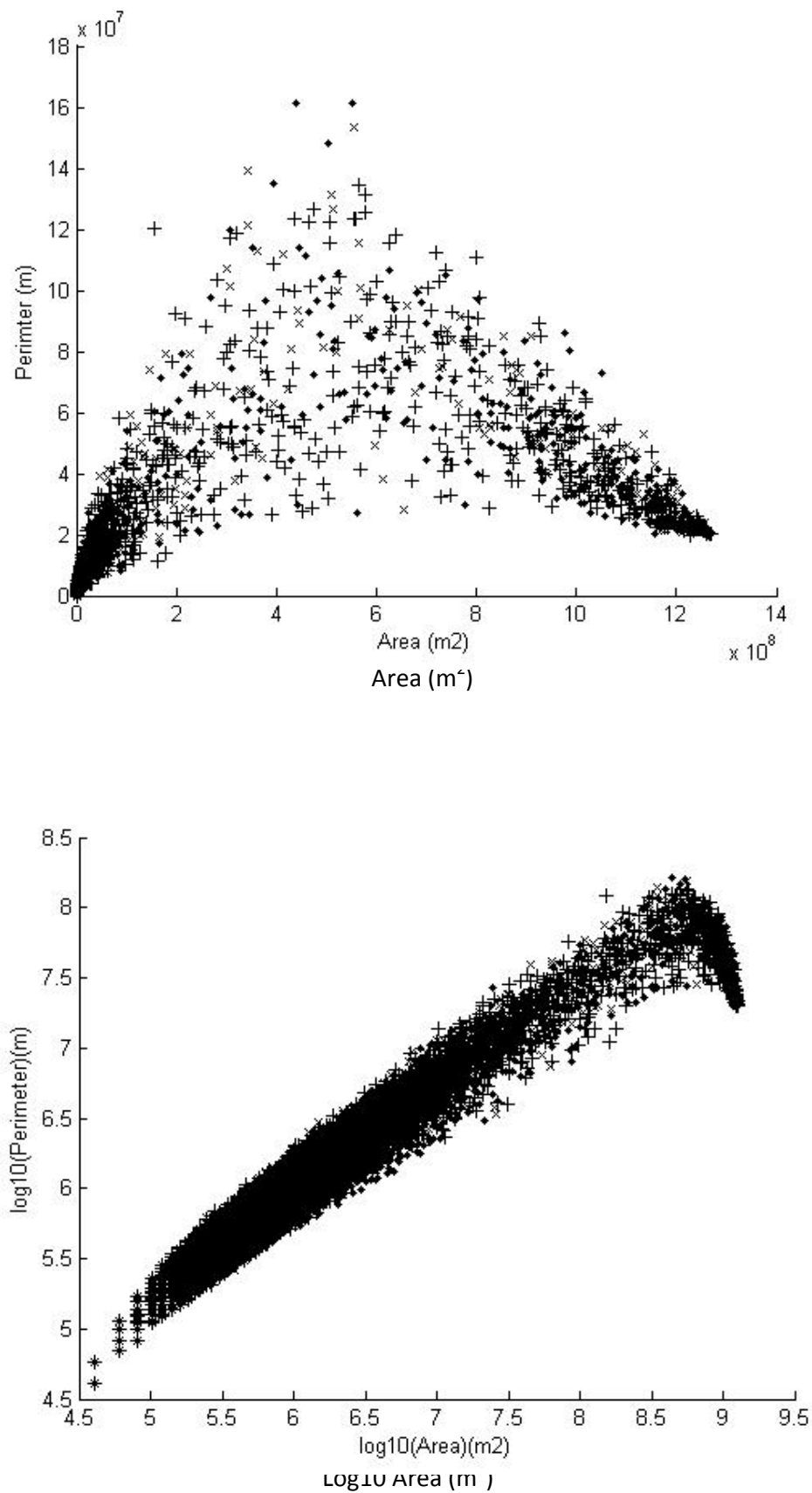
Figure 5.7   Perimeter vs. Area for all patches within the 104 sample units used in this study. Markers denote forest patches in Asia (+), Latin America (.) and Africa (x), respectively. Top: Standard, Bottom: Log10.

Observing the double log plot of figure 5.7, it can be seen that there is a slight curve in the distribution of the data both above and below the threshold. Ewers & Laurance (2006) applied a piecewise regression for the fractal dimensions of clearings within the Legal Amazon. This was justified by (a) a pattern that has a statistically significant break point between two scales that (b) corresponding processes operate within (i.e. small-scale clearings by simple means, and large scale clearings by mechanised means). The piecewise regression employed in this study was similarly considered from a physically motivated point of view. Break points in the data were found by smoothing the data by means of localised regression using weighted linear least squares and a 2nd degree polynomial model (LOESS). Taking the second derivative of the spline displays 'turning points' between the ratio of perimeter to area, i.e. turning points in the fractal dimension between certain scales.
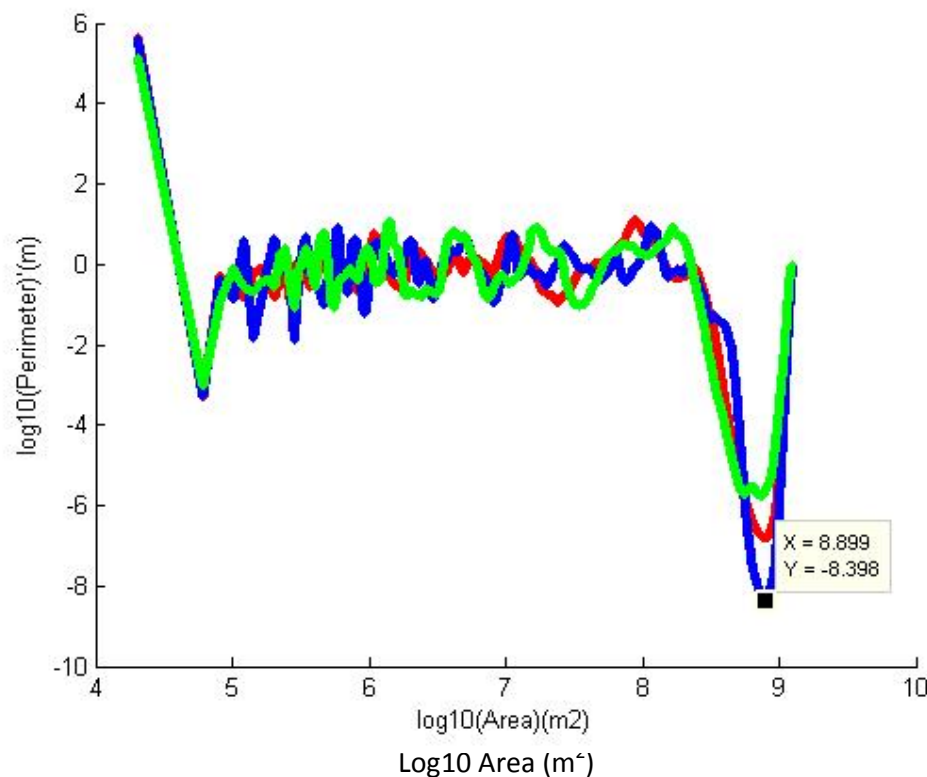
Figure 5.8   Turning points in the relationship between log10 (area) and log10 (perimeter) for each continent (Africa=green, Southeast Asia = blue, Latin America =red) based on the second derivative of their localised regressions.

It can be seen clearly in Figure 5.8 that the most significant turning point for all three continents is at what is presumed to be the transition from a 'forest-limited' to' a forest-replete' state, whereby the large amplitude in the curve represents a great magnitude of change between one relationship and the other. Whereas Southeast

Asia and Latin America share the same breakpoint (8.899 or 9.7724e+008m^2), African sites change state at a slightly lower point on the x axis (8.791 or 6.1802e+008 m^2).

Justification for fitting in a piecewise fashion is supported by the TREES results, which demonstrated that the fragmentation index of forest patches within 16x16 pixel sample blocks of AVHRR imagery across the tropics increases to a threshold of approximately 50% forest coverage whereupon it then *decreases* in complexity as an increase in forest size fills the landscape more and reduces fragmentation. This appears to also be the case for the data in this study, and was supported by a significant improvement in the ARS value between linear and log fits. Agreement between the results here and the TREES results (Figure 5.9) is encouraging. Although they appear similar, it should be noted that the TREES results were conducted at a much lower resolution (1km), and was effectively a box-counting analysis that used a fragmentation measure (Matheron Index) rather than the high resolution vector analysis of perimeter and area presented here. Furthermore, the TREES results are based upon fewer (1,800) sample sites.
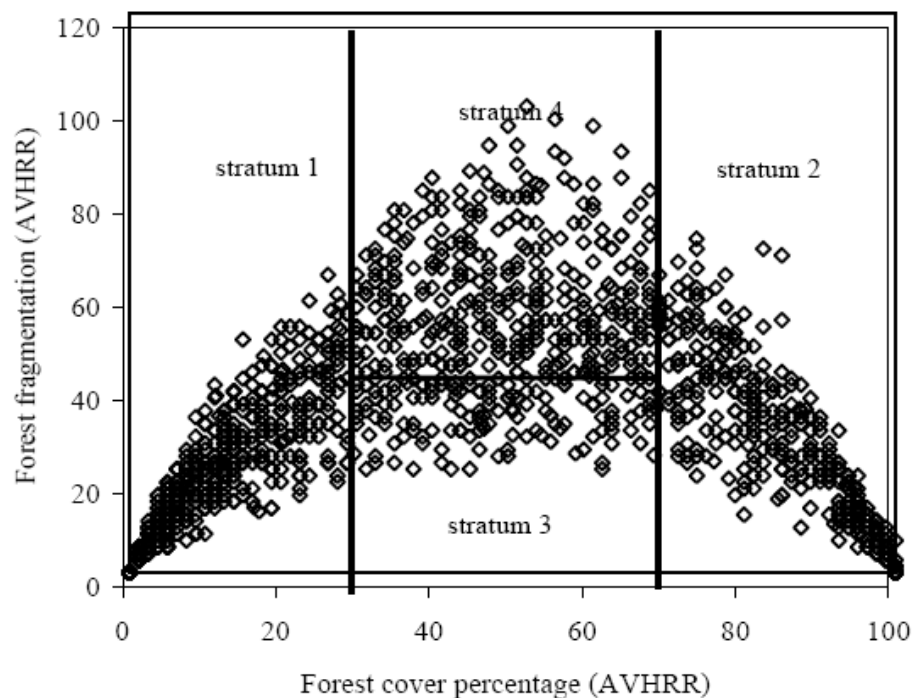
Figure 5.9   A graph of forest fragmentation vs. Forest percentage cover based on AVHRR imagery. Reproduced from Achard et al. (2002b).

From here on, points below the aforementioned breakpoint threshold will be referred to as a 'forest-remnant' state (i.e. < ~50% forest, see Figure 5.9), and those

points above the threshold will be considered a 'forest-perforation' state (i.e. > ~ 50% forest, see Figure 5.9). As the TREES results are based upon the proportion of forest cover, it is unsure as to whether the break point is an artefact of the effective image size, whereby very large forest patches become too large for the effective image size. This violates the assumptions of vector-based fractal analysis, and makes the analysis more similar to box-counting analyses. To test whether the pattern was an artefact of effective image size, analyses were repeated using image (section) sizes four times larger (i.e. equal to a quarter of a Landsat scene). The pattern remained unchanged, and therefore the negative gradient expressed for very large forests is not due to artefact, but instead much more likely to be due to a shift from remnant forests to insular deforestation and forest perforation. Therefore, the analyses presented here can truly be regarded as a vector-based analysis, which treats forest patches as separate entities. This is important, as without a vector-based product, stratification would not be scale-independent, but instead dependent on effective image/box size. It should be noted that comparative studies between sensors of disparate Instantaneous Field of View (IFOV) would suffer from this limitation for large forest patches. For data above and below the break point, it was found that a power law best described the data:

$$(f(x) = a * x^{b+c}) \qquad [-] \qquad \textit{(Equation 5.1).}$$

This means that the pattern expressed here is not a single fractal, but rather a combination of many fractals, i.e. a multifractal. This differs from the analysis of Ewers & Laurance (2006), who described patches of cleared forest as fractals described by two single scaling exponents above and below a breakpoint. Multifractal patterns are those characterised by multi-scaling behaviour, comprising a hierarchy of fractal sets. It can be seen that the fractal patterns of Southeast Asia and Latin America are similar, but that the African landscape is characterised by a higher fractal dimension in the 'forest remnant' state, and that forest areas in the 'forest perforation' state lose less perimeter as they increase in size. Thus, Africa appears to have a higher landscape complexity in both states. Whereas this is the case for the mean relationship, the perimeter-area regressions of data for each continent are not statistically distinct, demonstrating that the patterns of forest are similar across continents (Figure 5.10 and Table 5.1).

Log10 Area (m²)

Log10 Area (m²)
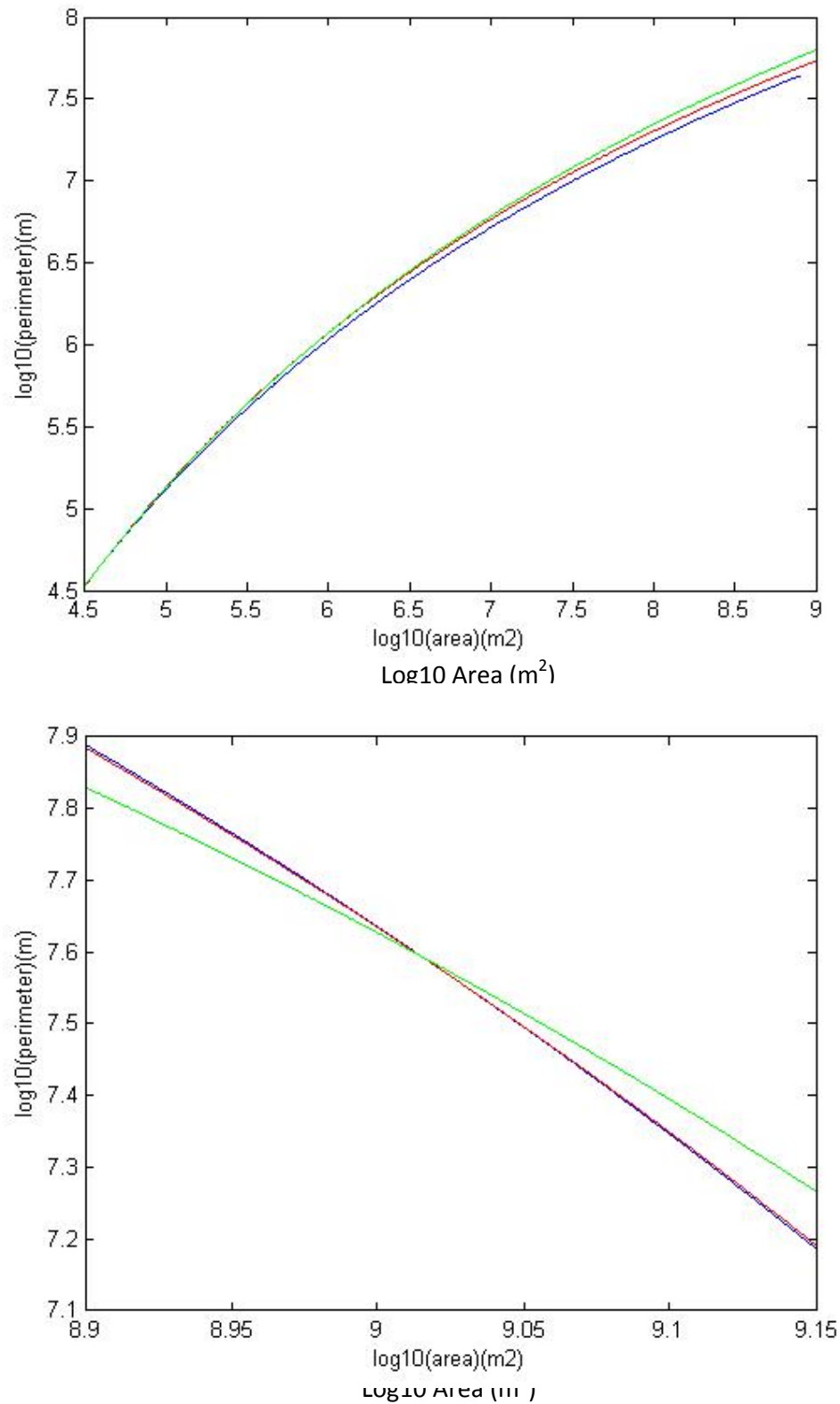
Figure 5.10 Power relationship regression curves of perimeter and area for Africa (green), Latin America (blue) and Southeast Asia (red), above (bottom figure) and below (top figure) the determined threshold. Data are omitted for clarity.

Continent	Latin America			Southeast Asia			Africa		
Term	a	b	c	a	b	c	a	b	c

'Forest Remnant' state:

Value	-23.60	-7.17	12.57	-24.84	-0.78	12.17	-24.10	-0.67	13.32
Upper Bound	-23.44	-0.69	12.79	-24.67	-0.77	12.31	-23.97	-0.65	13.61
Lower Bound	-23.75	-0.74	12.35	-25.00	-0.80	12.03	-24.22	-0.70	13.02

Adjusted r^2 =	0.97	0.97	0.97

'Forest Perforation' state:

Value	$-1.23E^{-12}$	12.78	9.54	$-1.11E^{-12}$	12.82	9.51	$-3.34E^{-13}$	13.25	9.10
Upper Bound	$7.05E^{11}$	38.48	13.48	$6.07E^{-11}$	40.95	13.72	$2.10E^{-11}$	41.35	12.11
Lower Bound	$-7.30E^{-11}$	-12.92	5.61	$-7.19E^{-11}$	-15.32	5.31	$-2.16E^{-11}$	-14.85	6.09

Adjusted r^2 =	0.77	0.73	0.71

Table 5.1: Confidence intervals (upper and lower bounds) and adjusted r^2 for a power curve describing the relationship f(x) = a*x^b+c between log10 perimeter and log10 area for all forest patches within each continent. Results are shown before and after the break points shown in Figures 5.8 and 5.9 of the perimeter to area relationship, defining a 'forest remnant' and 'forest perforation' state that are approximately the equivalent of <50% and >50% forest, respectively (Figure 5.9).

The similarities between patterns from different continents appear to confirm tentatively the hypothesis of Ewers & Laurance (2006), who argue that the process of deforestation is governed by the same rules regardless of location. It is important to note that this study is not strictly an analysis of deforestation pattern as in the case of Ewers & Laurance (2006) but rather an analysis of forest pattern. Therefore, other rules may guide the pattern of forest patches. However, it can be argued that the rules governing forest patterning are the same rules that govern the process of deforestation. For example, just as the process of deforestation is limited by physical factors such as topography, it follows that forest coverage will either be defined by

topography or, if not, it will be defined by the deforestation that itself will be limited by topography. The only other state that can exist is one whereby forest pattern is not limited (i.e. complete coverage of forest) or it is limited absolutely (i.e. complete non-forest coverage). Importantly, these rules are not governed by the geographic location of the continent, but instead are governed by common processes and patterns either intrinsic to each continent (topography, altitude, river networks etc.) or patterns and processes extrinsic to continents such as latitude, land-mass etc. The process of deforestation itself is limited by those intrinsic patterns, and furthermore cannot surmount these governing processes.

Whereas Ewers & Laurance (2006) sample scenes from a relatively large proportion of the Legal Amazon, it is commonly accepted that the deforestation within this region is highly stereotyped and indeed can be modelled by region (Laurance *et al.*, 1998b). Therefore, it follows that the analysis of Ewers & Laurance (2006) has much lower confidence intervals, and furthermore is likely to differ from this analysis. However, the distinct separation between large and small forest patches appears possible regardless of land cover type.

Examining the confidence intervals around the regressions (Table 5.1), it superficially seems like there is little deviation in the Fractal metric. However, given the range of the metric (1-2), a small variation in the value of D represents a large proportion of the theoretical range and this is something that cannot be ignored (Kojima *et al.*, 2006). Although stratifying the relationship by continent reduces the variation in the range of D values a large proportion of uncertainty remains. Therefore, further stratification is needed to classify regions accordingly in a more objective fashion. If an objective stratification is not possible by the sole practicable means of remote sensing, *in situ* regional stratification would be required but this could only be employed at a low frequency and at great cost. As the pattern is multifractal, however, a complete representation seems unwieldy, and thus patterns need to be addressed in a zonal fashion, which isolates fractal sets within the main 'multifractal' signal. An attempt to do this is made in the next section.

Linear combinations of texture measures were used to form principal underlying data components via PCA analysis. A total of 15 variables were included in the analysis, using (Table 3.2, Chapter 3):

1) Homogeneity,

2) Contrast,

3) Angular Moment,

4) Standard Deviation,

5) Summed mean,

applied to each of the three wavelet families (db1, db5, db10). The principal component accounted for 42% of the variation in the variables. Initial analyses indicated that stratification by texture did not separate the perimeter to area ratio into distinct populations. One possible reason for this is that the wavelet coefficients used were a combination of horizontal, vertical and diagonal components. Analysing the coefficients in this fashion effectively removes the directionality of the data, i.e. anisotropy is not accounted for. Analyses were modified to account for anisotropy, and repeated. The new principal component accounted for 45 % of the variation, indicating little improvement with the inclusion of anisotropy. It was found that the data of perimeter-to-area regressions as calculated in this thesis could not be stratified on a textural basis, either above or below the breakpoint.

The reason that the multifractal signal cannot be stratified may be down to the dimensionality reduction techniques employed in this study, where the mutually exclusive information provided by each texture measure actually confounds that of another. A recommendation, therefore, would be to attempt to stratify the perimeter-to-area ratios based on individual texture measures, rather than a linear combination of all measures. Such an approach would be cumbersome (Semler & Dettorri, 2007). It should also be noted that in creating a binary image of forest cover, a huge amount of textural information is lost. This means that the wavelet filters are operating upon a sparse textural signal, which may make wavelets ineffectual. Possible solutions for this second issue would include using a similar approach but substituting wavelets for ridgelets or curvelets, which are designed to be more

efficient in this kind of scenario and render a greater dynamic range for more sparse input data (Dettorri & Semler, 2007).

If it is not possible for wavelets to stratify the perimeter-to-area ratios in this fashion, it stands to reason that wavelets will also not be able to stratify scaling relationships, as the two are inherently related. This was found to be the case, whereby different texture classes did not offer separation between populations of AWMPFD or MPFD at different resolutions, and furthermore did not model each individual relationship well- with adjusted r^2 values rarely exceeding 0.2.

Although the poor stratification of pattern and pattern scaling may be due to the methods used in this study, a closer examination of the pattern expressed in each stratum offers some insight into why stratification is poor, and how it may be improved in the future. Mean patterns were examined using the second derivative of a spline function to indicate the 'turning' points between scales for each strata, in a similar fashion to that shown previously for each continent. Examining the mean signal in this fashion, as rudimentary as it is, follows various software packages which deliberately emphasise the mean of fractal signals (e.g. FRACLAC for ImageJ, http://rsbweb.nih.gov). Just as separation of scaling patterns into 'forest-remnant' and 'forest-perforation' states is possible for the greatest change in the relationship, it can be seen examining Figure 5.8 that other turning points are also present. These turning points represent 'singularities' within the multifractal signature, whereby the relationships around each singularity is consistent. In terms of this study and that of Ewers & Laurance (2006), the relatively localised pattern of Ewers & Laurance (2006) would be nested within the larger-scale relationship presented here. Given the stable scale relationship demonstrated by Ewers & Laurance (2006), it stands to reason that their study is situated between three singularities- i.e. they have selected a region expressing two singular scaling exponents. This viewpoint follows closely that of Pecknold *et al.* (1997). Analysing each scaling relationship between the singularities in this multifractal signal is certainly beyond the scope of this thesis. However, comparing the splines for each continent (Figures 5.8 and 5.11), and for n texture classes, it can be demonstrated as to why wavelets do not stratify a multifractal signature in generalised terms, and how it could be possible for them to stratify signatures by localising patterns into 'zones' between different patch sizes (and thus scales). This agrees in a converse fashion with the definition of 'multifractal' as *"if the measure has different fractal dimension on different parts of the support, the measure is a 'multifractal'"* (Pecknold *et al.*, 1997).

Observing Figure 5.8, it can be seen that the singularities within the multifractal pattern for each continent are correlated. This is because similar patterns of deforestation are expressed across all continents. However, analysing the same product for n texture strata shows an improved separability in the location of each singularity- i.e. the multifractal signal is being broken down in an objective fashion using textural measures as a proxy. This is demonstrated in Figure 5.11 using data from Latin America and four textural classes.
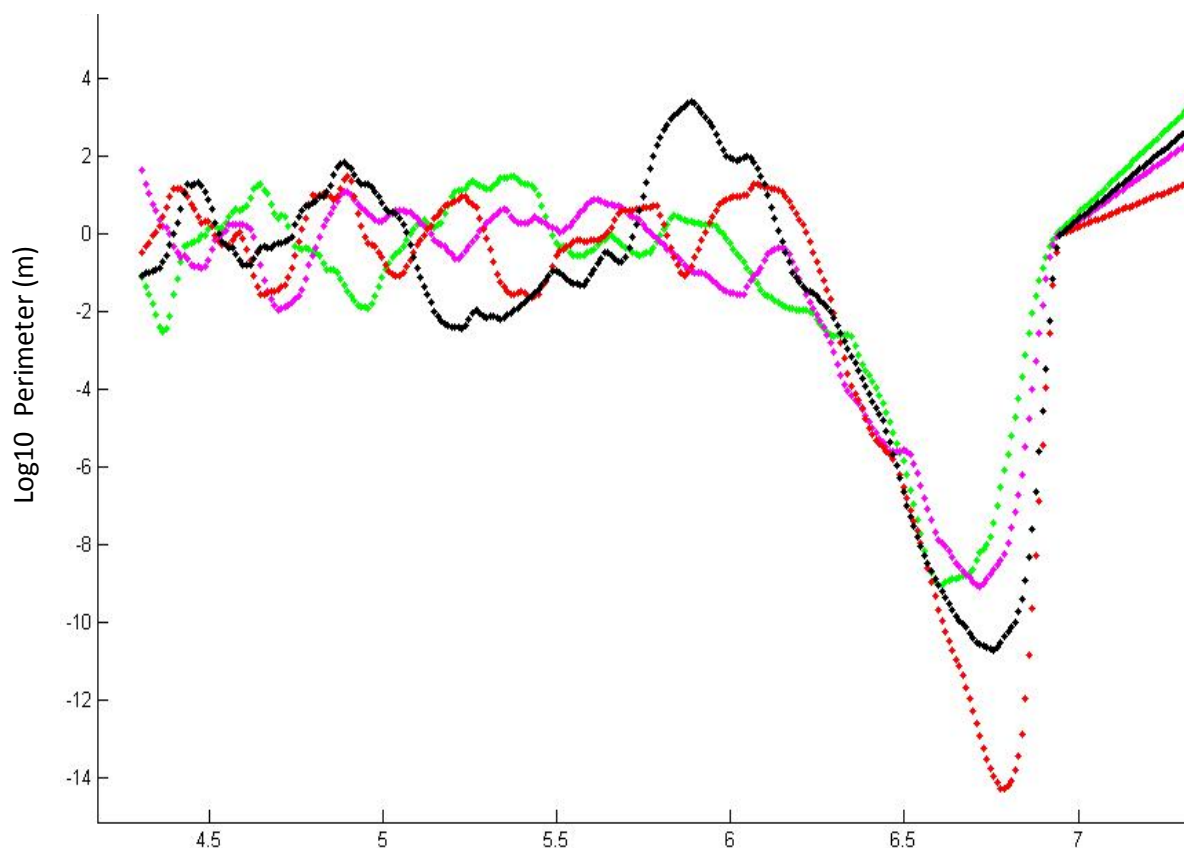
Figure 5.11   Turning points in the relationship between log10 (area) and log10 (perimeter) for forest patches stratified into four textural classes (represented by each colour) based on the second derivative of their localised regressions. Perimeter and area data used from Latin America.

Examining Figure 5.11 it can be seen that separability between scales in improved. This can be seen best by observing the point of greatest change at ~ 6.75, whereby the breakpoint between scales is staggered for different texture classes. Importantly, note that the taking the mean relationship until the breakpoint would yield poor separability between classes. It is exactly this that is being expressed by the poor separability between perimeter-to-area regressions for forest patches of each continent (Figure 5.10).

It must be noted, however, that the separation of singularities by texture does not necessarily mean that the scaling relationships between regions will be distinct. Further analysis will have to be conducted to see how well stratification in this fashion works in practice. However, by far the most important element to this relationship is the nested fractal patterns within a multifractal macro pattern, and its implications for scaling and extrapolating relationships from one region/scale to another. Just as Mandelbrot (1967) addressed the multifractal nature of the coastline of Britain, it must be similarly considered if the scaling properties of forest patterns have any particular significance *per se.* Whereas the study of Mandelbrot (1967) is significant in terms of observing multifractal patterns ubiquitous in nature (Mandelbrot, 1982), Pecknold *et al.* (1997) comment that the size of the coastline of Britain has no significance in geological terms. Similarly, it must be considered whether edge effects have any influence on regional or global climate at all, and whether the scale at which they are observed is crucial. This is addressed in the next section by making global estimates of forest cover and the proportion of forest that can be considered under the influence of an edge effect.

5.4   ESTIMATES OF REGIONAL AND GLOBAL TROPICAL FOREST COVERAGE

Estimates of 'Dense Tropical Humid Forest' are presented for this study alongside those estimates of the TREES project and also of the FAO in Table 5.2. It can be seen that the estimates made in this study broadly agree with those of -the other three estimates. Latin America has the most forest, then Southeast Asia, then Africa, in all four studies. There is an arguably broad agreement in the distribution of forests between continents and also the total amount of forest for each continent and globally (Table 5.2, Figure 5.12). It is not possible to say that one estimate is 'inaccurate' in terms of another, as each study processed data in different fashions. Given the possibility for estimates differing by 100% at the regional scale (Skole & Tucker, 1993) under different classification regimes, the proximity of the estimate presented here to those of others seems acceptable. In addition to differing classification regimes, each of the studies conducted had different minimum mapping units. TREES, for example, has a minimum mapping unit of 50 ha, which equates to a pixel size of just over 700m, versus the 140 m pixel size used in this study. However, just as one cannot say this classification is 'inaccurate' in terms of the others, it would violate the same logic to say this classification is 'accurate'. They are, simply, in broad terms, similar. This is best demonstrated by comparing the estimates of forest cover by each scheme (AFTE and TREES) for each observation site (Table 5.2).

Total Regional/Global Forest Cover (10^6 ha) as Estimated by Different Studies

	TREES	FAO CS	FAO RSS f2	AFTE
Year	2000	2000	2000	2000
SE Asia	264(+/-29)	278	224(+/-38)	280
Africa	191(+/-12)	207	484(+/-69)	280
Lat. America	649(+/-46)	624	767(+/-6)	676
Global	1,103(+/-52)	1,109	1,475(+/-124)	1,200

Note 1: FAO CS (Country Survey) estimates derived by TREES from the country tables (FAO, 2001, in Achard et al., 2002b). India is included with Southeast Asia but excluding 41 106 ha of dry forest for India. Africa and Latin America were corrected to the humid domain. Mexico is excluded from Latin America (Achard et al., 2002b).

Note2: FAO RSS (Remote Sensing Survey) (Achard et al., 2002b).

Source of TREES, FAO CS, FAO RSS f2 data: 'Methodology and results of the TREES-II research programme', Achard et al. (2002b), TREES Publications Series B, Research Report No.5, European Commission Directorate General Joint Research Centre Institute for Environment and Sustainability

Table 5.2: Comparison of estimated total forest cover (10^6 ha) between classifications of FAO, TREES and this study (AFTE) by continent, and globally. Dates refer to the mean imagery acquisition date. Tolerances of a given estimation are denoted +/-, where calculated.
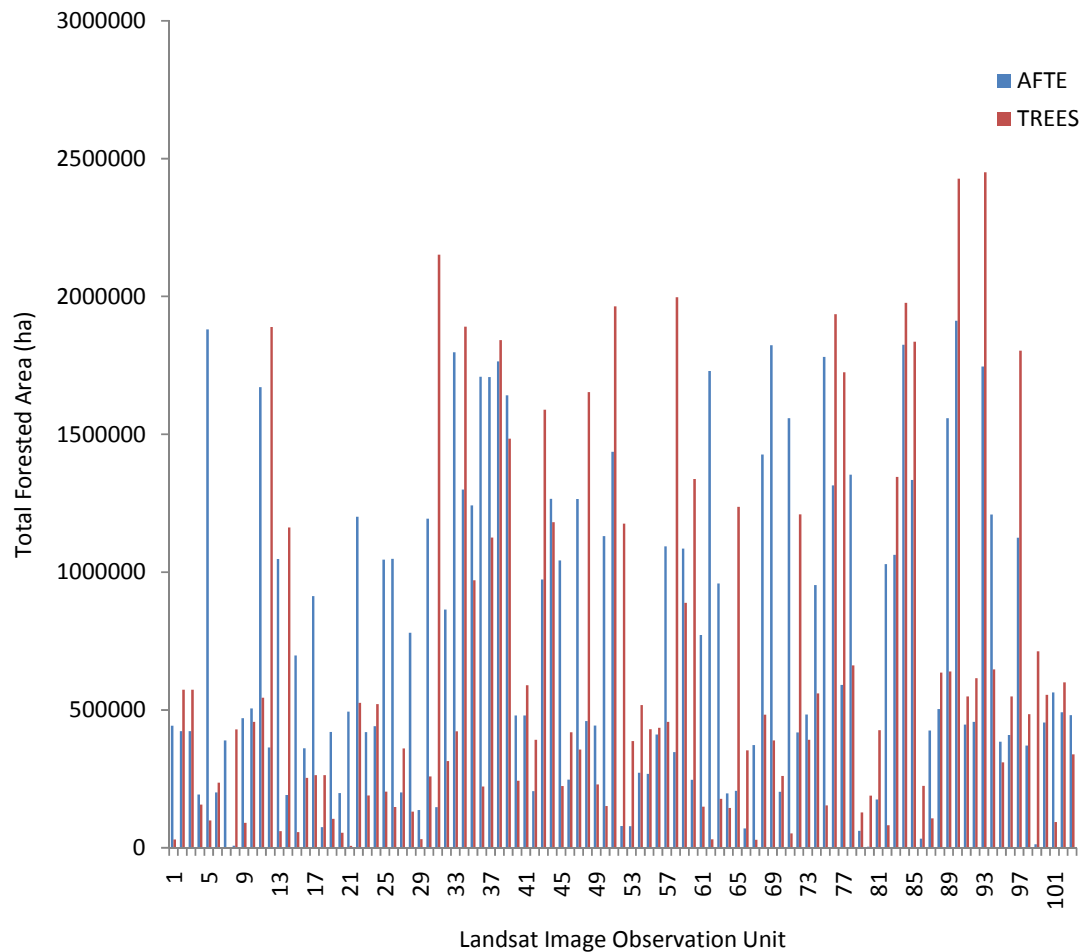
Figure 5.12   Comparison of estimated total forest coverage (ha) as derived from TREES (red) and AFTE (blue) classification schemes for 104 satellite image scenes or quarter scenes defining the 104 TREES observation units (blue boxes, Figure 3.8, Chapter 3, numbered 1-104, in Table 3.1, Chapter 3).

It can be seen that the classifications, whilst in broad agreement, produce very different estimates for some sites. Upon further inspection, the main reason for the difference between classification systems was due to the grouping of forest by the AFTE scheme into one main class for some sites, and the grouping of fragmented forest by the TREES scheme into a singular forest class at other sites. This, of course, is the reason why the AFTE scheme is employed in the first place. However, a broad agreement between the classification systems is encouraging and adds further support to the image accuracy assessments shown in the previous section. It should be also noted that the relative agreement between AFTE classifications at sites of low forest cover (i.e. high sampling weights) is improved. One advantage that the classification system here has is that it is physically motivated. As such, further work will be able to be compared directly to the work presented here, allowing room for future comparison and refinement.   Thus, the classification system imposed represents a practicable and consistent scheme that broadly agrees with other

schemes whilst affording analysis at an increased resolution in a fashion relevant to LSAIs.

5.5   Estimates of Regional and Global Tropical Forest Edge Coverage

The distributions of proportions of forest patches considered to be 'edge' are shown below for each continent. Graphs are shown for EEI (Extend of Edge Influence- i.e. distance of penetration of a given edge effect into the forest patch from its edge) values of 100, 500 and 1000m combined with patch metrics calculated at 140 m resolution. An increase in EEI shifts the distribution of the percentage of forest patches having a higher proportion of edge affected area (% AA) from a lower to higher value, whereby for the largest EEI many small patches become almost entirely influenced by edge area, as demonstrated by the increase in patches having 95%-100% edge influence (Figure 5.13c).

Given the distributions of the percentages of edge area for all patches within each continent, it would be tempting to conclude that a significant proportion of forest could be classed as 'edge affected'. Furthermore, it seems apparent that Southeast Asia has the most edge area in its landscape. However, viewing the total percentages of 'edge' for each continent and the tropical humid biome as a whole, it quickly becomes apparent that when the sampling scheme is accounted for, and so the appropriate weights applied for samples, the proportion of 'edge' decreases distinctly and shifts distribution (Table 5.3).

a) 100m
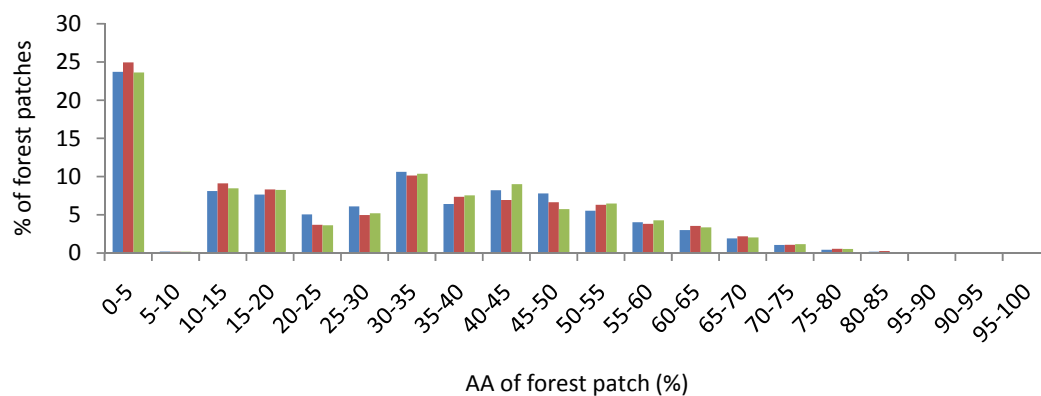
b) 500m
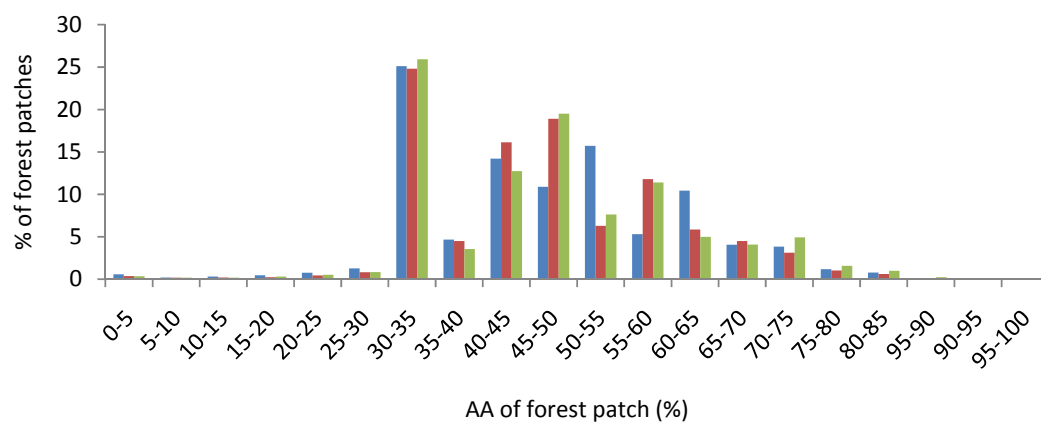
c) 1000m
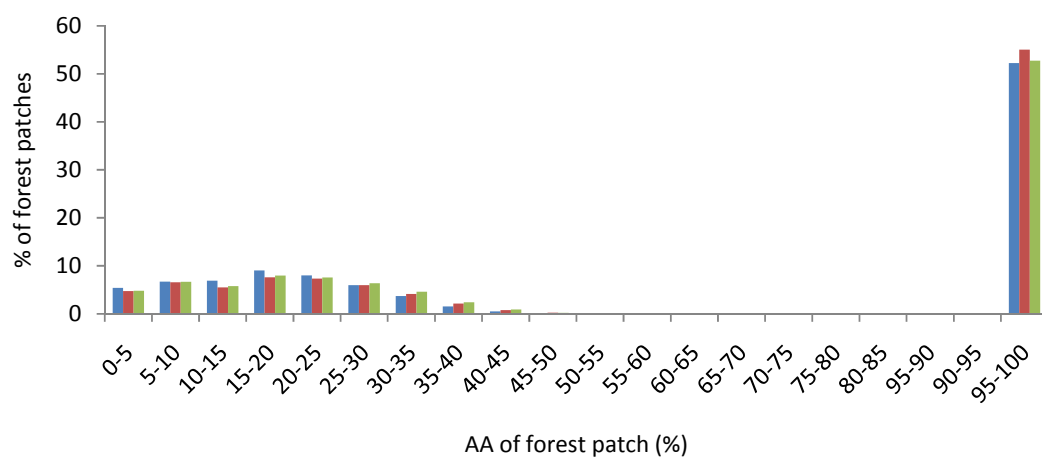
Figure 5.13   Percentage of forest patches having a given percentage of edge affected area (% AA) for each continent: Africa (green), Latin America (blue) and Southeast Asia (red), assuming three different prescribed EEI values as taken from the literature: (a) 100m, (b) 500m and (c) 1000m.

Observing Table 5.3, it can be seen that Africa has the highest percentage of edge, then Southeast Asia, then Latin America. This, at first, may seem to go against the common impression that Southeast Asia, as the most heavily deforested region, will also be the most fragmented. Indeed, observing the statistics for each continent (Table 5.4); Southeast Asia does indeed have the smallest average patch size, and also the greatest mean number of patches per sampling unit/patch.

Extent of Edge Influence (EEI)	% Forest under the Influence of Edge Effect			
	Africa	Latin America	Southeast Asia	Global
1000m	8.26	2.88	4.00	4.08
500m	3.77	1.31	1.84	1.86
100m	0.83	0.29	0.40	0.41
50m	0.42	0.15	0.20	0.21

Table 5.3: Percentage of forest area, as measured at a resolution of 140m by the AFTE classification of this thesis, to be under the influence of edge effects for each continent based on different extents of edge influence (EEI) prescribed by values taken from the literature.

Landscape Metric	Africa	Latin America	Southeast Asia
Total number of patches (n)	2.87 E+03	1.65 E+03	4.18 E+03
Mean patch size (ha)	2.57 E+06	3.81 E+06	2.28 E+06
Mean Patton Shape Index (-)	3.88	1.54	2.01

Table 5.4: The number forest patches and their mean size and shape (indicated by the Patton Shape Index) for each continent, as calculated by the AFTE classification of this thesis.

Africa, however, has the largest average Patton Index (3.88, Table 5.4), indicating its patches were on average less numerous and larger, but are much more complex than those of Southeast Asia. This is in agreement with Rudel & Roper (1997), who conclude that West Africa is the most fragmented region in the world (along with Central America, not considered in this study). It should also be noted that the mean

patch size of Africa is only slightly greater than that of Southeast Asia. It would seem, therefore, that Southeast Asia has a less complex landscape owing to the reduced size and increased numbers of its forest patches. Given that many areas of Southeast Asia are heavily deforested (Bernard & DeKonick, 1997; Brooks *et al.*, 1997; Sodhi & Brook, 2006) this seems a plausible explanation. Brooks *et al.* (1997), for example, showed that the average amount of deforestation in 36 islands of Southeast Asia was 56%, with some areas being up to 90% of forest removed. When the weighting system of TREES is applied, this leads to Africa having approximately twice the amount of forest edge than Southeast Asia. Although the Neotropics have the highest absolute forest loss (10 million ha yr^{-1}) followed by Asia (6 million ha yr^{-1}) and Africa (5 million ha yr^{-1}) (Sodhi & Brook, 2006), Laurance (1999b) states that the highest relative forest loss is in Southeast Asia, and Curran *et al.* (2004) demonstrate that even the 'protected' forests of Southeast Asia have declined by more than 56% between 1985 and 2001. However notwithstanding the reduced size of patches in Southeast Asia, and in agreement with this study, Rudel & Roper (1997) found this region to have a lower fragmentation index (0.723) than East (0.879) and West Africa (2.076). This appears a plausible agreement, as the results of this thesis consider Africa to be the most fragmented continent, based upon samples that predominantly came from West Africa, with a few samples having come from East Africa (Madagascar).

This raises an important issue on the way that climate scientists must perceive edges, which, importantly, fits in with the pattern analysis conducted in the previous section and the concept of localised fractal relationships. Climate (and thus climate modelling) is both a localized and global phenomenon. Whereas traditional (namely, ecological) views of forest edges look at local patterns of forest fragmentation, it is necessary for climate scientists to consider small changes in LSAIs both at local and regional/global scales. For example, Cochrane & Laurance (2002) consider the influence of fire disturbance at forest edges for two states in Amazonia. Whereas it is possible to conclude that the local pattern of deforestation there would play an important role in defining the amount of core/edge area, extrapolation to larger extents would be inappropriate as the measurement of forest pattern was conducted over two very small regions only. In this case, the two study areas, Tailandia (2470 km^2) and Paragominas (1280 km^2), are in the eastern Brazilian Amazon and have extensively fragmented forest cover. Problems would arise in extrapolation to larger scales for two reasons:

1) These regions of the Amazon express a distinct pattern that may not be found elsewhere.

2) The maximum size of the study area may not be large enough to encompass the 'true' size of the forest patches.

The wide variety of patterning shown previously supports point 1, and observing that the largest forest patch recorded in this study (approximately 1300 km^2) is slightly larger than the Paragominas area (1280km^2) covered by Cochrane & Laurance (2002) supports point 2. The possible errors in extrapolating to regional/global scales based on localized patterning are thus demonstrated in this study by comparing edge proportions before and after weighting. This would make approaches such as that of Laurance *et al.* (1998b) questionable, whereby the edge effect upon tree biomass is extrapolated to continental and global estimates of carbon dioxide emissions. It is questionable whether some estimate is better than none at all. Indeed, the work conducted in this thesis represents a first step in modelling the impact edges have upon climate, and, by virtue of this, has numerous limitations. Mary Watson (1978), quoted in Meentemeyer (1989), alludes to the ramifications of selecting inappropriate scales of analysis:

. . . We usually opt for one level of analysis exclusively, without considering the range of other alternatives. To judge from the literature this choice is a private act of faith, not to be reported publically.

The quotation above describes what is termed by Openshaw (1984) as 'Modifiable Areal Unit Problem' (MAUP) (Openshaw, 1984)), which is the problem associated with the bias of statistical interpretation arising from the necessary grouping of data into arbitrary units (i.e. modifiable areal units, such as pixels, geographical regions, satellite images) for analysis. In the case of Laurance *et al.* (1998b), basing large-scale estimates on results of relatively small geographic extents represents a potential example of MAUP, and indeed the results presented in this chapter seem to infer this is the case.

Although scaling considerations have been long analysed and appreciated within the social (e.g. Openshaw, 1984), geological/geographical (Meentemeyer, 1989; Quattrochi & Atkinson, 1999), and biological (Robinson, 1950) sciences, there is a

breakdown in the multidisciplinary case of climate modelling. The reason for this is a simple one: climate (modelling) encompasses a wide variety of scientific disciplines. In isolation, these disciplines work well at their characteristic scale. However there comes a point where disciplines, and hence large scales, must be crossed. Given the various scales and modifiable areal units imposed upon scientists within a certain discipline, the transition from one scale to another rapidly becomes clouded. Therefore, this study, by virtue of operating at a higher resolution and greater extent than previous studies, highlights the contrasts in conclusions made at different scales.

5.6 ESTIMATION OF ERRORS IN CLIMATE MODELS

In order to understand how the proportion of forest under the influence of edge effects could alter regional or global estimates of a given climatic variable, and thus outputs from both regional and global climate models based upon them, the percentage of forest edge affected area as determined for each continent in this chapter (Figures 5.12 and 5.13) was weighted according to different Extents of Edge Influence (EEI) and Magnitudes of Edge Influence (MEI) to estimate a generalised edge enhancement factor (EEF, *sensu* de Ridder *et al.*, 2004). Figures 5.14 and 5.15 demonstrate this procedure for the entire tropical humid domain and each continent, respectively. Figures 5.14 and 5.15 express, for a given variable, the divergence from its area-weighted regional/global estimation caused by including EEF, as represented by an 'error' percentage. 'Error' percentage thus represents the theoretical error incurred by ignoring edge effects in the process of regionalisation. Error was calculated using prescribed values of EEI and MEI combined with proportions of forest edge as estimated in this chapter for all forest patches within each continent, and globally (Figures 5.15 and 5.14, respectively).
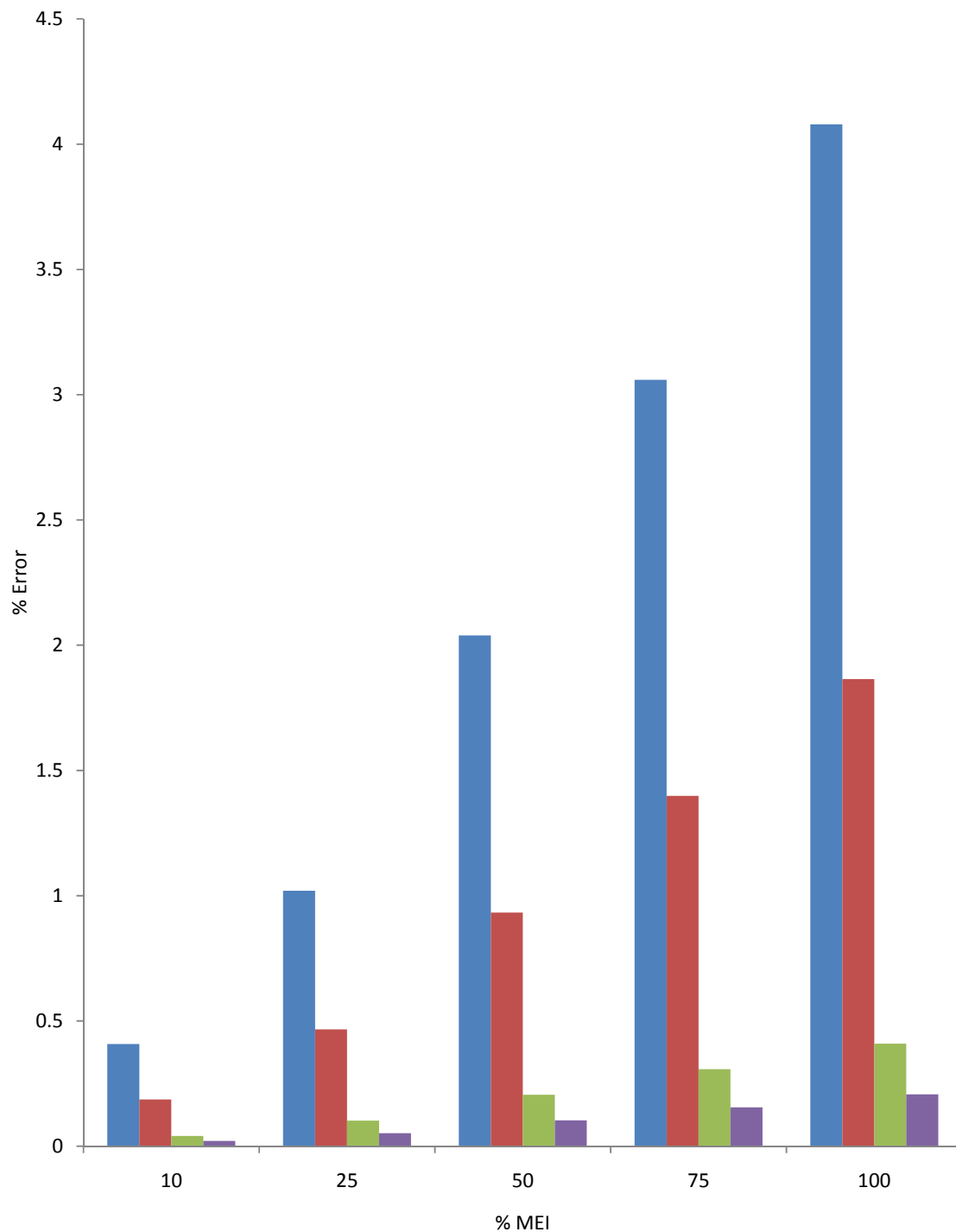
Figure 5.14   Theoretical % error (see text) incurred by not including edge effects in global estimations of a given variable for different magnitudes of edge influence (MEI) for extents of edge influence (EEI) penetrating 1000m (blue), 500m (red), 100m (green) and 50m (purple) into the forest edge.
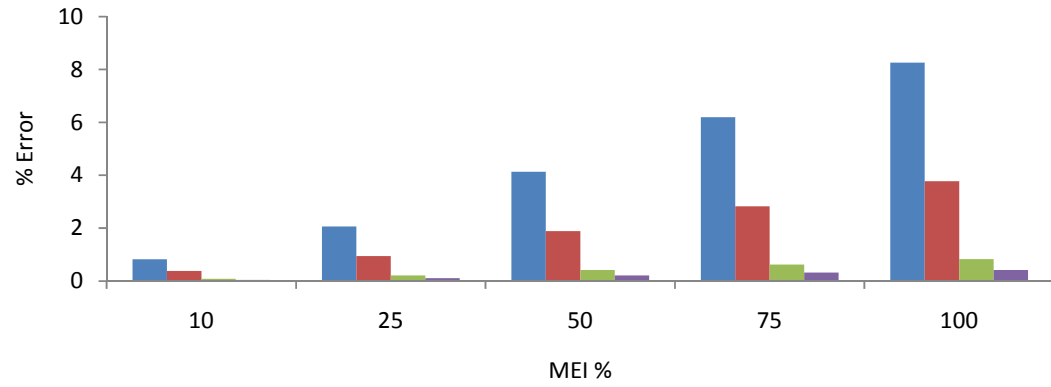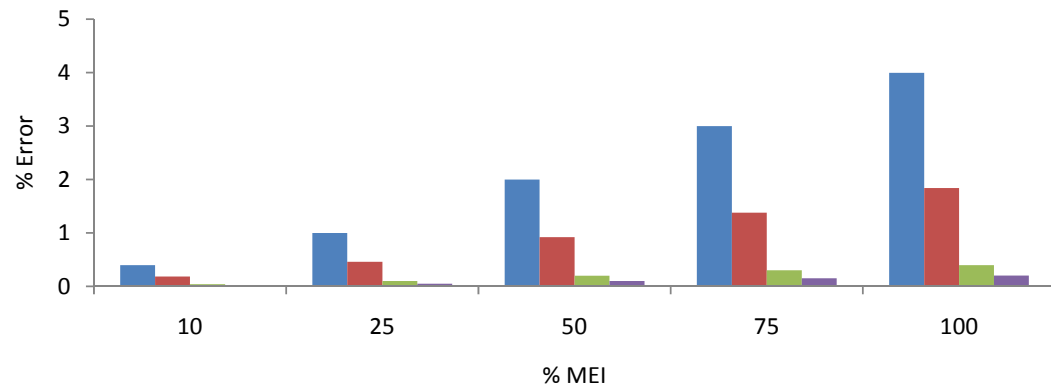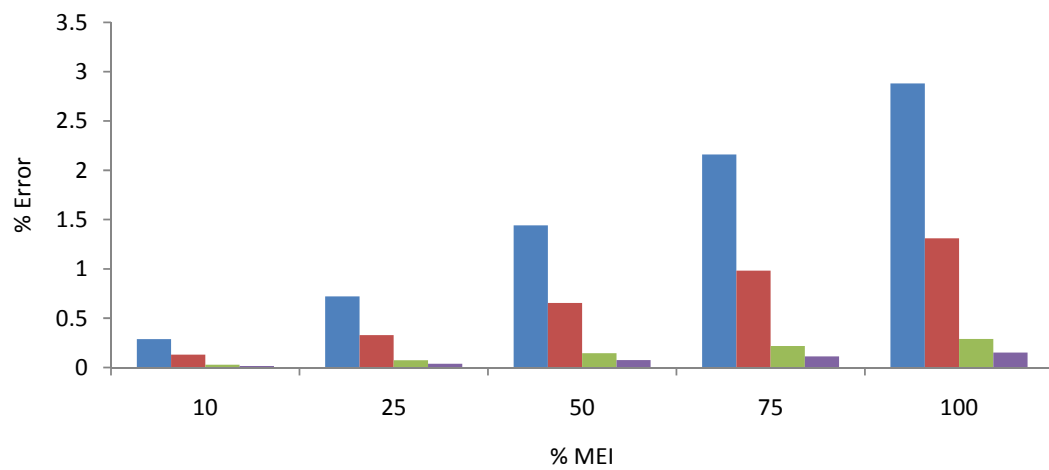
Figure 5.15   Theoretical % error (see text) incurred when making regional estimates of a given variable by not including edge effects for different magnitudes of edge influence (MEI) for extents of edge influence (EEI) penetrating 1000m (blue), 500m (red), 100m (green) and 50m (purple) into the forest edge.

From the literature review in the first chapter, three dominant scenarios of edge effect, which may potentially alter land surface atmosphere-interactions (LSAIs) are:

1) Microclimatic gradients

2) Evapotranspiration gradients

3) Mesoscale circulations

To give an indication of the expected errors associated with each process, typical values of extent and magnitude of edge influence (EEI and MEI respectively) are documented in Table 5.5, alongside EEI/MEI values from Laurance *et al.* (1998b), as used in the estimation of forest edge contribution to regional carbon dioxide fluxes.

Effect	MEI	EEI	Example citation
Microclimate	30%	50m	Murcia (1995)
Transpiration gradients	40%	60m	This study
Mesoscale circulations	?	1-2km	Roy *et al.* (2003)
Forest biomass	10.8%	100m	Laurance *et al.* (1998b)

Table 5.5: Typical values of MEI/EEI for common edge effects found to occur at forest edges, with respective examples as cited in the literature.

Examining Figures 5.14 and 5.15, and Table 5.5, it can be seen quite clearly that in most scenarios, the influence of edge effects upon microclimatic and transpiration gradients, or upon forest biomass loss, when extrapolated to regional or global scales, will alter estimates by less than 1%. Even within Africa - the most fragmented continent according to the work of this chapter- edge effects for these scenarios are still just over 1% (Figure 5.15a). Although this study concluded that edge effects upon transpiration do no penetrate more than 50m into the forest edge, it has been suggested by Giambelluca *et al.* (2003) that transpirative effects could extend beyond 200m into the forest edge. Even if this were the case, however, the greatest influence would not be more than 0.25% globally (Figure 5.14). For larger scale edge

effects the error term becomes significant (7-8%) in Africa (Figure 5.15a), but is unlikely to be greater than 4% across Latin America, Southeast Asia (Figure 5.15c, 5.15b), or the entire tropical humid biome (Figure 5.14). Whereas certain edge effects have been shown to extend beyond 1km into the forest, it is not at present possible to say what influence these effects would have upon climatically significant fluxes. In addition to this, such effects require a significant amount of deforestation, Avissar & Roy (2002) state that forest clearings need to be 150km^2 before any significant mesoscale alteration in boundary layer air circulation occurs. As this study measured the edges around clearings of all sizes, the model presented here cannot be applied to this kind of situation. Of particular interest, applying the relationships found in this study to those MEI/EEI values reported by Laurance *et al.* (1998b) yields a very different estimation of the global contribution of biomass loss to greenhouse gas emissions. Whereas Laurance *et al.* (1998b) suggest that this value would be in the region of 1-7%, the study here concludes such a contribution would be negligible. The reasons for this could be due to the differences in edge measurement (numerical modelling vs. direct measurement), or the definition of 'forest' maps upon which extrapolations were based (i.e. physiognomic vs. physical). However, as suggested earlier, it could be inappropriate extrapolation from one region to the other based upon stereotyped patterns that may not necessarily be present elsewhere around the globe.

5.7   CONCLUSIONS

It has been shown that not accounting for edge effects in regional and global climate models is unlikely to induce large errors in calculated quantities. Even though edge effects can appear to alter the response of the land surface as a whole, at lesser spatial extents extrapolation to regional and global scales renders the overall influence insignificant. The reason for this is that even though there exist numerous areas of significantly fragmented forest in which edge effects prevail, tropical regions and the tropics as a whole do not express forest patch sizes and shapes conducive to a high degree of edge influence.

In Latin America there remains so much intact forest that the forest as a whole cannot be considered fragmented. Southeast Asia, whilst heavily deforested, expresses remnant forest in the form of numerous smaller patches of simple shapes that do not afford sufficient perimeter for edge effects to play a significant role in calculations of climatic quantities at the regional scale. Africa is the most fragmented

region; expressing the most convoluted forest shapes where the average forest patch size is larger than Southeast Asia due to increased contiguity between patches. The increased contiguity in Africa leads to a more complex patch shape and thus a higher level of edge influence. However, even in Africa the error induced in the regional estimation of a given parameter having large MEI and EEI values by ignoring edge effects is not expected to exceed 7-8%.

The exercise presented in this chapter represents the first sensitivity analysis of its kind and in its completion highlights the more ubiquitous problem of scale and ecological fallacy induced by not accounting for scale and its connotations. In this particular case the importance of appreciating localised climatic responses at forest edges within locally fragmented forest represent part of regional and global systems is highlighted. Whereas this is an appropriate lesson for regional and global climate models it must be emphasised that there are scales over which edge effects will induce significant changes in the overall response of the land surface. A good example of this would be in water shed scale analyses. It should be also noted that the aggregated influence of edge effects is assumed to be linear in this sensitivity analysis and that this may not be the case. For example, it was commonly assumed up until recently that roughness elements operating in a landscape could simply be summed, but this is not the case and it has been shown that the combined effect of roughness elements in a landscape is greater than the sum of its constituents. Thus the simple work in this chapter is arguably simplistic.

With specific regard to the quantities measured in Chapter 4 of this thesis it is estimated that transpirative edge effects are unlikely to induce an error greater than 2% in even the most fragmented tropical forests of the world (Africa). Whereas studies previously have estimated that ignoring edge effects could lead to an error of 1-7% globally, entering the same process parameters into the parameterised forest size and shape distribution as measured here renders a total error an order of magnitude less.

This Chapter disseminates the main achievements of the work presented in this thesis, and how realising the aims and objectives of this work has contributed to understanding the hydrometeorology of fragmented tropical forests. Attention is drawn to the numerous problems associated with addressing the multi-scale and multi-faceted research discipline of land surface-atmosphere interactions in fragmented tropical forests, and the need to consider this as a field of research in its own right so that appropriate definition is brought to the subject.

Whilst modest, the work presented here is deemed a significant step forwards towards defining the discipline of fragmented forest hydrometeorology; having provided, for the first time, a review of the literature, field data, and remote sensing analysis combined in a fashion contributes significantly to formalising the theoretical and physical basis of land surface-atmosphere interactions in fragmented tropical forests.

However, it remains unclear whether the inclusion of tropical forest edge effects within climate models is necessary as the pioneering nature of this thesis, and of existing studies reviewed within it, means that solid conclusions will be dependent upon future work. This chapter thus makes suggestions for future research that will most effectively consolidate the provisional conclusions and recommendations made within this thesis.

Processes quantified in this thesis cover scales from the length of a thermal dissipation probe to the global extent of humid tropical forests. The important link between pattern and process is applied to scale up the sap velocity patterns measured at forest edges to the full extent of edge effects across the fragmented tropical forests of the world.

For the first time this thesis demonstrates an influence of distance from a forest edge upon the sap velocity of trees in tropical humid forest. Meteorological measurements support this conclusion and reinforce the concept of forest edges as high flux environments. The addition of meteorological measurements has allowed a demonstration of the influence of hot dry air advection from a clearing on the sap velocity response of trees at a forest edge. A reminder that tree physiology in addition to micrometeorological drivers confounds this relationship is made in light of variable responses of trees to heat advection and the necessity of combining measurements of meteorology and tree physiology highlighted.

Whereas at a single forest edge responses of sap velocity can hypothetically alter the net evapotranspiration of that patch, anthropogenic influences such as tree removal, hydrological components such as wet canopy evaporation and feedbacks within the soil-rhizosphere-xylem pathway, can be of equal much importance. Each process has its role at a specific scale, and small changes at one scale can aggregate to large effects at another. This is commonly appreciated for scales up to and including the scale of a forest stand. However, for the purpose of this study, extrapolation to scales many orders of magnitude larger are required, i.e. to the regional and global level. Scaling of this nature is performed for the first time using a simple physically-orientated classification procedure that allows the estimation of forest sizes and shapes, and consequently the proportion of forest that is expected to be influenced by an edge effect.

The combination of simple measurements of pattern and process parameterised in a relatively crude fashion represents the first sensitivity analysis of how forest edges in the humid tropics are expected to influence water budgets. Such is the novel nature of this work that its contribution to understanding hydrometeorological feedbacks of fragmented forests and its relationship to climate is deemed significant. However as a first step in a relatively new field the methods here have numerous limitations that

must be addressed in order to fulfil the main aim of this thesis, which is to provide a basis and starting point for a more comprehensive understanding of the hydrometeorology of fragmented tropical forests. This aim, whilst modest, is a realistic one, as there is much room for improvement and numerous other possible developments in this field.

A state-of-knowledge review, the literature review presented here is an important first step that attempts to formalise a route for the appropriate and accurate representation of tropical forest edges in climate models. This differs from previous works (*sensu* Laurance, 2004) by addressing climatically significant responses in terms of their raw quantities – namely momentum and sensible and latent heat fluxes. Drawing attention to these key elements is important as they constitute something of a missing piece of the jigsaw in what is essentially a broad and varied multidisciplinary subject.

If the simplistic nature of this study was deemed appropriate then it could be concluded that whereas forest edges appear to have evapotranspirative properties divergent from their interiors the pattern and extent of deforestation does not render a high enough proportion of tropical forests subject to edge effects to induce a great difference in regional or global estimates of a given property.

Although the simple conclusions drawn here can be used as a guide for future work it would be naive to consider them truly conclusive. The framework for solidifying these conclusions has however now been set in this thesis.

Although the site of field measurements can be considered representative of many regions of the tropical humid biome the natural variability in edge structures, clearing types and tree physiologies means that the one transect measured in this study is simply not sufficient to capture the inherent variability in hydrological responses. A roving scheme of sap flow sensors was designed in an approach convergent with that of Herbst *et al.* (2007) following similar roving arrangements of throughfall gauges (e.g. Lloyd *et al.*, 1988). However given the adverse conditions of working in such isolation and in a truly natural forest edge the roving arrangement designed here was not practicable. Whilst either the use of roving schemes or sap flow probes at forest edges is not new, the application of homemade thermal dissipation probes in a roving scheme way is highly recommended for measuring transpiration of trees at tropical forest edges. The only other means of achieving the replication required at a forest edge would be to use static stations and bought probes. This was the case for

Giambelluca *et al.* (2003), but without a similar budget (i.e. approximately $60,000) the purchase of commercially available probes (£500 each) would not be cost effective. Even using commercially available probes it is still necessary to maintain large lengths of wire and so the benefit of decreased maintenance is arguably negligible. A roving arrangement is also necessary given the wide variety of responses expected from different tree species. The application of a roving arrangement by Herbst *et al.* (2007) elegantly solves the problem of differing transpiration responses of different species.

Even with a roving arrangement it is unlikely that there will be a sufficient number of probes appropriately maintained to allow the simultaneous measurement of sap flow in many trees at once given limitations common to working in isolated areas. Standardisation of sap flux is therefore prerequisite to a study of this nature. However standardisation by adiabatic terms such as net radiation is questionable. Thus shortwave radiation and air psychrometrics should be measured alongside any sap flow measurements. Where fine wire thermocouples are available this permits the estimation of sensible and latent heat fluxes by surface renewal analysis (Castellvi *et al.*, 2004). A portable meteorological mast similar to that designed and employed in this study would permit the accurate measurement of all these quantities at the canopy level without the use of standard meteorological towers which are seldom found at forest edges. Although this thesis makes some attempt to qualify the controls driving the increased transpiration present at a forest edge the varied response of sap flux to different variables renders conclusions more suggestive than definitive. The additional measurement of a comprehensive soil moisture measurement suite would be greatly beneficial but repetition of sap flux measurements mediated by a roving arrangement would be much more practical. Results in this thesis suggest that wet canopy evaporation from highly fragmented secondary forest can constitute a large fraction of total evapotranspiration. This result may be due to the short measurement period of throughfall in the field campaign, but given the general agreement with other works and the presence of a weak edge effect a more thorough throughfall measurement campaign would be undoubtedly beneficial.

Site selection could be greatly improved using remotely sensed information of physical parameters such as albedo, soil moisture, vegetation and surface temperature. All these quantities can be derived from Landsat imagery and combined to make estimations of the surface energy balance and moisture status with the use

of Surface Energy Balance Algorithms such as 'SEBAL' (Bastiaanssen, 1998 a, 1998b). The selection of study sites based on specific and exact criteria of this nature would allow truly representative site selection. At this point it should be made clear that the site selected within the Yayasan Sabah concession in this study represents the most extreme contrast of land surface components in energetic terms, asides from those found in tropical urban heat islands. Whereas the region as a whole is representative of the tropical humid biome attention should be drawn to the fact that this may arguably not be the case for the study site itself.

The application of a physically motivated classification scheme would not only allow stratification and representative selection of study sites but it would also permit forests to be classified in a more appropriate way and into more than one class. It is expected that a more accurate classification scheme would render spatial metrics very different to those presented in chapter 3 for a simple 'forest/non-forest' classification. Immediate improvements can be made to the classification scheme presented in chapter 3 by using mosaic images to ensure no cloud coverage rather than the simple nearest neighbour replacement method.

The attempt at stratifying forest area to perimeter ratios presented in this thesis using texture proxies did not render a satisfactory separation of fragmentation classes. The expansion of this work would be more than worthwhile as it would permit the inverse calibration of low resolution imagery with that of a higher resolution. This would circumvent the need to use imagery mosaics and greatly improve the available time resolution to analyses. The stratification procedure outlined in this work could still hold much promise however, and instant improvements could be made by increasing the number of texture measures used. There is a very strong case for a false negative with this result as the expectation maximisation algorithm employed in this study is particularly sensitive to the initial starting values of the seeds that begin the iterative procedure. Although a series of different starting values were selected it is, with hindsight, unclear whether these values are appropriate. As the MATLAB code is already written for the stratification procedure the alteration of starting values should be a straight forward alteration that could render very valuable results. However this line of research was not pursued any further as the main aim of the remote sensing component of this work was to scale measurements to the tropical humid biome rather than look at scaling effects upon patterns of forest patch size and shape.

The improvements outlined here represent important considerations for the hydrological assessment of fragmented tropical forests and also far reaching ramifications for regional and global climate modelling and impact assessment.

Achard, F. & Estreguil, C. 1995. Forest Classification of Southeast Asia Using NOAA AVHRR Data. *Remote Sensing of Environment,* 54**,** 198-208.

Achard, F., Eva, H. & Mayaux, P. 2001. Tropical Forest Mapping from Coarse Spatial Resolution Satellite Data: Production and Accuracy Assessment Issues. *International Journal of Remote Sensing,* 22**,** 2741-2762.

Achard, F., Eva, H.D., Glinni, A., Mayaux, P., Stibig, H.J. & Richards, T. 1998. Identification of Deforestation Hot Spot Areas in the Humid Tropics. *The Humid Tropics, TREES Publications Series B.* Luxembourg.

Achard, F., Eva, H.D., Stibig, H.J., Mayaux, P., Gallego, J., Richards, T. & Malingreau, J.P. 2002a. Determination of Deforestation Rates of the World's Humid Tropical Forests. *Science,* 297**,** 999-1002.

Achard, F*.,* Eva, H.D., Stibig, H.J., Mayaux, P., Gallego, J., Richards, T. & Malingreau, J.P. 2002b. . Determination of Deforestation Rates of the World's Humid Tropical Forests – Methodology and Results of the TREES-II Research Programme. European Commission, Directorate General Joint Research Centre, Institute for Environment and Sustainability. TREES Publications Series B, Research Report No.5.

Ahmad, N., 2001. Frugivores and Fruit Production in Primary and Logged Tropical RainForest*s. Ph.D.* The*sis, Faculty of Science and Technology, University Kebangsaan Malaysia, Bangi, Malaysia.*

Albuz, E., Kocalar, E., and Khokhar, A. A., 1999. Vector-Wavelet Based Scalable Indexing and Retrieval System for Large Colour Image Archives. *IEEE Transactions on Geoscience and Remote Sensing.*14, 3021-3024.

Arai, K., 1993. A Classification Method with a Spectral-Spatial Variability. *International Journal of Remote Sensing.*14, 699-709.

Ashton, P.S. 1964. Ecological Studies in the Mixed Dipterocarp Forests of Brunei State. *Oxford Forest Mem*., 25.

Atkinson, P.M., 1993. The Effect of Spatial Resolution on the Experimental Variogram of Airborne MSS Imagery. *International Journal of Remote Sensing*, 14, 1005-1011.

Avery, T.E. & Berlin, G.l. 1992. *Fundamentals of Remote Sensing and Air Photo Interpretation,* NY, Macmillan Publishing Co.

Avissar, R. & Nobre, C.A. 2002. Preface to Special Issue on the Large-Scale Biosphere-Atmosphere Experiment in Amazonia (LBA). *Journal of Geophysical Research-Atmospheres,* 107.

Avissar, R. & Roy, S.B., 2002. Impact of Land Use/Land Cover Change on Regional Hydrometeorology in Amazonia. *Journal of Geophysical Research*, 107, 8037.

Bailey, R.G., 1976. Ecoregions of the United States, [map].

Baldocchi, D.D. & Rao, K.S. 1995. Intra-Field Variability of Scalar Flux Densities across a Transition Between A Desert and An Irrigated Potato Field. *Boundary-Layer Meteorology,* 76**,** 109-136.

Bastiaanssen, W.G.M. 2000. SEBAL-Based Sensible and Latent Heat Fluxes in the Irrigated Gediz Basin, Turkey. *Journal of Hydrology,* 229**,** 87-100.

Bastiaanssen, W.G.M. & Chandrapala, l. 2003. Water Balance Variability across Sri Lanka for Assessing Agricultural and Environmental Water Use. *Agricultural Water Management,* 58**,** 171-192.

Bastiaanssen, W.G.M., Menenti, M., Feddes, R.A. & Holtslag, A.A.M. 1998a. A Remote Sensing Surface Energy Balance Algorithm for Land (SEBAL) - 1. Formulation. *Journal of Hydrology,* 213**,** 198-212.

Bastiaanssen, W.G.M., Pelgrum, H., Wang, J., Ma, Y., Moreno, J. F., Roerink, G.J. & Van Der Wal, T. 1998b. A Remote Sensing Surface Energy Balance Algorithm for Land (SEBAL) - 2. Validation. *Journal of Hydrology,* 213**,** 213-229.

Bernard, S., & De Konick, R., 1997. The Retreat of the Forest in Southeast Asia: A Cartographic Assessment. *Singapore Journal of Tropical Geography*, 17, 1-14.

Bian, l. 1997. Multiscale Nature of Spatial Data in Scaling Up in Environmental Models. *In:* Quattrochi, D. A. & Goodchild, M. F., eds. *Scale in Remote Sensing and GIS.* Washington DC: Lewis Publishers.

Bidin, K. & Chapell, N.A. 2003. Net Rainfall and Wet Canopy Evaporation in A Small Selectively-Logged RainForest Catchment, Sabah, Malaysia. *Proceedings, 1st International Conference on Hydrology and Water Resources in Asia Pacific Region. Volume 2*. Kyoto. Japan:659-666.

Blyth, E.M. 1995. Using A Simple SVAT Scheme to Describe the Effect of Scale on Aggregation. *Boundary-Layer Meteorology,* 72**,** 267-285.

Blyth, E.M., Dolman, A.J. & Wood, N. 1993. Effective Resistance to Sensible-Heat and Latent-Heat Flux in Heterogeneous Terrain. *Quarterly Journal of the Royal Meteorological Society,* 119**,** 423-442.

Blyth, E.M. & Harding, R.J. 1995. Application of Aggregation Models to Surface Heat-Flux from the Sahelian Tiger Bush. *Agricultural and Forest Meteorology,* 72**,** 213-235.

Blyth, E.M., Harding, R.J. & Essery, R. 1999. A Coupled Dual Source GCM SVAT. *Hydrology and Earth System Sciences,* 3**,** 71-84.

Boegh, E., Soegaard, H., Friborg, T. & Levy, P.E. 1999. Models of CO_2 and Water Vapour Fluxes from a Sparse Millet Crop in the Sahel. *Agricultural and Forest Meteorology,* 93**,** 7-26.

Brakke, T.W., Verma, S.B. & Rosenberg, N.J. 1978. Local and Regional Components of Sensible Heat Advection. *Journal of Applied Meteorology,* 17**,** 955-963.

Brearley, F.Q., Prajadinata, S., Kidd, P.S., Proctor, J. & Suriantata 2004. Structure and Floristics of an Old Secondary Rain Forest in Central Kalimantan, Indonesia, and a Comparison with Adjacent Primary Forest. *Forest Ecology and Management,* 195**,** 385-397.

Brooks, S.M. & Spencer, T. 1997. Changing Soil Hydrology Due to Rain Forest Logging: An Example from Sabah Malaysia. *Journal of Environmental Management,* 49**,** 297-310.

Brooks, T.M., Pimm, S.L. & Collar, N.J., 1997. Deforestation Predicts the Number of Birds in Insular Southeast Asia. *Conservation Biology,* 11, 382-388.

Brown, N., Jennings, S., Wheeler, P. & Nabe-Nielsen, J. 2000. An Improved Method for the Rapid Assessment of Forest Understorey Light Environments. *Journal of Applied Ecology,* 37**,** 1044-1053.

Brown, P.J. 1982. Multivariate Calibration. *Journal of the Royal Statistical Society Series B-Methodological,* 44**,** 287-321.

Bruijnzeel, L.A. 1990. Hydrology of Moist Tropical Forests and Effects of Conversion: A State of Knowledge Review. *International Institute for Aerospace Survey and Earth Sciences.*

Brunet, Y., Itier, B., Mcaneney, J. & Lagouarde, J.P. 1994. Downwind Evolution of Scalar Fluxes and Surface-Resistance under Conditions of Local Advection. 2. Measurements Over Barley. *Agricultural and Forest Meteorology,* 71**,** 227-245.

Cain, D.H., Riitters, K. & Orvis, K. 1997. A Multi-Scale Analysis of Landscape Statistics. *Landscape Ecology,* 12**,** 199-212.

Calder, I.R., Wright, I.R, and Murdiyarso, D. (1986). A Study of Evaporation from Tropical Rainforest – West Java. *J. Hydrology*, 89, 13-31.

Caldwell, M.M., Dawson, T.E., Richards, J.H. 1998. Hydraulic Lift: Consequences of Water Efflux from the Roots of Plants, *Oecologia*, 151-161.

Camargo, J.L.C. & Kapos, V. 1995. Complex Edge Effects on Soil-Moisture and Microclimate in Central Amazonian Forest. *Journal of Tropical Ecology,* 11**,** 205-221.

Cao, C. & Lam, N.S.N. 1997. Understanding the Scale and Resolution Effects in Remote Sensing and GIS. *In:* Quattrochi, D.A. & Goodchild, M.F, eds. *Scale in Remote Sensing and GIS*. CRC Publishers.

Canny, J. 1986. A Computational Approach to Edge-Detection. *IEEE Transactions on Pattern Analysis and Machine intelligence,* 8**,** 679-698.

Castellvi, F. 2004. Combining Surface Renewal Analysis and Similarity theory: A New Approach for Estimating Sensible Heat Flux. *Water Resources Research,* 40.

Castellvi, F., Martinez-Cob, A. & Perez-Coveta, O. 2006. Estimating Sensible and Latent Heat Fluxes over Rice Using Surface Renewal. *Agricultural and Forest Meteorology,* 139**,** 164-169.

Castellvi, F., Perez, P.J. & Ibanez, M. 2002. A Method Based on High-Frequency Temperature Measurements to Estimate the Sensible Heat Flux Avoiding the Height Dependence. *Water Resources Research,* 38.

Chen, J.Q., Franklin, J.F. & Spies, T.A. 1995. Growing-Season Microclimatic Gradients from Clear-Cut Edges into Old-Growth Douglas-Fir Forests. *Ecological Applications,* 5**,** 74-86.

Chen, W., Novak, M.D., Black, A.T. & Lee, X., 1997. Coherent Eddies and Temperature Structure Functions for Three Contrasting Surfaces. Part II: Renewal Model for Sensible Heat Flux. *Boundary Layer Meteorology*, 84, 125-147.

Cienciala, E., Kucera, J. & Malmer, A. 2000. Tree Sap Flow and Stand Transpiration of Two *Acacia Mangium* Plantations in Sabah, Borneo. *Journal of Hydrology,* 236**,** 109-120.

Cienciala, E., Mellander, P. E., Kucera, J., Oplustilova, M., Ottosson-Lofvenius, M. & Bishop, K. 2002. The Effect of A North-Facing Forest Edge on Tree Water Use in A Boreal Scots Pine Stand. *Canadian Journal of Forest Research-Revue Canadienne De Recherche Forestiere,* 32**,** 693-702.

Clark, D.A. & Clark, D.B. 1992. Life-History Diversity of Canopy and Emergent Trees in a Neotropical Rain-Forest. *Ecological Monographs,* 62**,** 315-344.

Claussen, M. 1987. The Flow in a Turbulent Boundary-Layer Upstream of a Change in Surface-Roughness. *Boundary-Layer Meteorology,* 40**,** 31-86.

Claussen, M. 1991a. Estimation of Areally-Averaged Surface Fluxes. *Boundary-Layer Meteorology,* 54**,** 387-410.

Claussen, M. 1991b. Local Advection Processes in the Surface-Layer of the Marginal Ice-Zone. *Boundary-Layer Meteorology,* 54**,** 1-27.

Clearwater, M.J., Meinzer, F.C., Andrade, J.l., Goldstein, G. & Holbrook, N.M. 1999. Potential Errors in Measurement of Nonuniform Sap Flow Using Heat Dissipation Probes. *Tree Physiology,* 19**,** 681-687.

Cochrane, M.A. & Laurance, W.F. 2002. Fire as a Large-Scale Edge Effect in Amazonian Forests. *Journal of Tropical Ecology,* 18**,** 311-325.

Cox, P.M., Huntingford, C. & Harding, R.J. 1998. A Canopy Conductance and Photosynthesis Model for Use in a GCM Land Surface Scheme. *Journal of Hydrology,* 213**,** 79-94.

Cox, P.M., Betts, R.A., Jones, C.D., Spall, S.A. & Totterdell, I.J. 2000. Acceleration of Global Warming Due to Carbon-Cycle Feedbacks in a Coupled Climate Model. *Nature,* 408**,** 184-187.

Culf, A.D., Esteves, J.L., Marques Filho, A.D.O. & Da Rocha, H.R. 1996. Radiation, Temperature and Humidity over Forest and Pasture in Amazonia. *In:* Gash, J.H.C., Nobre, C.A., Roberts, J.M. & Victoria, R.L., eds. *Amazonian Deforestation and Climate.* Chichester: John Wiley.

Cumming, S. & Vernier, P. 2002. Statistical Models of Landscape Pattern Metrics, with Applications to Regional Scale Dynamic Forest Simulations. *Landscape Ecology,* 17**,** 433-444.

Curran, L.M., Trigg, S.N., McDonald, A.K., Astiani, D. & Kasischke, E. 2004. Lowland Forest Loss in Protected Areas of Indonesia. *Science, 303, 1000-1003.*

Cutrim, E., Martin, D.W. & Rabin, R. 1995. Enhancement of Cumulus Clouds Over Deforested Lands in Amazonia. *Bulletin of the American Meteorological Society,* 76**,** 1801-1805.

D'Alessandro, C.M., Saracino, A. & Borghetti, M. 2006. Thinning Affects Water Use Efficiency of Hardwood Saplings Naturally Recruited in a *Pinus radiata* Plantation. *Forest Ecology and Management,* 222**,** 116-122.

D'Angelo, S.A., Andrade, A.C.S., Laurance, S.G., Laurance, W.F. & Mesquita, R.C.G. 2004. Inferred Causes of Tree Mortality in Fragmented and Intact Amazonian Forests. *Journal of Tropical Ecology,* 20**,** 243-246.

Dal Moro, G. & Halounova, L., 2005. Haze Removal for High-Resolution Satellite Data: A Case Study. *International Journal of Remote Sensing*, 28, 2187 — 2205.

Da Rocha, H.R., Goulden, M.L., Miller, S.D., Menton, M.C., Pinto, L., de Freitas, H.C. & Figueira, A. 2004. Seasonality of Water and Heat Fluxes over a Tropical Forest in Eastern Amazonia. *Ecological Applications,* 14**,** S22-S32.

Da Silva, R.R. & Avissar, R. 2006. The Hydrometeorology of a Deforested Region of the Amazon Basin. *Journal of Hydrometeorology,* 7**,** 1028-1042.

Daubechies, I., 1992. Ten Lectures on Wavelets. *CBMS-NSF Regional Conference Series in Applied Mathematics*.

David, T.S., Gash, J.H.C., Valente, F., Pereira, J.S., Ferreira, M.I. & David, J.S. 2006. Rainfall Interception by an Isolated Evergreen Oak Tree in a Mediterranean Savannah. *Hydrological Processes,* 20**,** 2713-2726.

Davies, S.J. 1998. Photosynthesis of Nine Pioneer Macaranga Species from Borneo in Relation to Life History. *Ecology,* 79**,** 2292-2308.

Davies, S.J. 2001. Tree Mortality and Growth in 11 Sympatric Macaranga species in Borneo. *Ecology,* 82**,** 920-932.

de Bruin, H.A.R., Hartogensis, O.K., Allen, R.G. & Kramer, J. 2005. Regional Advection Perturbations in an Irrigated Desert (RAPID) Experiment. *Theoretical and Applied Climatology,* 80**,** 143-152.

Defries, R.S., Townsend, J.R. & Los, S.O. 1997. Scaling Land Cover Heterogeneity for Global Atmosphere-Biosphere Models. *In:* Quattrochi, D. A. & Goodchild, M. F., eds. *Scale in Remote Sensing and GIS.* Washington DC: Lewis Publishers.

de Jong, S.M. & Burrough, P.A. 1995. A Fractal Approach to the Classification of Mediterranean Vegetation Types in Remotely-Sensed Images. *Photogrammetric Engineering and Remote Sensing,* 61**,** 1041-1053.

de Jong, J.J.M. & Klaassen, W. 1997. Simulated Dry Deposition of Nitric Acid Near Forest Edges. *Atmospheric Environment,* 31**,** 3681-3691.

de Jong, J.J.M., de Vries, A.C. & Klaasen, W. 1999. Influence of Obstacles on the Aerodynamic Roughness of the Netherlands. *Boundary-Layer Meteorology,* 91**,** 51-64.

de Ridder, K. 2003. Horizontal Scale of Roughness Variations for Realistic Landscapes. *Boundary-Layer Meteorology,* 109**,** 49-57.

de Ridder, K. & Mensink, C. 2003. Surface Fluxes and Atmospheric Stability Obtained from a Surface Energy Balance Model With Parameters Estimated from Satellite Remote Sensing. *International Journal of Environment and Pollution,* 19**,** 22-31.

de Ridder, K., Neirynck, B. & Mensink, C. 2004. Parameterising Forest Edge Deposition Using Effective Roughness Length. *Agricultural and Forest Meteorology,* 123**,** 1-11.

Dettori, l. & Semler, l. 2007. A Comparison of Wavelet, Ridgelet, and Curvelet-Based Texture Classification Algorithms in Computed Tomography. *Computers in Biology and Medicine,* 37**,** 486-498.

Dias, M. A.F.S. & Regnier, P. 1997. Simulation of Mesoscale Circulations in A DeForested Area of Rondônia in the Dry Season. *In:* Gash, J. H. C., Nobre, C. A., Roberts, J. M. & Victoria, R. L., eds. *Amazonian Deforestation and Climate.* Chichester: John Wiley.

Dolman, A. J. & Blyth, E. M. 1997. Patch Scale Aggregation of Heterogeneous Land Surface Cover for Mesoscale Meteorological Models. *Journal of Hydrology,* 190**,** 252-268.

Draaijers, G.P.J., Vanek, R. & Bleuten, W. 1994. Atmospheric Deposition in Complex Forest Landscapes. *Boundary-Layer Meteorology,* 69**,** 343-366.

Duce, P., Spano, D., Snyder, R.l. & Paw, K.T. 1997. Surface Renewal Estimates of Evapotranspiration- Short canopies. *Second International Symposium on Irrigation of Horticultural Crops, Vols 1 and 2***,** 57-62.

Dyer, A. J. 1963. The Adjustment of Profiles and Eddy Fluxes. *Quarterly Journal of the Royal Meteorological Society,* 89**,** 276-280.

Dyer, A.J. & Crawford, T.V., 1965. Observations of the Modification of the Microclimate at a Leading Edge. *The Quarterly Journal of the Royal Meteorological Society*, 91, 345 - 348.

Earthsat. www.Earthsat.com

Edwards, G., Landary, R. & Thomson, K.P.B. 1988. Texture Analysis of Forest Regeneration Sites in High-Resolution SAR Imagery. *Proceedings of the International Geosciences and Remote Sensing Symposium (IGARSS 88).* Paris: European Space Agency.

Eva, H. D., Belward, A. S., de Miranda, E. E., Di Bella, C. M., Gond, V., Huber, O., Jones, S., Sgrenzaroli, M. & Fritz, S. 2004. A Land Cover Map of South America. *Global Change Biology,* 10**,** 731-744.

Ewers, R. M. & Laurance, W. F. 2006. Scale-Dependent Patterns of Deforestation in the Brazilian Amazon. *Environmental Conservation,* 33**,** 203-211.

Ferreira, L. V. & Laurance, W. F. 1997. Effects of Forest Fragmentation on Mortality and Damage of Selected Trees in Central Amazonia. *Conservation Biology,* 11**,** 797-801.

Fisch, G. 1986. Armazenamento E Fluxos De Energia Sobre Floresta Da Amazonia Central. MSc. Thesis. University of São Paulo, São Paulo, Brazil.

Fisch, G., Tota, J., Machado, L. A. T., Dias, M., Lyra, R. F. D., Nobre, C. A., Dolman, A. J. & Gash, J. H. C. 2004. The Convective Boundary Layer over Pasture and Forest in Amazonia. *Theoretical and Applied Climatology,* 78**,** 47-59.

Ford, C. R., Goranson, C. E., Mitchell, R. J., Will, R. E. & Teskey, R. O. 2004a. Diurnal and Seasonal Variability in the Radial Distribution of Sap Flow: Predicting total Stem Flow in *Pinus taeda* Trees. *Tree Physiology,* 24**,** 941-950.

Ford, C. R., Mcguire, M. A., Mitchell, R. J. & Teskey, R. O. 2004b. Assessing Variation in the Radial Profile of Sap Flux Density in *Pinus* Species and its Effect on Daily Water Use. *Tree Physiology,* 24**,** 241-249.

FRACLAC for ImageJ. http://rsbweb.nih.gov

Friedl, M. A. 1997. Examining the Effects of Sensor Resolution and Sub-Pixel Heterogeneity on Spectral Vegetation Indices: Implications for Biophysical Modelling. *In:* Quattrochi, D. A. & Goodchild, M. F., eds. *Scale in Remote Sensing and GIS.* Washington DC: Lewis Publishers.

Fritschen, L.J. 1985. Characterization of Boundary Conditions Affecting Forest Environmental Phenomena. *In:* Hutchison, B.A., & Hicks, B.B., eds. The Forest–Atmosphere interaction. D. Reidel Publishing Company, Dordrecht, the Netherlands (1985), 3–23.

Fu, R. & Li, W. 2004. The Influence of the Land Surface on the Transition from Dry to Wet Season in Amazonia. *Theoretical and Applied Climatology,* 78**,** 97-110.

Gabriel, P., Lovejoy, S., Schertzer, D. & Austin, G. l. 1988. Multifractal Analysis of Resolution Dependence in Satellite Imagery. *Geophysical Research Letters,* 15**,** 1373-1376.

Gardiner, B.A., Irvine,M.A., Hill, M.R., & Baker, M. 1995. Airflow and Turbulent Flux Development Across a Moorland/Forest Interface. *Agricultural and Forest Meteorology,* 21.

Gascon, C., Lovejoy, T. E., Bierregaard, R. O., Malcolm, J. R., Stouffer, P. C., Vasconcelos, H. L., Laurance, W. F., Zimmerman, B., Tocher, M. & Borges, S. 1999. Matrix Habitat and Species Richness in Tropical Forest Remnants. *Biological Conservation,* 91**,** 223-229.

Gascon, C., Williamson, G. B. & Da Fonseca, G. A. B. 2000. Ecology - Receding Forest Edges and Vanishing Reserves. *Science,* 288**,** 1356-1358.

Gash, J. H. C. 1986a. A Note on Estimating the Effect of a Limited Fetch on Micrometeorological Evaporation Measurements. *Boundary-Layer Meteorology,* 35**,** 409-413.

Gash, J. H. C. 1986b. Observations of Turbulence Downwind of a Forest-Heath Interface. *Boundary-Layer Meteorology,* 36**,** 227-237.

Gash, J. H. C. & Nobre, C. A. 1997. Climatic Effects of Amazonian *Deforestation*: Some Results from ABRACOS. *Bulletin of the American Meteorological Society,* 78**,** 823-830.

Gash, J. H. C. & Shuttleworth, W. J. 1991. Tropical Deforestation - Albedo and the Surface-Energy Balance. *Climatic Change,* 19**,** 123-133.

Gash, J. H. C., Nobre, C. A., Roberts, J. M. & Victoria, R.L. 1997. An Overview of ABRACOS. *In:* Gash, J. H. C., Nobre, C. A., Roberts, J. M. & Victoria, R.L., eds. *Amazon Deforestation and Climate.* Chichester: John Wiley.

Gay, l. W. & Berhoffer, C. 1991. Enhancement of Evapotranspiration by Advection in Arid Regions. *In:* Kienitz, G., Milly, P. C. D., Van Genuchten, M., Rosbjerg, D. & Shuttleworth, W. J., eds. *Hydrological Interactions Between Atmosphere Soil and Vegetation.* Great yarmouth: IAHS publications.

Gervin, J. C., Kerber, A. G., Witt, R. G., Lu, Y. C. & Sekhon, R. 1985. Comparison of Level-I Land Cover Classification Accuracy for MSS and AVHRR Data. *International Journal of Remote Sensing,* 6**,** 47-57.

Giambelluca, T. W., Fox, J., Yarnasarn, S., Onibutr, P. & Nullet, M. A. 1999. Dry-Season Radiation Balance of Land Covers Replacing Forest in Northern Thailand. *Agricultural and Forest Meteorology,* 95**,** 53-65.

Giambelluca, T. W., Nullet, M. A., Ziegler, A. D. & Tran, L. 2000. Latent and Sensible Energy Flux over Deforested Land Surfaces In The Eastern Amazon And Northern Thailand. *Singapore Journal of Tropical Geography,* 21**,** 107-130.

Giambelluca, T. W., Ziegler, A. D., Nullet, M. A., Truong, D. M. & Tran, L. T. 2003. Transpiration in a Small Tropical Forest Patch. *Agricultural and Forest Meteorology,* 117**,** 1-22.

GLCF –'Global Land Cover Facility'. www.landcover.org

Goldstein, G., Andrade, J. l., Meinzer, F. C., Holbrook, N. M., Cavelier, J. Jackson, P. & Celis, A. 1998. Stem Water Storage and Diurnal Patterns of Water Use in Tropical Forest Canopy Trees. *Plant Cell and Environment,* 21**,** 397-406.

Granier, A. 1985. A New Method of Sap Flow Measurement in Tree Stems. *Annales Des Sciences Forestieres,* 42**,** 193-200.

Granier, A. 1987. Evaluation of Transpiration in a Douglas-Fir Stand by Means of Sap Flow Measurements. *Tree Physiology,* 3**,** 309-319.

Granier, A., V. Bobay, J.H.C. Gash, J. Gelpe, B. Saugier & Shuttleworth, W.J. 1990. Vapour Flux Density and Transpiration Rate Comparisons in a Stand of Maritime Pine (*Pinus pinaster* Ait.) in Les Landes Forest. *Agricultural and Forest Meteorology,* 51,309-319.

Granier, A., Biron, P., Breda, N., Pontailler, J.Y. & Saugier, B. 1996a. Transpiration of Trees and Forest Stands: Short and Longterm Monitoring Using Sapflow Methods. *Global Change Biology,* 2, 265-274.

Granier, A., Huc, R. & Barigah, S. T. 1996b. Transpiration of Natural Rain Forest and its Dependence on Climatic Factors. *Agricultural and Forest Meteorology, 78*, 19-29.

Granier, A., Huc, R. & Colin, F. 1992. Transpiration and Stomatal Conductance of 2 Rain-Forest Species Growing in Plantations (*Simarouba-amara and Goupia-glabra*) in French-Guyana. *Annales Des Sciences Forestieres, 49*, 17-24.

Granier, A., Biron, P. & Lemoine, D. 2000. Water Balance, Transpiration and Canopy Conductance in Two Beech Stands. *Agricultural and Forest Meteorology, 100*, 291-308.

Green, S., Clothier, B. & Jardine, B. 2003. Theory and Practical Application of Heat Pulse to Measure Sap Flow. *Agronomy Journal, 95*, 1371-1379.

Gustafson, E. J. 1998. Quantifying Landscape Spatial Pattern: What Is the State of the Art? *Ecosystems, 1*, 143-156.

Hales, K., Neelin, J. D. & Zeng, N. 2004. Sensitivity of Tropical Land Climate to Leaf Area Index: Role of Surface Conductance Versus Albedo. *Journal of Climate, 17*, 1459-1473.

Harding, R.J., Blyth, E.M. & Huntingford, C. 1997. Issues in the Aggregation of Surface Fluxes from A Heterogeneous Landscape: from Sparse Canopies Up to the GCM Grid Scale, *In:* Van Gardingen, P.R., Foody, G.M., Curran, P.J., eds. *Scaling-Up from Cell to Landscape,* 386. Society for Experimental Biology, Seminar Series 63. Cambridge: Cambridge University Press.

Hargis, C. D., Bissonette, J. A. & David, J. L. 1998. The Behaviour of Landscape Metrics Commonly Used in the Study of Habitat Fragmentation. *Landscape Ecology, 13*, 167-186.

Harper, K. A., Macdonald, S. E., Burton, P. J., Chen, J. Q., Brosofske, K. D., Saunders, S. C., Euskirchen, E. S., Roberts, D., Jaiteh, M. S. & Esseen, P. A. 2005. Edge influence on Forest Structure and Composition in Fragmented Landscapes. *Conservation Biology, 19*, 768-782.

Hatton, T. J., Moore, S. J. & Reece, P. H. 1995. Estimating Stand Transpiration in a Eucalyptus-Populnea Woodland With the Heat Pulse Method - Measurement Errors and Sampling Strategies. *Tree Physiology, 15*, 219-227.

Herbst, M., Roberts, J. M., Rosier, P. T. W. & Gowing, D. J. 2006. Measuring and Modelling the Rainfall Interception Loss by Hedgerows in Southern England. *Agricultural and Forest Meteorology, 141*, 244-256.

Herbst, M., Roberts, J. M., Rosier, P. T. W. & Gowing, D. J. 2007a. Seasonal and Interannual Variability of Canopy Transpiration of a Hedgerow in Southern England. *Tree Physiology,* 27**,** 321-333.

Herbst, M., Roberts, J. M., Rosier, P. T. W., Taylor, M. E. & Gowing, D. J. 2007b. Edge Effects and Forest Water Use: A Field Study in a Mixed Deciduous Woodland. Forest *Ecology and Management,* 250**,** 176-186.

Hill, R. A. 1999. Image Segmentation for Humid Tropical Forest Classification in Landsat TM data. *International Journal of Remote Sensing,* 20**,** 1039-1044.

Hodnett, M. G., DaSilva, L. P., Darocha, H. R. & Senna, R. C. 1995. Seasonal Soil-Water Storage Changes Beneath Central Amazonian Rain-Forest and Pasture. *Journal of Hydrology,* 170**,** 233-254.

Hodnett, M. G., Oyama, M. D., Tomasella, J. & Marques Filho, A. D. O. 1997a. Comparisons of Long-Term Soil Water Storage Behaviour Under Pasture and Forest in Three Areas of Amazonia. *In:* Gash, J. H. C., Nobre, C. A., Roberts, J. M. & Victoria, R. L., eds. *Amazonian Deforestation and Climate.* Chichester: John Wiley.

Hodnett, M. G., Tomasella, J., Marques Filho, A. D. O. & Oyama, M. D. 1997b. Deep Soil Water Uptake by Forest and Pasture in Central Amazonia: Predictions from Long-Term Daily Rainfall Data Using a Simple Water Balance Model. *In:* Gash, J. H. C., Nobre, C. A., Roberts, J. M. & Victoria, R. L., eds. *Amazonian Deforestation and Climate.* Chichester: John Wiley.

Hoffmann, W. A. & Jackson, R. B. 2000. Vegetation-Climate Feedbacks in the Conversion of Tropical Savanna to Grassland. *Journal of Climate,* 13**,** 1593-1602.

Holdridge, L. R. 1947. Determination of World Plant formations from Simple Climatic Data. *Science,* 105**,** 367-368.

Hölscher, D., De A. Sá, T.D., Bastos, T.X., Denich, M. & Fölster, H. (1997) Evaporation from Young Secondary Vegetation in Eastern Amazonia, *Journal of Hydrology*, 193, 293-305.

Horowitz, P., & Hill, W., 1964, The Art of Electronics. Cambridge University Press.

Hubbard, R. M., Ryan, M. G., Giardina, C. P. & Barnard, H. 2004. The Effect of Fertilization on Sap Flux and Canopy Conductance in a *Eucalyptus Saligna* Experimental Forest. *Global Change Biology,* 10**,** 427-436.

Hujtes, R. W. A., Klaassen, W., Kruijt, B. & Veen, A. W. L. 1991. Predicting Near-Surface Meteorological Variations Over Different Vegetation Types. *In:* Kienitz, G., Milly, P. C. D., Van Genuchten, M. T., Rosbjerg, D. & Shuttleworth, W. J., eds. Hydrological interactions Between Atmosphere, Soil and Vegetation, 1991 Vienna. *International Association of Hydrological Sciences*, 75-84.

Hutley, l. B., O'grady, A. P. & Eamus, D. 2000. Evapotranspiration from Eucalypt Open-Forest Savanna of Northern Australia. *Functional Ecology,* 14**,** 183-194.

Hutley, l. B., O'grady, A. P. & Eamus, D. 2001. Monsoonal Influences on Evapotranspiration of Savanna Vegetation of Northern Australia. *Oecologia,* 126**,** 434-443.

Imbernon, J. & Branthomme, A. 2001. Characterization of Landscape Patterns of Deforestation in Tropical Rain Forests. *International Journal of Remote Sensing,* 22**,** 1753-1765.

Irvine, M. R., Gardiner, B. A. & Hill, M. K. 1997. The Evolution of Turbulence Across a Forest Edge. *Boundary-Layer Meteorology,* 84**,** 467-496.

James, S. A., Clearwater, M. J., Meinzer, F. C. & Goldstein, G. 2002. Heat Dissipation Sensors of Variable Length for the Measurement of Sap Flow in Trees with Deep Sapwood. *Tree Physiology,* 22**,** 277-283.

James, S. A., Meinzer, F. C., Goldstein, G., Woodruff, D., Jones, T., Restom, T., Mejia, M., Clearwater, M. & Campanello, P. 2003. Axial and Radial Water Transport and Internal Water Storage in Tropical Forest Canopy Trees. *Oecologia,* 134**,** 37-45.

Jarvis, P. G. 1976. Interpretation of Variations in Leaf Water Potential and Stomatal Conductance Found in Canopies in Field. *Philosophical Transactions of the Royal Society of London Series B-Biological Sciences,* 273**,** 593-610.

Jarvis, P. G. & McNaughton, K. G. 1986. Stomatal Control of Transpiration - Scaling Up from Leaf to Region. *Advances in Ecological Research,* 15**,** 1-49.

Jimenez, M. S., Nadezhdina, N., Cermak, J. & Morales, D. 2000. Radial Variation in Sap Flow in Five Laurel Forest Tree Species in Tenerife, Canary Islands. *Tree Physiology,* 20**,** 1149-1156.

Jipp, P. H., Nepstad, D. C., Cassel, D. K. & De Carvalho, C. R. 1998. Deep Soil Moisture Storage and Transpiration in Forests and Pastures of Seasonally-Dry Amazonia. *Climatic Change,* 39**,** 395-412.

Jupp, T. E. & Twiss, S. D. 2006. A Physically Motivated Index of Subgrid-Scale Pattern. *Journal of Geophysical Research-Atmospheres,* 3, 111.

JRC – 'Joint Research Centre'. http://www-tem-jrc.it/activities.htm

Kabat, P., Claussen, M., Dirmeyer, P. A., Gash, J. H. C., Bravo de Guenni, l., Meybeck, M., Pielke SR., R. A., Vörösmarty, C. J., Hutjes, R. W. A. & Lütkemeier, S., eds., 2003. *Vegetation, Water, Humans and the Climate: A New Perspective on an interactive System*, Springer, Berlin, Heidelberg, New York.

Kapos, V. 1989. Effects of Isolation on the Water Status of Forest Patches in the Brazilian Amazon. *Journal of Tropical Ecology,* 5**,** 173-185.

Kapos, V., Ganade, G., Matsui, E. & Victoria, R. L. 1993. Partial-Derivative-C-13 As An Indicator of Edge Effects in Tropical Rain-Forest Reserves. *Journal of Ecology,* 81**,** 425-432.

Karnieli, A., Kaufman, Y. J., Remer, l. & Wald, A. 2001. AFRI - Aerosol Free Vegetation Index. *Remote Sensing of Environment,* 77**,** 10-21.

Kaufman, Y. J. & Tanre, D. 1992. Atmospherically Resistant Vegetation index (ARVI) for EOS-MODIS. *IEEE Transactions on Geoscience and Remote Sensing,* 30**,** 261-270.

Klaassen, W. 1992. Average Fluxes from Heterogeneous Vegetated Regions. *Boundary-Layer Meteorology,* 58**,** 329-354.

Klaassen, W. & Claussen, M. 1995. Landscape Variability and Surface Flux Parameterization in Climate Models. *Agricultural and Forest Meteorology,* 73**,** 181-188.

Klaassen, W., Lankreijer, H. J. M. & Veen, A. W. L. 1996. Rainfall interception Near a Forest Edge. *Journal of Hydrology,* 185**,** 349-361.

Klaassen, W. & Sogachev, A. 2006. Flux Footprint Simulation Downwind of a Forest Edge. *Boundary-Layer Meteorology,* 121**,** 459-473.

Klaassen, w., van Breugel, P. B., Moors, E. J. & Nieveen, J. P. 2002. Increased heat fluxes near a Forest edge. *Theoretical and Applied Climatology,* 72**,** 231-243.

Kleidon, A. & Heimann, M. 2000. Assessing the Role of Deep Rooted Vegetation in the Climate System with Model Simulations: Mechanism, Comparison to Observations and Implications for Amazonian Deforestation. *Climate Dynamics,* 16**,** 183-199.

Kochendorfer, J., Kyaw, T.P.U., Park, Y.S., 2007, Estimates of Horizontal Advection Using Field Measurements in a Crop Canopy. ams.confex.com/ams/pdfpapers/111168.pdf

Kohsiek, W. 1981. A Rapid-Circulation Evaporation Chamber for Measuring Bulk Stomatal-Resistance. *Journal of Applied Meteorology,* 20**,** 42-52.

Kojima, N., Laba, M., Liendo, X. M. V., Bradley, A. V., Millington, A. C. & Baveye, P. 2006. Causes of the Apparent Scale independence of Fractal indices Associated With Forest Fragmentation in Bolivia. *ISPRS Journal of Photogrammetry and Remote Sensing,* 61**,** 84-94.

Komatsu, H., Kang, Y. H., Kume, T., Yoshifuji, N. & Hotta, N. 2006a. Transpiration from a *Cryptomeria japonica* Plantation, Part 1: Aerodynamic Control of Transpiration. *Hydrological Processes,* 20**,** 1309-1320.

Komatsu, H., Kang, Y. H., Kume, T., Yoshifuji, N. & Hotta, N. 2006b. Transpiration from a *Cryptomeria japonica* Plantation, Part 2: Responses of Canopy Conductance to Meteorological Factors. *Hydrological Processes,* 20**,** 1321-1334.

Koppen, W. 1936. Das Geographische System Der Klimate. *In:* Koppen, W. & Geiger, R., eds. *Handbuch der Klimatologie, vol. 5, part C.* Berlin: Gebruder Borntrager.

Kroon, L.J.M. 1989. Profile Derived Estimation of Evaporation After A Change in Vegetative Cover: A Numerical Approach. IAHS Publ. no. 177,175.

Kroon, L. J. M. & Bink, N. J. 1996. Conditional Statistics of Vertical Heat Fluxes in Local Advection Conditions. *Boundary-Layer Meteorology,* 80**,** 49-78.

Bibliography

Kroon, L. J. M. & DeBruin, H. A. R. 1993. Atmosphere Vegetation Interaction in Local Advection Conditions - Effect of Lower Boundary-Conditions. *Agricultural and Forest Meteorology,* 64**,** 1-28.

Kroon, L. J. M. & DeBruin, H. A. R. 1995. The Crau Field Experiment - Turbulent Exchange in the Surface-Layer Under Conditions of Strong Local Advection. *Journal of Hydrology,* 166**,** 327-351.

Kruijt, B., Klaassen, W., Hutjes, R. W. A. & Veen, A. W. L. 1991. Heat and Momentum Fluxes Near a Forest Edge. *In:* Kienitz, G., Milly, P. C. D., Van Genuchten, M. T., Rosbjerg, D. & Shuttleworth, W. J., eds. Hydrological interactions Between Atmosphere, Soil and Vegetation, 1991 Vienna. *International Association of Hydrological Sciences*, 107-116.

Kumagai, T., Katul, G. G., Saitoh, T. M., Sato, Y., Manfroi, O. J., Morooka, T., Ichie, T., Kuraji, K., Suzuki, M. & Porporato, A. 2004a. Water Cycling in a Bornean Tropical Rain Forest Under Current and Projected Precipitation Scenarios. *Water Resources Research,* 40**,** 12.

Kumagai, T., Saitoh, T. M., Sato, Y., Morooka, T., Manfroi, O. J., Kuraji, K. & Suzuki, M. 2004b. Transpiration, Canopy Conductance and the Decoupling Coefficient of a Lowland Mixed Dipterocarp Forest in Sarawak, Borneo: Dry Spell Effects. *Journal of Hydrology,* 287**,** 237-251.

Kumagai, T., Saitoh, T. M., Sato, Y., Takahashi, H., Manfroi, O. J., Morooka, T., Kuraji, K., Suzuki, M., Yasunari, T. & Komatsu, H. 2005. Annual Water Balance and Seasonality of Evapotranspiration in a Bornean Tropical RainForest. *Agricultural and Forest Meteorology,* 128**,** 81-92.

Kume, T., Kuraji, K., Yoshifuji, N., Morooka, T., Sawano, S., Chong, L. & Suzuki, M. 2006. Estimation of Canopy Drying Time After Rainfall Using Sap Flow Measurements in an Emergent Tree in A Lowland Mixed-Dipterocarp Forest in Sarawak, Malaysia. *Hydrological Processes,* 20**,** 565-578.

Kushwaha, S. P. S., Kuntz, S. & Oesten, G. 1994. Applications of Image Texture in Forest Classification. *International Journal of Remote Sensing,* 15**,** 2273-2284.

Kyaw, T. P. U., Qiu, J., Sun, H. B., Watanabe, T. & Brunet, Y. 1995. Surface Renewal Analysis - A New Method to Obtain Scalar Fluxes. *Agricultural and Forest Meteorology,* 74**,** 119-137.

Lambers, H., Stuart Chapin, F. S. & PONS, T. H. Plant Physiological Ecology. *1998,* NY, Springer.

Lang, A. R. G., Evans, G. N. & Ho, P. Y. 1974. Influence of Local Advection on Evapotranspiration from Irrigated Rice in a Semi-Arid Region. *Agricultural Meteorology,* 13**,** 5-13.

Laurance, W. F. 1991. Edge Effects in Tropical Forest Fragments - Application of a Model for the Design of Nature-Reserves. *Biological Conservation,* 57**,** 205-219.

Laurance, W.F., 1997. Hyper-Disturbed Parks: Edge Effects and the Ecology of Isolated Rainforest Reserves in Tropical Australia, 71-83. *In:* Laurance, W.F. & Bierregaard, Jr., eds. Tropical Forest Remnants: Ecology, Management and Conservation of Fragmented Communities. University of Chicago Press, Chicago.

Laurance, W. F. 1999a. Gaia's Lungs. *Natural History,* 108**,** 96-96.

Laurance, W.F., 1999b. Reflections on the Tropical Deforestation Crisis. *Biological Conservation, 91, 109-117.*

Laurance, W. F. 2002. Hyperdynamism in Fragmented Habitats. *Journal of Vegetation Science,* 13**,** 595-602.

Laurance, W. F. 2004. Forest-Climate Interactions in Fragmented Tropical Landscapes. *Philosophical Transactions of the Royal Society of London Series B-Biological Sciences,* 359**,** 345-352.

Laurance, W. F. & Yensen, E. 1991. Predicting the Impacts of Edge Effects in Fragmented Habitats. *Journal of Clinical Microbiology,* 55**,** 77-92.

Laurance, W. F. & Williamson, G. B. 2001. Positive Feedbacks Among Forest Fragmentation, Drought, and Climate Change in the Amazon. *Conservation Biology,* 15**,** 1529-1535.

Laurance, W. F., Laurance, S. G., Ferreira, L. V., Rankindemerona, J. M., Gascon, C. & Lovejoy, T. E. 1997. Biomass Collapse in Amazonian Forest Fragments. *Science,* 278**,** 1117-1118.

Laurance, W. F., Ferreira, L. V., Rankin-De Merona, J. M. & Laurance, S. G. 1998a. Rain Forest Fragmentation and the Dynamics of Amazonian Tree Communities. *Ecology,* 79**,** 2032-2040.

Laurance, W. F., Laurance, S. G. & Delamonica, P. 1998b. Tropical Forest Fragmentation and Greenhouse Gas Emissions. *Forest Ecology and Management,* 110**,** 173-180.

Laurance, W. F., Delamonica, P., Laurance, S. G., Vasconcelos, H. L. & Lovejoy, T. E. 2000. Conservation – Rain Forest Fragmentation Kills Big Trees. *Nature,* 404**,** 836-836.

Laurance, W. F., Williamson, G. B., Delamonica, P., Oliveira, A., Lovejoy, T. E., Gascon, C. & Pohl, L. 2001. Effects of a Strong Drought on Amazonian Forest Fragments and Edges. *Journal of Tropical Ecology,* 17**,** 771-785.

Laurance, W. F., Lovejoy, T. E., Vasconcelos, H. L., Bruna, E. M., Didham, R. K., Stouffer, P. C., Gascon, C., Bierregaard, R. O., Laurance, S. G. & Sampaio, E. 2002. Ecosystem Decay of Amazonian Forest Fragments: A 22-year investigation. *Conservation Biology,* 16**,** 605-618.

Li, L. H. & Yu, Q. 2007. Quantifying the Effects of Advection on Canopy Energy Budgets and Water Use Efficiency in an Irrigated Wheat Field in the North China Plain. *Agricultural Water Management,* 89**,** 116-122.

Bibliography

Li, Q. L., Chen, J. Q., Song, B., Lacroix, J. J., Bresee, M. K. & Radmacher, J. A. 2007. Areas influenced By Multiple Edges and their Implications in Fragmented Landscapes. *Forest Ecology and Management,* 242**,** 99-107.

Lindsay, R. W., Percival, D. B. & Rothrock, D. A. 1996. the Discrete Wavelet Transform and the Scale Analysis of the Surface Properties of Sea Ice. *IEEE Transactions on Geoscience and Remote Sensing,* 34**,** 771-787.

Lloyd, C. R. 1995. The Effect of Heterogeneous Terrain on Micrometeorological Flux Measurements - A Case-Study from HAPEX-SAHEL. *Agricultural and Forest Meteorology,* 73**,** 209-216.

Lloyd, C. R., Gash, J. H. C., Shuttleworth, W. J. & Marques, A. D. 1988. The Measurement and Modeling of Rainfall interception By Amazonian Rain-Forest. *Agricultural and Forest Meteorology,* 43**,** 277-294.

Loescher, H. W., Gholz, H. l., Jacobs, J. M. & Oberbauer, S. F. 2005. Energy Dynamics and Modeled Evapotranspiration from A Wet Tropical Forest in Costa Rica. *Journal of Hydrology,* 315**,** 274-294.

Lopes, J. L. M. 2001. Observacoes De Umidade Do Solo Em Areas De Pastagem E Floresta Em RondoˆNia Utilizando Refletometros No Dominio Da Frequencia. *Dissertacao de mestrado*. Universidade de Sao Paulo, Sao Paulo, Brasil.

Lovejoy, S. 1982. Area-Perimeter Relation for Rain and Cloud Areas. *Science,* 216**,** 185-187.

Lovejoy, S., Schertzer, D., Tessier, Y. & Goanac'h, H. 2001. Multifractals and Resolution-Independent Remote Sensing Algorithms: The Example of Ocean Colour. *International Journal of Remote Sensing,* 22**,** 1191-1234.

Lowman, M., & Rinker, H.B., 2004, Forest Canopies. Elsevier

Lu, P. 1997. A Direct Method for Estimating the Average Sap Flux Density Using a Modified Granier Measuring System. *Australian Journal of Plant Physiology,* 24**,** 701-705.

Lynn, B. H., Rind, D. & Avissar, R. 1995. The Importance of Mesoscale Circulations Generated By Subgrid-Scale Landscape Heterogeneities in General-Circulation Models. *Journal of Climate,* 8**,** 191-205.

Lyra, R. F. F., Molion, L. C. B., Da Silva, M. R. G., Fisch, G. & Nobre, C. A. 2003. Some Aspects of the Atmospheric Boundary Layer Over Western Amazonia: Dry Season 1994. *Revista Brasileira de Meteorologia,* 18**,** 79-85.

Malcolm, J. R. 1994. Edge Effects in Central Amazonian Forest Fragments. *Ecology,* 75**,** 2438-2445.

Malhi,Y., Nobre, A.D., Grace,J., Kruijt, B., Pereira, M.G.P., Culf, A. & Scott, S. 1998. Carbon Dioxide Transfer Over a Central Amazonian Rain Forest. - geog.ox.ac.uk

Malingreau, J.P., Achard, F., D'Souza, G., Stibig, H.J., D'Souza, J., Estreguil, C., & Eva, H. 1995. The AVHRR for Global Tropical Forest Monitoring: Lessons of the Trees Project. *Remote Sensing Reviews*, 12 29–40.

Mallat, S. & Zhong, S. 1992. Characterization of Signals from Multiscale Edges. *IEEE Transactions on Pattern Analysis and Machine intelligence,* 14**,** 710-732.

Mallat, S. G. 1989. A theory for Multiresolution Signal Decomposition - The Wavelet Representation. *IEEE Transactions on Pattern Analysis and Machine Intelligence,* 11**,** 674-693.

Mandelbrot, B.B., 1967. How Long is the Coast of Britain? Statistical Self-Similarity and Fractional Dimension*. Science,* 156, 3775, 636-638.

Mandelbrot, B.B., 1975. LES OJECTS Fractals: Forme, Hasard et Dimension. Flammarion Press.

Mandelbrot, B. 1982. The Fractal Geometry of Nature. W. H. Freeman: San Francisco.

Markham, B. L. & Townshend, J. R. G. 1981. Land Cover Classification Accuracy as a Function of Sensor Spatial Resolution. *Proc. of 15th International Symposium on Remote Sensing of the Environment.* West Lafayette, In.

Marsh, C.W., 1995. Danum Valley Conservation Area Management Plan 1995-2000, Sabah. *Yayasan Sabah and Innoprise Corporation Sdn Bhd, Kota Kinabalu, Sabah, Malaysia*, *unpublished report.*

Marsh, C. W. & Greer, A. G. 1992. Forest Land-Use in Sabah, Malaysia - An Introduction to Danum Valley. *Philosophical Transactions of the Royal Society of London Series B-Biological Sciences,* 335**,** 331-339.

Mas, J. F., Puig, H., Palacio, J. L. & Sosa-Lopez, A. 2004. Modelling Deforestation Using GIS and Artificial Neural Networks. *Environmental Modelling & Software,* 19**,** 461-471.

Mason, P. J. 1988. The Formation of Areally-Averaged Roughness Lengths. *Quarterly Journal of the Royal Meteorological Society,* 114**,** 399-420.

Matlack, G. R. 1993. Microenvironment Variation Within and Among Forest Edge Sites in the Eastern United-States. *Biological Conservation,* 66**,** 185-194*.*

MATLAB, Mathworks Inc. www.mathworks.com.

MATLAB Users Guide, MATLAB, Mathworks Inc. www.mathworks.com.

Mayaux, P. & Lambin, E. F. 1995. Estimation of Tropical Forest Area from Coarse Spatial-Resolution Data - A 2-Step Correction Function for Proportional Errors Due to Spatial Aggregation. *Remote Sensing of Environment,* 53**,** 1-15.

Mayaux, P. & Lambin, E. F. 1997. Tropical Forest Area Measured from Global Land-Cover Classifications: Inverse Calibration Models Based on Spatial Textures. *Remote Sensing of Environment,* 59**,** 29-43.

Mayaux, P., Achard, F. & Malingreau, J. P. 1998. Global Tropical Forest Area Measurements Derived from Coarse Resolution Satellite Imagery: A Comparison With Other Approaches. *Environmental Conservation,* 25**,** 37-52.

Mayaux, P., Richards, T. & Janodet, E. 1999. A Vegetation Map of Central Africa Derived from Satellite Imagery. *Journal of Biogeography,* 26**,** 353-366.

Mayaux, P., Holmgren, P., Achard, F., Eva, H., Stibig, H. & Branthomme, A. 2005. Tropical Forest Cover Change in the 1990s and Options for Future Monitoring. *Philosophical Transactions of the Royal Society B-Biological Sciences,* 360**,** 373-384.

Mcaneney, k. J., Brunet, Y. & Itier, B. 1994. Downwind Evolution of Transpiration by 2 Irrigated Crops Under Conditions of Local Advection. *Journal of Hydrology,* 161**,** 375-388.

McNaughton, K. G. 1976a. Evaporation and Advection. 1. Evaporation from Extensive Homogeneous Surfaces. *Quarterly Journal of the Royal Meteorological Society,* 102**,** 181-191.

McNaughton, K. G. 1976b. Evaporation and Advection. 2. Evaporation Downwind of a Boundary Separating Regions Having Different Surface Resistances and Available Energies. *Quarterly Journal of the Royal Meteorological Society,* 102**,** 193-202.

McNaughton, K.G. & Jarvis, P.G., 1983. Predicting Effects of Vegetation Changes on Transpiration and Evaporation. *Water deficits and plant growth*, Academic Press

McGarigal, K., S. A. Cushman, M. C. Neel, & E. Ene. 2002. FRAGSTATS: Spatial Pattern Analysis Program for Categorical Maps. Computer software program produced by the authors at the University of Massachusetts, Amherst. Available at the following web site: www.umass.edu/landeco/research/fragstats/fragstats.html

McWilliam, A.-L. C., Cabral, O. M. L., Gomes, B. M., Esteves, J. L. & Roberts, J. M. 1996. Forest and Pasture Leaf-Gas Exchange in South-Western Amazonia. *In:* Gash, J. H. C., Nobre, C. A., Roberts, J. M. & Victoria, R. L., eds. *Amazonian Deforestation and Climate.* Chichester: John Wiley.

McWilliam, A. L. C., Roberts, J. M., Cabral, O. M. R., Leitao, M., DeCosta, A. C. L., Maitelli, G. T. & Zamparoni, C. 1993. Leaf-Area index and Aboveground Biomass of Terra-Firme Rain-Forest and Adjacent Clearings in Amazonia. *Functional Ecology,* 7**,** 310-317.

Meentemeyer, V., 1989. Geographical Perspectives of Space, Time and Scale. *Landscape Ecology*, 3, 163-173

Meinzer, F. C., Goldstein, G., Holbrook, N. M., Jackson, P. & Cavelier, J. 1993. Stomatal and Environmental-Control of Transpiration in A Lowland Tropical Forest Tree. *Plant Cell and Environment,* 16**,** 429-436.

Meinzer, F. C., Andrade, J. L., Goldstein, G., Holbrook, N. M., Cavelier, J. & Jackson, P. 1997. Control of Transpiration from the Upper Canopy of a Tropical Forest: the Role of Stomatal, Boundary Layer and Hydraulic Architecture Components. *Plant Cell and Environment,* 20**,** 1242-1252.

Meinzer, F. C., Clearwater, M. J. & Goldstein, G. 2001a. Water Transport in Trees: Current Perspectives, New insights and Some Controversies. *Environmental and Experimental Botany,* 45**,** 239-262.

Meinzer, F. C., Goldstein, G. & Andrade, J. L. 2001b. Regulation of Water Flux Through Tropical Forest Canopy Trees: Do Universal Rules Apply? *Tree Physiology,* 21**,** 19-26.

Meinzer, F. C., James, S. A., Goldstein, G. & Woodruff, D. 2003. Whole-Tree Water Transport Scales with Sapwood Capacitance in Tropical Forest Canopy Trees. *Plant Cell and Environment,* 26**,** 1147-1155.

Mesquita, R. C. G., Delamonica, P. & Laurance, W. F. 1999. Effect of Surrounding Vegetation on Edge-Related Tree Mortality in Amazonian Forest Fragments. *Biological Conservation,* 91**,** 129-134.

Millington, A.C., Velez-Liendo, X.M., Bradley, A.V. 2003. Scale Dependence in Multitemporal Mapping of Forest Fragmentation in Bolivia: Implications for Explaining Temporal Trends in Landscape Ecology and Applications to Biodiversity Conservation. *ISPRS Journal of Photogrammetry and Remote Sensing*, 57, 289-299.

Monteith, J. L. 1965. Evaporation and Environment. *Symposium of Experimental Biology,* 19**,** 205-34.

Moody, A. & Woodcock, C. E. 1994. Scale-Dependent Errors in the Estimation of Land-Cover Proportions - Implications for Global Land-Cover Datasets. *Photogrammetric Engineering and Remote Sensing,* 60**,** 585-594.

Mooney, H. A., Pearcy, R. W. & Ehleringer, J. 1987. Plant Physiological Ecology today. *Bioscience,* 37**,** 18-20.

Moorcroft, P. R. 2003. Recent Advances in Ecosystem-Atmosphere interactions: An Ecological Perspective. *Proceedings of the Royal Society B-Biological Sciences,* 270**,** 1215-1227.

Murcia, C. 1995. Edge Effects in Fragmented Forests - Implications for Conservation. *Trends in Ecology & Evolution,* 10**,** 58-62.

Myers, N. 1996. The World's Forests: Problems and Potentials. *Environmental Conservation,* 23, 156–169.

Myint, S. W. 2003. Fractal Approaches in Texture Analysis and Classification of Remotely Sensed Data: Comparisons with Spatial Autocorrelation Techniques and Simple Descriptive Statistics. *International Journal of Remote Sensing,* 24**,** 1925-1947.

Myint, S. W. 2006. A New Framework for Effective Urban Land Use and Land Cover Classification: A Wavelet Approach. *GIS Science & Remote Sensing,* 43**,** 155-178..

Myint, S. W., Lam, N. S. N. & Tyler, J. M. 2002. An Evaluation of Four Different Wavelet Decomposition Procedures for Spatial Feature Discrimination in Urban Areas. *Transactions in GIS,* 6**,** 403-429.

Myint, S. W., Lam, N. S. N. & Tyler, J. M. 2004. Wavelets for Urban Spatial Feature Discrimination: Comparisons with Fractal, Spatial Autocorrelation, and Spatial Co-Occurrence Approaches. *Photogrammetric Engineering and Remote Sensing,* 70**,** 803-812.

Nadezhdina, N., Cermak, J. & Ceulemans, R. 2002. Radial Patterns of Sap Flow in Woody Stems of Dominant and Understory Species: Scaling Errors Associated With Positioning of Sensors. *Tree Physiology,* 22**,** 907-918.

Naot, O. & Mahrer, Y. 1991. 2- Dimensional Microclimate Distribution Within and Above A Crop Canopy in an Arid Environment - Modelling and Observational Studies. *Boundary-Layer Meteorology,* 56**,** 223-244.

Nascimento, H. E. M., Andrade, A. C. S., Camargo, J. L. C., Laurance, W. F., Laurance, S. G. & Ribeiro, J. E. L. 2006. Effects of the Surrounding Matrix on Tree Recruitment in Amazonian Forest Fragments. *Conservation Biology,* 20**,** 853-860.

Nascimento, H. E. M. & Laurance, W. F. 2002. Total Aboveground Biomass in Central Amazonian Rain Forests: A Landscape-Scale Study. *Forest Ecologyand Management,* 168**,** 311-321.

Nascimento, H. E. M. & Laurance, W. F. 2004. Biomass Dynamics in Amazonian Forest Fragments. *Ecological Applications,* 14**,** S127-S138.

Neal, C., Robson, A. J., Hall, R. L., Ryland, G., Conway, T. & Neal, M. 1993. Hydrological Impacts of Hardwood Plantation in Lowland Britain - Preliminary Findings on Interception at a Forest Edge, Black-Wood, Hampshire, Southern England. *Journal of Hydrology,* 146**,** 459-459.

Newbery, D. M., Campbell, E. J. F., Lee, Y. F., Ridsdale, C. E. & Still, M. J. 1992. Primary Lowland Dipterocarp Forest at Danum Valley, Sabah, Malaysia - Structure, Relative Abundance and Family Composition. *Philosophical Transactions of the Royal Society of London Series B-Biological Sciences,* 335**,** 341-356.

Niedermeier, A., Romaneessen, E. & Lehner, S. 2000. Detection of Coastlines in SAR Images Using Wavelet Methods. *IEEE Transactions on Geoscience and Remote Sensing,* 38**,** 2270-2281.

Nieuwnhuis, C.J.M. (2005). MSc Thesis. Faulty of Earth and Life Sciences, Vrije Universiteit Amsterdam, the Netherlands. May 2005.

Nik Muhamad, M., Mohd Basri, H. & Shaharuddin, A. 1979. Rainfall Interception, Throughfall and Stemflow in a Secondary Forest. *Pertanika,* 2**,** 152-154.

Noilhan, J., Lacarrere, P., Dolman, A. J. & Blyth, E. M. 1997. Defining Area-Average Parameters in Meteorological Models for Land Surfaces with Mesoscale Heterogeneity. *Journal of Hydrology,* 190**,** 302-316.

Nussbaum, R. (1991). Water and Nutrient Dynamics in Rain Forests After Logging. *Unpublished report*, University of Exeter.

O'Brien, J. J., Oberbauer, S. F. & Clark, D. B. 2004. Whole Tree Xylem Sap Flow Responses to Multiple Environmental Variables in a Wet Tropical Forest. *Plant Cell and Environment,* 27**,** 551-567.

O'Neill, R. V., Milne, B. T., Turner, M. G. & Gardner, R. H. 1988. Resource Utilization Scales and Landscape Pattern. *Landscape Ecology,* 2**,** 63-69.

Oke, T.R., 1983. Boundary Layer Climates. 2nd ed. Methuen, New York, NY, USA.

Okuda, T., Suzuki, M., Adachi, N., Quah, E. S., Hussein, N. A. & Manokaran, N. 2003. Effect of Selective Logging on Canopy and Stand Structure and Tree Species Composition in a Lowland Dipterocarp Forest in Peninsular Malaysia. *Forest Ecology and Management,* 175**,** PII S0378-1127(02)00137-8.

Oliveira, R. S., Bezerra, L., Davidson, E. A., Pinto, F., Klink, C. A., Nepstad, D. C. & Moreira, A. 2005. Deep Root Function in Soil Water Dynamics in Cerrado Savannas of Central Brazil. *Functional Ecology,* 19**,** 574-581.

Openshaw, S. 1984. The Modifiable Areal Unit Problem. *Concepts and Techniques in Modern Geography*, 38, 41.

Oren, R. & Pataki, D. E. 2001. Transpiration in Response to Variation in Microclimate and Soil Moisture in Southeastern Deciduous Forests. *Oecologia,* 127**,** 549-559.

Oren, R., Phillips, N., Ewers, B. E., Pataki, D. E. & Megonigal, J. P. 1999a. Sap-Flux-Scaled Transpiration Responses to Light, Vapor Pressure Deficit, and Leaf Area Reduction in a Flooded *Taxodium Distichum* Forest. *Tree Physiology,* 19**,** 337-347.

Oren, R., Sperry, J. S., Ewers, B. E., Pataki, D. E., Phillips, N. & Megonigal, J. P. 2001. Sensitivity of Mean Canopy Stomatal Conductance to Vapor Pressure Deficit in a Flooded *Taxodium Distichum* Forest: Hydraulic and Non-Hydraulic Effects. *Oecologia,* 126**,** 21-29.

Oren, R., Sperry, J. S., Katul, G. G., Pataki, D. E., Ewers, B. E., Phillips, N. & Schafer, K. V. R. 1999b. Survey and Synthesis of Intra- and Interspecific Variation in Stomatal Sensitivity to Vapour Pressure Deficit. *Plant Cell and Environment,* 22**,** 1515-1526.

Parrinello, T. & Vaughan, R. A. 2002. Multifractal Analysis and Feature Extraction in Satellite Imagery. *International Journal of Remote Sensing,* 23**,** 1799-1825.

Pataki, D. E., Oren, R. & Phillips, N. 1998. Responses of Sap Flux and Stomatal Conductance of *Pinus taeda* l. Trees to stepwise reductions in leaf area. *Journal of Experimental Botany,* 49**,** 871-878.

Pecknold, S., Lovejoy, S., Schertzer, D. & Hooge, C. 1997. Multifractals and Resolution Dependence of Remotely Sensed Data. *In:* Quattrochi, D. A. & Goodchild, M. F., eds. *Scale in Remote Sensing and GIS.* Washington DC: Lewis Publishers.

Pereira, A. R. 2004. The Priestley-Taylor Parameter and the Decoupling Factor for Estimating Reference Evapotranspiration. *Agricultural and Forest Meteorology,* 125**,** 305-313.

Pereira, F.L., Gash, J.H.C., David, J.S., Valente, F., 2009. Evaporation of intercepted Rainfall from Isolated Evergreen Oak Trees: Do the Crowns Behave Like Wet Bulbs? *Agricultural and Forest Meteorology*, 149, 667-679.

Pesaresi, M. 2000. Texture Analysis for Urban Pattern Recognition Using Fine-Resolution Panchromatic Satellite Imagery. *Geographical and Environmental Modelling,* 4**,** 43-63.

Philip, J. R. 1959. The Theory of Local Advection. *Journal of Meteorology,* 16**,** 535-547.

Philip, J. R. 1987. Advection, Evaporation, and Surface-Resistance. *Irrigation Science,* 8**,** 101-114.

Phillips, N., Bond, B. J. & Ryan, M. G. 2001. Gas Exchange and Hydraulic Properties in the Crowns of Two Tree Species in a Panamanian Moist Forest. *Trees-Structure and Function,* 15**,** 123-130.

Phillips, N. & Oren, R. 1998. A Comparison of Daily Representations of Canopy Conductance Based on Two Conditional Time-Averaging Methods and the Dependence of Daily Conductance on Environmental Factors. *Annales Des Sciences Forestieres,* 55**,** 217-235.

Phillips, N., Oren, R. & Zimmermann, R. 1996. Radial Patterns of Xylem Sap Flow in Non-, Diffuse-, and Ring-Porous Tree Species. *Plant Cell and Environment,* 19**,** 983-990.

Phillips, N., Oren, R., Zimmermann, R. & Wright, S. J. 1999. Temporal Patterns of Water Flux in Trees and Lianas in a Panamanian Moist Forest. *Trees- Structure and Function,* 14**,** 116-123.

Pielke, R. A. 2001. Influence of the Spatial Distribution of Vegetation and Soils on the Prediction of Cumulus Convective Rainfall. *Reviews of Geophysics,* 39**,** 151-177.

Pielke, R. A., Avissar, R., Raupach, M., Dolman, A. J., Zeng, X. B. & Denning, A. S. 1998. Interactions Between the Atmosphere and Terrestrial Ecosystems: Influence on Weather and Climate. *Global Change Biology,* 4**,** 461-475.

Pinard, M. A. & Putz, F. E. 1996. Retaining Forest Biomass by Reducing Logging Damage. *Biotropica,* 28**,** 278-295.

Pinker, R.T., Thompson, O.E. & Eck, T.F. 1980. The Energy Balance of a Tropical Evergreen Forest, *Journal of Applied Meteorology*, 19, 1,341-349.

Pitman, A., Pielke S.R., R., Avissar, R., Claussen, M., Gash, J. & Dolman, H. 2003. The Role of the Land Surface in Weather and Climate: Does the Land Surface Matter? *IGBP Newsletter.*

Pitman, A. J., Narisma, G. T., Pielke, R. A. & Holbrook, N. J. 2004. Impact of Land Cover Change on the Climate of Southwest Western Australia. *Journal of Geophysical Research-Atmospheres,* 109.

Polcher, J. 1995. Sensitivity of Tropical Convection to Land-Surface Processes. *Journal of the Atmospheric Sciences,* 52**,** 3143-3161.

Poyatos, R., Cermak, J. & Llorens, P. 2007. Variation in the Radial Patterns of Sap Flux Density in Pubescent Oak (*Quercus pubescens*) and its Implications for Tree and Stand Transpiration Measurements. *Tree Physiology,* 27**,** 537-548.

Priestley, C. H. B. & Taylor, R. J. 1972. On the Assessment of Surface Heat Flux and Evaporation Using Large-Scale Parameters. *Monthly Weather Review,* 100**,** 81-92.

Proctor, J., Anderson, J. M., Chai, P. & Vallack, H. W. 1983. Ecological-Studies in 4 Contrasting Lowland Rain Forests in Gunung-Mulu National-Park, Sarawak. 1. Forest Environment, Structure and Floristics. *Journal of Ecology,* 71**,** 237-260.

Proctor, J., Lee, Y. F., Langley, A. M., Munro, W. R. C. & Nelson, T. 1988. Ecological-Studies on Gunung Silam, a Small Ultrabasic Mountain in Sabah, Malaysia. 1. Environment, Forest Structure and Floristics. *Journal of Ecology,* 76**,** 320-340.

Prueger, J. H., Hatfield, J. L., Aase, J. K. & Pikul, J. L. 1997. Bowen-ratio Comparisons with Lysimeter Evapotranspiration. *Agronomy Journal,* 89**,** 730-736.

Quattrochi, D. A. & Atkinson, P. M. 1999. Introduction to this Special Issue on Geostatistics and Scaling of Remote Sensing and Spatial Data. *Photogrammetric Engineering and Remote Sensing,* 65**,** 40-40.

Rabin, R. M., Stadler, S., Wetzel, P. J., Stensrud, D. J. & Gregory, M. 1990. Observed Effects of Landscape Variability on Convective Clouds. *Bulletin of the American Meteorological Society,* 71**,** 272-280.

Rao, K. S., Wyngaard, J. C. & Cote, O. R. 1974. Structure of 2-Dimensional Internal Boundary-Layer Over A Sudden Change of Surface-Roughness. *Journal of the Atmospheric Sciences,* 31**,** 738-746.

Raynor, G. S. 1971. Wind and Temperature Structure in a Coniferous Forest and a Contiguous Field. *Forest Science,* 17**,** 351-&.

Richards, J.F. & Flint, E.P., 1994. Historic Land Use and Carbon Estimate for South and Southeast Asia: 1880±1980. *In:* Daniels, R.C. (ed.). Carbon Dioxide information Analysis Center, OakRidge National Laboratory, Environmental Sciences Division, Publication No. 4174.

Richards, T., Gallego, J. & Achard, F. 2000. Sampling for Forest Cover Change Assessment at the Pan-Tropical Scale. *International Journal of Remote Sensing,* 21**,** 1473-1490.

Rider, N. E., Philip, J. R. & Bradley, E. F. 1963. The Horizontal Transport of Heat and Moisture - A Micrometeorological Study. *Quarterly Journal of the Royal Meteorological Society,* 89**,** 507-531.

Riitters, K. H., O'Neill, R. V., Hunsaker, C. T., Wickham, J. D., Yankee, D. H., Timmins, S. P., Jones, K. B. & Jackson, B. L. 1995. A Factor-Analysis of Landscape Pattern and Structure Metrics. *Landscape Ecology,* 10**,** 23-39.

Roberts, J.M., 1983. Forest Transpiration: A Conservative Hydrological Process? *Hydrology*, 66, 133–141.

Roberts, J., O. M. R. Cabral, J. P. De Costa, A. L. C. McWilliam & T. D. De A. SÁ, 1996: An Overview of the Leaf Area index and Physiological Measurements during ABRACOS. *Amazonian Deforestation and Climate,* J. H. C. Gash, C. A. Nobre, J. M. Roberts & Victoria, R. L ., eds. John Wiley, 287–306.

Roberts, J., Cabral, O. M. R., Fisch, G., Molion, L. C. B., Moore, C. J. & Shuttleworth, W. J. 1993. Transpiration from An Amazonian Rain-Forest Calculated from Stomatal Conductance Measurements. *Agricultural and Forest Meteorology,* 65**,** 175-196.

Robinson, W.S., 1950. Ecological Correlations and the Behaviour of Individuals. *American Sociological Review*, 15, 351-357.

Rosenberg, N.J 1969. Advective Contribution of Energy Utilized in Evaportranspiration By Alfalfa in East Central Great Plains (USA). *Agricultural Meteorology,* 6**,** 179-&.

Rosenberg, N. J., Blad, B.L., & Verma, S.B. 1983. *Microclimate: the Biological Environment,* New York, John Wiley and Sons.

Roy, S. B. & Avissar, R. 2000. Scales of Response of the Convective Boundary Layer to Land-Surface Heterogeneity. *Geophysical Research Letters,* 27**,** 533-536.

Roy, S. B., Weaver, C. P., Nolan, D. S. & Avissar, R. 2003. A Preferred Scale for Landscape forced Mesoscale Circulations? *Journal of Geophysical Research-Atmospheres,* 108.

Rudel, T. & Roper, J. 1997. Forest Fragmentation in the Humid Tropics: A Cross-National Analysis. *Singapore Journal of Tropical Geography,* 18**,** 99-109.

Sa, T. D., Da Costa, P. R. & Roberts, J. M. 1996. Forest and Pasture Conductances in Southern Pará, Amazonia. *In:* Gash, J. H. C., NOBRE, C. A., Roberts, J. M. & Victoria, R. L., eds. *Amazonian Deforestation and Climate.* Chichester: John Wiley.

Sagar, R. & Singh, J. S. 2006. Tree Density, Basal Area and Species Diversity in a Disturbed Dry Tropical Forest of Northern india: Implications for Conservation. *Environmental Conservation,* 33**,** 256-262.

Santos, B. A., Peres, C. A., Oliveira, M. A., Grillo, A., Alves-Costa, C. P. & Tabarelli, M. 2008. Drastic Erosion in Functional Attributes of Tree Assemblages in Atlantic Forest Fragments of Northeastern Brazil. *Biological Conservation,* 141**,** 249-260.

Saunders, D. A., Hobbs, R. J. & Margules, C. R. 1991. Biological Consequences of Ecosystem Fragmentation - A Review. *Conservation Biology,* 5**,** 18-32.

Savill, P. S. 1983. Silviculture in Windy Climates. *Commonwealth Forestry Bureau,* 44**,** 473-483.

Scatena, F. N. 1990. Watershed Scale Rainfall interception on 2 Forested Watersheds in the Luquillo Mountains of Puerto-Rico. *Journal of Hydrology,* 113**,** 89-102.

Schellekens, J., Scatena, F. N., Bruijnzeel, L. A. & Wickel, A. J. 1999. Modelling Rainfall Interception by A Lowland Tropical Rain Forest in Northeastern Puerto Rico. *Journal of Hydrology,* 225**,** 168-184.

Semler, L. & Dettori, L. 2007. A Comparison of Wavelet-Based and Ridgelet-Based Texture Classification of Tissues in Computed Tomography. *Advances in Computer Graphics and Computer Vision,* 4**,** 240-250.

Sgrenzaroli, M., DE Grandi, G. F., Eva, H. & Achard, F. 2002. Tropical Forest Cover Monitoring: Estimates from the GRFM JERS-1 Radar Mosaics Using Wavelet Zooming Techniques and Validation. *International Journal of Remote Sensing,* 23**,** 1329-1355.

Sheikholeslami, G., Zhang, A. & Bian, L. 1999. A Multi-Resolution Content-Based Retrieval Approach for Geographic Images. *Geoinformatica,* 3**,** 109-139.

Sheil, D. 1995. A Critique of Permanent Plot Methods and Analysis with Examples from Budongo-Forest, Uganda. *Forest Ecology and Management,* 77**,** 11-34.

Shuttleworth, W., 1988. Macrohydrology - The New Challenge for Process Hydrology. *Journal of Hydrology*, 100, 31.

Shuttleworth, W. J., 1989. Micrometeorology of Temperate and Tropical Forest. *Philosophical Transactions of the Royal Society of London B,* 324,299–334.

Shuttleworth, W. J. & Calder, I. R. 1979. Has the Priestley-Taylor Equation Any Relevance to Forest Evaporation? *Journal of Applied Meteorology,* 18**,** 639-646.

Shuttleworth, W. J., Gash, J. H. C., Lloyd, C. R., Moore, C. J., Roberts, J., Marques, A. D., Fisch, G., Silva, V. D., Ribeiro, M. D. G., Molion, L. C. B., Sa, L. D. D., Nobre, J. C. A., Cabral, O. M. R., Patel, S. R. & Demoraes, J. C. 1984. Eddy-Correlation Measurements of Energy Partition for Amazonian Forest. *Quarterly Journal of the Royal Meteorological Society,* 110**,** 1143-1162.

Shuttleworth, W.J., Bastable, H.G., Dallarosa, R.L.G., Fisch, G., Nobre, C.A., 1993. Observations of Climate, Albedo, and Surface Radiation Over Cleared and Undisturbed Amazonian Forest. *International Journal of Climatology*, 13,783-796

Sinun, W., Meng, W. W., Douglas, I. & Spencer, T. 1992. Throughfall, Stemflow, Overland-Flow and Throughflow in the Ulu Segama Rain-Forest, Sabah, Malaysia. *Philosophical Transactions of the Royal Society of London Series B-Biological Sciences,* 335**,** 389-395.

Skole, D. & Tucker, C. 1993. Tropical Deforestation and Habitat Fragmentation in the Amazon - Satellite Data from 1978 to 1988. *Science,* 261**,** 1104-1104.

Slik, J. W. F. 2005. Assessing Tropical Lowland Forest Disturbance Using Plant Morphological and Ecological Attributes. *Forest Ecology and Management,* 205**,** 241-250.

Smith, D. M. & Allen, S. J. 1996. Measurement of Sap Flow in Plant Stems. *Journal of Experimental Botany,* 47**,** 1833-1844.

Smith, D. M., Jarvis, P. G. & Odongo, J. C. W. 1997. Energy Budgets of Windbreak Canopies in the Sahel. *Agricultural and Forest Meteorology,* 86**,** 33-49.

Snyder, R. L., Paw, K. T., Spano, D. & Duce, P. 1997. Surface Renewal Estimates of Evapotranspiration- Theory. *Second International Symposium on Irrigation of Horticultural Crops, Volumes 1 and 2***,** 49-55.

Sodhi, N.S., & Brook, B.W., 2006. Southeast Asian Biodiversity Crisis. *Cambridge University Press. 05218393000.*

Sogachev, A., Leclerc, M. Y., Karipot, A., Zhang, G. & Vesala, T. 2005. Effect of Clearcuts on Footprints and Flux Measurements above a Forest Canopy. *Agricultural and Forest Meteorology,* 133**,** 182-196.

Somerville, A. 1980. Wind Stability - Forest Layout and Silviculture. *New Zealand Journal of Forestry Science,* 10**,** 476-501.

Souza, E. P., Renno, N. O. & Dias, M. 2000. Convective Circulations Induced By Surface Heterogeneities. *Journal of the Atmospheric Sciences,* 57**,** 2915-2922.

Spano, D., Duce, P., Snyder, R. L. & Paw, K. T. 1997a. Surface Renewal Estimates of Evapotranspiration- Tall canopies. *Second International Symposium on Irrigation of Horticultural Crops, Volumes 1 and 2***,** 63-68.

Spano, D., Duce, P., Snyder, R. L., Paw, K. T. & Ferreira, M. I. 2000a. Estimating Tree and Vine Evapotranspiration with Emphasis on Surface Renewal. *Proceedings of the Third International Symposium on Irrigation of Horticultural Crops, Volumes 1 and 2***,** 37-43.

Spano, D., Snyder, R. L., Duce, P. & Paw, K. T. 2000b. Estimating Sensible and Latent Heat Flux Densities from Grapevine Canopies Using Surface Renewal. *Agricultural and Forest Meteorology,* 104**,** 171-183.

Spano, D., Snyder, R. L., Duce, P. & U, K. T. P. 1997b. Surface Renewal Analysis for Sensible Heat Flux Density Using Structure Functions. *Agricultural and Forest Meteorology,* 86**,** 259-271.

Sperry J.S. & Tyree M.T. 1988. Mechanism of Water Stress-Induced Xylem Embolism. *Plant Physiology*, 88, 581-587.

Stohlgren, T. J., Chase, T. N., Pielke, R. A., Kittel, T. G. F. & Baron, J. S. 1998. Evidence That Local Land Use Practices Influence Regional Climate, Vegetation, and Stream Flow Patterns in Adjacent Natural Areas. *Global Change Biology,* 4**,** 495-504.

Tanaka, N., Kume, T., Yoshifuji, N., Tanaka, K., Takizawa, H., Shiraki, K., Tantasirin, C., Tangtham, N. & Suzuki, M. 2008. A Review of Evapotranspiration Estimates from Tropical Forests in Thailand and Adjacent Regions. *Agricultural and Forest Meteorology,* 148**,** 807-819.

Taylor, P. J., Nuberg, I. K. & Hatton, T. J. 2001. Enhanced Transpiration in Response to Wind Effects at the Edge of a Blue Gum (*Eucalyptus globulus*) plantation. *Tree Physiology,* 21**,** 403-408.

Tessier, Y., Lovejoy, S., Hubert, P., Schertzer, D. & Pecknold, S. 1996. Multifractal Analysis and Modelling of Rainfall and River Flows and Scaling, Causal Transfer Functions. *Journal of Geophysical Research-Atmospheres,* 101**,** 26427-26440.

Thom, A.S. & H.R. Oliver. 1977. On Penman's Equation for Estimating Regional Evaporation. *Quarterly Journal of the Royal Meteorological Society,* 103, 345–357.

Tinker, D. B., Resor, C. A. C., Beauvais, G. P., Kipfmueller, K. F., Fernandes, C. I. & Baker, W. L. 1998. Watershed Analysis of Forest Fragmentation by Clearcuts and Roads in a Wyoming Forest. *Landscape Ecology,* 13**,** 149-165.

Todd, R. W., Evett, S. R. & Howell, T. A. 2000. The Bowen Ratio-Energy Balance Method for Estimating Latent Heat Flux of Irrigated Alfalfa Evaluated in A Semi-Arid, Advective Environment. *Agricultural and Forest Meteorology,* 103**,** 335-348.

Torrence, C. & Compo, G. P. 1998. A Practical Guide to Wavelet Analysis. *Bulletin of the American Meteorological Society,* 79**,** 61-78.

Townsend, J. R. G. & Justice, C. O. 1988. Selecting the Spatial-Resolution of Satellite Sensors Required for Global Monitoring of Land Transformations. *International Journal of Remote Sensing,* 9**,** 187-236.

Tucker, C.J., Grant, D.M., Dykstra, J.D., 2004. NASA'S Global Orthorectified Landsat Data Set. *Photogrammetric Engineering & Remote Sensing*, 70, 313–322.

Turner, M. G., O'Neill, R. V., Gardner, R. H. & Milne, B. T. 1989. Effects of Changing Spatial Scale on the Analysis of Landscape Pattern. *Landscape Ecology,* 3**,** 153-162.

Tyree, M.T., Fiscus, E.L., Wullschleger, S.D. & Dixon, M.A. 1986. Detection of Xylem Cavitation in Corn Under Field Conditions. *Plant Physiology*, 82, 597-599.

TREES – 'Tropical Rainforest Environment Observation by Satellite'. http://www-tem.jrc.it/activities.htm)

Ubarana, B. N. 1996. Observation and Modelling of Rainfall Interception Loss in Two Experimental Sites in Amazonian Forest. *In:* Gash, J. H. C., Nobre, C. A., Roberts, J. M. & Victoria, R. L., eds. *Amazonian Deforestation and Climate.* Chichester: John Wiley.

Uuemaa, E., Roosaare, J. & Mander, U. 2005. Scale Dependence of Landscape Metrics and their Indicatory Value for Nutrient and Organic Matter Losses from Catchments. *Ecological indicators,* 5**,** 350-369.

Van Atta, C.W., 1977. Effect of Coherent Structures on Structure Functions of Temperature in the Atmospheric Boundary Layer. *Archives of Mechanics*, 29, 161–171.

Van Breugel, P. B., Klaassen, W. & Moors, E. J. 1999a. Fetch Requirements Near A Forest Edge. *Physics and Chemistry of the Earth Part B-Hydrology Oceans and Atmosphere,* 24**,** 125-131.

Van Breugel, P. B., Klaassen, W. & Moors, E. J. 1999b. The Spatial Variability of Turbulence Above A Forest. *Theoretical and Applied Climatology,* 62**,** 43-50.

Bibliography

Veen, A. W. L., Hutjes, R. W. A., Klaassen, W., Kruijt, B. & Lankreijer, H. K. M. 1991. Evaporative Conditions Across A Grass-Forest Boundary: A Comment on the Strategy for Regionalizing Evaporation. *In:* Kienitz, G., Milly, P. C. D., Van Genuchten, M. T., Rosbjerg, D. & Shuttleworth, W. J., eds. Hydrological interactions Between Atmosphere, Soil and Vegetation, 1991 Vienna. *International Association of Hydrological Sciences*, 43-52.

Veen, A. W. L., Klaassen, W., Kruijt, B. & Hutjes, R. W. A. 1996. Forest Edges and the Soil-Vegetation-Atmosphere Interaction at the Landscape Scale: the State of Affairs. *Progress in Physical Geography,* 20**,** 292-310.

Vertessy, R.A., R.G. Benyon, S.K. O'Sullivan & Gribben, P.R. 1995. Relationships Between Stem Diameter, Sapwood area, Leaf area and Transpiration in a Young Mountain Ash Forest. *Tree Physiology*, 15,559-567.

Vertessy, R.A., T.J. Hatton, P. Reece, S.K. O'Sullivan & Benyon, R.G. 1997. Estimating Stand Water Use of Large Mountain Ash Trees and Validation of the Sap Flow Measurement Technique. *Tree Physiology*, 17,747-756.

Von Randow, C., Manzi, A.O., Kruijt, B., de Oliveira, P.J., Zanchi, F.B., Silva, R.L., Hodnett, M.G., Gash, J.H.C., Elbers, J.A., Waterloo, M.J., Cardoso, F.L., Kabat, P. 2004. Comparative Measurements and Seasonal Variations in Energy and Carbon Exchange Over Forest and Pasture in South West Amazonia. *Theoretical and Applied Climatology,* 78, 5-26.

Voss, R. F. 1986. Characterization and Measurement of Random Fractals. *Physica Scripta,* T13**,** 27-32.

Walsh, R. P. D. 1982. The influence of Climate, Lithology and Time on Drainage Density and Relief Development in the Tropical Volcanic Landscapes of the Windward Islands. *Journal of the Geological Society,* 139**,** 656-656.

Walsh, R. P. D. 1996. Drought Frequency Changes in Sabah and Adjacent Parts of Northern Borneo Since the Late Nineteenth Century and Possible Implications for Tropical Rain Forest Dynamics. *Journal of Tropical Ecology,* 12**,** 385-407.

Walsh, R. P. D. & Newbery, D. M. 1999. The Ecoclimatology of Danum, Sabah, in the Context of the World's RainForest Regions, with Particular Reference to Dry Periods and their Impact. *Philosophical Transactions of the Royal Society of London Series B-Biological Sciences,* 354**,** 1869-1883.

Walsh, S. J., Moody, A., Allen, T. R. & Brown, D. G. 1997. Scale Dependence of NDVI and its Relationship to Mountainous Terrain. *In:* Quattrochi, D. A. & Goodchild, M. F., eds. *Scale in Remote Sensing and GIS.* Washington DC: Lewis Publishers.

Walter, H., Harnickell, E. & Mueller-Dombois, D. 1975. Climate Diagram Maps of the individual Continents and the Ecological. NY: Springer.

Weathers, K. C., Cadenasso, M. L. & Pickett, S. T. A. 2001. Forest Edges as Nutrient and Pollutant Concentrators: Potential Synergisms Between Fragmentation, Forest Canopies, and the Atmosphere. *Conservation Biology,* 15**,** 1506-1514.

Bibliography

Weaver, C. P. & Avissar, R. 2001. Atmospheric Disturbances Caused By Human Modification of the Landscape. *Bulletin of the American Meteorological Society,* 82**,** 269-281.

Weaver, C. P., Roy, S. B. & Avissar, R. 2002. Sensitivity of Simulated Mesoscale Atmospheric Circulations Resulting from Landscape Heterogeneity to Aspects of Model Configuration. *Journal of Geophysical Research-Atmospheres,* 107.

Werth, D. & Avissar, R. 2002. the Local and Global Effects of Amazon Deforestation. *Journal of Geophysical Research-Atmospheres,* 107.

Whitmore, T.C., 1984. Tropical Rain Forest of the Far East. 2nd ed. Oxford University Press, Oxford, UK.

Willott, S. J., Lim, D. C., Compton, S. G. & Sutton, S. L. 2000. Effects of Selective Logging on the Butterflies of a Bornean RainForest. *Conservation Biology,* 14**,** 1055-1065.

Wilson, J.D., & T.K. Flesch, 1999. Wind and Tree Sway in Forest Cutblocks, Iii: A Windflow Model to Diagnose Spatial Variation. Agricultural and Forest Meteorology, 93, 259-282.

Woodcock, C. & Harward, V. J. 1992. Nested-Hierarchical Scene Models and Image Segmentation. *International Journal of Remote Sensing,* 13**,** 3167-3187.

Woodcock, C. E. & Strahler, A. H. 1987. The Factor of Scale in Remote-Sensing. *Remote Sensing of Environment,* 21**,** 311-332.

Woodward, F.I. 1987. Climate and Plant Distribution. Cambridge University Press.

Woodward, F. I. & Lomas, M. R. 2001. Integrating Fluxes from Heterogeneous Vegetation. *Global Ecology and Biogeography,* 10**,** 595-601.

Woodward, F. I. & McKee, I. F. 1991. Vegetation and Climate. *Environment International,* 17**,** 535-546.

Wright, I. R., Gash, J. H. C., DaRocha, H. R., Shuttleworth, W. J., Nobre, C. A., Maitelli, G. T., Zamparoni, C. & Carvalho, P. R. A. 1992. Dry Season Micrometeorology of Central Amazonian Ranchland. *Quarterly Journal of the Royal Meteorological Society,* 118**,** 1083-1099.

Wright, I. R., Manzi, A.O., da Rocha, H.R. 1995. Surface Conductance of Amazonian Pasture: Model Application and Calibration for Canopy Climate. *Agricultural and Forest Meterology,*75, 51-70.

Wright, I. R., Gash, J. H. C., Da Rocha, H. R. & Roberts, J. M. 1996a. *Modelling Surface Conductance for Amazonian Pasture and Forest, in* Gash, J. H. C., Nobre, C. A., Roberts, J. M. & Victoria, R.L., eds. *Amazonian Deforestation and Climate*. Wiley and Sons, Chichester, UK.

Wright, I. R., Nobre, C.A., Tomasella, J., da Rocha, H.R., Roberts, J.M., Vertamatti, E., Culf, A.D., Alvala, R.C.S., Hodnett, M.G. and Ubarana, V.N. 1996b. Towards a GCM surface parameterization of Amazonia. Pages 473–504 *in* Gash, J. H. C., Nobre, C. A., Roberts, J. M. & Victoria, R.L., eds. *Amazonian Deforestation and Climate*. Wiley and Sons, Chichester, UK.

Wullschleger, S. D., Hanson, P. J. & todd, D. E. 2001. Transpiration from a Multi-Species Deciduous Forest As Estimated By Xylem Sap Flow Techniques. *Forest Ecologyand Management,* 143**,** 205-213.

Wullschleger, S. D. & King, A. W. 2000. Radial Variation in Sap Velocity as a Function of Stem Diameter and Sapwood Thickness in Yellow-Poplar Trees. *Tree Physiology,* 20**,** 511-518.

Wullschleger, S. D., Meinzer, F. C. & Vertessy, R. A. 1998. A Review of Whole-Plant Water Use Studies in Trees. *Tree Physiology,* 18**,** 499-512.

Xue, Y. K. & Shukla, J. 1996a. The Influence of Land-Surface Properties on Sahel Climate .1. Desertification. *Journal of Climate,* 6**,** 2232-2245.

Xue, Y. K. & Shukla, J. 1996b. The Influence of Land Surface Properties on Sahel climate .2. Aforestation. *Journal of Climate,* 9**,** 3260-3275.

Zang, D. Q., Beadle, C. L. & White, D. A. 1996. Variation of Sapflow Velocity in Eucalyptus Globulus with Position in Sapwood and Use of A Correction Coefficient. *Tree Physiology,* 16**,** 697-703.

Zeng, N. & Neelin, J. D. 2000. The Role of Vegetation-Climate Interaction and Interannual Variability in Shaping the African Savanna. *Journal of Climate,* 13**,** 2665-2670.

Zhang, Y., Guindon, B. & Cihlar, J. 2002. An Image Transform to Characterize and Compensate for Spatial Variations in Thin Cloud Contamination of Landsat Images. *Remote Sensing of Environment,* 82**,** 173-187.

Zhu, C. Q. & Yang, X. M. 1998. Study of Remote Sensing Image Texture Analysis and Classification Using Wavelet. *International Journal of Remote Sensing,* 19**,** 3197-3203.

APPENDIX I: AIR PSYCHROMETRICS

A1.1   SPECIFIC HUMIDITY RELATIVE HUMIDITY AND VAPOUR PRESSURE DEFICIT

Mixing ratio, W, can be determined if the dry and wet bulb temperatures (T and Twb, respectively) are known:

$W=[(Tc-Twb)(Cp)-Lv(Eswb/P)]/[-(Tc-Twb)(Cpv)-Lv]$ [-]   equation A.1.1

Where Cp is specific heat of dry air at constant pressure (J/g)~1.005 J/g, Cpv is specific heat of water vapor at constant pressure(J/g)~4.186 J/g, Lv, Latent heat of vaporization(J/g)~2500 J/g, Eswb is saturation vapour pressure at the wet bulb temperature(mb) and P is atmospheric pressure at surface~1013 mb at sea-level. The saturated vapour pressure is calculated from empirically. The equation given here is simplified to 3 significant figures and a third order polynomial:

$e_s \approx$ $\underline{0.01[6.107+4.43E\text{-}1(T)+1.42E\text{-}2(T^2)+2.54E\text{-}4(T^3)]}$ $T \geq 0$

           $0.01[6.109+5.03E\text{-}1(T)+1.89E\text{-}2(T^2)+4.18E\text{-}4(T^3)]$ $T<0$

                                         [KPa]   equation A.1.2,

where T is the air temperature expressed in degrees centigrade.

The saturation mixing ratio for air can thus be calculated:

$Ws=Es/P$ [-]   equation A.1.3

Relative humidity can be calculated:

$RH = (W/Ws)*100$ [%]   equation A.1.4

Note: The latent heat of vapourization(Lv) varies slightly with temperature. The value given used in this thesis is an approximate value for the standard atmosphere at 37 degrees Celsius.

Specific Humidity (q) can be calculated from relative humidity, air temperature and atmospheric pressure using the following approximating algorithm (Monteith and Unsworth, 1990):

$$q \approx e\varepsilon/P \qquad\qquad [kgkg^{-1}] \qquad\qquad equation\ A.1.5$$

Where ε is the ratio of the molecular weights of water and air, P is the atmospheric pressure and the vapour pressure (e) is derived as

$$RH = e\ /\ es \qquad\qquad [-] \qquad\qquad equation\ A.1.6$$

Where RH is the calculated relative humidity expressed as a fraction of the vapour pressure (e) over the saturated vapour pressure (es). The vapour pressure deficit (VPD) can thus be calculated:

$$VPD = (100\text{-}RH)/100\ *\ Edb \qquad\qquad [KPa] \qquad\qquad equation\ A\ 1.7$$

A1.2 AIR DENSITY AND ABSOLUTE HUMIDITY

In order to calculate air density, the Ideal Gas Law equation is employed after converting temperature to Kelvin and converting pressure in kPa to Pa.The gas law equation:

$$D=P/(T*R) \qquad\qquad [kgkg^{-1}] \qquad\qquad equation\ A1.8$$

Where P is pressure, D is density, T is temperature, R is the gas constant for air=287 (J/kg*Kelvin), Rw is the gas constant for water vapour= 461.5 (J/kg*Kelvin).

To calculate absolute humidity, if the dew point temperature is known, it is possible to calculate vapour pressure in millibars. Application of the gas law allows the calculation of absolute humidity by substituting Rw in place of R and be using the vapour pressure in the gas law formula, rather than the total atmospheric pressure that you would use to calculate air density.

A1.3 ADJUSTING WIND SPEED TO COMMON REFERENCE HEIGHT

Wind speed at a standard height of 2m (u_2) can be estimated:

$u_2 = u_z \dfrac{ln(2-d)/z_{om}}{ln(z-d)/z_{om}}$ $[ms^{-1}]$ equation A1.9,

where wind speed at 2m (u_2) is derived from the wind speed (u_z) measured at height (z) given the displacement height (d = 0.67h) and aerodynamic roughness length (z_{om} = 1.23h) for a particular vegetation of height (h).

A1.4 MATHEMATICAL REPRESENTATION OF TERM Δ

Term 'Δ' represents the curve of saturation vapour pressure versus temperature (T). If mean temperature is known then:

$\Delta = 0.200 [0.00738T+0.8072]^7 - 0.000116$ $[KPa\ °C^{-1}]$ equation 1.10

In: Environmental Hydrology (1995): Ward, A.D., Trimble, S.W., & Wolman, M.G. CRC press.

APPENDIX II: STAND BIOMETRICS

A2.1 ⎯⎯⎯⎯⎯⎯⎯⎯⎯⎯⎯⎯⎯⎯⎯⎯⎯⎯⎯⎯ TREE HEIGHT

By measuring the distance from the base of a tree to the observer (d) and the angle from the observer to the top of the same tree, following Pythagoras theorem it is possible to derive the height for that tree (h), assuming it is at a right angle to the plane on which the observation is made:

$$h = d\ tan\theta \qquad\qquad [m] \qquad equation\ A2.1,$$

where:

$$tan\ \theta = \frac{h}{d} \qquad\qquad [\text{-}] \qquad equation\ A2.2.$$

By measuring the angle from the observer to the lowest branch and subtracting the two heights an estimate of crown depth can be derived.

A2.2 ⎯⎯⎯⎯⎯⎯⎯⎯⎯⎯⎯⎯⎯⎯⎯⎯ CROWN AREA AND STEM RADIUS

Crown width (d) was measured in n=4 planes at 45 degrees to one another. The projected circular area (A) was calculated for each measurement plane and then averaged:

$$A = \left(\pi \left(\frac{d}{2} \right)^2 \right) \frac{1}{n} \qquad\qquad [m^2] \qquad equation\ A2.3$$

Stem radius (r) was calculated from girth breast-height (GBH) measurements:

$$r = \left(\frac{\frac{GBH}{2}}{\Pi} \right) \qquad\qquad [cm] \qquad equation\ A2.4$$

Girth measurement protocol follows those practices recommended by Clark and Clark (2002).

A2.3 ⎯⎯⎯⎯ ESTIMATION OF GAP FRACTION HEMISPHERICAL PHOTOGRAPHY

Hemispherical photos were classified into forest/non-forest areas using HEMIVIEW software (Delta T Systems Ltd., Cambs.) via supervised image classification. Although measures were taken to ensure even lighting conditions for hemispherical photos, such conditions were not met, and therefore thresholding classification cannot be deemed appropriate or accurate.

APPENDIX III: CONVERSIONS

A3.1   ENERGETIC CONVERSIONS

Wm^{-2}-MJ^{-dy}:

Given that 1 Wm^{-2} = 1 $Jm^{-2}s^{-1}$, and 1MJ= 1x10⁶J:

$$x(MJ^{-dy}) = x(Wm^{-2}) * LI/1e^6 \qquad [MJ^{-dy}] \qquad \text{equation A2.5}$$

Where LI is the logging interval in s (e.g. 30minutes =1800) and ni the number of intervals in a diel cycle.

A3.2   CONVERTING DN TO RADIANCES FOR ETM+ PLATFORM

Taken mainly from the Landsat 7 ETM+ Handbook, NASA.

To render a '1G' product image pixels digital number (DN) values are converted to units of absolute radiance using 32 bit floating point calculations, and then scaled to byte. Absolute radiance:

L_λ = "gain" * QCAL + "offset",   []   equation A2.6

is also expressed as:

L_λ = ((LMAX$_\lambda$ - LMIN$_\lambda$)/(QCALMAX-QCALMIN)) * (QCAL-QCALMIN) + LMIN$_\lambda$

                                      []   equation A2.7

where:

L_λ	= Spectral Radiance at the sensor's aperture in watts/(meter squared * ster * µm)
"gain"	= Rescaled gain (the data product "gain" contained in the Level 1 product header or ancillary data record) in watts/(meter squared * ster * µm)
"offset"	= Rescaled bias (the data product "offset" contained in the Level 1 product header or ancillary data record) in watts/(meter squared * ster * µm)
QCAL	= the quantized calibrated pixel value in DN
LMIN$_\lambda$	= the spectral radiance that is scaled to QCALMIN in watts/(meter

squared * ster * μm)

LMAX$_\lambda$ = the spectral radiance that is scaled to QCALMAX in watts/(meter squared * ster * μm)

QCALMIN = the minimum quantized calibrated pixel value (corresponding to LMIN$_\lambda$) in DN
= 1 for LPGS products
= 1 for NLAPS products processed after 4/4/2004
= 0 for NLAPS products processed before 4/5/2004

QCALMAX = the maximum quantized calibrated pixel value (corresponding to LMAX$_\lambda$) in DN
= 255

Spectral Radiance Range (watts/(meter squared * ster * μm))

| | Before July 1, 2000 | | | | After July 1, 2000 | | | |
| | Low Gain | | High Gain | | Low Gai | | High Gain | |
Band	LMIN	LMAX	LMIN	LMAX	LMIN	LMAX	LMIN	LMAX
1	-6.2	297.5	-6.2	194.3	-6.2	293.7	-6.2	191.6
2	-6.0	303.4	-6.0	202.4	-6.4	300.9	-6.4	196.5
3	-4.5	235.5	-4.5	158.6	-5.0	234.4	-5.0	152.9
4	-4.5	235.0	-4.5	157.5	-5.1	241.1	-5.1	157.4
5	-1.0	47.70	-1.0	31.76	-1.0	47.57	-1.0	31.06

Three techniques to calculate the final reflectance product exist. The first method (apparent reflectance model) corrects the effects caused by the solar radiance and sun zenith angle. This method is very simple and easy to apply because it does not require in-situ field measurements.

$R_\lambda = PI * D^2 * L_\lambda sensor/(Esun * COS(\theta))$ []   *equation A2.8.*

d = (distance Earth-Sun) = 1 - 0.01674*cos(0.9856*(JD-4))

JD= Julian Day

θ = sun zenith angle = 90-Sun Elevation angle

Esun= Mean solar exoatmospheric irradiances for a given band, from the following table:

ETM+ Solar Spectral Irradiances	
Band	Watts (meter squared * μm)
1	1969.000
2	1840.000
3	1551.000
4	1044.000
5	225.700

The other two methods use Dark Object Subtraction (DOS model) which uses a dark object that is assumed to have a reflectivity of zero. Thus, any reflectivity value over this body is equal the reflectivity of haze ($L_{\lambda.haze}$). The first of these DOS models corrects for the effects caused by sun zenith angle, solar radiance, and atmospheric scattering, but cannot correct the atmospheric absorption.

$R_\lambda = PI * D^2 * (L_{\lambda\,sensor} - L_{\lambda.haze})/(Esun_\lambda * COS(\theta))$ [-]   *equation A2.9.*

The third method (improved DOS model) has the all functions of the above two models and also takes into account the atmospheric multiplicative transmittance components.

$R_\lambda = PI * (L_{\lambda\,sensor} - L_{\lambda.haze})/(TAUv * Esun_\lambda * COS(\theta) * TAUz)$ [-]   *equation 2.10.*

The cosine of the solar zenith angle is used to estimate TAUz (COST model). TAUv is equal to 1 because the viewing angle for Landsat TM images is zero.

Conversion to radiaces allows the calculation of 'Top of Atmosphere' reflectance, pTOA:

$$\rho TOA = \frac{\pi * L * d^2}{ESUN * \cos(z)}$$ *equation 2.11.*